The University of Nottingham

UNITED KINGDOM · CHINA · MALAYSIA

Development of Injectable Cell Delivery Systems for High Accuracy Cell Therapy Applications

Mahetab H. Amer, MSc

Thesis submitted to the University of Nottingham for the degree of Doctor of Philosophy (PhD)

December 2016

Abstract

Cell-based therapeutic interventions are being developed for a variety of clinical indications, including irreversible retinal pathologies and stroke. Numerous cell therapy procedures use injection-based administration to deliver high density cell preparations, either systemically or directly. The mode of delivery of fragile cells can compromise treatment efficacy, which is dependent on cell viability and functionality post-injection. Reviewing current literature, there is a lack of comprehensive testing of the effects of injection-based cell delivery on the various parameters of cell function. This study investigated the effects of the administration process on a range of cell characteristics, and aimed to answer critical questions regarding possible reasons for failure to deliver a sufficient numbers of viable cells. Biomaterial-assisted cell delivery was also investigated to determine improvement of cell recovery and possible influence on cell fate.

Primary human mesenchymal stem cells (hMSCs) and Swiss mouse embryonic fibroblast cell line (NIH 3T3) suspensions were drawn up into 100 µL Hamilton syringes with 30- and 34G needles. They were then ejected at rates ranging from 10-300 µL/min. A comprehensive toolset was employed to assess the effects of various injection parameters, including ejection rate and needle size. Cell dose recovery, viability, apoptosis, senescence and other parameters of cellular health were evaluated using various standard and multiplex assays. Trilineage differentiation potential of ejected hMSCs was also assessed. Moreover, various injectable cell carriers were explored in terms of improvement of cell recovery and potential influence on differentiation capacity.

Ejections at slower flow rates resulted in a significantly lower percentage of dose delivered as viable cells, with ejections at 300 μL/min showing the maximum percentage of hMSCs dose delivered at 77.6 ± 11.7%. Lower cell numbers delivered at slower ejection rates were mainly attributed to cell retention within the delivery device. Normalised caspase-3/7 activity measurements ejected at 10 μL/min were also significantly higher than control. Quantification of differentiation of ejected hMSCs revealed that both ejection rate and cell carrier employed may exert an effect on differentiation capacity. The use of biomaterials as cell carriers significantly improved cell recovery. Ejection of hMSCs in 2% (w/v) gelatin solution resulted in 87.5 ± 14% of the cell dose being delivered as viable cells, in comparison with 32.2 ± 19% of the dose ejected in phosphate buffered saline (PBS) at 10 μL/min.

This study shows that ejection rate, needle size and cell carrier have a significant impact on the percentage of cell dose delivered as viable cells, cellular health and differentiation potential post-ejection. Optimal delivery strategies for injectable cell-based therapeutics are required to enhance their efficacy and reproducibility. This study emphasises the importance of careful consideration of administration protocols, according to the nature of the administered cells and cellular responses post-ejection. The combination of the investigated factors, among others, may also influence the fate of stem cells injected, thereby affecting the success of cell-based therapies.

Publications, Conferences and Awards

The following publications and awards have resulted from the work presented in this thesis.

Publications in peer-reviewed journals

Amer, M., Rose, F., White, L. & Shakesheff, K. (2016). "A Detailed Assessment of Varying Ejection Rate on Delivery Efficiency of Mesenchymal Stem Cells Using Narrow-Bore Needles"; *Stem cells translational medicine,* 5(3):366-378

Amer, M., White, L. and Shakesheff, K. (2015). "The effect of injection using narrow-bore needles on mammalian cells: administration and formulation considerations for cell therapies". *Journal of Pharmacy and Pharmacology*, 67(5):640-650

Journal papers under review

Amer, M., Rose, F., Shakesheff, K., Modo M., White, L. "Translational considerations in injectable cell-based therapeutics: concepts, progress and challenges".

Published conference abstracts

Amer, M., Rose, F., White, L., Shakesheff, K. (2016). "Comprehensive evaluation of the impact of injectable delivery on mesenchymal stem cells: Finding the winning combination"; *eCells and materials, Vol 32 (4)*

Amer, M., Rose, F., White, L., Shakesheff, K. (2015). "Evaluation of delivery of mesenchymal stem cells using small-gauge needles: Tailoring administration of

cell-based therapies for efficient clinical translation"; *Tissue Engineering: Part A, Vol 21(1)*

Amer, M., Rose, F., White, L., Shakesheff, K. (2015). "Quantifying the impact of delivery of mesenchymal stem cells using narrow-bore needles for cell therapy applications"; *eCells and materials, Vol 29 (3)*

Awards

- University of Nottingham Tri-Campus Endowed Postgraduate Award, Andrew Hendry Scholarship - University of Nottingham (April 2016).
- "Faculty for the Future" Fellowship - Schlumberger Foundation (2014-2016).
- Vice-Chancellor's Scholarship for Research Excellence (International) - University of Nottingham (2013-2016)

Acknowledgements

First and foremost, praise is due to Allah (God) Almighty, for empowering and supporting me to successfully complete this PhD thesis.

I would like to seize this opportunity to thank my supervisors for their support. Their comments and suggestions have strongly enhanced the quality of this work.

I would like to begin by thanking Prof. Kevin Shakesheff for allowing me the opportunity to undertake a project in which I had a great deal of interest but no relevant research background at the time. I am also grateful to him for allowing me the freedom to work independently and take the project down the routes I found most interesting. Prof. Shakesheff has provided me with many remarkable opportunities whilst working towards my PhD, for which I am very thankful. My sincere appreciation goes to him for allowing me the opportunity to be a member of the UK Regenerative Medicine Platform Hub "Acellular Approaches for Therapeutic Delivery", which has been an extremely valuable learning experience.

I am deeply thankful to Dr. Lisa White for her unwavering support since day 1. I am grateful for her thorough guidance concerning the various aspects of my PhD work and my training. Without her constant support, encouragement and understanding, I am not sure I would have made it this far in my PhD. I have learned a lot from her, and I truly thank her for being a mentor and a remarkable role model.

I would like to thank Dr. Felicity Rose for the guidance she has provided during my studies. Much appreciation goes to the members of the Tissue Engineering group at

the University of Nottingham, who have offered advice, support, many amazing friendships and an enjoyable working atmosphere. My endless gratitude goes to Hoda ElTaher, Nesma Abouelkheir, Nashwa Ibrahim and Aiswarya Viswanath, who have been a constant source of support throughout my PhD, and accompanied me on countless coffee breaks that helped push me through stressful times in the lab.

My thanks also go to Dr. Charles Mathews for his assistance during the first few months of my PhD, for which I am grateful. I would like to thank Dr. Glen Kirkham and Gemma Bray for training and support with stem cells. My thanks also go to Teresa Marshall, Dr. Helen Cox, and Dr. Omar Qutachi for training and advice on various techniques and materials. I am also grateful to Dr. James Dixon for provision of NIH 3T3 cells, Noura Alom for provision of bECM digests, Dr. David Onion for assistance with flow cytometry data, and Dr. Robert Markus for assistance with microscopy.

I would like to express my gratitude to Prof. Glen McDowell, Ms Stacy Johnson and fellow members of the pastoral care team at Hugh Stewart Hall. They have provided constant moral support and a family-like atmosphere that was greatly needed, and have contributed to my amazing experience in Nottingham.

I would especially like to thank the University of Nottingham, Schlumberger's "Faculty for the Future" program and Misr ElKheir foundation for funding. They have allowed me the opportunity to study what I love at one of the world's best universities.

Finally, I am truly grateful to my family for their endless love, unwavering support, enthusiastic encouragement and for always being there for me. They are my constant source of strength and inspiration. I would not be where I am now without their presence in my life. I dedicate this thesis to them.

Table of Contents

List of Figures

List of Tables

List of Abbreviations

ALP	Alkaline phosphatase
ALS	Amyotrophic lateral sclerosis
bECM	Bone-derived extracellular matrix
BSA	Bovine serum albumin
CBER	Centre for Biologics Evaluation and Research
CBF	Cerebral blood flow
CMC	Carboxymethyl cellulose
CNS	Central nervous system
Col-I	Collagen type 1
Coll	Collagen
Ctrl	Control
DAPI	4',6-Diamidino-2-phenylindole
DMEM	Dulbecco's modified eagle medium
DMSO	Dimethyl sulphoxide
DP	Directly plated control
ECM	Extracellular matrix
EDTA	Ethylenediaminetetraacetic acid
EthD-1	Ethylene homodimer-1
FCS	Fetal calf serum
FITC	Fluorescein isothiocyanate
GAG	Glycosaminoglycan
G	Gauge
g	Centrifugal G force
Gel	Gelatin
GRPs	Glial-restricted precursors
HA	Hydroxyapatite
hMSC(s)	Human mesenchymal stem cell(s)
HSA	Human serum albumin
HXYPR	Hydroxyproline

ID	Internal diameter
MPs	Microparticles
MSCGM	Mesenchymal stem cell growth medium
MSCs	Mesenchymal stem cells
NIH 3T3	Swiss mouse embryonic fibroblast cell line
NPCs	Neural progenitor cells
OCN	Osteocalcin
Pa	Pascal
PBS	Phosphate-buffered saline
PD	Parkinson's disease
PFA	Paraformaldehyde
PI	Propidium iodide
R_e	Reynold's number
RBD	Radially branched deployment
STS	Staurosporine
TGF-β	Transforming Growth Factor-β
UV	Ultraviolet
v/v	Volume per volume
w/v	Weight per volume

Chapter 1| General Introduction

Regenerative medicine is defined as an intervention that "replaces or regenerates human cells, tissues or organs, to restore or establish normal function" [1]. Cell-based therapies can be an appropriate treatment for various medical conditions that occur in a variety of tissues [2]. Injectable cell-based therapeutics offer the ability to administer cells into irregularly shaped defects in a minimally invasive manner, which is a necessity for most clinical applications [3, 4]. In addition, they allow site specificity and localised delivery [5]. However, its clinical translation is hindered by the limited supply of stem cells, substantial loss of transplanted cells following delivery, and difficulties obtaining regulatory approval [6]. Nevertheless, there has been inadequate development of tools and protocols to facilitate surgical delivery of cell-based therapies. Accordingly, research is required to improve handling and injectability of cell suspensions and biomaterial-based cellular therapies for use *in vivo*.

Since 1928, human fetal tissues and stem cells have been used to treat numerous conditions, with transplantation strategies continuously being optimised [7, 8]. Preclinical studies utilising cell transplantation have been translated into clinical trials for conditions including Parkinson's disease (PD) [9, 10], Huntington's disease [11, 12], amyotrophic lateral sclerosis (ALS) [13], and stroke [14-16]. Clinical trials have focused on the delivery of purified cellular suspensions, for example in spinal cord injuries and stroke [17-19]. The large number of cells currently used to achieve satisfactory cell retention indicates that researchers must focus on developing efficient cell delivery platforms without significant loss of cellular function or viability. Producing an appropriate number of therapeutic cells is challenging, and re-

consideration of the current administration procedures is needed to translate cell therapy to clinical use at a scale that can meet the needs of millions of patients a year.

Cell suspensions provide a delivery advantage, since they can be easily delivered via small diameter needles/cannulas into the target site, causing minimal injury. Therefore, one of the main translational challenges to the implementation of cell therapy is the need to determine suitable delivery protocols in order to ensure sufficient accuracy, survival and reproducibility in administering cells for therapeutic efficacy [20].

Despite the availability of studies investigating effects of needle-based cell delivery, a lack of administration protocol optimisation and a deficiency of comprehensive understanding of the effects of the delivery procedure on cells still exist. In this chapter, critical considerations for the various stages of cell administration are identified, studies that have evaluated the performance of injected cells are outlined, and criteria for designing cell delivery devices for minimally invasive cell therapy are discussed. The various approaches used to attempt to maximise cell viability and functionality in high accuracy applications are described, mainly focusing on neurological cell therapies as an example of high accuracy applications.

1.1 Cells as therapeutic agents

Cellular injection helps bypass many of the body's defence barriers and facilitates minimally invasive delivery [21]. Principally, three stages make up a typical cell therapy procedure: 1) *in vitro* preparation of cell suspensions; 2) injection procedure; and 3) retention of the administered cells post-injection (diffusion from injection site, survival, retention, differentiation, and immune responses) [22]. Focusing on one stage only can yield optimised settings that are not favourable to the entire procedure, and

therefore it is essential that systematic investigations consider all three stages to outline optimal transplantation parameters (Figure 1.1).

Poor cell retention at the injection site is a main barrier to the implementation of cell-based therapies to date [23]. Cell loss has been reported to be observed within the first minutes of implantation [24], with quantified survival rate of transplanted cells from approximately 1% [25], up to an immediate post-injection cell survival of 60% [26]. Cell loss has been attributed to be possibly due to retention in the dead space of the syringe and leakage from the puncture site [26]. Afterwards, a large number of cells that have been originally retained die, possibly due to exposure of cells to the inflammatory microenvironment, washout, immune destruction, dispersion through impaired local vascular system [27, 28], apoptosis and anoikic cell death [29, 30]. Variable clinical outcomes observed in two trials for PD [9, 10] have been partially ascribed to a failure to properly distribute cells to the target site [31, 32]. Attaining efficient delivery of an adequate number of cells without loss of functionality is therefore a key step in the development of regenerative medicine approaches.

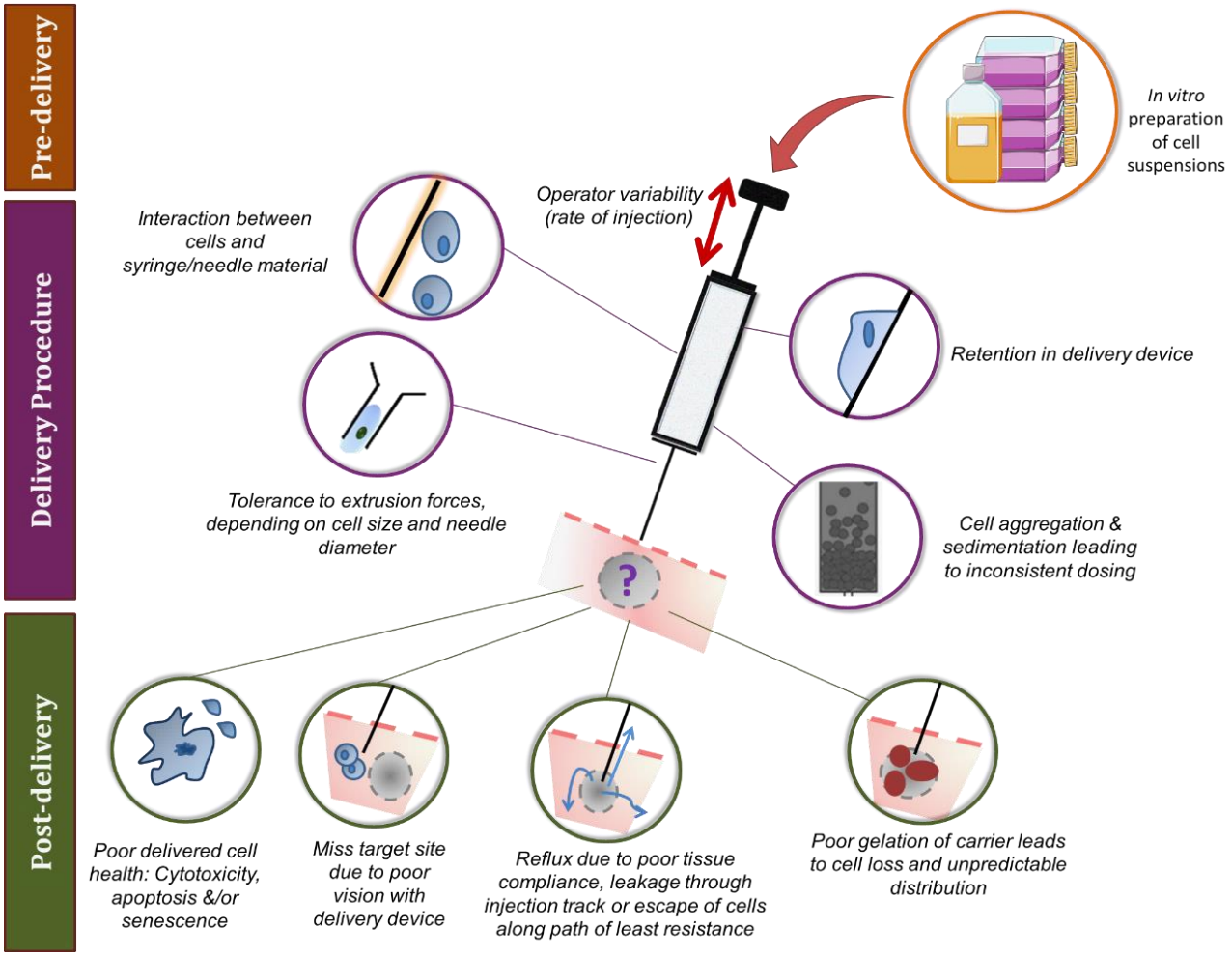

Figure 1.1: **Common problems with injectable cell delivery and possible cell fates**. Three stages make up a typical cell therapy protocol: *in vitro* preparation (pre-delivery), injection (delivery), and subsequent retention (post-delivery) of injected cells.

1.2 Pre-delivery factors: Scaling up pre-clinical models to human therapy

The number of cells required to achieve the desired therapeutic effect will have an impact on the ease of clinical translation, so satisfactory survival and incorporation of injected cells are critical for efficient cell therapy. To overcome low cell transplantation efficiency, one popular approach to translational scale-up has been to administer large numbers of cells to one site [33], with typical doses of up to hundreds of millions of cells [33, 34]. This makes cell therapy approaches technically complex and expensive, as well as offering limited control over cell fate in terms of both site-specificity and differentiation [35, 36].

1.2.1 Cell density

In cell transplantation studies, cell concentration within suspensions is often reported, with suspensions of over 100,000 cells/μL considered highly concentrated [37]. As well as higher costs of cell processing, these suspensions can be viscous, and may cause needle clogging and uneven injection flow. Moreover, as cell size varies widely depending on the site or species of origin, the maximum concentration suspended within a certain volume will therefore vary. Hence, it is more accurate to express the cellular component as a volume fraction [22].

Highly dense cell suspensions result in an increased cellular density within grafts, which may lead to cell death attributable to limited oxygen and nutrient diffusion [38]. Large doses of administered cells also pose higher safety risks of tumorigenesis [39] and micro-embolism [40]. In a study aiming to treat intervertebral disk degeneration, large osteophytes were formed that were composed of mineralised tissue surrounded

by chondrocytes derived from the injected mesenchymal stem cells (MSCs) [41]. Moreover, higher injected cell concentrations result in exposure to increased shear forces [42], yet a reduced tendency for sedimentation [22]. On the other hand, diluting cell suspensions by increasing injection volumes to over 100 μL per site can mechanically increase damage to CNS tissue [43]. The limited capacity to generate appropriately large numbers of standardised cells consistently while meeting quality criteria has also led to small clinical trials. Consequently, a balance between cell density and volumes injected needs to be attained for maximal efficacy.

1.2.2 **Cell suspension vehicles**

Suspension vehicles have been found to affect the viability of cells pre-delivery and their survival upon implantation [22, 44, 45]. Preparing a cell suspension that maintains homogeneous distribution and viability is essential to ensure effective clinical translation. Studies have suggested that MSCs viability is reduced to levels significantly below the permitted limit of 70% in a short time when stored in parenteral solutions, with other biological functions being slightly affected [44]. Cells at different temperatures will also have different requirements for storage solutions [46]. Viability at room temperature can be well preserved by the proper selection of suspension vehicles [22].

1.2.3 **Injection volume and cell number**

The human brain is 800–2300 times larger than that of rodents used for preclinical research [47]. To enable scale-up to larger target volumes, cell distribution can be increased by making multiple, lower volume injections for improved engraftment [27]. The adjustment of the needle/catheter for adequate cell distribution can lead to multiple

needle tracks and entry points. Multiple transcortical brain penetrations have been used for a range of clinical trials [9, 10, 12, 48, 49]. This is a cause for concern, as each penetration carries a risk of intracranial haemorrhage and damage to white matter tracts [43].

A study by Gutierrez *et al.* [50] evaluates the spinal cord's tolerance to varying volumes and numbers of cell injections in Göttingen minipigs. Complete functional recovery was achieved by 2 weeks, even when injection volume and numbers were increased. However, histological analysis revealed tissue damage when large volumes (50 µL) of cell suspensions were injected per site. Increased numbers of injections did not cause an increase in tissue damage, but there was an optimal number of injections required to attain the best engraftment.

In many clinical trials, doses are extrapolated from data of pre-clinical animal studies. Such extrapolations may be inaccurate and, depending on how they are calculated, doses of 100 million or more cells may result, yielding massive volumes being required. Thus, it is vital that detailed dosing studies are performed in animal models to determine the minimum effective and maximum tolerated doses [51].

No agreement exists regarding the optimal cell number to be transplanted, although this is likely to vary depending on cell type, disease and administration route. For example, $3\text{-}5\times10^7$ cells/kg MSCs were administered per multiple sclerosis patient [52], whereas in spinal cord injury, $5\text{-}6\times10^6$ cells/kg have been transplanted [53]. Use of MSCs has had positive effects on functional stroke recovery across doses of $1x10^4$ - $3.25x10^7$ cells [54]. Taguchi *et al.* reported that the higher dose of 3.4×10^8 cells gave more improved neurologic outcomes than the lower dose of 2.5×10^8 cells [55]. A

further rationale for using a higher concentration of MSCs (up to 75 million/mL) was that lower percentage loss was exhibited which seemed to level off with increasing concentrations, possibly due to the finite number of cells being able to attach to the available inner surface of the device [56]. In contrast, other clinical studies have reported that low cell doses were as effective as higher doses in inducing a response [57]. Furthermore, a phase II trial using 5-10 million NT2N cells in stroke patients showed that patients receiving the lower dose performed better [15]. A recent study demonstrated that a suitable cell dose, rather than a higher one, can better aid the repair of injured tissue in stroke patients [58].

1.3 Cell delivery challenges

1.3.1 Cell injector system design requirements & challenges

The main delivery platform for cell-based therapeutics has traditionally been a needle and syringe [59], with cell preparations delivered either systemically or directly [60]. There is a growing recognition that conventional needle- and catheter-based cell transplantation tools have considerable inadequacies that may affect clinical translation [61-63]. Key considerations for clinical translation of cell delivery devices include ease of loading and use, reproducibility, possibility of sterilisation, and ensuring no visual obstruction through a surgical microscope in high accuracy applications.

Although many clinical trials have used syringe/needle systems without cannulas [17, 64-68], CNS cell transplantation trials have typically utilised a frame-based platform for the insertion of a stereotactically guided straight cell delivery cannula or needle [9-12, 43, 49, 67, 69-71].

1.3.2 **Role of mechanical forces**

Burguera *et al.* described calculations to prove the effect of needle size on ejection force [72]. This mechanical stress may be negligible for customary needle sizes (i.e. 16–22G) [73], but may become crucial if the inner diameter is smaller. To comprehend the fluid dynamics in action in the injection device, the mechanical forces exerted on the cells being injected must be explored.

While flowing through a needle, cells may experience several types of mechanical forces, comprising shear forces characteristic of linear shear flow, pressure drop across the cell, and extensional (stretching) forces [74]. The nature of flow, whether laminar or turbulent, should be confirmed at the ejection rate and syringe/needle size used for the transplantation procedure. This can be verified through the calculation of Reynold's number (R_e), which determines flow conditions (transitional level to turbulence is R_e=2100):

$$Re = \frac{\rho Q}{15\pi D\eta}$$

where ρ is carrier fluid density (water at room temperature=999.97 kg/m^3), Q is volumetric flow rate (mL/min), D is needle diameter, and η is dynamic viscosity of the medium. Given that the flow is laminar, the velocity profile is parabolic across the diameter (Figure 1.2A), with maximum velocity at the centre of the lumen. Cells and fluid in the middle of a cannula travel at a different flow velocity to those at the walls. This difference in velocity exposes cells to shear stress [42]. Changes in shear rate and shear stress have been suggested to affect cell viability and function [74]. Shear stress (τ) can be calculated by Poiseuille's equation,

$$\tau = \frac{4Q\eta}{\pi R^3}$$

where τ_{max} is shear stress (dyn/cm^2); Q is flow rate (cm^3/s); η is dynamic viscosity of the medium; and R denotes needle radius. The magnitude of shear stress is maximal at the walls of the syringe/needle, zero at the centre, and changes linearly with distance between those two. Even low levels of shear stress (10 dynes/cm^2) have been stated to have a major influence on the activation of molecular cascades [75, 76]. Any change in the system's geometry, such as the sudden tapering of a syringe to the needle, can also result in cells experiencing extensional flow and an increase in velocity and, consequently, high shear [77]. The range of shear stress values generated by clinicians may exceed physiological values. As a useful reference, average wall shear stress is 1–6 dyn/cm^2 for venous circulation and 15 dyn/cm^2 for arterial circulation [78, 79]. However, previous reports have also stated that low shear forces of 3.5 [80] and 15 dyn/cm^2 [81] can influence cells. Studies have concluded that cell damage is based on the extent of shear stress as well as exposure time to zones of shear [42, 82]. Damage may also occur due to collisions with the stationary surfaces of the device [83]. Complete damage of the cell may not necessarily be the only adverse result, as investigations carried out on erythrocytes have shown that excessive stretching or deformation of the cell membrane might result in loss of function [84]. Extensional flow also causes cells to experience stretching and deformation, leading to cell death [85, 86]. A larger difference between diameters of the syringe and needle will result in larger extensional forces, whereas a longer needle will increase the time a cell is exposed to extensional forces. In addition, cell aggregation may intensify shear stress experienced by cells during delivery. Forces acting on cells during their administration may have two effects: cell destruction along with stretch pre-conditioning [26].

Biomaterial assisted cell delivery (reviewed in detail in Section 1.6.2) has the potential to mediate the impact of mechanical forces during cell delivery. Shear thinning hydrogels are injectable materials that exhibit a viscosity decrease under shear strain; the viscosity returns to normal when the shear is removed. Shear-thinning materials typically display plug flow behaviour when their flow within a capillary reaches a steady state. They exhibit a central wide region where material and cells experience little or no shear rate and a narrow zone of shear adjacent to the walls (Figure 1.2B). Numerous hydrogels have been reported to undergo plug flow [87, 88].

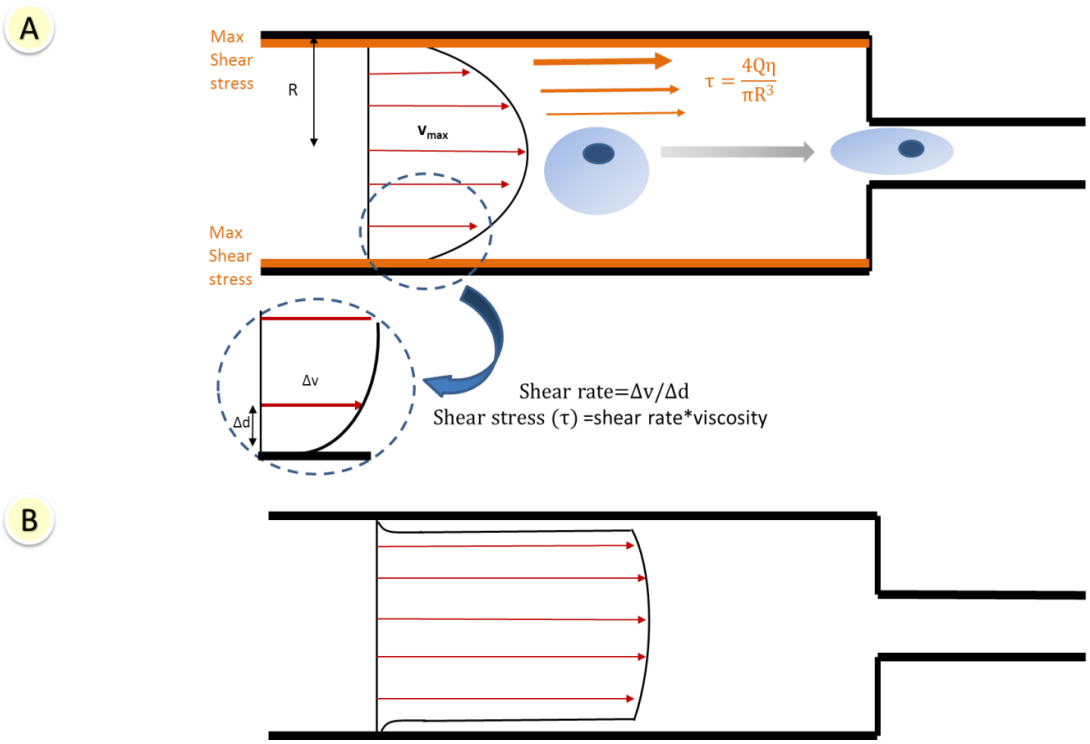

Figure 1.2: **Schematic of a section of a syringe/needle lumen of radius R.** (A) *Shear stress and velocity distribution in delivery device for Newtonian fluid and laminar flow*. The velocity profile across the diameter is parabolic. Shear stress (**τ**) is zero at the centre and increases linearly to its maximum value at the wall. As a cell flows from the syringe to the needle, it will experience increasing velocities along its length, causing it to stretch. (B) *Plug flow behaviour* - Flow velocities are almost equal across the whole diameter. Shear-thinning materials display this behaviour when their flow in a capillary reaches a steady state.

1.3.3 **Needle characteristics**

Critical parameters in injectable cell delivery include needle characteristics and/or diameter of the tubing used [89]. Needle characteristics include inner and outer diameters, length, stiffness, and bevel design. Deep subcortical target structures, such as the caudate nucleus or corpus striatum, require a long, thin needle/cannula of sufficient rigidity to penetrate to the target site without injuring the overlying structure. This cannula can be as long as 19 cm or more. Shorter needles (8–10 cm) would require direct brain exposure, which is more invasive [89].

Various needle gauge sizes have been used for neurological applications, typically starting from 25G [70, 90]. Devices with needle sizes of 30G have been developed for CNS applications [91, 92], and 30-34G are typically used for applications requiring high accuracy, particularly in ophthalmic cell transplantations [93-95]. However, smaller bore size needles, e.g.: 27–34G, are more prone to obstruction by concentrated cell suspensions, especially when successive injections are required. Smaller gauge needles cause less tissue trauma, minimise leakage through the track created by needle insertion, and have been suggested to reduce gliosis [96]. Mehta *et al.* [97] reported a 53% headache rate with the use of a 22G needle in neurological patients, and suggested that this high incidence might be caused by the large-bore spinal needle employed, which was used to prevent mechanical damage to the infused cells. Karussis *et al.* [98] also reported a high incidence of headache with MSCs in multiple sclerosis and ALS patients, attributing this to the lumbar puncture itself; needle size was not reported. Care should be taken to choose the correct needle size that accounts for cell type, injection speed, site of transplantation, and the viscosity of the suspension. Veraitch *et al.* [99] reported that 45 passages through a bore of 500 μm diameter were

needed before a significant reduction in viability was detected. Longer, finer needles have resulted in the delivery of a smaller volume [89], and are reported herein to result in a lower percentage of the cell dose being recovered [82, 100]. Faster acceleration of fluid and cells within longer needles may be more prone to clogging, perhaps because there is less time for cells to dislodge from transient adhesions to other cells and the injector [89]. Bevel angle and length may also influence injectate dispersion and direction.

1.3.4 **Material employed for construction of delivery device**

Cell retention has been reported to be more pronounced on glass than on metal surfaces [101]. Whether the adherence of the cells to the surfaces is due to chemical, physical, or charge effects has not been studied, but all of these might possibly be manipulated to decrease adhesion and settling [101]. Additionally, coating the inner surface of needles or catheters with proteins may reduce cell adhesion to the device [102]. The use of hydrophilic and siliconized coatings on internal walls of the cannula has also been suggested to decrease friction between the needle and tissue *in vivo* [101].

Although glass cannulas present several advantages, including small diameters, higher precision and minimal penetration injuries [37], glass may not be sufficiently rigid to endure injection pressure. Novel materials such as electroactive polymers and magnetorheological elastomers [103] show promise for the development of tailored needles whose rigidity could be adjusted by current, magnetic field or temperature.

1.3.5 **Sedimentation**

Uniformity of cell dosing may be affected by aggregation or sedimentation of cells in suspension over time, with clumping of cells being found to affect cell viability [104]. Unless the syringe is kept in constant motion, cells will naturally sediment, usually at the end attached to the cannula [47]. This gradient of cell density within the syringe barrel can lead to the first partial injection from a syringe possibly containing more cells than those dispensed afterwards [22].

The possibility of cell sedimentation during the course of the surgical procedure, especially in large diameter needles/cannula [101], and the potential for inconsistent cell dosing need to be considered in designing cell therapy protocols, particularly given that orientation will vary depending on application. In vertical cannulas, cells sediment towards the tip of the needle, with most cells appearing in the first 10–20% of the injectate. In horizontal cannulas, settling and adherence of cells on the side caused most of the cell dose to emerge in the final 10–20% of injectate [101]. A suspension medium should preferably have a density of ~2 g/cm^3 and a viscosity >3 cP to reduce cell settling at 20-40% cell volume fraction [22]. Negative impacts of cell sedimentation, observed post cell therapy, include graft-induced dyskinesias in PD trials, which may have occurred due to formation of dopamine “hot spots” in the brain, resulting in abnormal activation of neural circuits [105]. Moreover, some cells, such as NPCs, have a natural tendency to form clusters that may settle at the tip of the needle [89]. Therefore, it is essential to maintain an even cell suspension using agitation or other approaches.

1.4 Administration protocols

As cell injections move on to extensive clinical testing, procedural standardisation is necessary to reduce the probability of technical failures and measure the effects of interventions on patient outcome and other endpoints (e.g. injection-associated trauma and graft survival). Clinical trial design to enhance the final number of cells that integrate within the diseased tissue will require re-examining the current lack of optimisation of transplantation protocols. For a given clinical trial, optimum parameters for cell implantation are normally estimated from pre-clinical research or the investigator's judgement [106]. Whilst inappropriately administered cells may in most cases result in no functional impact, in some cases transplanted cells may result in undesirable side effects.

1.4.1 Injection rate

Injection rates employed in clinical trials for cell injection are inconsistent. For neural cell transplantation for instance, studies have used a rate of 5 µL/min [19, 107], 300 µL/min for spinal injury [108], and between 10-1000 µL/min for stroke [109-111].

Although small volume injections may be made over extended periods in the laboratory, clinical injections must be made within limited surgical duration. It has been suggested that delivering the required volume over a longer time will potentially reduce mechanical forces acting on the cells and the creation of damaging pressure gradients [37]. Delivery of 44 nL in 5 min was linked to good tissue preservation [112]. However, such a rate would be impractical, with 1 µL requiring over an hour to deliver. Notably, brain microinjections in rats at a rate greater than 1 µL/min have been linked to tissue damage [113].

Recently, intracarotid transplantation of glial-restricted precursors (GRPs) and MSCs through a microcatheter at an infusion rate of ≥ 1 mL/min resulted in stroke in 27 out of 44 rats, even with a vehicle-only infusion. A lower rate (0.2 mL/min) was safe for the infusion of both vehicle and GRPs [114]. Moreover, at high flow rates, backflow along the catheter shaft may occur if the applied force is removed from the plunger and affect delivery. It was determined that backflow can be avoided in grey matter with a 32G catheter at rates below 0.5 μL/min in a rat model [115].

1.4.2 **Cells employed**

Optimal injection parameters will vary depending on the particular morphological, physiological and growth characteristics of each cell type. Thus, it is not surprising that preparation and ejection protocols optimised for one type of cells are not necessarily applicable to others [45]. Some cell types, such as MSCs, may be especially disposed to clumping, leading to blockage of flow within the needle [116] whereas other cell types, e.g. NSCs, are sensitive to manipulation and undergo apoptosis easily. During handling, BMSCs were observed to have a greater inclination than NPCs to come out of suspension and form tight clusters [116].

1.4.3 Tissue compliance and volume of administered cell suspensions

If injections are made into cavities, larger volumes can be introduced without generating large pressure gradients if fluid drainage from the cavity is adequate, i.e. match injection to lesion volumes [117]. The shortage of human studies with lesion volume calculations, such as those occurring in human spinal cord injuries [118], make it challenging to decide on optimal injection volumes. Hydrodynamic injury will occur if intraparenchymal pressure surpasses the tensile limits of the parenchyma. Given that many microsyringes are manufactured to tolerate 1000 psi or more before failure, the likelihood of producing large tissue pressures during injection exists. Larger injection volumes also worsen the reflux of infused materials along the penetration tract [119, 120], making cell dosing unpredictable in terms of numbers and final location, and contributing to injection-related injury [37]. The low elastic modulus of brain tissue also provides little resistance to reflux of infusions [47]. In a study in minipigs, injections of greater than 6 µL caused clear neuronal damage [51].

1.5 Post-delivery complications: Functional performance of injected cells

Given the number of clinical trials that use needle- or catheter-based systems for cell delivery, surprisingly few studies have focused on the impact of small-bore needle injection on cell function. Transplantation studies have focused on the outcome of the trial rather than the variables that affected results. These variables should be studied so that they may be optimised prior to transplantation, maximising the chance of success. Investigating viability and potency of transplanted cells at the time of delivery is crucial, since a small level of cell death within a concentrated cell population could have a significant effect on the remaining viable portion through the release of

cytotoxic agents [43]. To date, research has been carried out to evaluate the impact of injection on cell viability [42, 56, 73, 74, 89, 121-123]. Studies have highlighted parameters needed to achieve an adequate cell density for therapy, such as the period between cell preparation and implantation [124], injection rate, needle length and bore size [89], and cell concentration [96, 125].

There has been wide variability in how the effects of delivery devices on cell performance are assessed. Therefore, it is vital to develop standardised assays to consistently characterise cellular therapy products. Discrepancies in the employed delivery devices and administration methodologies has complicated comparisons and led to contradictory results. This is illustrated by studies demonstrating that cell manipulation through a needle did not significantly affect viability [42, 73, 121], whereas other studies show that it did exert a significant effect [122]. A study by Heng *et al.* showed reduced cell recovery at the higher flow rate (1600 µL/min), with large variation in their samples [56].

Another potential concern is the inadequate testing of many aspects of cellular health in most studies, thereby not providing the complete picture needed to develop appropriate clinical administration protocols. The lack of comprehensive testing of the various parameters of cellular health is illustrated in Table 1.1. Conventional tests such as propidium iodide (PI) can reveal which cells are dead, but are not a useful predictor of potential delayed damage to the cells. The transient exposure to shear forces when injected does not make membrane integrity measurements, such as trypan blue exclusion assay, a good method of uncovering delayed apoptotic and senescent responses triggered. This is evident in some studies that have only relied on the analysis of cell viability to conclude that cells were not affected by the injection

parameters under investigation [73, 89, 123]. In addition, some studies have utilised a relatively small sample size of $n \leq 3$ for their investigations [42, 56, 122]. Moreover, different studies had different definitions of what constitutes effective cell transplantation. While the Centre for Biologics Evaluation and Research (CBER) states that cellular therapy products should display ≥70% viability [126], a study by Kondziolka *et al.,* considered a reduction of almost 50% in viability of cells post-injection acceptable [70].

The aforementioned issues illustrate that an enhanced understanding of what happens to cellular therapeutics post-injection, specifically regarding vital cellular health parameters, will facilitate the development of more efficient administration and formulation approaches. This reinforces the need for defining crucial parameters and trial-specific pre-clinical GLP validation of any injection protocol before human application. One method to enhance cell functionality testing in pre-clinical and clinical studies is to assess the viability of a small aliquot of injected cells. Further investigations into proliferative capacity, phenotypic expressions, apoptotic responses and other transcription-level changes of the various cell types under clinical investigation is critical. Without this, the uncertainty of whether delivery was effective will undermine interpretations of efficacy.

Most investigations carried out on the impact of injection on cell functionality and viability are completely *in vitro*, and although this data is important, other issues can undermine cell viability *in vivo*. For example, reflux and rejection can eliminate grafts in animals. *In vitro* experiments presented in this introduction will need to be augmented with *in vivo* data. The possibility that cells may experience significant biological changes on catheter/syringe/needle passage outside the conditions

examined in studies cited in this chapter cannot be excluded. Optimisation of injection protocols, materials from which delivery devices are constructed, injection rates, and cell dose is therefore crucial to in order to achieve higher efficacy and reduce variability using the smallest possible cell dose.

Table 1.1: **Overview of investigations carried out to assess the effects of various injection parameters on cell viability and functionality.** This table provides a summary of the investigations carried out into the effects of injection-based administration of cells on various parameters of cell health. Trials shown below represent a systematic review of the studies carried out, and should not be taken as an indication of the quality of any particular study.

Aim of study	Experimental design	Cell type	Syringe & needle	Flow rate(s) & other parameters	Brief description of results	Assays for Assessment of Cellular Health				Ref
						Viability	***Apoptosis***	***Senescence***	***Others***	
Viability after cell transfusion	*In vitro*	Bone marrow-derived mono-nuclear cells	Injection pump and 16-, 18-, 22G needles	1 and 0.5 mm/s	No difference detected in viability ratios.	√	X	X	X	[73]
Changes in hMSCs by transcatheter injection	*In vitro*	hMSCs	1-mL syringe and 26G (155 cm) Nitinol needle	400 or 1600 µL/min	Viability not affected. Slightly altered gene expression, but effects not translated into significant differences in protein production.	√	X	X	Clonogenicity, gene expression profile, cytokine secretion	[56]

Response after manipulation in narrow-bore syringe system	*In vitro*	Murine MSCs	10 μL syringes and 26s-, 25- or 22G needles	Drawn up at 30 μL/min; ejected at 20, 5 and 1 μL/min	Needle bore size and time within the syringe affected viable cell density.	√	√	X	Cell attachment and spreading	[122]
Effect of cell delivery via needles & catheters	*In vitro*	Rat and human MSCs	20-, 25-, and 30G needles, & SL-10 microcatheter attached to 10 mL syringe	60, 120, 240, and 500 mL/hr	No sig. effect on viability (>70%). Delayed viability drop at 24 hr. No change in cell surface markers.	√	√	X	Immunophe-notyping & multilineage differentiation	[42]
Small bore size to deliver single/multiple cell injections	*In vitro* and *in vivo*	hMSCs	24, 25 & 26G needles and 1 mL syringe. Multiple injections (10x): 26G needle & 1mL syringe	2000 μL/min	26G can be safely used. Multiple injections non-detrimental to cells (kept functional characteristics).	√	X	√	Morphology, immunophenotyping, trilineage differentiation, *in vivo* migration	[121, 127]

Impact of manual handling procedures	*In vitro*	Mouse ESC cell line	20mL syringes: one containing cell suspension, luer-locked to stainless steel capillary (500 µm D, 1 cm L).	-Pass cells between syringes at 0.80 mL/s -Centrifuge: 300*g*, 600*g* & 1000*g* -Inoculation cell density	Gentle cell handling needed to maintain viability. Inoculation density and time exposed to ambient conditions impacted phenotype.	√	X	X	Phenotyping	[99]
Impact of injection parameters in automated delivery for the brain	*In vitro*	Neural progenitor cells and bone marrow stromal cells	Automated injection device; 250 µL syringes with 20G and 27G needles, 3.8 or 15.2 cm in length	Flow rate of 1 µL or 10 µL/s; initial acceleration rate of 42 or 208 µL/s^2. Delay between loading and injection.	Longer, thinner cannulas and greater cell concentrations were harmful for delivery.	√	X	X	X	[89]

Effect of DMSO, cell density and needle size on viability in 3D hydrogels	*In vitro*	NIH 3T3 cells	27G needle	-	Viability of cryopreserved cells was significantly lower than freshly collected cells. Needle size affected survival rates. DMSO lowered survival.	√	X	X	X	[123]
Effect of varying ejection rate, cell density and needle gauge on cell health *(Chapter 3)*	*In vitro*	NIH-3T3 cells	30- and 34G needles attached to 100 µL syringes	Drawn up at 300 µL/min, and ejected at 20-300 µL/min controlled using a syringe pump	Ejections at 150 µL/min resulted in highest percentage of dose delivered. Difference in proportions of apoptotic cells 48 hrs post-ejection was	√	√	√	Cytotoxicity	[82]

					higher at slower rates.					
Investigation of cell suspensions in large injection cannulas oriented at various angles	*In vitro*	Primary rat embryonic cell suspensions of neural tissue	18-, 21- & 25G metal cannulas. Glass cannulas (ID: 0.8 mm) attached via silicone tubing to 100 µL syringe	10 µL/min using a syringe pump. Delay of 20 mins between loading & injection	Cell behaviour was affected by cannula diameter, orientation and material.	X	X	X	Mean cell counts	[101]
Effect of transcatheter injections on viability and cytokine release	*In vitro*	Mononuc-lear cells	Cell suspension was aspirated into a 5-mL syringe and then infused through a 25G needle. Cells were passed through an Excelsior SL-10 catheter; Iodine and	0.5 to 5 mL/min	Flow rates from 0.5-2 mL/min did not alter viability, but 5 mL/min reduced viability by 19%. Catheter delivery at 2 mL/min did not affect VEGF, IL-10, or IGF-1 levels. Iodine	√	√	X	Cellular function was assessed by production and release of VEGF, IL-10, and IGF-1.	[128]

			heparin exposure		did not affect viability. High-dose heparin caused cell death.					
Effect of ejection rate and needle gauge on cell health *(Chapter 4)*	*In vitro*	hMSCs	30- and 34G needles attached to 100 µL syringes	Drawn up at 300 µL/min, and ejected at 10-300 µL/min using a syringe pump	300 µL/min gave highest viable cell recovery. Apoptosis levels at 10 µL/min were significantly higher than control. CD105 expression downregulated at 10 µL/min.	√	√	√	Immunophe-notyping, trilineage differentiation	[100]

G, gauge; CBF, cerebral blood flow

1.6 Approaches to improve cell injectability

1.6.1 Improvement of cell transplantation protocols and tools

Insufficient development of surgical tools and methods for cell delivery to the human brain and spinal cord may result in the failure of cell transplantation trials despite the reliability of the basic biological concepts [61-63, 89, 91, 116, 129]. In addition to possible adherence to device materials, cells may encounter residual trace amounts of manufacturing agents that could induce apoptosis or undesired differentiation. Moreover, there is a lack of available catheter-based delivery devices for pre-formed scaffolds.

To decrease variations encountered in manual injection, automated devices (e.g: computer-controlled syringe pumps) have been suggested to offer better control [116, 130, 131]. Automated brain injections were more reproducible compared to manual injections, with variability 2-20 fold higher in manual techniques [116]. For cell aggregates or encapsulated cells, automated cell delivery methods may prove useful to control the cell dose and preserve structure integrity.

To overcome the need for multiple injections, Mendez *et al.* developed a two-hole cannula tip design [63], while Lim and colleagues created a system capable of radially branched deployment (RBD) of a catheter at adjustable angles [43, 47]. Notably, cells at high density ($6x10^7$ cells/mL) were not damaged by transit at a high rate of delivery (50 µL/min, 99.6% viability) [47]. While it represents an improvement, RBD still does not fully repeat the cell distribution achieved in pre-clinical models.

The use of syringe/cannula rotation during the injection procedure is a strategy described in the literature [70, 101, 132]. In a clinical trial for Parkinson's disease, the injection protocol incorporated rotations of the cannula between deposits, with transplant survival confirmed up to 12 months after surgery [63]. Skewed distribution of cells in horizontally oriented cannulas can also be amended by rotation at regular intervals during the procedure [101]. Robot-assisted surgery, image-based needle guidance systems can also facilitate accurate delivery. These include needles that automatically stop and lock into position by sensing drops in mechanical resistance [133]. Technological improvements to platform and cannula design have reduced procedural invasiveness while improving injection accuracy, resulting in progress from single unilateral microinjections to multiple bilateral injections without long-term neurological consequences [91].

As the number of clinical cell therapy trials increases, the need for improvement of transplantation procedures has correspondingly increased. Optimisation of injection rates used in pre-clinical and clinical trials is critical to improve delivery success rates. However, most trials do not specify infusion volumes, rates or duration of administration. Few clinical trials thoroughly optimise and state their cell transplantation protocols, which may lead to variability and lower transplantation efficiency. Table 1.2 displays a selection of clinical trials that do not state the ejection rates used in the cell transplantation procedures, which may influence the success of cell delivery. This table shows various clinical trials that have not reported important variables of the cell administration protocol, such as volumes of cell suspensions administrated and injection rates utilised. However, recent studies are beginning to recognise the importance of optimisation of transplantation protocols, both in pre-clinical and clinical trials [114, 125, 134-137]. In a model of retinal dysfunction,

photoreceptor integration was 20- to 30-fold increased by improved transplantation procedures including single and dual injections and optimisation of the number of cells injected per µL [138]. Another study defined optimised conditions for an autologous stem cell therapy to treat a craniofacial traumatic deficiency, regenerating 80% of the original jawbone deficiency in only 4 months versus a minimum healing period of 6–8 months with typical protocols [134]. To successfully achieve optimal delivery *in vitro* preparation of cell suspensions, the suitability of the suspending vehicle [22], amongst other variables, must be optimised.

Table 1.2: **Selection of clinical trials for neural applications carried out using injectable cell therapy.** This table is illustrative of the numerous clinical cell therapy trials undertaken in the field of neurodegenerative diseases. Trials shown were selected to exemplify the range of therapies currently under investigation, and should not be taken as an indication of the quality of any particular trial.

Cells	Application	Injection device	Cell dose	Volume injected	Flow rate	Outcome	Ref
MSCs	*Amyotrophic lateral sclerosis*	Syringe with 18G cannula needle mounted on a table fixed arm with a micrometric system. Cannula pre-modified to inject upwards and downwards.	110×10^6 cells. During treatment, different cell numbers were obtained in each subject. Only one patient received $<15\times10^6$ cells.	Cells suspended in about 1 mL of autologous CSF.	Not stated	MSC transplantation into the spinal cord is safe, but no definitive conclusion about cell vitality after transplantation.	[139]
	Parkinson's disease	Each patient was mounted with a Leksell stereotactic headframe. A 50 μL Hamilton syringe, fitted with a custom-made microinjector. The cell suspension was deposited along each of four putaminal trajectories.	Final cell concentration of ≈ 80,000/μL. Total of 3.2×10^6 cells in one patient and about 4.8×10^6 cells in the other.	One patient received 40 μL (3.2×10^6 cells) along 4 tracks in the right postcommissural putamen, and 32 μL (2.6×10^6 cells) in the left side in the first patient.	Not stated	Results demonstrate that such therapies can be effective in some patients at advanced stages of disease. Changes in methodology may result in better clinical outcome.	[71]

	Chronic spinal cord injury	Cobra 2 catheter (tubular, polyurethane 4 Fr and 65 cm long,	2.5 x10^6 CD 34+ cells/kg	Not stated	10 mL/min	Recovery of somatosensory evoked response to peripheral stimuli. During a 2.5-year follow-up, this protocol proved safe.	[140]
		Not stated	5 × 10^6 to 10 × 10^6/kg of mononuclear cells	Not stated	Not stated	No statistical improvement demonstrated. One case of encephalomyelitis after 3rd injection. 24 patients developed neuropathic pain.	[53]
LBS-Neurons	*Ischemic or haemorrhagic stroke*	0.9 mm-OD cannula with 20 µL. Cells were aspirated into 100 µL syringe.	5x10^6 or 1x10^7 cells	10 µL was injected slowly at each site over 2 mins.	5 µL/min. Total time = 150 minutes.	A quantifiable improvement was noted in some patients, but no evidence of significant value in motor function.	[15]
MSCs and NSPCs	*Ischemic stroke*	Not described	Either 4 IV injections of MSCs at 0.5×10^6/kg body weight; or one IV injection of MSCs at 0.5×10^6/kg followed by	Four IV injections of MSCs were in 250 mL saline; and the one intravenous injection in 250 mL saline followed	Not stated	No evidence of neurological deterioration, infection or tumorigenesis at 2-year follow-up. Neurological functions and	[59]

			3 injections at 5×10^6/patient and NSPCs at 6×10^6/patient	by injections of MSCs and NSPCs in 10 mL saline.		disability levels were improved.	
RPE cells on gelatin microcarriers	*Parkinson's disease*	Cosman-Roberts-Wells stereotactic frame. Injection device parameters not described.	≈ 325000 cells on microcarriers	Two deposits of 25 µL each were made in each of the 5 targets. A total of 250 µL was injected.	Not stated	Implants appeared to be safe and well tolerated, improving symptoms.	[21]
NSI-566RSC (Neuralstem, Inc)	*Amyotrophic Lateral Sclerosis*	Microinjection platform base attached to a custom self-retaining retractor system. Five sequential unilateral injections.	$1x10^4$ cells/mL	5 injections of 10 µL at 4-mm intervals.	Not stated	Delivery was well tolerated	[141]
Olfactory ensheathing cells	*Complete, thoracic paraplegia*	25 µL Hamilton syringe with 28G bevelled needle.	80,000 cells/µL	Four injections of 1.1 µL during each penetration	Injections frame-assisted & freehand.	Transplantations were feasible and safe up to 3 years post-implantation	[17, 66]
		Automatic micropump and 3D micromanipulator. 25 µL glass syringe & 26G bevelled needle	30,000–200,000 cells/µL	Volume of single injections was 0.5 µL	2 µL/min	Neurological improvements in the 3 patients. Confirmation of significance requires larger sample.	[65]

IV: Intravenous

1.6.2 **Biomaterial-assisted delivery**

Cell suspensions in saline do not have the capability to retain cells at the target site, and do little to provide for the requirements of cell viability, behaviour and fate [142]. Thus, alternatives to saline have included cells embedded within hydrogels or microencapsulated within polymers, attached to the surfaces of microcarriers, or injected as multicellular aggregates [143]. Injectable biomaterial scaffolds as cell carriers have demonstrated improved spatial and temporal administration compared to saline injections [4, 144] along with enhanced cellular retention [145-147]. In addition, the use of biomaterials provides an opportunity to deliver growth factors alongside cells.

Hydrogels are hydrated, polymeric networks with great potential as cell carriers [148-152] that have been well utilised in regenerative medicine applications [4, 153, 154]. Shear thinning hydrogels exhibit a viscosity decrease under shear strain; the viscosity returns to normal when the shear is removed due to physical cross-linking of hydrogel nanostructures. When injected, only the hydrogel at the edges experiences shear [155], leaving the rest of the hydrogel intact under plug flow to protect cells and maintain their viability and distribution [87, 156]. Hydrogels such as alginate may experience 'shear banding' along inner walls of the needle [74] whereby a layer of hydrogel shear-thins to form a fluid, acting as a lubricant, allowing the rest of the intact hydrogel to slip through the needle. The width of the plug flow region is dependent upon rigidity of the hydrogel and flow rate [155], therefore altering the hydrogel's formulation may impact plug flow. This mechanical protection is independent of cell properties [74] and is therefore applicable to different cell types.

In biomaterial-based cell delivery systems, challenging criteria exist. Firstly, gelation kinetics must be rapid enough to ensure that cells become homogeneously integrated within the matrix. In addition, the delivery device must maintain the liquid pre-polymer during transit, allow rapid gelation once injected, and account for multiple injections if needed without needle blockage. Aguado *et al.* [74] tested 1% alginate with three different molecular weights, and demonstrated protective effects with optimised mechanical properties. HUVECs had significantly lower cell viability in phosphate-buffered saline (PBS) or in non-crosslinked alginate when compared to crosslinked alginates. In addition, choice of biomaterials will depend on the biomechanical properties of the target tissue. For example, it has been established that native spinal cord tissue is soft and viscoelastic [157]. Therefore, low stiffness and viscoelasticity are expected to be key parameters for the selection of candidate biomaterials [157].

Considerable research on hydrogel cell carriers has focused on their role post-delivery, including cell localisation [150], support of tissue growth [158, 159] and protection from local inflammatory conditions [160]. More focus is required on their role during the injection procedure, as opposed to post-delivery, where the presence of an optimised viscoelastic material may protect cells from damaging mechanical forces [74, 82]. This has been only investigated on a small scale (Table 1.3), and needs to be explored further.

Table 1.3: **A selection of investigations carried out into potential protective approaches for protection of cell cargos.**

Aim of study	Cell type	Needle size	Flow rate	Brief description of results	Ref.
Use of Hydrogels					
Improving viability during injection by alginate hydrogels	Human umbilical vein endothelial cells and adipose stem cells, rat MSCs, & mouse neural progenitor cells	28G needle on 1mL syringes	1000 µL/min	Cross-linked alginate hydrogel produced highest viability. Increasing or decreasing G' reduced protective effect. Cells in non-crosslinked alginate exhibited lower viabilities than media. Data suggested extensional flow at needle entrance was chief cause of cell death.	[74]
β-hairpin peptide hydrogel as carrier during syringe flow	MG63	26G borosilicate capillary on 1mL syringe	4, 6 and 8 mL/hr	Only gel material at the capillary wall experienced a velocity gradient, while the rest was subject to minimal shear rate. Hydrogels had no apparent effect on viability of encapsulated cells.	[88]
Injectable fibrin matrix to enhance vascularisation	Bone marrow mononuclear cells (BMMNCs)	100 µL injection – Needle size not mentioned	Not mentioned	Device was constructed for simultaneous injection of fibrinogen and thrombin solutions. Implantation of BMMNCs in fibrin resulted in better tissue regeneration and neovascularisation.	[161]
Growth-factor supplemented Matrigel for cell delivery	C2C12 myoblasts	Not mentioned	Slow- exact rate not mentioned	Results showed that the combination of matrigel as a cell carrier for myoblasts with growth factors is recommended for the generation of muscle *in vivo.*	[162]

Use of Microparticles					
PLGA particles for intra-cerebral delivery	Neural stem cells	22G needle on a 50 µL gastight Luer-tip syringe	2 µL/min	Plasma polymerised allylamine-treated MPs were used. Cell attachment was influenced by curvature, material, electrostatic charge and surface motif of particles, and the number of cells in the culture	[163, 164]
Nerve growth factor (NGF)-releasing PLGA microparticles	Fetal rat (E16-E17) brain cells	22s-G needle on a 10µL syringe	<1µL/min	Dose of NGF delivered can be modified by changing quantity of microparticles or NGF release rate. Activity of neo-tissues with NGF-enriched microenvironments increased *in in vivo* and *in vitro*.	[165]
Automated vs Manual systems					
Compare manual & automated injection	Neural progenitor cells and bone marrow stromal cells	Automated device for µL syringes (MEDRAD Inc.)	-	Automated delivery resulted in less variability in amount delivered. No significant difference in viability attributable to method of injection.	[116]

G', hydrogel storage modulus

1.7 Aims and objectives of this study

Delivery of cells in a minimally invasive manner, while ensuring maximum cell survival and retention, poses considerable challenges. An integrated approach to the evaluation of cell delivery success is needed to improve the assessment of delivery efficacy and to allow for sound interpretations of clinical results. In addition, improved cell delivery administration protocols and systems are required to facilitate the delivery of cell-based therapeutics.

This project is a response to the translational requirements of regenerative medicine research presented in this chapter, addressing a vital challenge that needs to be overcome to successfully translate promising cell therapy findings (Figure 1.3). As described previously in this introduction, studies have demonstrated a significant and rapid loss of implanted cells shortly after transplantation. It was hypothesised that a combination of delayed cell death by apoptosis and senescence, cell loss within the delivery device, as well as mechanical stresses during the ejection process have a significant influence on the success of cell delivery procedures. Once the reasons behind low cell recovery are elucidated, it would be possible to develop appropriate biomaterial-based cell delivery systems for efficient injectable cell delivery.

The main aim of this work is to inform researchers and clinicians of the impact of cell administration, using syringe-based delivery systems and narrow-bore needles, on cellular health in clinically relevant scenarios. This study also aims to identify potential solutions to the identified administration difficulties. To achieve this, there is a need to quantify the effect of administration stresses on cells, and to use this information to

design efficient injectable cell delivery systems that can protect cells during administration and enhance their functionality *in vivo*. If the variables associated with optimal cell survival can be elucidated, cell loss may be reduced and efficacy of cellular therapies improved.

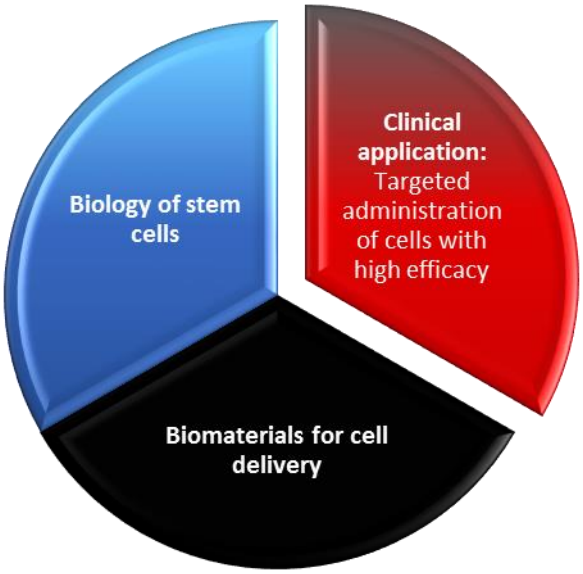

Figure 1.3: **Main areas of regenerative medicine research, highlighting the area that this project addresses**

It was hypothesised that early cell loss within the delivery device, in addition to delayed cell death, e.g.: due to induction of apoptosis by exposure to mechanical forces associated with the ejection procedure, may be the main reasons behind the failure to deliver sufficient numbers of viable cells. To assess the impact of injectable administration on the efficiency of cellular delivery, a detailed and comprehensive assessment of cellular health post-ejection was required. In order to achieve this, the objectives were to:

- Use a mammalian cell model system to assess the impact of various injection variables (ejection rate, needle gauge, and cell density) on different parameters of cellular health (Chapter 3).
- Perform a detailed assessment of the impact of varying key parameters, such as ejection rate and needle gauge, on cellular health and delivery efficacy of the clinically relevant hMSCs (Chapter 4).
- Investigate the impact of varying ejection rate on tri-lineage differentiation potential of hMSCs (Chapter 5).

Once the reasons behind low cell recovery were elucidated, it was hypothesised that suitable biomaterial-based cell delivery systems could be developed to improve the efficiency of injectable cell delivery. Therefore, the second aim of this work was to improve the viability and recovery of cells administered by syringe-based devices, especially for high accuracy applications, by investigating potential protective mechanisms such as biomaterial-based cell delivery. This might be achieved by the incorporation of hydrogels and viscous carriers as an integral component of the cell delivery system. The objectives in order to achieve this were to:

- Investigate the effects of co-delivery of cells with injectable hydrogels or viscous carriers on viability and proliferation post-ejection (Chapter 6).
- Investigate the impact of biomaterial-based cell delivery on differentiation capacity of hMSCs using an appropriate differentiation model (Chapter 6).

Chapter 2| Materials and methods

This chapter focuses on the experimental methodologies used throughout the study. Many methods are utilised in more than one results chapter and form the basis for several of the experiments performed. General cell culture and differentiation procedures are described below. Assays and staining protocols used throughout the results are justified and explained. Additional details explaining experimental design is available in each of the separate results chapters.

2.1 Cell culture

Swiss mouse embryonic fibroblast cell lines (NIH 3T3) were kindly supplied by Dr. James Dixon (University of Nottingham, UK). They were cultured in DMEM media (Gibco Life Technologies, UK) supplemented with 10% (v/v) foetal calf serum (FCS), 1% (v/v) penicillin-streptomycin and 1% L-glutamine. Cells were cultured in a humidified 5% CO_2 incubator at 37°C. For routine detachment and passaging, a standard trypsinisation protocol was carried out using 0.25% (w/v) trypsin/2 mM EDTA solution. In Annexin V/PI analyses, cells were detached using Accutase® solution (Sigma-Aldrich, UK). Cells were pelleted by centrifugation at 180x*g* using a Sigma Laboratory centrifuge 2–16K (Scientific Laboratory Supplies, UK) for 5 minutes. Subsequently, pellets were re-suspended in the appropriate volume of vehicle or re-seeded at the desired cell density in the corresponding culture vessel. Cells used were between passages 29-41.

Primary human bone marrow mesenchymal stem cells (hMSCs) were obtained from Lonza, Cologne, Germany. They were cultured in mesenchymal stem cell growth

medium (MSCGM; #PT-3001, Lonza, Germany) with 5% CO_2 at 37ºC. On receipt, the cells were at passage 2. Lot numbers of hMSC batches obtained from both male and female donors were as follows: #0000351482, #0000411107, and #0000422610, and were cultured as individual patient stocks. Cells were tested for the ability to differentiate into osteogenic, adipogenic and chondrogenic lineages. All routine passaging and differentiation procedures were performed according to Lonza's Poietics™ human mesenchymal stem cells protocols. StemPro Accutase® Cell Dissociation Reagent (Invitrogen Life Technologies, Paisley, UK) was used for cell detachment in Annexin V/PI analyses. Cells used in this study were between the third to fifth passages for cellular health assays, and up to the sixth passage for biomaterial-based delivery investigations. Donor characteristics are shown in Table 2.1.

Table 2.1: **Donor characteristics of hMSCs used**

Donor	Sex	Age
1	Male	20
2	Female	21
3	Male	25

2.2 General apparatus, chemicals and consumables

Cell ejection experiments required the use of the following:

- 100 µL Hamilton® GASTIGHT® syringes (model 1710RN), in addition to 30- and 34G removable (RN) needles (20mm or 51mm), were purchased from Hamilton, Bonaduz, Switzerland. Hamilton syringes and needles were sterilised by drawing up and immersing in 70% ethanol for 20 minutes.
- Harvard® Infuse/Withdraw syringe pump (model PHD 2000) was purchased from Harvard Apparatus®, Massachusetts, USA.

Consumable lab ware used for routine cell culture and experimental work included:

- Tissue culture flasks (25 cm^2, 75 cm^2, and 175 cm^2) (Nunc, Fisher, Loughborough, UK).
- Tissue culture treated 6-well, 12-well, and 24-well plates (Falcon, Becton Dickinson, Oxford, UK). Costar 96-well plates were purchased from Corning Inc., NY, USA.
- Cryovials, sterile pipettes, pipette tips (1mL, 200 µL 20 µL and 10 µL), 0.22 µm filters and 1.5 mL/0.5 mL Eppendorf tubes (Fisher Scientific, Loughborough, UK);
- Improved Neubauer haemocytometer, 7 mL bijoux, 100 mL sterile plastic containers, cell scrapers, Pasteur pipettes, syringes of various volumes and parafilm (Scientific Laboratory Supplies, Nottingham, UK);
- 15 and 50 mL sterile centrifuge tubes (Grenier Bio One, Stonehouse, UK);
- 30 mL universal tubes (Sarstedt, Leicester, UK);

Absorbance and fluorescence measurements were carried out on a Tecan Infinite M200 microplate reader (Tecan, Reading, UK). Brightfield and fluorescent images were taken using a Leica DM-IRB inverted microscope (Leica Microsystems Ltd., Milton Keynes, UK) or a Nikon Eclipse TS100 microscope (Nikon, UK).

Most general chemicals and assays were purchased from Sigma-Aldrich (Poole, UK) and are of analytical grade, unless otherwise stated:

- ApoTox-Glo™ Triplex Assay – Catalogue number G6320 (Promega, UK).
- AdipoRed™ Adipogenesis Assay – Catalogue number PT-7009, Lonza (Cologne, Germany).

- 1,9-Dimethyl-methylene blue- Catalogue number 341088, Sigma-Aldrich, UK.
- BD Stemflow™ hMSCs Analysis Kit- Catalogue number 562245 (BD Biosciences, UK).
- Dulbecco's Modified Eagle Medium (DMEM) - Life Technologies (Paisley, UK)
- Ethylenediaminetetraacetic acid (EDTA) - Catalogue number ED2SS, Sigma-Aldrich (Poole, UK).
- EnzChek Caspase-3 Assay Kit #1 - ThermoFisher Scientific (Loughborough, UK).
- Dead Cell Apoptosis Kit with Annexin-V FITC and PI, for flow cytometry – Catalogue number V13242, ThermoFisher Scientific (Loughborough, UK).
- Fluorometric Alkaline Phosphatase Assay Kit – Catalogue number ab83371, Abcam (Cambridge, UK)
- Foetal Calf Serum (FCS) - Sigma-Aldrich (Poole, UK).
- Human Serum Albumin (HSA) – Catalogue number A9511, Sigma-Aldrich (Poole, UK)
- L-Glutamine – Catalogue number G7513, Sigma-Aldrich (Poole, UK).
- OsteoImage™ Mineralisation Assay – Catalogue number PA-1503, Lonza (Cologne, Germany)
- Phosphate buffered saline (PBS) tablets (Oxoid, UK): One tablet made up to 100 ml in distilled water and heat sterilised (0.01M pH 7.4).
- Penicillin/Streptomycin (Pen/Strep) – Catalogue number 15070-063, Life Technologies (Paisley, UK).

- Quant-iT™ PicoGreen® dsDNA Assay Kit - Invitrogen Life Technologies (Paisley, UK)
- Live/Dead® Viability/Cytotoxicity Kit - Invitrogen Life Technologies (Paisley, UK).
- Senescence Cell Histochemical Staining Kit - Sigma-Aldrich (Poole, UK).
- Trypan Blue – Catalogue number SV3008401, ThermoFisher Scientific (Loughborough, UK).
- Trypsin – Catalogue number T4549, Sigma-Aldrich (Poole, UK).
- Trypsin/EDTA – Catalogue number 25-053-CI, Mediatech (Manassas, USA) or mixture of Sigma-Aldrich trypsin and EDTA to final concentration of 0.25% (w/v) trypsin and 0.02% (w/v) EDTA.

2.3 Standard cell preparation protocol for experimental procedures

After trypsinisation of cells as previously described (Section 2.1), cells were centrifuged (180x*g* for NIH 3T3 or 580x*g* for MSCs) for 5 minutes. They were then reconstituted to the required cell density in PBS, unless otherwise stated ($5X10^5$ cells/mL for NIH 3T3 and $7x10^5$ cells/mL for hMSCs). Density of suspensions used in this study was selected conservatively based on earlier pre-clinical and clinical studies [59, 166, 167]. Aliquots (100 µL) of this final concentration were used for cell ejection experiments. Cells were directly plated into well-plates to provide a control (i.e.: not ejected through a needle).

For cell ejection, 100 µL Hamilton GASTIGHT® syringes (model 1710RN) were fitted with 30- or 34G removable (RN) Point Style 3 stainless steel needles (Hamilton, Switzerland). Cell suspensions were drawn up into the syringes using a Harvard®

Infuse/Withdraw syringe pump (Harvard Apparatus®, USA) at a constant rate of 300 µL/min, before being ejected at various controlled rates into Eppendorf tubes (Figure 2.1). This ensured that any variability in cell recovery or health parameters was due to differences in ejection and not loading. Programming of syringe diameter allowed ejection to occur at the required rate determined by µL/min, rather than mm/min. Ejection was carried out into Eppendorf tubes to ensure no cell suspension was lost during the ejection process. All studies were performed at room temperature. Ejected cells were then transferred into the appropriate tissue culture well-plates.

Figure 2.1: **Experimental setup of the Hamilton syringes on the Harvard Infuse/withdraw pump.** The Harvard® PHD 2000 syringe pump was placed within a class II safety cabinet. RN needles of various gauges were attached to Hamilton 1701RN syringes, and 100 µL of cell suspensions was then drawn up into the needle and syringe. Eppendorf tubes were placed at the end of the delivery device to ensure no cell suspension was lost during ejection.

Blunt tip needles were used because needles of this kind have been utilised in several clinical and pre-clinical studies [168-170]. Syringe volume [15, 70, 171] and needle sizes were chosen to be relevant to high accuracy cell therapy applications (Section 1.3.3). Reviewing the literature, ejection rates used in clinical trials were found to be highly variable. For neural cell transplantation for example, some clinical trials have used a rate of 5 µL/min [19, 107], 300 µL/min for spinal injury [108], and ejection rates ranging between 10-1000 µL/min for stroke [109-111]. Therefore, ejection rates employed in this study (10-300 µL/min) were selected to assess a range of clinically relevant ejection rates previously used in clinical trials, while still being feasible to use with a syringe pump to provide accurate control over ejection rates.

2.4 Determination of cell viability and other cellular health parameters

2.4.1 Trypan blue exclusion method

After ejection, trypan blue (Fisher Scientific, Loughborough, UK) was added to 10 µL of the cell suspension in a ratio of 1:1 and mixed gently, then counted using the improved Neubauer haemocytometer (Scientific Laboratory supplies, UK).

2.4.2 PrestoBlue® cell viability reagent

PrestoBlue® Cell Viability Reagent (Invitrogen Life Sciences, Paisley, UK) is a resazurin-based reagent that indicates cell viability by using the reducing power of viable cells [172]. To each well, 1 mL of a 1:9 mixture of PrestoBlue™: culture medium was added. After incubating at 37 °C in the dark for the appropriate time (45 mins for NIH 3T3 and 60 mins for hMSCs), 100 µL aliquots from each well were

transferred in triplicate to a black 96-well plate (Costar, Corning Inc.). Fluorescence intensity was measured using a Tecan Infinite M200 microplate reader ($\lambda_{exc}/\lambda_{em}$: 560/590 nm), and average readings from the medium-only control were subtracted from that of tested samples.

Prestoblue® is minimally toxic [172], so assays were run on the same batch of cells over various time points to assess proliferation. Cells were cultured over several days, with directly plated cells acting as controls. With the aid of a standard curve prepared at the time of seeding, an estimate of cell numbers at each time point could be determined.

2.4.3 **CyQUANT® NF assay**

The CyQUANT® NF assay (Invitrogen, Paisley, UK) is based on measurement of cellular DNA content via fluorescent dye binding. Because cellular DNA content is highly regulated, it is closely proportional to cell number [173].

Cell suspensions ($1.5x10^5$ cells/mL) were ejected at various flow rates, as described above, then transferred to clear 96-well plates (Costar, Corning Life Sciences, UK) and incubated for 24 hours. Cell number was then determined by quantification of total DNA by CyQUANT® NF Cell Proliferation Assay according to manufacturer's instructions using a Tecan Infinite M200 microplate reader, with excitation at 485 nm and emission detection at 535 nm. DNA content (shown by fluorescence intensity) can be correlated to the number of cells by a reference standard curve, thereby providing an accurate measure of cell number.

CyQUANT was also used to assess cell adhesion capacity two hours post-ejection, according to manufacturer's instructions. Briefly, well-plates were prepared in duplicates and test well-plates were washed gently with PBS to remove non-adherent cells. To determine total cell number, the directly plated control plate was centrifuged and culture medium was carefully removed. CyQuant® working solution (100 µL) was added to each well. Plates were then incubated in the dark at 37°C for 1 hour. Adhesion capacity is expressed as fold difference relative to total cell number in the control plate.

2.4.4 **LIVE/DEAD® Viability/Cytotoxicity assay**

The Live/Dead® Viability/Cytotoxicity assay is used to determine cell viability in a population based on cellular esterase activity and plasma membrane integrity. Assessment of cell viability was performed according to the manufacturer's instructions (Invitrogen Life Technologies, Paisley, UK). Calcein AM and ethidium homodimer-1 (EthD-1) were prepared in PBS to produce the Live/Dead® staining solution. Samples were visualised using fluorescence microscopy (see section 2.2), where viable cells stained green and dead cells stained red. Stained cells were also analysed using flow cytometry after incubating with Live/Dead® staining solution for 30 minutes before analysis (see section 2.4.7).

2.4.5 **Apo-Tox Glo™ Triplex assay**

Multiplex assays are capable of measuring cell cytotoxicity, viability, and apoptosis simultaneously in a single well. Viability, cytotoxicity and apoptosis were measured using the ApoTox-Glo Triplex Assay (Promega, UK) according to manufacturer's instructions. This assay evaluates cell membrane integrity by measuring two protease

biomarker activities, in addition to a signal from the cleavage of the luminogenic caspase-3/7 substrate.

Cells were plated at 20,000 cells/well in clear-bottom 96-well plates (Costar, Corning Life Sciences) for NIH 3T3 experiments. Cell suspensions of $1.5x10^5$ cells/mL were used in hMSCs investigations. Fluorescence and luminescence readings were made using a Tecan Infinite 200 plate reader, and data was normalised to the medium-only sample. To provide a means of normalising well-to-well variability, cytotoxicity fluorescence measurements were represented as normalised to viability measurements (dead/live cell ratio). Caspase luminescence measurements were represented as normalised to viability (apoptotic/live cell ratio). Cells subjected to three hours of 10μM staurosporine treatment were used to provide a positive control.

2.4.6 **Senescence assay**

Cellular senescence is the process whereby cells permanently lose the ability to proliferate, moving from an actively dividing to a non-dividing state [174]. In conjunction with the loss of the ability to divide, changes occur in their morphology and physical appearance, as well as a changed pattern of gene expression [175].

Seventy microliters of cell suspensions were ejected at various flow rates (section 2.3) then transferred to T-25 tissue culture flasks and incubated (5 days for NIH 3T3 cells and 3 days for hMSCs). Cells were tested for senescence using the Senescence Cells Histochemical Staining Kit (#CS0030, Sigma-Aldrich, UK) according to the manufacturer's protocol. The assay is based on a histochemical stain for β-galactosidase activity at pH 6. Under these conditions, β-galactosidase activity is easily detectable in senescent cells only. Cells were stained with freshly prepared staining

solution (pH 6) for 18 hours at 37°C in the dark. Senescence-associated β-galactosidase (SA-β-Gal) activity was quantified by counting the number of blue-stained cells, determining a final average percentage of the number of stained to total cells. At least 200 cells were counted for each flow rate from a minimum of 10 non-overlapping microscopic fields in each flask. Hydrogen peroxide (150μM for 3 hours) was used as positive control.

2.4.7 **Flow cytometry analysis**

Following ejection into Eppendorf tubes, cell suspensions were then transferred to flow cytometry tubes and analysed. Cell suspensions were analysed using a Beckman Coulter Cytomics FC500 flow cytometer (High Wycombe, UK) using a 488nm laser. For NIH 3T3 Live/Dead analysis, a sorting parameter of 50,000 total events was used in each sample, or 300 seconds. For Annexin V/PI, a sorting parameter of 30,000 total events was used. Data was analysed using WEASEL software (F. Battye, Walter and Eliza Hall Institute, Melbourne, Australia). For data analysis, quadrants were determined using unstained and single stain control samples.

In Live/Dead analysis, percentage viability was determined by dividing the number of viable events (events fluorescing in the lower right quadrant) by the total number of events that occurred within the control. Using this method allows the number of cells that may have lysed, and therefore not produced an event, to be taken into account. However, this method does assume that no cells lysed within the control group. Dead cells were prepared for single population controls by incubating with 10% ethanol for 10 minutes at room temperature.

For apoptosis detection, cells were analysed using the Alexa Fluor® 488 Annexin V/Dead Cell Apoptosis Kit (Molecular Probes, UK). The method used was loosely based on the protocol described by Rieger *et al.* [176]. Briefly, cells were detached using Accutase® after the desired period of incubation following injection, washed with PBS and centrifuged (335x*g* for 8 minutes for NIH 3T3 and 380x*g* for 5 minutes for hMSCs). Cells were then re-suspended in 100 µL of 1X Annexin V-binding buffer, then added 5 µL Annexin V-FITC and incubated for 10 minutes. Afterwards, propidium iodide (PI) was added (1 µL for NIH 3T3 and 2 µL for hMSCs), and incubated for a further 15 minutes. 400 µL of the Annexin-binding buffer was then added, and cells were kept on ice in the dark until analysis. Cells treated with 3µM staurosporine (STS) were used as positive control for NIH 3T3 cells and with 10µM STS for hMSCs.

2.5 Immunophenotyping for hMSCs

After ejection of cell suspensions ($7x10^5$ cells/mL) at the various flow rates, cells were incubated overnight (n=3). After 24 hours, flow cytometry-based immunophenotyping was carried out. Immunophenotypic analysis was carried out using a BD Stemflow hMSCs analysis kit and BD LSR II flow cytometer (#562245, BD Biosciences, UK). Cells were prepared following manufacturer's instructions. Mouse antihuman monoclonal antibodies CD90 FITC, CD73 APC, and CD105 PerCP-Cy5.5 were used for positive identification of hMSCs, while CD19, CD11b, CD34, CD45, and HLA-DR PE were used for negative expression. Isotype controls were prepared for all antibodies, and 10,000 events were recorded per sample.

2.6 Multi-lineage differentiation protocols and assays for hMSCs

Cell suspensions were ejected through 30G needles at the various flow rates under investigation and tested for their ability to differentiate into adipogenic, osteogenic and chondrogenic lineages. Uninduced controls were maintained in basal medium Mesenchymal Stem Cell Growth Medium (MSCGM; Lonza, Cologne, Germany; #PT-3001).

2.6.1 Adipogenic differentiation

- *Differentiation protocol*

Ejected hMSCs were seeded in 12 well-plates for adipogenic differentiation. Cells were cultivated in MSCGM until confluence, and then differentiation was induced using commercial adipogenic differentiation media. The medium was alternated between adipogenic induction and adipogenic maintenance media (#PT-3004; Lonza, Germany) for three days each time, as per the manufacturer's instructions.

- *Qualitative and quantitative assessments of adipogenesis*

Adipogenic differentiation of hMSCs is accompanied by the accumulation of intracellular droplets of triglycerides. This accumulation of intracellular triglycerides is often used as a marker of adipocyte differentiation [177]. After 21 days, cultures were rinsed with 70% (v/v) isopropanol for five minutes and differentiation was qualitatively assessed by specific staining of lipid droplets with 0.5% Oil Red O solution (Sigma-Aldrich, Poole, UK). Intracellular lipid accumulation was quantified using the AdipoRed™ Adipogenesis Assay (Lonza, Cologne, Germany) following the manufacturer's protocol. Briefly, cells were pre-washed with PBS and incubated with

the AdipoRed™ Reagent, which is a solution of Nile Red, for 10 minutes. Fluorescence was measured using a plate reader ($\lambda_{exc}/\lambda_{em}$ 485/572 nm).

2.6.2 **Osteogenic differentiation**

- *Differentiation protocol*

Ejected cell suspensions ($1.5x10^5$ cells/mL for monopotential media and $7x10^5$ cells/mL for bipotential media) were seeded in 12 well-plates and cultured in osteogenic differentiation medium (#PT-3002; Lonza, Germany). Media was changed every 3 days. After 21 days of incubation, cells were fixed in 10% (v/v) formalin and the presence of extracellular calcium deposits in differentiated samples was verified using Alizarin Red staining solution and von Kossa silver staining kit (Millipore, UK).

- *Qualitative detection of mineralisation*

For Alizarin Red S staining at day 21, cells were treated with Alizarin Red S for 5 minutes at room temperature. After washing three times in deionised water, cells were observed microscopically. For von Kossa staining, the silver staining kit (#100362, Millipore, UK) was used. Briefly, cells were incubated with silver nitrate solution under exposure to UV light for 20 minutes. Wells were then washed with deionised water three times, and treated with sodium thiosulfate solution for 5 minutes. Wells were then washed again three times with deionised water. Mineralised nodules were visualised as black spots.

- *OsteoImage staining for quantitation of hydroxyapatite deposition*

At day 21 from osteogenic induction, *in vitro* mineralisation was assessed using the OsteoImage™ Mineralisation Assay kit (Lonza, Germany) according to the

manufacturer's instructions. The assay is based on the specific binding of the fluorescent OsteoImage Staining Reagent to the hydroxyapatite portion of mineralised bone nodules in osteogenic cultures. Briefly, cells were fixed in 10% (v/v) formalin, rinsed twice using the OsteoImage Wash Buffer, stained with the staining solution provided (1:100 dilution in the wash buffer) and incubated for 30 minutes. Following incubation, cells were rinsed three more times with wash buffer. The OsteoImage Assay allows the assessment of *in vitro* mineralisation both visually by fluorescent microscopy and quantitatively using a plate reader ($\lambda_{exc}/\lambda_{em}$: 492/520 nm).

- *Quantitative alkaline phosphatase staining*

ALP activity was assayed to provide information on possible osteogenic changes occurring at the protein level. For the quantitative determination of alkaline phosphatase activity, the Fluorometric Alkaline Phosphatase Assay Kit (#ab83371, Abcam, UK) was used, as per manufacturer's protocol. Cultured cells were lysed using three freeze-thaw cell lysis steps. The samples to be measured (culture media or cell lysate) were incubated with the non-fluorescent 4-methylumbelliferyl phosphate disodium salt (MUP) as a substrate. The resultant fluorescence was measured using a plate reader and compared with the standards provided in the kit. ALP activity was normalised to total DNA content, measured using the Quant-iT PicoGreen dsDNA Assay Kit (#P11496; Invitrogen), following the manufacturer's protocol. DNA content of samples was estimated using the DNA standard provided in the assay kit.

- *Osteocalcin (OCN) immunostaining*

hMSCs cultured in 12 well-plates were rinsed with warm PBS and fixed with 3.7 % (w/v) paraformaldehyde (PFA) in PBS for 20 minutes, followed by a wash with warm PBS for 5 minutes. The cells were then permeabilised using warm 0.1% (w/v) Triton-

X 100 in PBS (Sigma-Aldrich, UK) for 30 minutes. Non-specific binding sites were blocked by incubation in 10% (v/v) normal donkey serum (D9663, Sigma-Aldrich, UK) and 1% bovine serum albumin (BSA) in PBS for 1 hour. The primary antibody was Mouse Anti-Human Osteocalcin Monoclonal Antibody (MAB1419, R&D Systems) diluted in 1% (w/v) BSA in PBS at 10 µg/mL for 3 hours at room temperature. This was followed by two washes with PBS supplemented with 0.1% (w/v) BSA (5 minutes each). The secondary antibody, a Donkey Anti-Mouse IgG antibody (NL007, R&D Systems), diluted in 1% (w/v) BSA in PBS (1:200), was then added for 1 hour in the dark, followed by two washes with PBS (5 minutes each). Samples were counterstained with DAPI NucBlue® Fixed Cell ReadyProbes for 5 minutes to stain cell nuclei, then visualised using a Leica DM-IRB inverted microscope (Leica Microsystems Ltd., Milton Keynes, UK).

2.6.3 Chondrogenic differentiation

- *Differentiation protocols*

Micro-mass cultures were used for qualitative chondrogenic differentiation. Ejected cell suspensions were seeded in 20 µL chondrogenic induction medium (#PT-3003; Lonza, Germany) in 96-well plates (Costar, Corning Life Sciences, UK), which includes transforming growth factor β3 (TGF-β3; PT- 4124, Lonza, Germany) to a concentration of 20 µg/mL. After 2 hours, 200 µL of chondrogenic induction medium was added to adherent cells, and media was changed three times a week. After 21 days, fixed cells were stained in 1% (w/v) Alcian blue solution (pH 1.5) overnight to identify the proteoglycan extracellular matrix. Nuclear fast red (Sigma #N3020) counterstain was incubated for 5 minutes.

For quantitative chondrogenic differentiation studies, pellet cultures were prepared based on the protocol described by Penick *et al*. [178]. Cells were centrifuged for 5 min at 580×*g*, then re-suspended in chondrogenic medium. Cell suspensions were mixed by gentle pipetting to ensure homogeneity. One hundred-microliter aliquots were then dispensed into U-type 96 well-plates (Costar, Corning Life Sciences, UK). The plates were centrifuged for 5 min at 500×*g* and incubated at 37°C in a humidified atmosphere of 5% CO_2. Cells coalesce overnight and form high-density cell aggregates [179]. Twenty-four hours post-seeding, it was ensured that aggregates could float freely by releasing them from the bottom of the wells via aspirating some of the medium and gently releasing it back into the wells. Chondrogenic induction was run for 28 days in culture volumes of 200 µL of chondrogenic induction medium. Media was changed three times a week.

- *Biochemical characterisation*

Triplicate cultures were removed from the culture medium after 28 days of *in vitro* culture and digested in 200 µL of papain solution (125 µg/mL papain in 10 mM EDTA and 2 mM L-cysteine (Sigma)) for 18 hours at 65°C.

Quantification of sulphated GAGs in the digested aggregates was carried out spectrophotometrically using the dimethylmethylene blue dye (DMMB) assay. Absorbance at 525 nm was measured using a plate reader, and proteoglycan content was estimated using bovine chondroitin-4-sulphate as standard (#C6737, Sigma-Aldrich, UK).

DNA content of the aggregates was quantified spectrofluorimetrically using the Quant-iT PicoGreen dsDNA Assay Kit (#P11496; Invitrogen), following the

manufacturer's protocol. DNA content in the samples was estimated using the DNA standard provided in the assay kit.

Collagen content was quantified by a colorimetric analysis using the Hydroxyproline assay kit (#MAK008, Sigma), according to the manufacturer's instructions. Hydroxyproline content was used as a measure of total collagen content. Hydroxyproline is a major component of collagen that serves to stabilise the helical structure. [180, 181]. Hydroxyproline content was determined in duplicates by the oxidation of hydroxyproline residues in collagen with chloramine T, developed with *p*-dimethylaminobenzaldehyde (DMAB), resulting in a product that can be measured at 560 nm. Hydroxyproline content was estimated using the standard provided.

2.7 Investigation of cell retention in the delivery device

To investigate whether cells were preferentially retained in the syringe or needle, the syringe barrel and needle were separated following cell ejection at 10 µL/min, and each was then re-attached to a corresponding clean syringe or needle. These were then flushed with PBS three times to dislodge retained cells, and washes were assessed for viable cells using PrestoBlue. To visualise cells retained in the delivery device, a Nikon SMZ1500 dissection microscope and a Zeiss LSM 510 UV META Kombi confocal system on an Axiovert 100 stand (Carl Zeiss, Germany) were used.

To investigate the possible extent of adhesion to the delivery device, 100 µL of cells suspensions with different densities ($7x10^5$ and $1.5x10^5$ cells/mL) were seeded into 96-well glass-bottom plates (Greiner Bio-One, Gloucester, UK) and incubated for ten minutes at room temperature. Suspensions were then removed from the "test" wells using a pipette, and were left in the "control" wells. Some test wells were then gently

washed three times with PBS to remove weakly adherent cells, and others were not washed and hence designated as "no-wash" wells. Control, no-wash and washed wells were incubated for a further 4 hours to allow cell attachment, and cell numbers were quantified using the CyQUANT assay. Fluorescence intensities of triplicate samples were normalised to control.

To assess whether the morphological changes of apoptosis, such as cellular shrinkage and membrane blebbing, might have led to a loss of cell-cell adhesion, ejected cell dose recovery of apoptotic cells versus viable cells (at 10 µL/min) were investigated. Apoptosis was induced in hMSCs using 10µM STS. Cell numbers ejected were then determined using CyQUANT® NF Cell Proliferation Assay (Invitrogen, Paisley, UK), as previously described.

2.8 Measurement of cell size

To measure cell size, cells from each of the three batches of hMSCs used in this study (passage 5) were suspended to a concentration of $7x10^5$ cells/mL and analysed on a Coulter LS230 particle size analyser (Beckman Coulter, High Wycombe, UK). Size distributions were obtained using the Fraunhofer approximation model, and size distribution plots based on volume distribution were generated.

2.9 Formulation and preparation of biomaterial-based carriers for cell delivery

2.9.1 Alginate carriers for NIH 3T3 cells

Alginate gels were prepared in tissue culture water under aseptic conditions, and sterilised by tyndallisation to maintain alginate's properties. Conventional UV

irradiation or autoclaving damaged cross-linking, and the 1% solution was too thick for filter sterilisation. Tyndallisation was carried out by heating the prepared gels three times at 70°C for 20 min each at 24hr intervals. The 1% (w/v) alginate solution (#177775000, Acros Organics, Belgium) was mixed 20 times using two luer-locked syringes with sterile-filtered 0.25% (w/v) calcium chloride solution (Sigma-Aldrich, UK) for cross-linking. Cells were suspended in PBS and incorporated into alginate gels indirectly via gentle mixing in a ratio of 1:1 (v/v) to give a final cell density of $5x10^5$ NIH 3T3 cells/mL.

2.9.2 **Formulation of carriers for ejection of hMSCs**

Cells were incorporated into the biomaterials via gentle mixing after suspension in PBS. The carrier was gently mixed with the cells at a ratio of 1:1 (v/v). The final cell density was always $7x10^5$ hMSC cells/mL.

- *Carboxymethyl cellulose (CMC)*

Aqueous cell carriers were prepared using high viscosity CMC (#12M31P, Ashland Speciality Ingredients, Poole, UK) in tissue culture water at a concentration of 0.5% (w/v), and were tyndallised as described in section 2.9.1. The carrier was then mixed with the cells at a ratio of 1:1.

- *Type I collagen*

Commercially available high concentration rat-tail collagen type I (#354249, 10 mg/mL, BD Biosciences, Oxford, UK) was prepared at a concentration of 1.75 mg/mL following manufacturer's instructions. Briefly, collagen was freshly prepared for ejection experiments by combining rat-tail collagen type I with 10x PBS, ice-cold 1N

sodium hydroxide, and sterile ice cold deionised water to achieve a final collagen concentration of 1.75 mg/mL. The solution was mixed and kept at 4°C.

- *Bone extracellular matrix (ECM)*

Decellularised and demineralised bone ECM was obtained from bovine bone as described previously [182]. Briefly, liquid nitrogen has been used to freeze and fragment bovine cancellous bone. Cancellous fragments were next demineralised using a solution of 0.5 M HCl at RT for 24 hours. Following demineralisation, a solution of chloroform/methanol was used to remove lipids. Then, demineralised powder was subjected to 24 hours of the decellularisation process in 0.05% Trypsin/0.02% EDTA at 37°C. To obtain bECM digests, powder bone was combined with 1 mg/mL pepsin in 0.01 M HCl for a final concentration of 10 mg/mL. Next, the suspension was stirred at RT for 96 hours until the matrix was dissolved. The resultant bECM digests were aliquoted and stored at -20°C until required[1]. Neutralisation of the required digest volume was carried out by addition of one tenth of the digest volume of NaOH (0.1 N) and one ninth of the digest volume of PBS (10×), then diluting to the desired final ECM concentration with 1× PBS on ice. A concentration of 1.75 mg/mL bECM was always freshly prepared for ejection studies.

- *Gelatin*

Commercially available 2% (w/v) gelatin solution in water, derived from bovine skin (Type B; #G1393, Sigma-Aldrich, UK), was used for biomaterial-based cell ejection studies.

[1] bECM digests were prepared by Ms Noura Alom, University of Nottingham.

2.10 Rheological analysis of biomaterial-based carriers

Rheology is the study of the viscoelastic behaviour of materials, and can provide important insight into their potential uses. For easy understanding of the fundamental rheological parameters, a two-plate model is used whereby the sample is between two plates and sheared in the gap. The upper plate is set in motion by a shearing force, while the lower plate remains fixed. Two assumptions are made: the sample does not slip/slide out of the gap, and conditions are for laminar flow [183-185]. Measurements were performed on thin sample layers between narrowly separated plates to prevent significant edge effects or variability of mechanical properties throughout the sample.

Biomaterials were subjected to rheological assessment using a Physica MCR 301 rheometer (Anton Paar, Hertford, UK). Rotational and oscillatory measurements were carried out to assess the mechanical properties of the biomaterial-based carriers. Prepared materials were loaded between 50-mm diameter cone-plate (CP 50-1) for most rheological measurements. Thixotropy recovery studies were performed using a PP 25 parallel plate with a 0.2 mm measuring gap. All rheological measurements were carried out at a controlled temperature of 25°C. A pipette was used to place approximately 200 μL of the material to be tested on the bottom plate of the rheometer, and any excess was removed once the upper cone plate was lowered into measuring position. The samples were allowed to equilibrate for at least 2 minutes prior to analysis. Typically, a minimum of three independent measurements were taken for each sample, and each reported value is the average of those measurements.

Steady shear rotational experiments were performed to determine viscosity (η) as a function of shear rate. Viscosity was determined using a constant shear rate of 1 s^{-1}. The average value of all readings at 6 sec intervals over a span of 120 secs was taken

as the viscosity measurement. Steady shear rheology was performed with shear rate varying from 0.01 to 1000 s^{-1} to determine whether the material is Newtonian or exhibits signs of elasticity. The resulting viscosity of the samples were recorded. Different flow behaviours include: Newtonian, with constant viscosity along the applied shear rates; shear thinning, when there is a decrease of viscosity with shear rate; and shear-thickening, when the viscosity increases with shear rate [185]. Shear thinning is often related to the way molecules in the sample are originally entangled, and disentangle as shear is applied. This results in intermolecular forces yielding less flow resistance with the increase of shear load [184, 186]. Viscometric thixotropy testing was carried out by applying a high magnitude strain (10000 s^{-1}) to break the biomaterial's structure, followed by a low level strain (1 s^{-1}) to observe the rate and extent of recovery of their bulk properties.

Rheological properties of biomaterials were further studied by oscillatory strain-dependent rheology to measure the material's relative viscous and elastic responses. Dynamic rheological experiments were performed to obtain additional information on the mechanical properties. Samples were subjected to oscillatory strain sweeps from 0.1-1000% performed at 6 rad/s to determine the linear viscoelastic (LVE) region and assess failure strain for these biomaterials. Storage (G′) and loss (G″) moduli helped illuminate the elastic and viscous natures of the materials under investigation.

2.11 Contact angle measurement

In any given material the individual atoms or molecules are subjected to attractive and repulsive forces from their surroundings. In the bulk of the material, attraction between the same molecules dominates, which is the same in all directions. At the surface, however, the attractive forces of the molecules from the bulk are in equilibrium with

forces acting from the adjacent material (e.g. air) [187]. Sessile drop measurements are obtained when a stationary droplet is at an equilibrium on the surface.

The contact angles of the various biomaterial-based carriers under investigation with glass slides were measured using the sessile drop method. Contact angles were measured with a CAM 200 instrument (KSV Instruments, Helsinki, Finland), after 10 seconds spreading time. A drop of the material to be tested was formed on the end of a precision syringe and lowered onto the sample surface, and then the syringe was retracted until the drop detached. After positioning the droplet onto the surface, 10 images of the drop were taken in 1-second intervals. All measurements were made at 25°C. The contact angle was calculated for each image using a Young-Laplace curve fit, and was measured relative to a manually positioned surface baseline. The drop image was processed by an image analysis system that calculated both sides of the drops, and the average was stated. A minimum of five repeat measurements were made for each biomaterial using a number of separate glass slides.

2.12 **Statistical Analysis**

Statistical analyses were performed using GraphPad Prism 6 software. Experiments were conducted with n=5 needles for each batch of cells tested, unless stated otherwise. Data sets were tested for normality, and appropriate tests of comparisons were subsequently chosen. For comparisons of two groups, the Student's unpaired *t*-test was used. For normally distributed multiple data comparisons, one-way or two-way analysis of variance (ANOVA) was carried out, with Dunnett's or Tukey–Kramer *post-hoc* tests. For n<5 or non-normal data distributions, analysis was carried out using the non-parametric Kruskal-Wallis analysis of variance, unless stated otherwise. Results were considered statistically significant if $p < 0.05$.

Chapter 3| The effects of ejection using narrow bore needles on mammalian NIH 3T3 cells

A research article based on the work described in this chapter has been published in the *Journal of Pharmacy and Pharmacology* [82].

3.1 Introduction

The success of cell therapies relies on the effective and reliable delivery of viable cells to the target site, where they can produce the desired therapeutic effect. Preclinical animal studies on cell therapy have been translated into clinical trials for a multitude of CNS disorders, including Parkinson's disease [9, 10] and stroke [15, 16, 54, 110, 188]. However, the clinical translation of cellular therapeutics is hindered by substantial loss of transplanted cells following delivery [6, 189, 190].

There are numerous challenges to the delivery of the delicate cell-based therapeutics, especially those requiring micro-volumes of cell suspensions to be delivered with high accuracy, such as in the treatment of retinal diseases. Since many cell therapy procedures require the use of syringe-based devices to deliver cells, particularly in the case of small defects and sites of limited accessibility, there is an urgent need for the development of delivery systems to provide improved cell viability and function. With the growing number of clinical trials studying the applicability of cell therapy procedures, a detailed understanding of the limitations of cell delivery is vital. Currently, injection protocols mainly rely on the operator's personal experience

through trial-and-error [106, 191]. Therefore, robust cell delivery systems must be developed and standardised to accelerate the translation of cell therapies to the clinic.

Reviewing current literature, there is a lack of comprehensive testing of the various parameters of cell health and functionality following their ejection. The aim of this study was to investigate the different aspects of successful delivery of the mammalian NIH 3T3 cells following ejection from clinically relevant, narrow-bore needles. With a growing number of clinical trials exploring potential applications of cell therapy, understanding the factors that may impact the viability and functionality of cells post-injection is of considerable importance.

3.2 Experimental design

NIH 3T3 was used as a mammalian cell model to carry out a preliminary investigation on the potential impact of the needle-based ejection process on cellular viability and functionality. The main advantage of this cell line is that a large supply of cells can be obtained with high reproducibility [192]. This cell line has been widely used as a standard model system for testing wound healing activity *in vitro,* since the cells deposit ECM and fill spaces within tissues [193, 194]. NIH 3T3 cells have also been frequently used in studies of cell functions such as cell adhesion, movement, and proliferation [195, 196]. Cell doses in this study were selected conservatively on the basis of previous clinical studies [197-200] and the rapid growth characteristics of the cells. Experiments were carried out as described in Chapter 2, with flow rates investigated herein ranging from 20-300 µL/min. An overview of the assays used to evaluate the various aspects of cellular health post-injection is shown in Figure 3.1.

For multiple data comparisons, analysis was carried out using the Kruskal-Wallis analysis of variance, unless stated otherwise. Results were considered statistically significant if $p<0.05$.

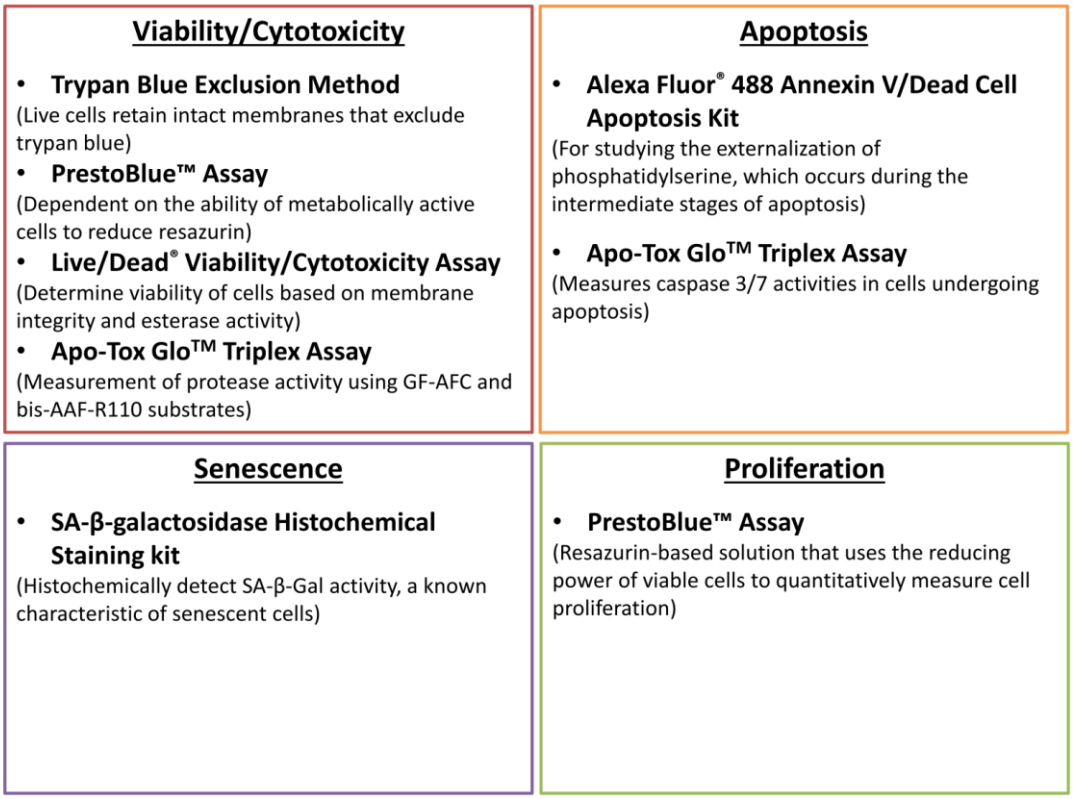

Figure 3.1: **An overview of assays used to evaluate the various aspects of cellular health post-ejection**.

3.3 Results

3.3.1 Effect of varying ejection rates

The graph in Figure 3.2A shows immediate (6 hour) and 24-hour cell viability measurements following ejection of cell suspensions at various flow rates, measured using the PrestoBlue assay. The percentage of the dose delivered as viable cells was only significantly reduced from the control value at the slower flow rates tested ($p<0.05$). Cells ejected at 150 μL/min showed the highest percentage of viable cells delivered at 99.9 ± 12.2%, with all other ejection rates exhibiting a lower percentage of cells delivered. Ejection at 20 μL/min resulted in the lowest cell recovery, with only 31.7 ± 5.1% of the cell dose delivered as viable cells.

The proliferative ability of the NIH 3T3 cells was significantly affected following ejection, with all ejection rates showing significantly lower cell numbers than the directly plated control. However, fibroblasts seemed to proliferate normally, with a significant recovery in proliferative ability after 72 hours (Figure 3.2B).

Cell counts, using the trypan blue exclusion method, after ejection of cells at different flow rates are presented in Figure 3.2D. The percentage of dead cells was only 1.5 to 2% of the total number of cells in all samples tested. However, the total number of cells ejected was significantly lower at slower flow rates, suggesting loss of cells during ejection.

All samples attached to culture surfaces within four hours of ejection and showed normal morphology. The Live/Dead staining kit, which relies on esterase activity of living cells (green fluorescence indicates living cells stained by Calcein-AM) and

compromised membranes of dead cells (red fluorescence indicated by EthD-1), was used to assess viability. Among ejection rates tested, the percentage of viable cells was high (Figure 3.3), and a visibly lower number of cells appeared in ejected samples relative to the control, especially at 20 μL/min.

Senescence-associated pH 6 β-galactosidase (SA-β-Gal) was used as a senescence marker to investigate the percentage of cells undergoing senescence post-ejection. Figure 3.4 shows the quantitation of blue-stained SA-β-gal-positive cells observed in cells after manipulation. A trend could be observed whereby a higher percentage of senescent cells was observed with higher ejection rates.

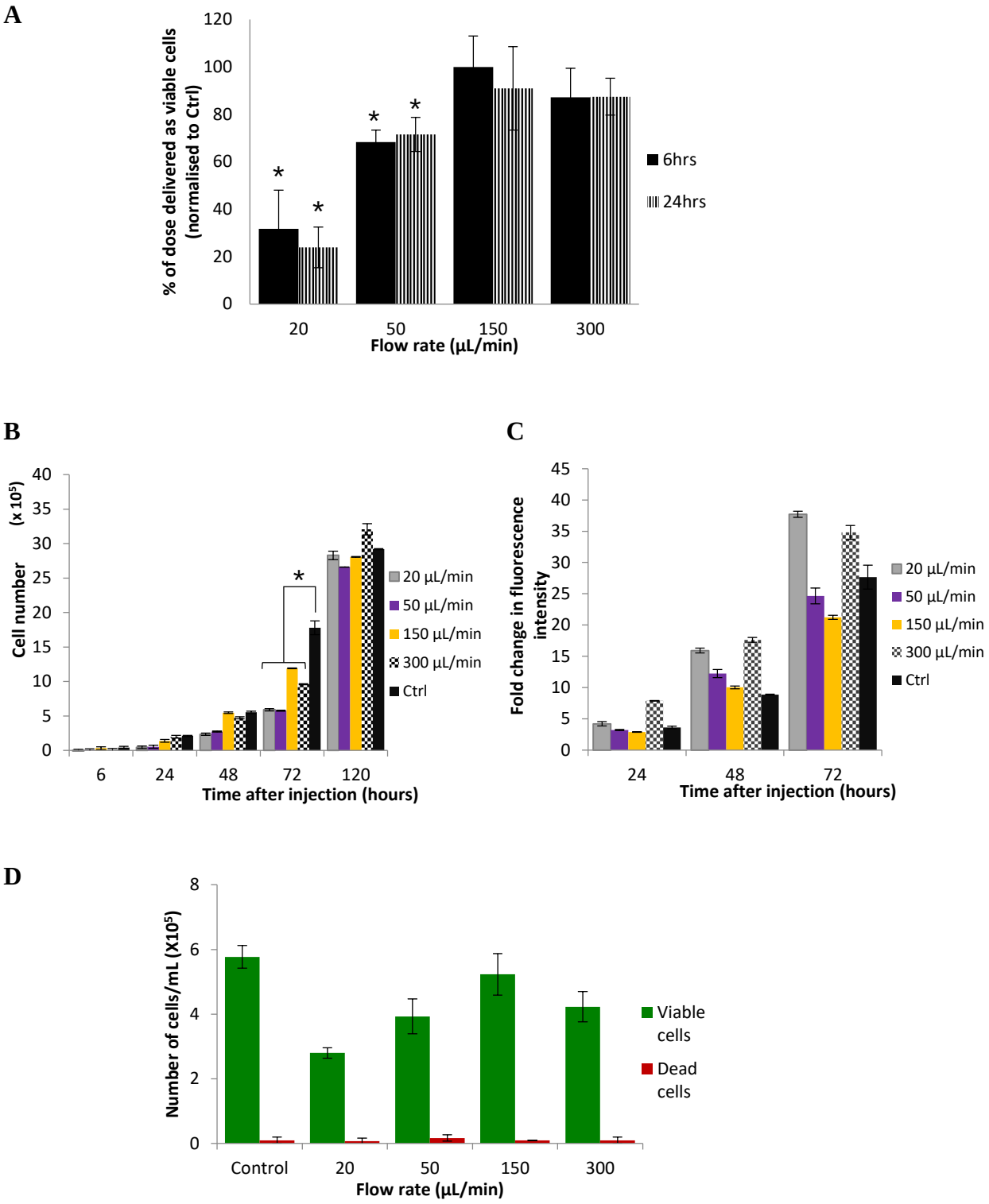

Figure 3.2: **Effect of varying ejection rate on viability and proliferation of NIH 3T3 cells ejected via 30G needles.** (A) Percentage of NIH 3T3 cells delivered as viable cells, determined using PrestoBlue, following ejection at various flow rates. Results are mean values ± SD (n=3). Data were normalised against control value of directly plated cells and expressed as percentage dose delivered. Asterisks represent significant difference between samples (p<0.05) and control. (B) Proliferation of NIH 3T3 cells, measured using PrestoBlue, following ejection at various flow rates. Results are mean values ± SD (n=3). (C) Proliferation data given as the fold change in mean fluorescence intensity, measured using PrestoBlue, following ejection at various flow rates through a 30G needle from Day 0 of each sample. Results are mean values ± SD (n=3). (D) Quantitation of cell viability using Trypan blue following ejection of NIH 3T3 cells at various flow rates (mean ± SD; n=2).

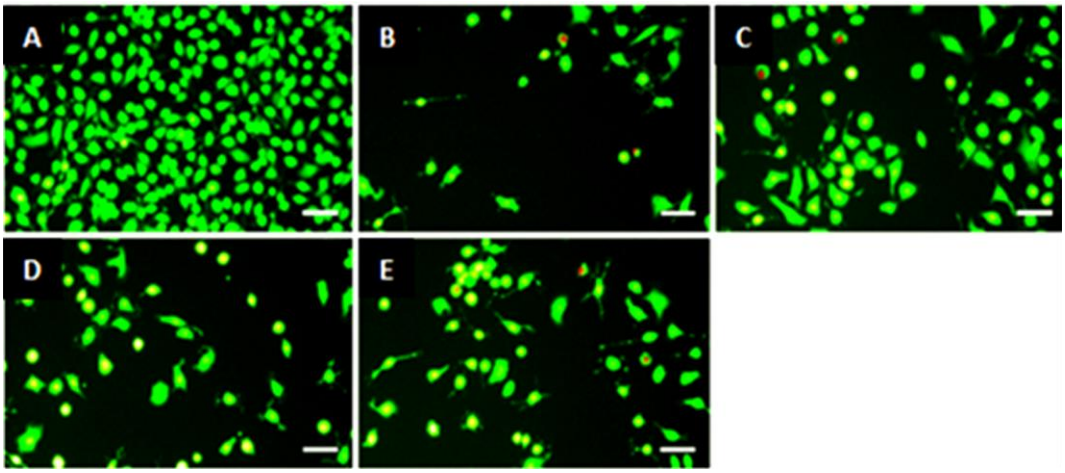

Figure 3.3: **Representative fluorescence images showing LIVE/DEAD®-stained NIH-3T3 cells ejected at various flow rates at 48 hours of incubation**. Live cells exhibited green fluorescence while dead cells showed red fluorescence (Scale bar=100 µm); (A) Control; (B) 20 µL/min; (C) 50 µL/min; (D) 150 µL/min; (E) 300 µL/min.

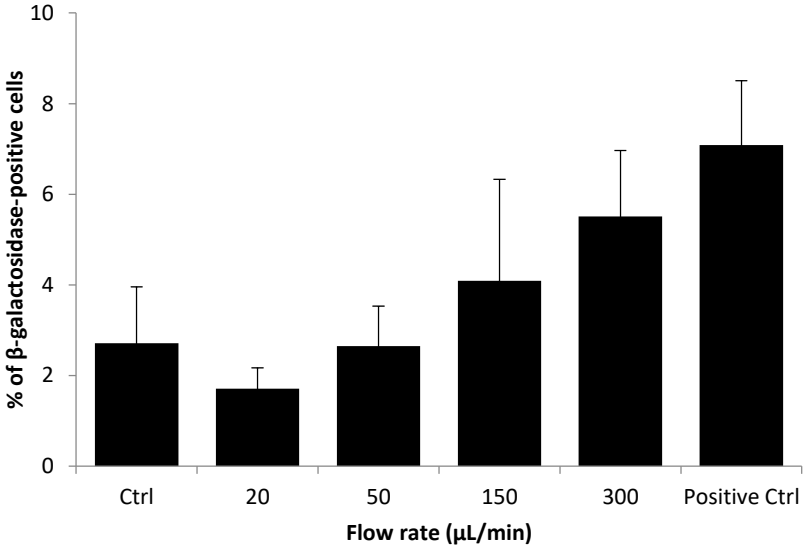

Figure 3.4**: NIH 3T3 cells undergoing senescence following delivery via 30G needles (*n*=3).** SA-β-galactosidase assay was performed at 5 days after injection, with addition of 150 µM H_2O_2 for 2 hours as positive control. Results are mean values ± SD.

3.3.2 **Effect of varying needle gauges and lengths**

Finer needles are required for high accuracy applications in order to minimise injury, especially for neuronal or retinal regenerative applications. To investigate cell viability following injection through different needle sizes, two different experiments were performed. In the first set of experiments, NIH 3T3 cells were ejected through 30G (internal diameter (ID) =159 μm), 32G (ID=108 μm) and 34G (ID=51 μm) needles of two lengths, 51 and 20 mm, at 150 μL/min. In the second set, they were ejected through 30G and 34G 20 mm needles at the various flow rates under investigation.

Due to the extremely small diameter of 34G needles, it was impossible to draw up cell suspensions using the 51mm needle. After 15 minutes of pulling the plunger to withdraw the cell suspension into the syringe there was no liquid drawn in, verified by visualisation through the glass syringe barrel. Other needles had suspensions withdrawn into the syringe almost immediately following withdrawal of the plunger. This length was therefore excluded.

Figure 3.5A shows that varying needle gauge and length had a significant effect on the percentage of cells successfully delivered; this was reduced by decreasing internal diameter and increasing needle length. In terms of the cells' proliferative ability, only the 51mm 32G and 20mm 34G needles exhibited significant differences in cell number compared to the control after 96 hours of incubation (Figure 3.5B).

Both 30G and 34G 20mm needles displayed the same trend of cell viability with the different ejection rates tested, with cells ejected at 150 μL/min exhibiting the highest viability (Figure 3.5C). However, the 34G needle showed an evidently larger decrease

in the percentage of cell dose delivered than the 30G needle at most of the ejection rates under investigation (Figure 3.5C).

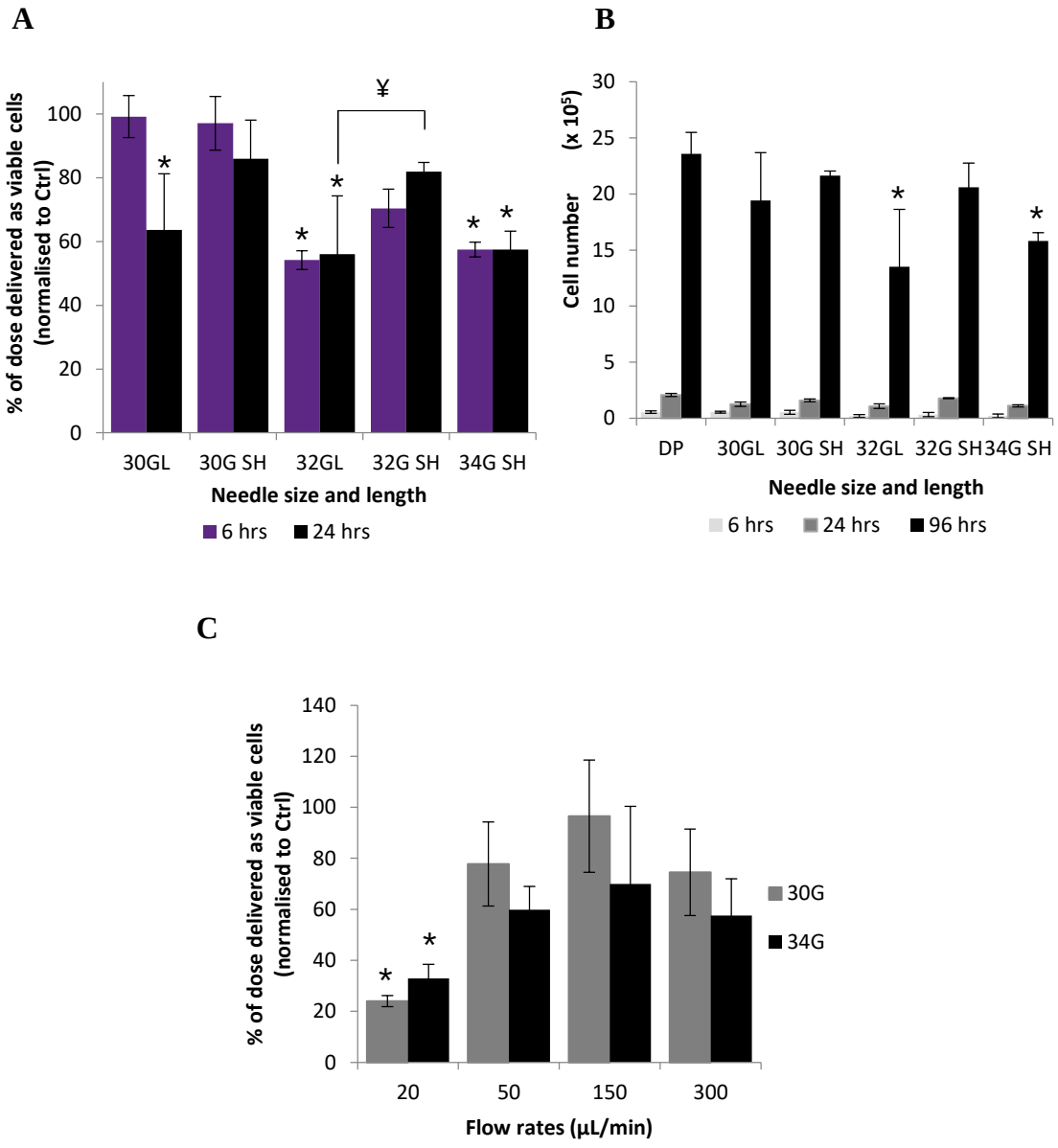

Figure 3.5: **Effect of varying needle gauges and lengths used for ejection of NIH 3T3s on their viability and proliferation ability.** (A) Percentage of NIH 3T3 cells, delivered as viable cells, after ejection at 150 µL/min using various needle gauges and lengths. Results are mean values ± SD% (n=3). Asterisks represent significant difference between samples and control, and ¥ represent significant difference between needle lengths (Short (SH) = 20 mm; Long (L) = 51 mm) of the same needle gauge, using the Kruskal–Wallis test. (B) Proliferation of NIH 3T3 cells ejected at 150 µL/min using different needle gauges and lengths (mean values ± SD). Asterisks represent significant difference between samples (p<0.05) and control (DP: directly plated control). (C) Percentage of NIH 3T3 cells, delivered as viable cells, 6 hrs following ejection at various flow rates using 30G and 34G 20mm needles. Results are normalised mean values to control ± SD (n=3). Asterisks indicate statistically significant differences between control and ejected samples using the Kruskal–Wallis test (p<0.05).

3.3.3 **Flow cytometric analysis of NIH 3T3 cells post-ejection**

Flow cytometry was used as an additional tool for analysis of cellular health. Flow cytometry-based Live/Dead assay was used for the simultaneous detection of viable and dead cells, giving an indication of both esterase activity and cell membrane integrity. At all ejection rates tested, over 97% of the cells were positive for the cell viability marker calcein AM (Figure 3.6A, lower right quadrant of dot plots), with no major differences in dead cell fractions for different flow rates. This correlates with the previous findings by microscopical examination (Figure 3.3). However, the sample ejected at 20 μL/min displayed a lower total number of events in comparison with all the other tested samples and control (Figure 3.6B).

Apoptosis was investigated by analysing the percentage of apoptotic cells using Annexin V/PI double staining. This method enables the detection of viable, apoptotic, and necrotic cell populations: Annexin V^-/PI^- cells were considered viable, Annexin V^+/PI^- as early apoptotic, Annexin V^+/PI^+ as late apoptotic, and Annexin V^-/PI^+ necrotic. After 48 hours of incubation, differences in percentages between the samples were apparent at the slower ejection rate used (Figure 3.6C). The proportion of apoptotic cells was higher in the samples ejected at slower ejection rates (6.22 ± 4.6% early apoptotic cells at 20 μL/min, versus 1.88 ± 1.7% at 300 μL/min). The results indicate that a significant loss of NIH 3T3 cell viability may still occur 48 hours post-injection, with the differences in apoptotic cell populations between the ejected samples and control being statistically significant at 20 μL/min using one-way ANOVA, with a Tukey–Kramer multiple comparisons test.

Figure 3.6D summarises flow cytometric analyses using Live/Dead staining for cell populations ejected at 150 μL/min. There was no visible difference in non-viable cell numbers with various needle sizes, with viable cells ranging between 98-99.2% of total cells analysed. However, 34G needles displayed a lower total number of events through the flow cytometer, which was hypothesised to occur due to cell lysis.

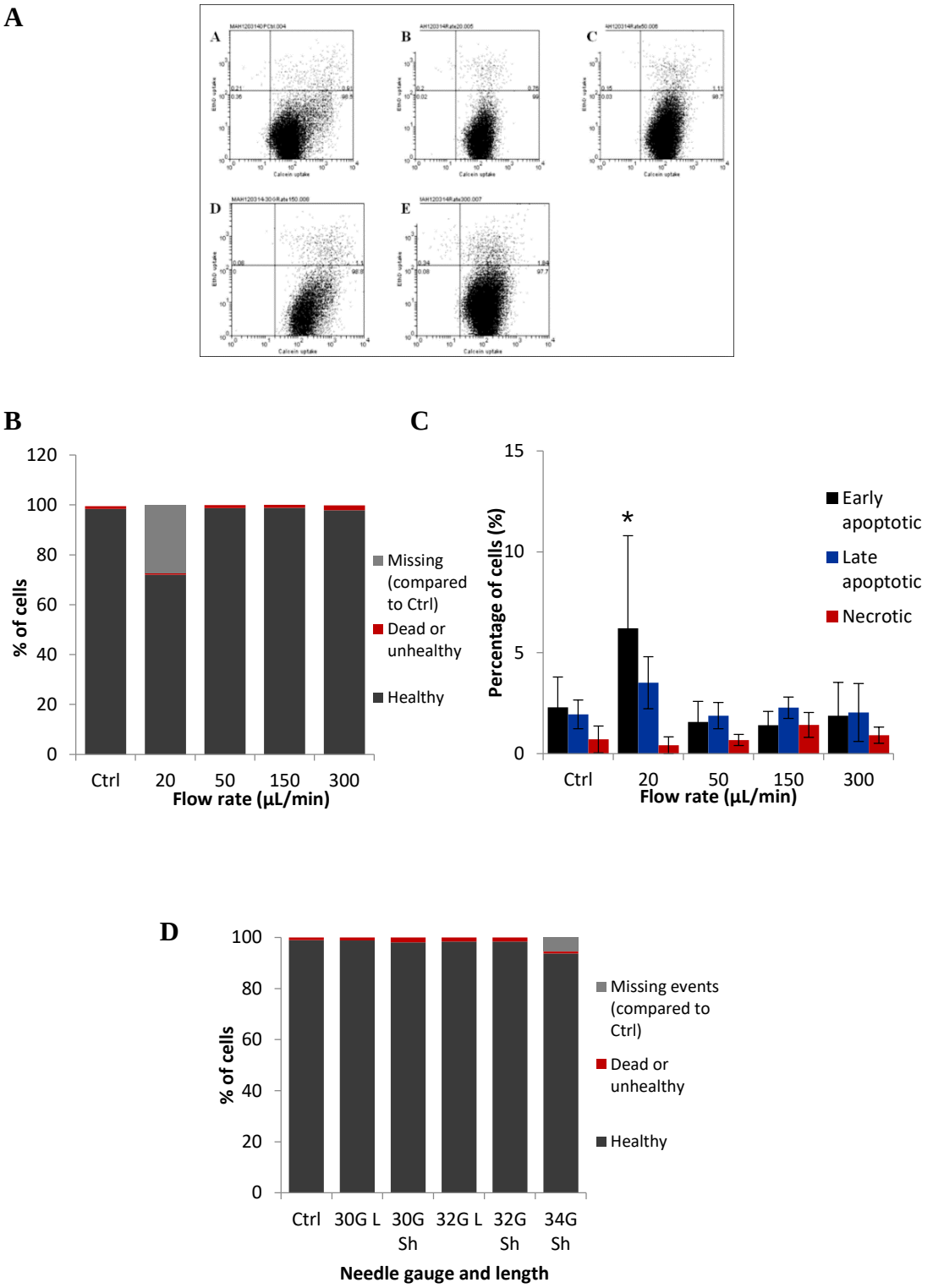

Figure 3.6: **Flow cytometric analysis of NIH 3T3 cells post-ejection.** (A) Flow cytometric dot plot quadrant analysis of NIH 3T3 cells, using Live/Dead stain, directly plated (*A*), or ejected at 20 (*B*) 50 (*C*), 150 (*D*) or 300 (*E*) µL/min. (B) Graph showing results of flow cytometric analysis of NIH 3T3 cells ejected at various flow rates, classified as healthy, dead/unhealthy, or missing events (compared to control). (C) Percentages of apoptotic and necrotic cells analysed 48 hrs post-ejection, by double labelling with Alexa Fluor® 488 Annexin V and PI. Mean values of five independent experiments are shown ± SD. Asterisk represents significant difference between samples and control using two-way ANOVA followed by Tukey's *post hoc* test ($p<0.05$) (D) Graph showing results of flow cytometric analysis of NIH 3T3 cells ejected using various needle gauges and lengths, classified as healthy, dead/unhealthy, or missing events (compared to control); Sh: Short (20mm); L: Long (51 mm).

3.3.4 **Effect of varying cell density**

Cell viability was analysed for cell suspensions of different densities ejected using a 30G needle at two flow rates to investigate possible effects of cell densities at both low and high ejection rates (20 and 150 μL/min).

With the exception of the highest cell density tested ($5x10^6$ cells/mL), which showed a higher percentage of dose delivered than other densities under investigation; there were no significant differences in cell delivery between the lower cell densities (Figure 3.7A). Flow cytometric analyses of samples of different cell densities ejected at 150 μL/min through a 30G needle showed no significant differences in viability (Figure 3.7B).

3.3.5 **Investigating cell fate at low ejection rates**

Further investigations were required to identify the reason behind the lower number of cells ejected at the slower ejection rates. For a more complete picture, the slower ejection rate of 10 μL/min was also assessed. After ejecting cells, each ejection was followed by 3x100 μL PBS washes at an ejection rate of 300 μL/min to dislodge any cells that may have adhered to the inner surface of the needle. Washes were pooled together, placed in 2 mL media in 6-well plates and assessed for the presence of viable cells.

Figure 3.8A shows cell numbers after ejection and for the following PBS washing step. A trend can be clearly observed, where the number of viable cells in PBS washes increases with slower ejection rates, indicating that the adhesive nature of this fibroblast cell line may be causing them to adhere to needle's inner surface at slower

ejection rates. In the case of smaller needle gauges, the number of NIH 3T3 cells in PBS washes was not substantial (Figure 3.8B), indicating that the lower number of events in 34G flow cytometry analyses was probably due to cell lysis (Figure 3.6).

A

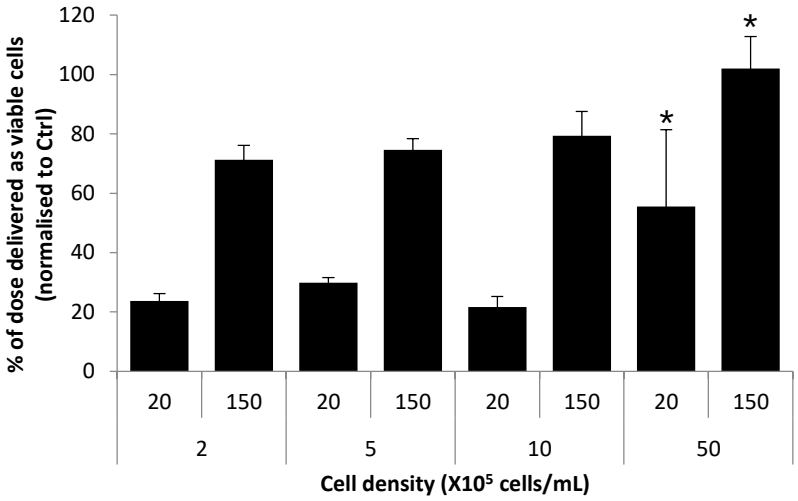

B

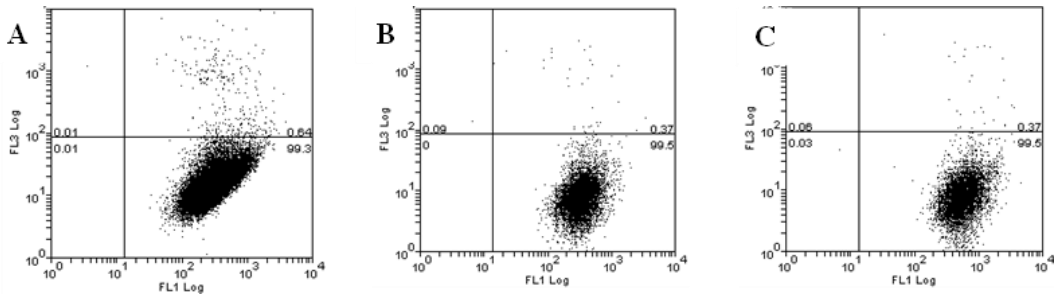

Figure 3.7: **Effect of varying cell density on cell delivery *in vitro*.** (A) Comparison of 6-hour viability of different cell densities of NIH 3T3 cells injected, using a 30G needle, at two different flow rates (20 and 150 μL/min); Results are mean ± SD% (n=3). Asterisks indicate statistically significant difference between ejected samples and 5x10^5 cells/mL (p<0.05) (B) Flow cytometric dot plot quadrant analysis of NIH-3T3 cells, using Live/Dead stain, of a cellular density of 5x10^5 (a) 1x10^6 (b) and 5x10^6 (c) cells/mL, ejected at 150 μL/min.

A

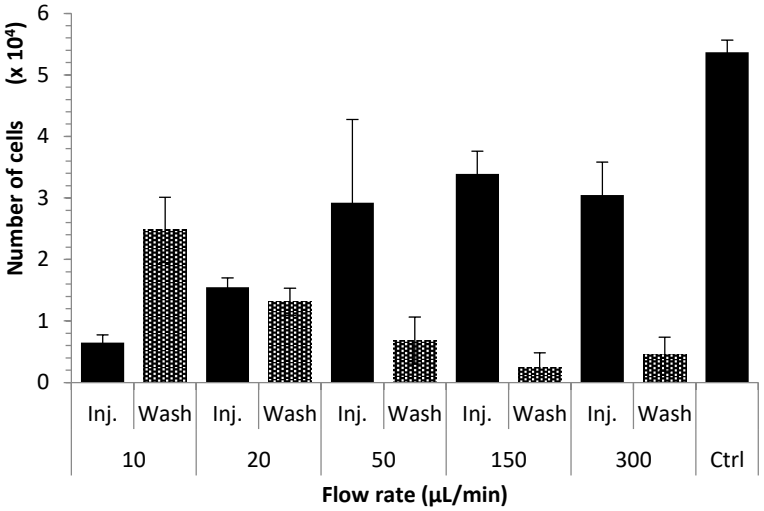

B

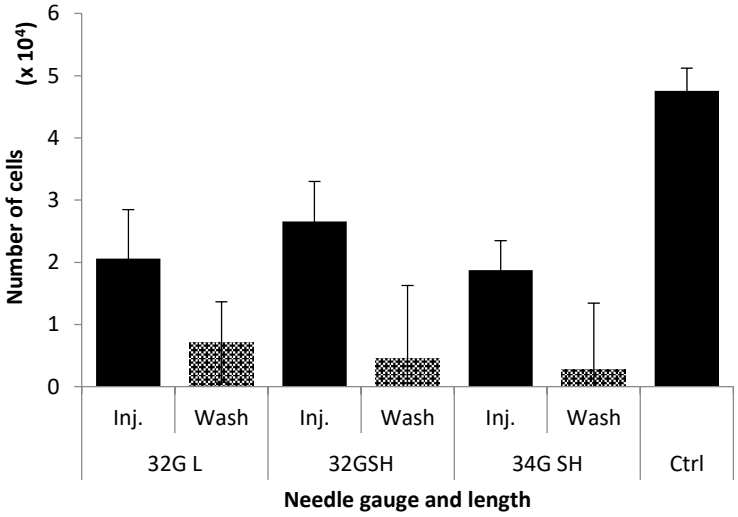

Figure 3.8: **Investigation of cell fate at low ejection rates**. (A) To investigate cell fate at low flow rates, each cell ejection was followed by needle washes (3X100 µL PBS ejected at 300 µL/min each), and the number of cells recovered was measured using PrestoBlue (mean ± SD, *n*=3). (B) Ejections through needles of various gauges and lengths were followed by washes using 3×100 µL of PBS ejected at 300 µL/min each, and the number of cells recovered was measured using PrestoBlue (mean ± SD).

3.3.6 **Assessing compound effects of ejection using a multiplex assay**

Multiplex assays are capable of measuring multiple parameters (cell viability, cytotoxicity and apoptosis) in a single well independent of cell number. This is desirable to help to provide normalised controls to overcome well-to-well variations in cell numbers.

Despite the high sensitivity of this assay, there was no statistically significant change in cytotoxicity or caspase-3/7 activity between the various ejection rates under investigation (Figure 3.9A & B). There were no significant differences in normalised cytotoxicity or caspase-3/7 activity measurements between samples ejected using 30- and 34G 20 mm needles and the directly pipetted control, with the exception of cytotoxicity in cells injected at 20 μL/min through 34G needles (Figure 3.9C). Apoptosis levels with decreasing needle bore size are presented in Figure 3.9D.

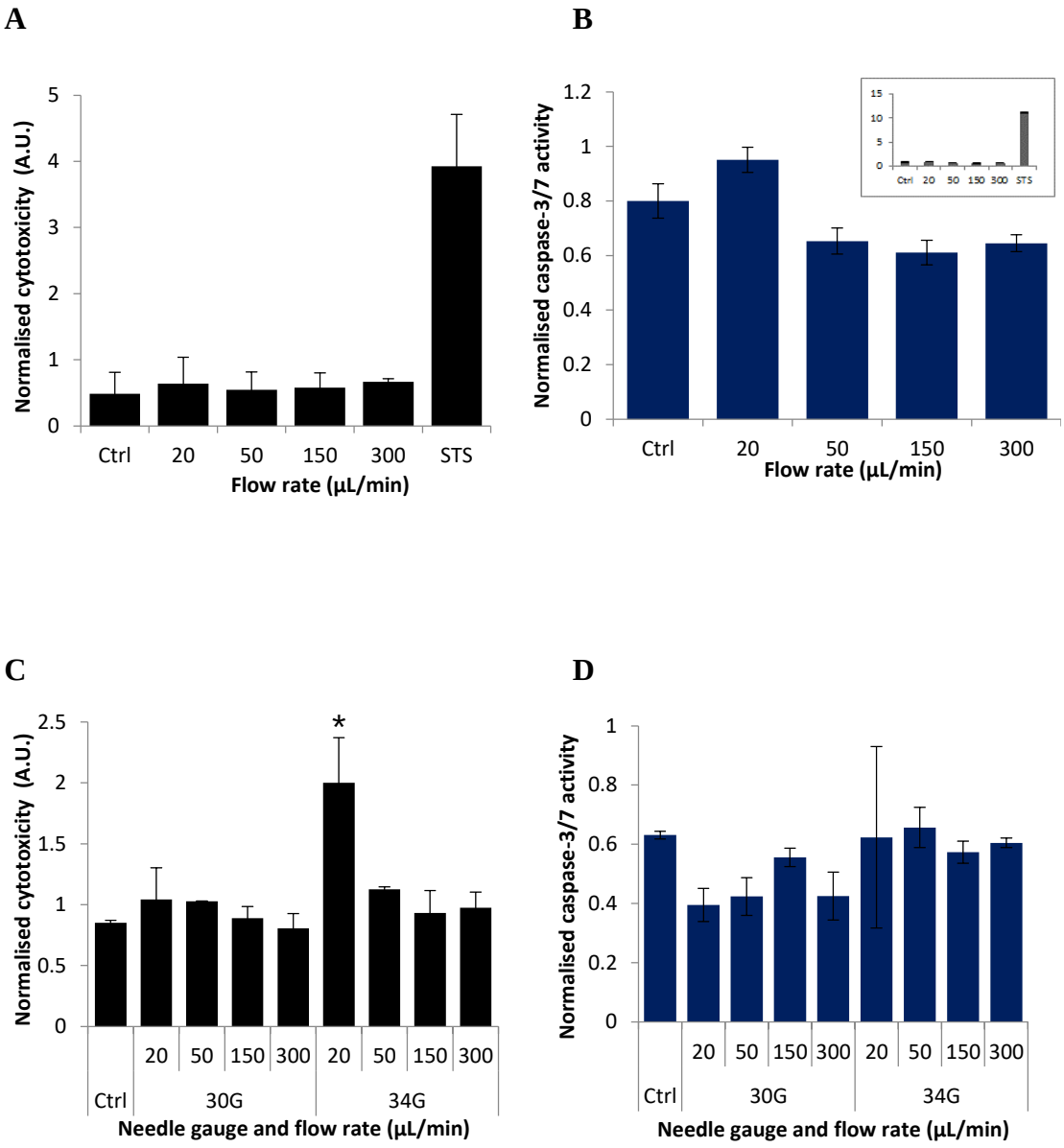

Figure 3.9: **Assessing cellular health of NIH 3T3 cells post-ejection using the multiplex ApoTox-Glo Triplex Assay.** (A) Cytotoxicity in NIH 3T3 cells 4 hrs post-injection. Cytotoxicity fluorescence at wavelengths 485_{exc} and 520_{em} were normalised to viability within the same well. (B) Caspase-3/7 activity luminescence was represented as normalised to viability in well-to-well normalisation. Staurosporine treatment (STS; 1µM) was used as a positive control, and the graph showing its effect is superimposed for clarity (n=3; mean ± SD) (C) Cytotoxicity in NIH 3T3 cells 4 hrs post-injection (analysed by ApoTox-Glo Triplex Assay). Cytotoxicity readings were normalised to viability within the same well. (D) Caspase-3/7 activity luminescence was represented as normalised to viability measurements. Asterisks represent significant difference between sample and control (p<0.05). (n=2; mean ± SD).

3.3.7 **Improving viability during needle flow using viscous carriers**

Since shear stress experienced during the cell ejection process may result in a decrease in proportion of viable cells delivered, it was hypothesised that co-injecting the cells with viscous carriers may improve viability. Solutions of 1% uncross-linked alginate, cross-linked alginate (1% w/v, 1:4 Ca^{2+} : alginate cross-linking ratio), and high viscosity CMC were used to test this hypothesis.

By incorporating the cells in a protective viscous medium, significantly improved cell delivery was demonstrated *in vitro* compared to cells ejected within PBS. Figure 3.10A shows significantly lower cell numbers delivered as viable cells using PBS and uncrosslinked alginate relative to the control. Suspending cells within cross-linked alginate hydrogels significantly improved the 6-hour viability of ejected cells to 95.6% ± 32.4%, while suspending in the viscous CMC carrier improved viability to 85.4% ± 9.10%. In contrast, uncrosslinked alginate did not provide any significant cell protection. The protective effects of the cross-linked alginate also resulted in an increased proliferation of the cells, with significantly higher cell numbers being present after three days of incubation (Figure 3.10B).

A

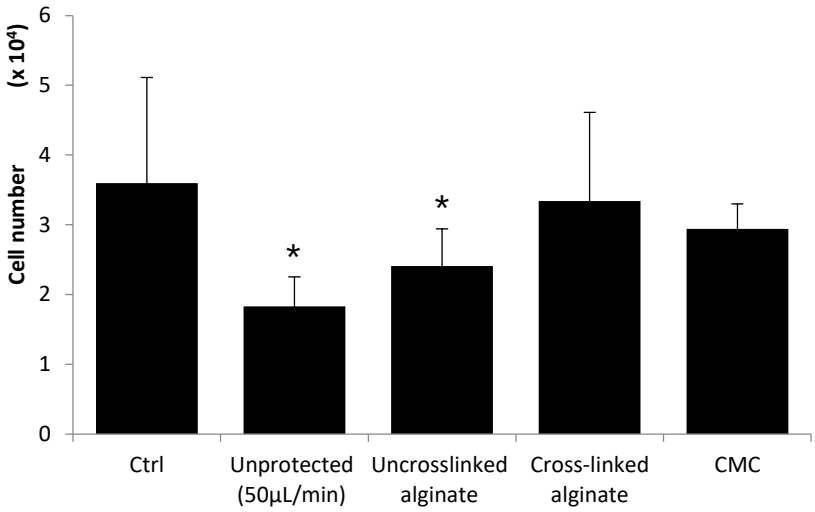

B

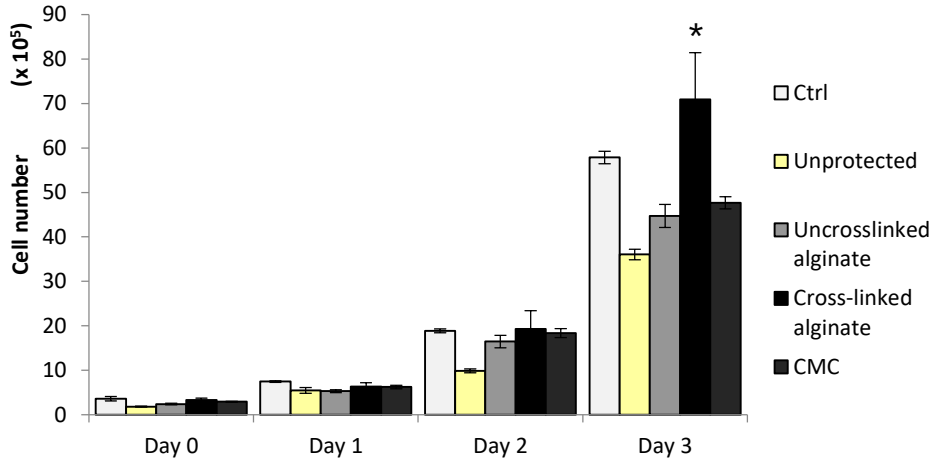

Figure 3.10: **Investigating the use of biomaterial-based delivery of NIH 3T3 cells to improve viability.** (A) To investigate the proportion of NIH 3T3 cells delivered within PBS, uncrosslinked 1% alginate solution, 1:4 cross-linked alginate gels and high viscosity CMC after ejection through a 30G syringe needle at 50 µL/min, normalised to directly-plated control (mean ± SD, n=3). Asterisks indicate significantly lower cell numbers delivered relative to the control. (B) Cell proliferation of NIH 3T3 cells when injected unprotected in PBS and in several carriers (n=3, mean values ± SD); Asterisks indicate statistically significant improvement in proliferation of ejected cells compared with the directly-plated control cells at 72 hours (p<0.05).

3.4 Discussion

The treatment potential of cellular therapies depends on the viability and functionality of cells post-injection. Presently, limited data exists regarding factors vital for the survival of cells during and following ejection via narrow-bore needles at clinically relevant ejection rates. This study demonstrates the effects of administration stresses on NIH 3T3 cells, a widely used model in cellular biology. This study highlights potential parameters, such the use of optimum ejection rates, different needle sizes and the nature of injected cells, required to deliver the high viable cell number needed for cell therapy applications.

The effects of injectable delivery on NIH 3T3 cells were quantified in terms of immediate and 24-hour viability, apoptosis and other parameters of cellular health. The PrestoBlue™ assay measured viability in terms of cell numbers acquired relative to a directly pipetted control. Following manipulation within a syringe, the percentage of NIH 3T3 cells delivered as viable cells was not directly proportional to ejection rate as was expected, with cells ejected at 150 μL/min demonstrating a higher percentage of cells delivered than those ejected at other rates. This may be due to striking an optimal balance between the magnitude of shear stress exerted and the time period exposed to mechanical forces within the delivery device. These viability findings were in agreement with results obtained from counting cells with the trypan blue exclusion test, where slower ejection rates resulted in the ejection of a lower total number of cells. Flow cytometric analyses measured the actual proportions of dead cells which came out of the needle within samples under investigation. LIVE/DEAD analyses demonstrated that cells obtained by ejecting through 30G needles at all ejection rates were not discernibly impacted in terms of membrane integrity. The improved

proliferation after 72 hours of injection may be due to cellular repair mechanisms being activated, which suggests that cell recovery is possible in a favourable environment. In addition, cells may have undergone exponential growth by this time point.

Needle gauge and length also have a significant effect on cell viability post-injection. A lower percentage of cell dose delivered as viable cells was observed with increasing needle length and decreasing needle diameter. This can be explained by the mechanical forces to which cells are exposed as they flow through the needle: cells are exposed to shear and extensional forces for a longer period of time in longer needles, while smaller needle diameters will result in higher force magnitudes.

No significant difference in caspase-3/7 protein levels, an early regulatory event in apoptosis, occurred upon cell injection. The multiplex assay used confirmed that the ejection rates under investigation did not significantly increase NIH 3T3 cytotoxicity or apoptosis levels at the tested time point. Even upon decreasing needle bore diameter, no significant increase in caspase-3/7 levels was observed (Figure 3.9). Forty-eight hours post-ejection, more visible differences between ejection rates under investigation became apparent with Annexin V/PI staining. Since the lowest ejection rates were translated into a significant increase in apoptotic cell proportions (Figure 3.6C), this confirms the hypothesis that a balance is needed between the magnitude of mechanical forces exerted on the cells and the time spent exposed to these forces. NIH 3T3 cells are also known to be quite resistant to the induction of apoptosis [201], which may explain the non-significant difference in caspase activity despite decreasing needle gauge or increasing ejection rate.

Since apoptosis and cytotoxicity results did not fully explain the significant differences in the percentages of doses delivered as viable cells, PBS washes were made to investigate the possibility of cells adhering to the inner walls of the needle, since cells used in this work are anchorage-dependent. Results show that the cells were retained in the dead space of the syringe and on the inner walls of the needle, and were only dislodged by PBS washes at a flow rate of 300 μL/min. NIH 3T3 cells adhesive properties are well known and have been studied previously [202, 203]. These results highlight the importance of tailoring cell delivery systems to the nature of the transplanted cells.

It was hypothesised that increasing cell concentration may increase shear forces, resulting in more cell death. On the contrary, increasing NIH 3T3 cell concentration caused a significant improvement in viability at the highest cell density under investigation. It was observed that significant cell clumping occurred at cell densities higher than $5x10^6$ cells/mL, which did not allow for reproducible experimentation. The clumping that occurred at this density, whilst not being substantial enough to cause experimental problems, may have exerted a protective action on the cells. This agrees with previous findings regarding cell aggregation [204].

Preliminary viability studies carried out on the use of hydrogels and viscosity-modifying excipients for cellular delivery demonstrated the protective effects of shear-thinning alginate hydrogels on cells undergoing needle flow. Cross-linked hydrogels have been reported to undergo plug flow [87]. The hydrogel adjacent to the walls undergoes shear thinning to form a fluid layer that acts as a lubricant. This lubricating fluid layer and plug flow behaviour may be the mechanisms by which an increased proportion of the cells are delivered, reducing the detrimental effects of shear and

extensional forces as well as retention of the cells in the delivery device. A similar result was previously obtained by Aguado *et al.* with 28G needles and 1mL syringe [74]. This work confirms that the protective action of co-delivery with alginate gels is also applicable to the adverse effects induced by injection flow in microsyringes and smaller needle sizes. This may be vital to high accuracy applications and cells that may display biological changes after exposure to mechanical forces. Such delivery strategies have promising applications for the clinical translation of cell therapy in high accuracy regenerative medicine applications.

3.5 Conclusions

In contrast to previous studies, which have focused on viability as the chief indicator of cellular response to ejection through needle-based devices (Chapter 1), this work assesses an extensive range of viability and cellular health indicators *in vitro* to elucidate cellular response to the ejection procedure.

In summary,

- Ejections at 150 µL/min resulted in the highest percentage of the cell dose being delivered as viable cells among ejection rates tested.
- The difference in proportions of apoptotic cells became apparent 48 hours after ejection, with these proportions being higher in samples ejected at slower rates.
- Co-delivery of NIH 3T3 cells with viscous carriers demonstrated a protective action on the cell payload.

The use of a comprehensive set of tools in this study for the assessment of cell delivery post-ejection will allow clinicians to make informed judgements regarding the most suitable administration and formulation requirements for cell therapy clinical trials.

This will also help answer critical questions regarding possible reasons for failure to deliver sufficient numbers of viable cells.

This work demonstrates the effects of manipulation of NIH 3T3 cells using various needle gauge sizes and lengths, cell densities and ejection rates through a needle-based delivery device. Early loss of injected cells may be due to a combination of cell disruption by mechanical forces exerted during the ejection process, and cell retention in the needle or the syringe's dead space. The higher proportion of apoptotic cells appearing 48 hours post-ejection suggests that the ejection process may also induce delayed death through induction of apoptosis. Co-delivery with viscosity-modifying excipients demonstrated a protective action on cell payload. Therefore, this study demonstrates the importance of careful consideration of the administration protocol of cell suspensions and the optimisation of delivery parameters according to the nature and cellular responses of cells post-ejection.

Chapter 4| A detailed assessment of the effects of ejection using narrow bore needles on hMSCs

A research article based on the work described in this chapter has been published in *Stem Cells Translational Medicine* [100].

4.1 Introduction

Mesenchymal stem cells (MSCs) have been the focus of numerous pre-clinical and clinical studies, affording promise in the treatment of various conditions using cell therapy [142, 205, 206]. MSCs have been investigated to regenerate damaged tissue resulting from brain and spinal cord injury, myocardial infarction, diabetes, stroke, and bone injuries [207].

MSCs have demonstrated valuable therapeutic potential due to their relatively convenient isolation, multi-lineage differentiation potential [208], and ability to promote vascularisation [209]. However, a major barrier to the implementation of MSC therapy is achieving the required cell dose at the injection site [190]. Early cell loss has been observed within the first minutes of implantation [24], with one study quantifying immediate post-injection cell survival at 60% [26] and another stating that only 44.8% of cells survived 10 minutes after implantation [210].

In an attempt to improve the number of cells that are successfully delivered to the target site, typical doses used in clinical trials comprise up to hundreds of millions of MSCs [190]. However, no agreement exists regarding the optimal cell number to be

transplanted, although this is likely to vary depending on cell type and treatment. One of the main translational challenges of cell therapy is the need to determine and achieve suitable delivery protocols of the administered cell dose [211]. An enhanced understanding of what happens to hMSC-based therapeutics post-injection, specifically with regard to vital cellular health parameters, will facilitate the development of more efficient administration and formulation approaches in order to achieve higher efficacy and reduce variability.

4.2 Experimental design

Following on from the previous chapter, a broad toolset was used for the assessment of cell delivery and health post-ejection. This was carried out by exploring different aspects of administration of primary human MSCs after ejection from clinically relevant, narrow-bore needles. The delivery devices used for this study are 30- and 34G 20mm needles attached to 100 µL Hamilton syringes.

4.3 Results

4.3.1. Cell size measurement

Cells from the three different donors at passage 5 were measured in triplicates. Based on Coulter Counter measurements, cells used in this study had a mean size of 22.57±1.34 µm and median size of 21.29±1.02 µm (Figure 4.1).

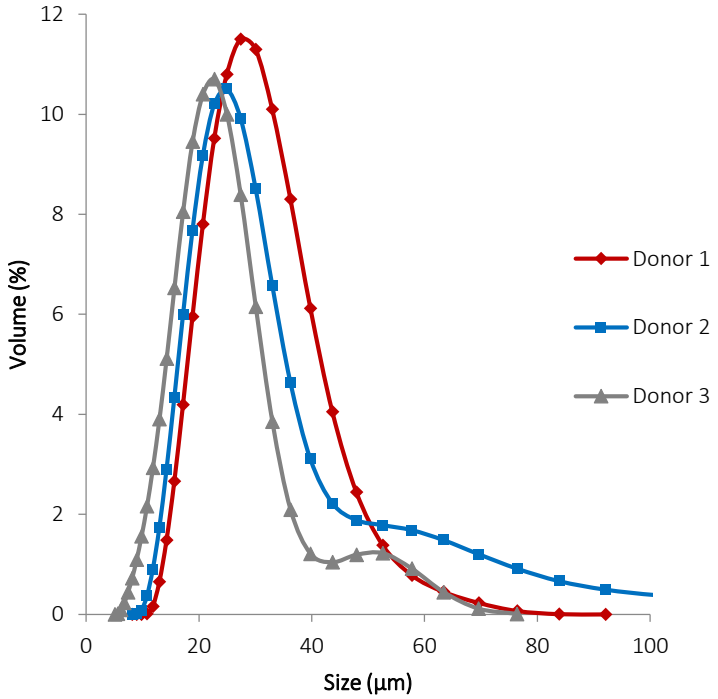

Figure 4.1: **Size distribution, expressed as volume %, of hMSCs at passage 5**. This was determined using a Coulter LS230 particle size analyser and plotted as a function of the percentage of distribution volume.

4.3.2. Effect of varying ejection rates on viability and percentage recovery of dose delivered

Figure 4.2A shows mean cell numbers quantified 24 hours after ejection of cell suspensions (prepared from three individual donors) through 30G needles, measured using the CyQUANT assay. Percentage of dose delivered was significantly lower than the control value of directly pipetted cells at all flow rates tested ($p \leq 0.01$). In all donors tested, cells ejected at 300 μL/min showed the highest percentage cell dose delivered at 77.6 ± 11.7%. PrestoBlue was used to measure percentage of the dose delivered as viable cells 24 hours post-ejection to confirm these findings (Figure 4.2B).

Figure 4.2C shows the proliferation of hMSCs from one donor, given as fold change in number from day 0 of each sample, measured using PrestoBlue. The proliferative ability of hMSCs at Day 10 was not significantly affected following ejection.

All ejected cells attached to culture surfaces within three hours of ejection, and displayed typical fibroblast-like morphology. Live/Dead staining kit, which relies on esterase activity of living cells (green fluorescence) and compromised membranes of dead cells (red fluorescence), was used to assess viability within cells ejected. The proportion of viable cells was high among the flow rates tested (Figure 4.2D & E). However, a visibly lower number of cells appeared in ejected samples, particularly at 10 μL/min, suggesting cell loss during ejection and endorsing the results acquired using CyQuant and PrestoBlue assays.

Figure 4.2E presents the flow cytometric analysis, which revealed a viability of >97% at all flow rates under investigation.

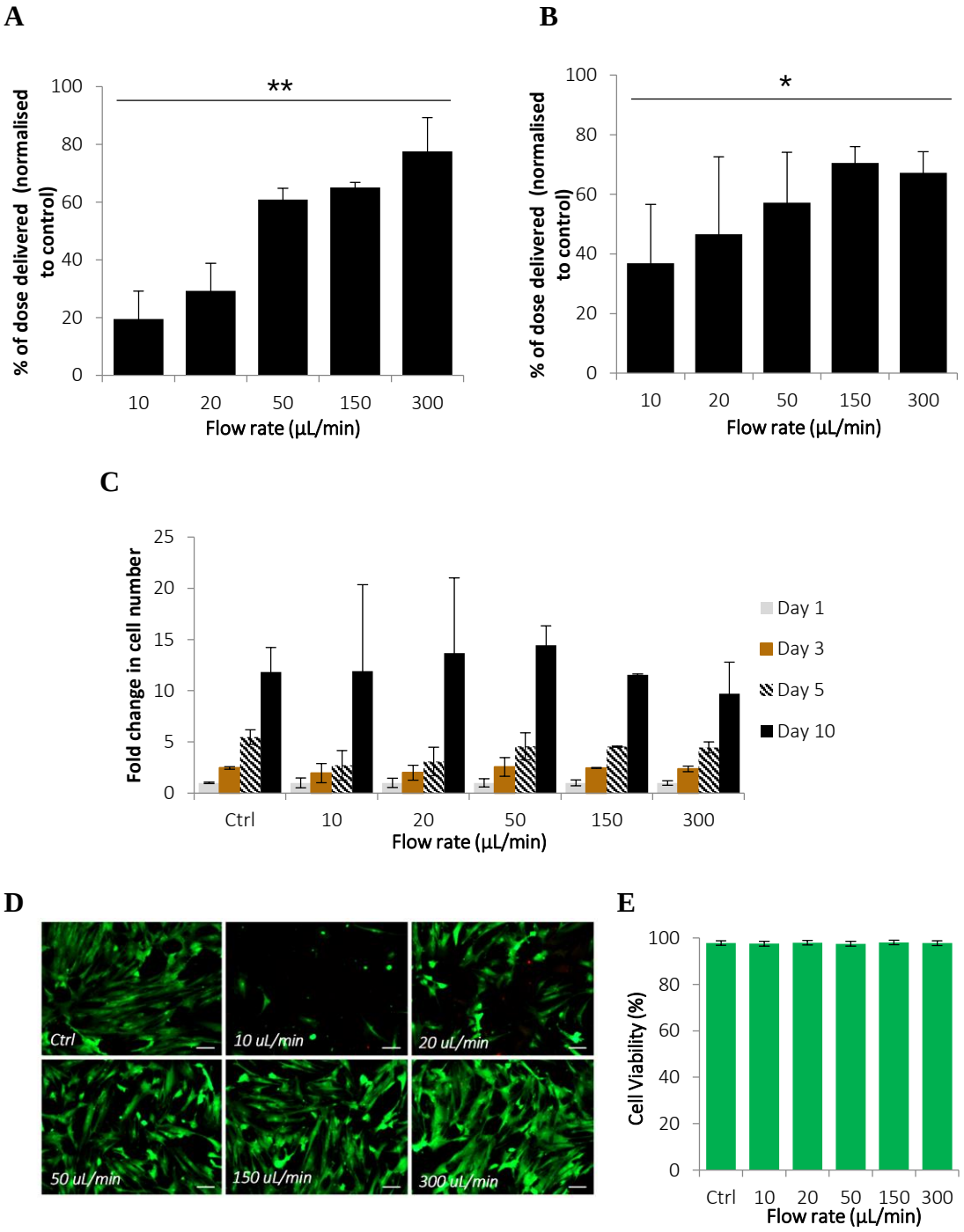

Figure 4.2: **Viability of hMSCs and percentage of cell dose delivered via 30G needles.** (A) Percentage of hMSCs delivered, determined using CyQUANT, 24 hrs post-ejection through a 30G 20mm needle. Data were normalised against control. Data represents averages from three donors (*n*=5 each) in five independent experiments (mean ± SD); Asterisk indicates statistical significance between number of ejected cells compared with control (**$p \leq 0.01$ - one-way ANOVA with Dunnett's *post-hoc*). (B) Percentage of hMSCs delivered as viable cells, measured using PrestoBlue, 24 hrs following ejection (mean ± SD). Data is combined from three independent donors (*n*=3 each), each measured in triplicate (*$p \leq 0.05$; one-way ANOVA with Dunnett's *post-hoc*). (C) Graph showing proliferation of hMSCs, given as fold change in number from day 0 of each sample, measured using PrestoBlue (mean ± SD; *n*=3, measured in triplicate) (D) Representative Live/Dead-stained fluorescence images of hMSCs 48 hrs following ejection (Scale bar=50 µm). (E) Graph shows flow cytometric analysis of ejected hMSCs (*n*=3), illustrating high viable cell proportions at all flow rates under investigation.

4.3.3. Effects of varying ejection rates on various markers of cellular health

To overcome well-to-well variations in cell numbers ejected with different ejection rates, ApoTox-Glo Triplex Assay was used to measure cytotoxicity and apoptosis. Measurements were normalised to viability within the same well. There were statistically significant increases in cytotoxicity ($p \leq 0.05$) and caspase-3/7 activity levels ($p \leq 0.0001$) in both donor samples ejected at 10 µL/min through 30G 20mm needles, compared to the directly pipetted control 4 hours post-ejection (Figure 4.3A).

Apoptosis was also assessed using Annexin V/PI. Annexin V^-/PI^- cells were considered viable, Annexin V^+/PI^- early apoptotic, Annexin V^+/PI^+ late apoptotic, and Annexin V^-/PI^+ as necrotic. After 24 hours, differences between samples were evident at the slower ejection rates employed (Figure 4.3B). The proportion of apoptotic cells was significantly higher in the samples ejected at slower flow rates, with 7.12 ± 2.2% early apoptotic cells at 10 µL/min versus 4.93 ± 1.1% in control samples. A trend of increasing necrotic cell proportions with increased ejection rates was also observed. The results indicate that loss of hMSC viability may still arise 24 hours post-injection, with the increase in apoptotic cell populations in the ejected samples being statistically significant relative to the control at lower ejection rates.

Senescence-associated pH6 β-galactosidase (SA-β-Gal) was used to investigate whether cells undergo senescence due to the injection process. Figure 4.3C shows the quantification of stained SA-β-gal-positive cells observed after ejection, with no statistical difference in senescence with increasing ejection rates in cells derived from two donors.

To assess the influence of ejection rate on the adhesion capacity of hMSCs, the numbers of adherent cells were determined by the CyQUANT NF Cell Proliferation Assay Kit 120 mins post-ejection, after gently washing twice with PBS. Adherent cell density was stated as fold difference relative to the control plate. Cell adhesion in test samples was not significantly different to control samples (Figure 4.3D).

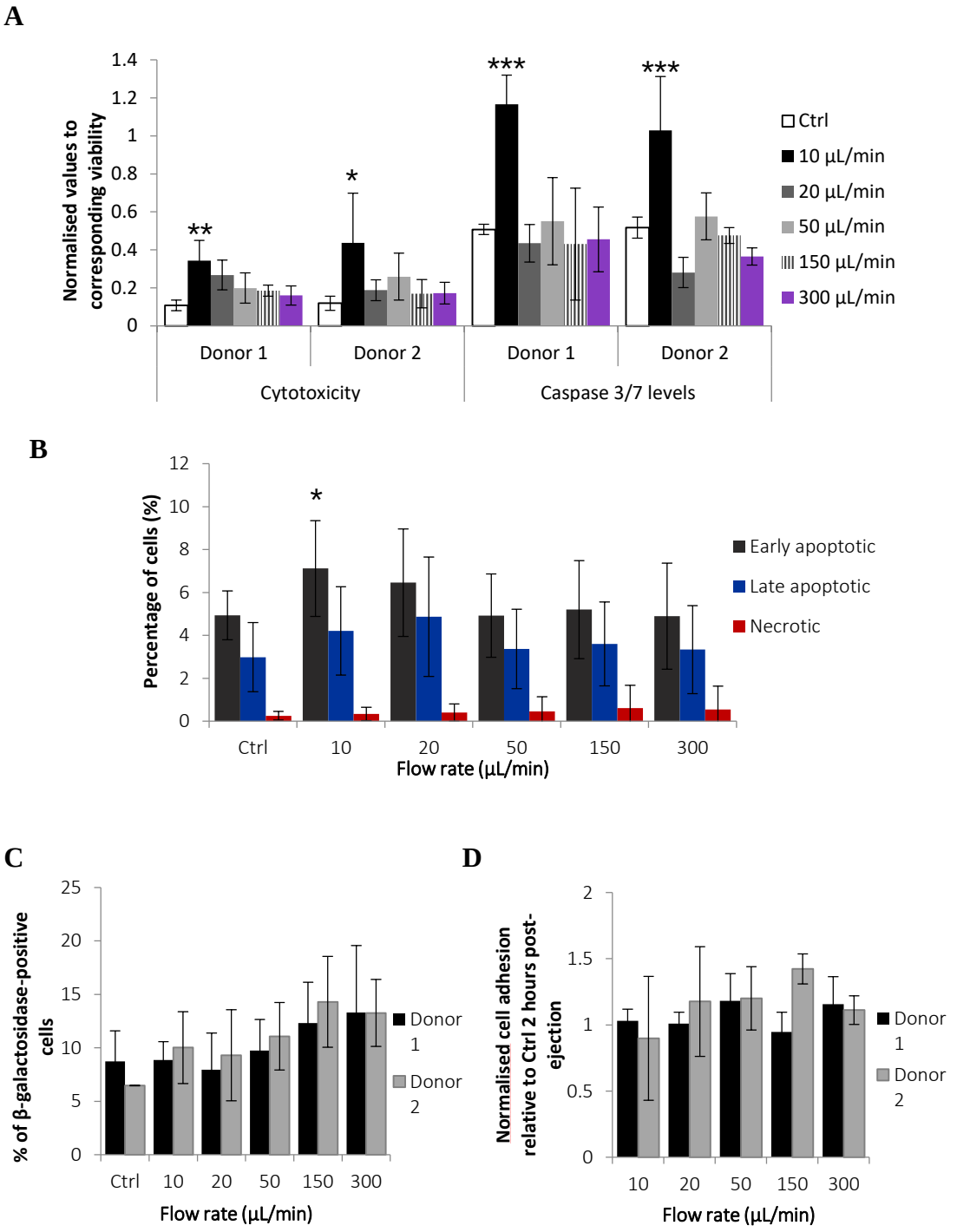

Figure 4.3: **Various parameters of cellular health assessed in hMSCs ejected via 30G needles**. (A) Cytotoxicity and apoptosis measurements in hMSCs from two donors 4 hrs post-ejection, analysed by ApoTox-Glo Triplex Assay. Measurements were normalised to viability within the same well (n=5; mean ± SD; two-way ANOVA and Dunnett's *post-hoc*; *$p \leq 0.05$; **$p \leq 0.01$; ***$p \leq 0.0001$). (B) Percentages of apoptotic and necrotic cells 24 hrs post-ejection, measured using Alexa Fluor® 488 Annexin V/PI (3 donors in six independent experiments; n=15). Asterisks represent significant difference between samples and control using ANOVA with Dunnett's *post-hoc* (*$p \leq 0.05$). (C) SA-β-galactosidase assay was performed 3 days post-ejection (mean ± SD; 2 donors, n=3 each). (D) Adhesion capacity of hMSCs after incubation of control and ejected hMSCs for 120 mins. Adhesion capacity is shown as fold difference relative to total cell numbers in centrifuged control plate. Data from two donors shown as mean ± SD (n=5 each); *Ctrl*: control.

4.3.4. Immunophenotyping

Following observations of apoptosis and senescence, it was deemed necessary to determine whether ejection rate could also cause changes in expression of cell surface markers 24 hours post-ejection. Flow cytometry-based immunophenotyping was carried out to measure surface markers as recommended by ISCT [212].

Analysis showed that mesenchymal surface markers CD73, CD90 and CD105 were highly expressed (>95%) in all control samples, whereas the markers CD11b, CD19, CD45, HLA-DR and CD34 were negative (<1%). There was a statistically significant downregulation of expression of CD105 (Table 4.1) in both donor samples (93.2 ± 0.6% and 93.5 ± 1.2%) at the slowest flow rate under investigation relative to controls ($p \leq 0.05$).

Table 4.1**: Immunophenotypic characteristics of hMSCs in control and samples ejected through 30G needles by multi-colour flow cytometry 24 hours post-ejection**. Data is % of positive cells ± SD (n=6 using cells from two independent donors). Asterisks represent significant difference to the control sample using one-way ANOVA followed by Dunnett's multiple comparisons test (* $p \leq 0.05$).

Marker	**Average % of positive cells ± SD**					
	Control	**10 µL/min**	**20 µL/min**	**50 µL/min**	**150 µL/min**	**300 µL/min**
CD90	99.3±0.45	98.5±1.26	99.3±0.44	99.6±0.15	99.5±0.35	99.5±0.18
CD105	95.4±0.50	***93.3±0.85****	94.3±2.18	96.1±0.76	95.8±0.98	95.7±1.25
CD73	99.0±0.73	97.9±1.73	98.9±0.61	99.2±0.45	99.2±0.55	99.2±0.33
Negative markers	0.21±0.24	0.18±0.13	0.98±2.0	0.15±0.11	0.11±0.093	0.15±0.17

4.3.5. Effects of varying needle gauge

Smaller needles are essential clinically for high accuracy applications in order to reduce physical damage, especially for retinal or neural regenerative applications. To explore cell viability and recovery following ejection through smaller needle sizes, hMSCs were ejected through 34G 20mm needles at all the flow rates under investigation. Cells ejected through both 30G and 34G 20mm needles exhibited the same trend of percentage cell recovery with flow rates tested, with cells ejected via 34G needles at 300 μL/min displaying the greatest cell recovery of 64.4 ± 16.3%. However, the use of 34G needles resulted in a larger reduction in the percentage of cell dose delivered (Figure 4.4A) compared with the 30G needle at all rates under investigation. Microscopic examination of ejected cells stained with Live/Dead staining solution exhibited a high percentage of cells positive for calcein AM (Figure 4.4B).

Figure 4.4C shows the apoptotic and necrotic cell fractions in cell samples from three donors ejected via 34G needles, across all flow rates after 24 hours of incubation. A trend towards increased apoptosis was observed with this smaller needle diameter. Additionally, a significant increase in early apoptotic cell proportions was observed with the highest flow rate under investigation as well as the slowest flow rate ($p<0.05$), unlike the results previously observed with the larger needle gauge (Figure 4.3B). Shear forces exerted on the cells ejected through 34G needles at the lowest flow rate under investigation are higher than those calculated for all flow rates with a 30G needle (Appendix 1). This suggests that there may be an optimum flow rate that balances the exerted mechanical forces with the time spent exposed to these forces. The high

variability of apoptotic cell proportions in the case of 34G needles is possibly attributable to uneven injection flow due to its extremely small diameter (51 μm).

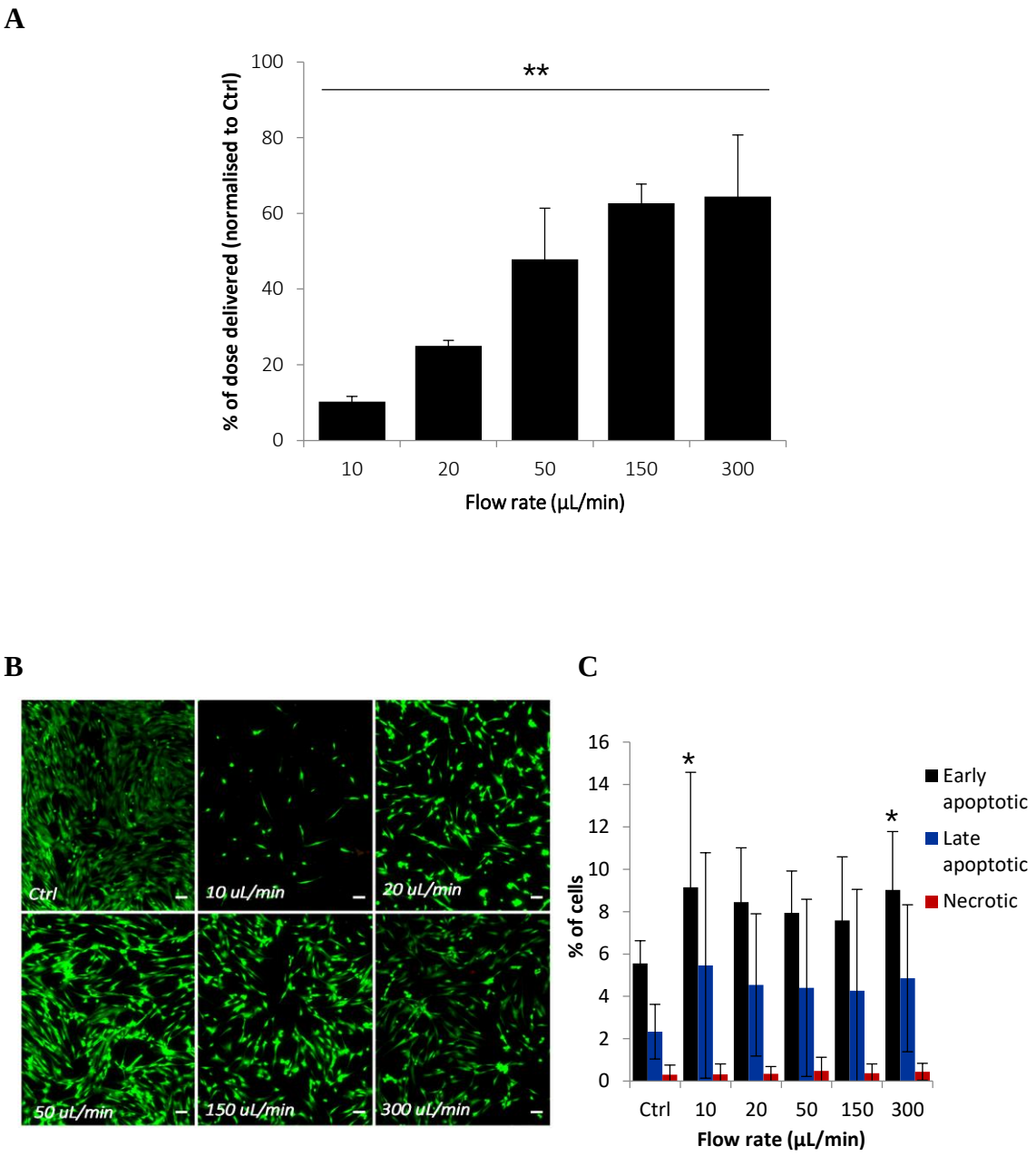

Figure 4.4: **Viability and apoptosis levels of hMSCs delivered via 34G needles.** (A) Percentage of hMSCs delivered, measured using CyQuant, 24hrs post-ejection via 34G 20mm needles. Results are normalised mean values to control ± SD (averages from 2 donors and two independent experiments, each *n*=5). Asterisks indicate statistically significant difference between control and ejected samples using one-way ANOVA (**$p \leq 0.01$). (B) Representative fluorescence images depicting Live/Dead-stained hMSCs ejected at several flow rates 48 hrs post-ejection (Scale bar=100 µm). (C) Mean percentages (± SD) of apoptotic and necrotic cells 24 hrs post-injection via 34G needles, measured using Alexa Fluor® 488 Annexin V/PI (3 donors in five independent experiments; *n*=11). Asterisk denotes significant difference between samples and control using ANOVA and Dunnett's *post-hoc* test (* $p \leq 0.05$).

4.3.6. Tri-lineage differentiation potential of ejected hMSCs

The ability of hMSCs to differentiate into multiple lineages is a functional criterion defining them [212]. Figure 4.5 is representative of results obtained with cells from at least two donors (*n*=5 each), and shows that all control and ejected samples completed multi-lineage differentiation. After 21 days of induction towards an adipogenic lineage, a distinctive morphological change with appearance of lipid vacuoles was observed. Osteogenesis was assessed by staining for calcium and phosphate after 21 days of culture under osteogenic conditions, with all samples exhibiting positive staining with alizarin red and von Kossa stains. Additionally, all cells retained chondrogenic differentiation capacity, as shown by positive staining using Alcian blue. All hMSCs showed similar differentiation patterns. However, there was an observable difference in both the number of cells at day 21 and the extent of both adipogenic and osteogenic differentiation in the samples ejected at 10 μL/min.

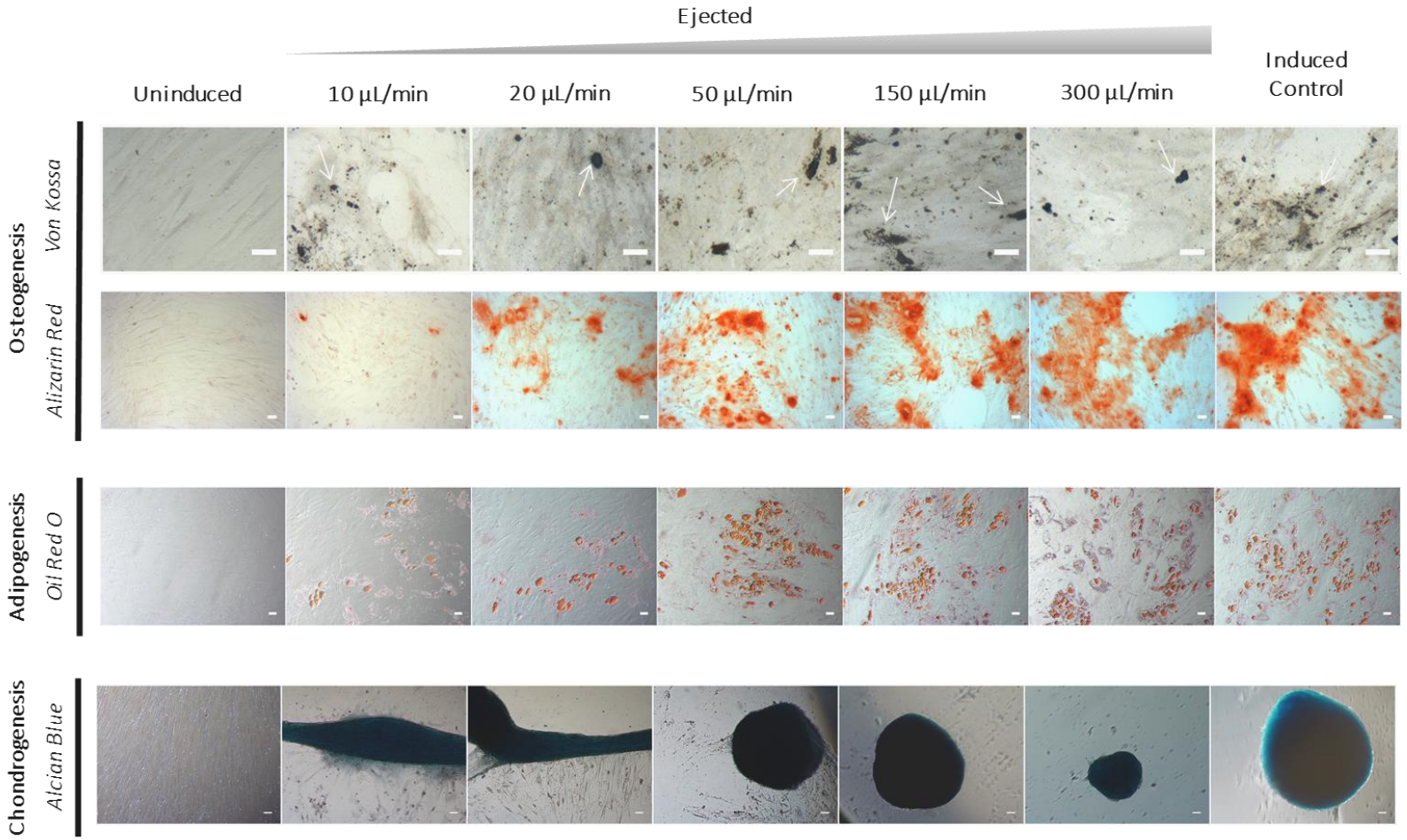

Figure 4.5: **Trilineage differentiation potential of cultured hMSCs ejected via 30G needles.** To verify the differentiation capacity of ejected hMSCs via 30G needles, adipogenic, osteogenic and chondrogenic differentiation was carried out on ejected and control samples following 21 days of differentiation. Adipogenic differentiation was assessed by Oil Red O staining. Osteogenic differentiation was assessed by Alizarin Red staining of calcified matrix and von Kossa stain. Phase-contrast microscopy of micro-mass cultures shows differentiation down the chondrocyte lineage, as confirmed by Alcian Blue staining (Scale bar=50µm). Cells cultured in MSGCM without induction served as negative control.

4.3.7. Investigating low cell recovery at slow ejection rates

Additional investigations were undertaken to explore potential reasons behind the smaller cell numbers ejected at lower ejection rates. Each ejection was followed by 5x100 µL PBS washes at 300 µL/min to dislodge cells that may have transiently adhered to the inner surfaces of the syringe or needle. Washes were combined, and cell numbers measured using PrestoBlue.

Figure 4.6A shows cell numbers of the directly plated controls, ejected samples, and those quantified in the succeeding PBS washes. A trend can be clearly detected, where the number of viable cells in the PBS washes is increased at lower flow rates, signifying that the adhesive nature of hMSCs may be causing them to adhere to the delivery device at the lower flow rates. Cells could also be observed visibly aggregating in the syringe barrel as the plunger advanced during PBS washes post-ejection at the slowest flow rates (Figure 4.6B), and can also be microscopically visualised in the syringe post-ejection before PBS washes (Figure 4.6C).

To explore whether cells were preferentially retained in the syringe or needle, components of the delivery device (syringe barrel and needle) were separated following ejection of cell suspensions at 10 µL/min, and each was then re-attached to a corresponding clean syringe or needle. These were then flushed with 100 µL of PBS three times to dislodge any retained cells, and washes were assessed for viable cells using PrestoBlue. Most of the cells were retained in the syringe (21.5 ± 9.45%) relative to 5.6 ± 6.35% (mean ± SD %) retained in the needle (Figure 4.7A).

To investigate whether ten minutes in the delivery device (in the case of 10 µL/min samples) would account for the loss in cell dose delivered, cells suspensions with

different densities ($7x10^5$ and $1.5x10^5$ cells/mL) were seeded into well-plates with glass bottom (made of borosilicate glass to simulate the Hamilton syringe), and incubated for ten minutes at room temperature. A comparison was then made between wells where the cell suspensions were removed and the ones that were gently rinsed with gentle washes of PBS after removal of cell suspensions. Fluorescence readings were normalised to control wells. After ten minutes of incubation, almost 55% of the cells seeded adhered to the surface following removal of the suspension from the wells. Gentle washes resulted in 26.9% of cells still being retained in the wells with high density suspensions, and 10.7% of cells being retained in the low density suspensions under investigation (Figure 4.7B).

Moreover, a comparison of cell dose delivery between apoptotic *vs* viable cells at 10 µL/min was carried out (n=4) using cells from two different donors. Apoptosis was induced in hMSCs using 10 µM staurosporine, which was shown by Annexin V/PI staining (Figure 4.7C) to result in an apoptotic population of 89.95 ± 2.14% (mean ± SD, n=4) in comparison with 7.58 ± 1.85% (mean ± SD, n=4) apoptotic cells in normal, viable populations. Results obtained are displayed in Figure 4.7D. At an ejection rate of 10 µL/min, 8.89 ± 3.98% of the viable cell dose was ejected, in comparison to 28.8 ± 15.30% (mean ± SD) of the apoptotic cell dose ejected at the same rate (p<0.05, Mann-Whitney test).

A

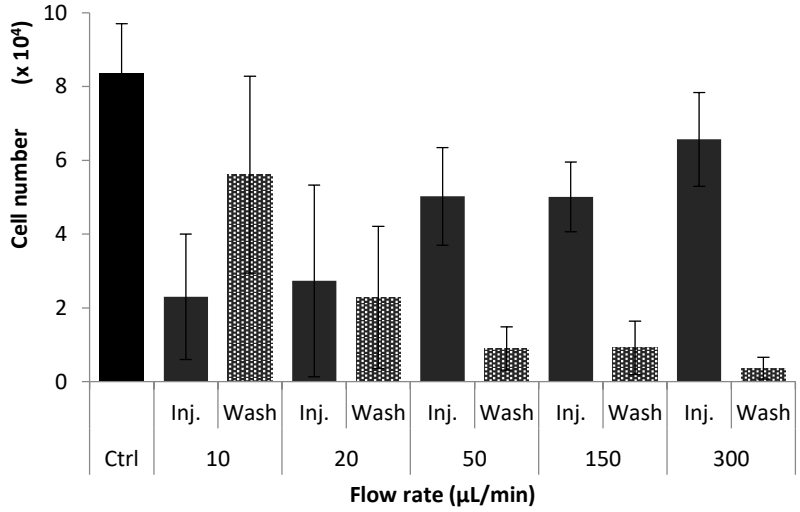

B

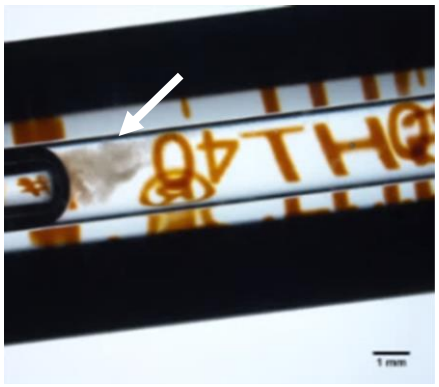

C

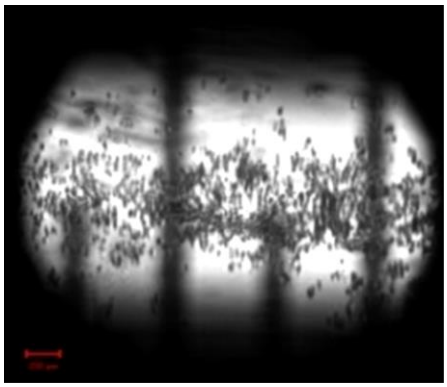

Figure 4.6: **Investigation of cell recovery and retention in the delivery device following ejection via 30G needles.** (A) To investigate poor cell recovery at slow flow rates, each ejection was followed by PBS washes (5×100 µL at 300 µL/min), and number of cells recovered was quantified using PrestoBlue (mean ± SD, 2 donors, each *n*=3). (B) A representative dissection microscope image of a syringe barrel post-ejection at 10 µL/min, depicting cells that have been retained in the syringe aggregating during PBS wash following ejection (Scale bar=1mm). (C) Confocal microscopy was used to image cells retained in the syringe after ejection at 10 µL/min (Scale bar=200µm).

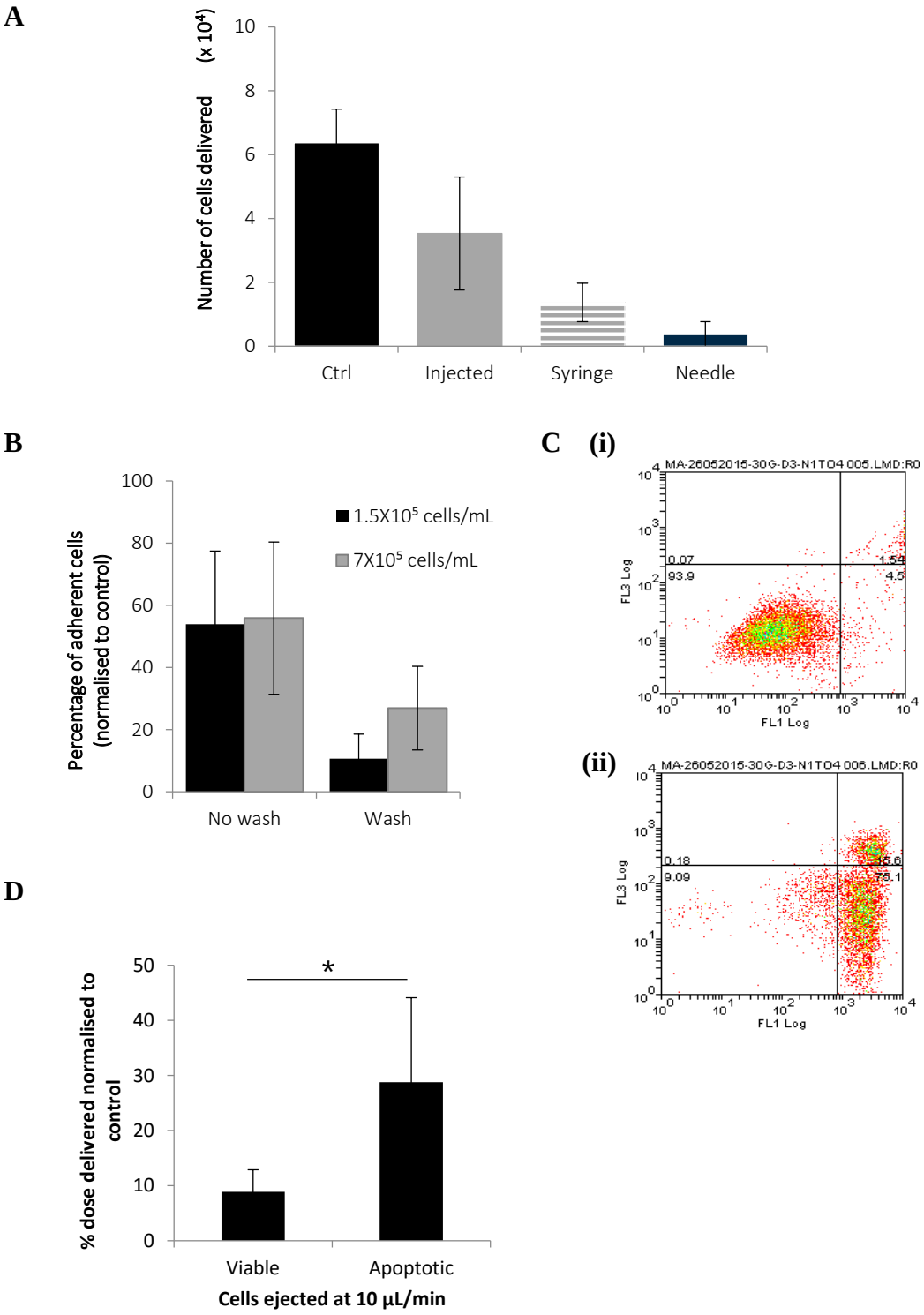

Figure 4.7: **Investigation into cell retention and adhesion in the delivery device**. (A) To investigate where cells were being retained in the delivery device, its components (syringe barrel and needle) were separated after ejection at 10 µL/min, and each was separately washed with PBS. Number of cells recovered was measured using PrestoBlue (mean ± SD, *n*=3). (B) Adhesion of cells to a borosilicate glass surface was assessed, comparing number of cells adhering with no wash following removal of cell suspensions from wells, and after gentle PBS washes (100 µL×3) (*n*=3, three independent experiments using cells from three donors). (C) Representative Annexin V/PI flow cytometric dot plots showing viable (*i*) and apoptotic cell (*ii*) proportions. (D) A comparison of cell dose recovery between viable and apoptotic cells (induced using 10 µM staurosporine) ejected at 10 µL/min (mean ± SD, *n*=4). Asterisk represents significant difference between the two groups using the Mann-Whitney test ($p \leq 0.05$).

4.4 **Discussion**

The aim of this study was to assess the impact of administration of hMSCs via a syringe-based delivery system on cellular health. With the increase in number of cell therapy clinical trials and variability of results obtained, there is an urgent need to step back and evaluate key factors required for the optimal delivery of viable cells. The impact of injectable delivery on hMSCs was quantified in terms of 24-hour viability, apoptosis, and other aspects of cell health.

Limited studies are currently available which assess clinically relevant cell types, needles and ejection rates. hMSCs used in this study were found to have a mean size of 22.57 µm, therefore making them comparatively large relative to needle gauges appropriate for high accuracy cell therapy applications. All donors used were within a small age range (Table 2.1), and there were no apparent differences in cellular health parameters pre- or post-ejection between male and female donors in this study.

PrestoBlue™ and CyQUANT® assays were used to measure viability in terms of cell numbers obtained relative to directly pipetted control samples. A significant loss of cells at all flow rates under investigation was observed at 24 hours post-ejection. The percentage of hMSCs delivered was directly proportional to the ejection rate employed, with cells ejected at 300 µL/min displaying the highest percentage of cells delivered. This may be due to the shorter time spent exposed to mechanical forces within the delivery device at higher ejection rates, which appears to have a more prominent effect on the cells than the magnitude of shear stress exerted at the rates under investigation. This is interesting to compare with the smaller NIH 3T3 cells used previously (mean size of 14.9 µm), which, unlike hMSCs, had an optimum cell dose delivery at 150 µL/min after which delivery efficiency decreased. Percentages of cell

recovery at slower ejection rates were confirmed microscopically, where lower flow rates resulted in the ejection of a visibly lower number of cells. Flow cytometric analyses measured proportions of dead cells delivered through the needle within samples under investigation. LIVE/DEAD analyses (Figure 4.2) confirmed that cells obtained by ejecting through 30G needles at all flow rates were not discernibly affected (viable cells > 97%). This is comparable with previous viability findings with several cell types, where viability was > 90% at the needle sizes explored in those studies [56, 122, 213]. Since cell viability levels were high at all the flow rates under investigation, it was concluded that cell loss was probably mainly due to retention in the delivery device.

Cell viability assays are a valuable and vital indicator of potential damage to cells. However, the transient exposure of ejected cells to supra-physiological shear stress forces (Appendix 1) may trigger apoptotic responses and other changes at the molecular level. Consequently, further investigation into the apoptotic, senescence and phenotypic expressions of the ejected hMSCs was carried out. The proliferative capacity of the cells ejected through 30G needles did not show any significant changes at all flow rates under investigation.

A significant increase in caspase-3/7 protein levels occurred as early as four hours post-ejection. Multiplexing viability, cytotoxicity and apoptosis assays in the same culture well provided us with internal controls in order to determine caspase-3/7 levels while taking the differences in cell numbers ejected into account, in contrast with previous studies [42, 122]. This multiplex assay indicated that the slowest ejection rate under investigation (10 µL/min) resulted in a significant increase in cytotoxicity and apoptosis levels in ejected hMSCs. An increase in the apoptotic cell proportions at the

slowest flow rates and an increase in the necrotic cell proportions were also observed at 24 hours post-ejection with Annexin V/PI staining. This suggests that slower flow rates prolonged cell exposure to shear forces, possibly inducing apoptosis. Since the lowest flow rates resulted in a significant increase in apoptotic cell proportions compared to the control, this endorsed the hypothesis that an equilibrium needs to be achieved between the mechanical forces exerted on the cells and the period of time spent subjected to these forces. The senescence results displayed a different trend, whereby SA-β-galactosidase activity increased with increasing flow rates, but this failed to reach statistical significance.

The International Society of Cellular Therapy (ISCT) defines MSCs as cells which are capable of osteogenesis, adipogenesis and chondrogenesis under *in vitro* conditions, and that are positive (>95%) for CD73, CD90 and CD105 but negative for CD11b, CD14, CD34, CD45, CD79a and HLA-DR surface markers [212]. Down-regulation in the expression of CD105, a stromal cell-associated marker, to less than 95% at 24 hours post-ejection at the slowest rate of ejection under investigation (10 µL/min) represented the greatest significant change observed in flow cytometric immunophenotyping. This is lower than the value stated by ICST as minimal criteria to define hMSCs [212]. Down-regulated expression of CD105 has been observed after the beginning of MSC differentiation [214] and can be used to indicate their differentiation status [215]. Therefore, altered expression of this surface marker at the slowest flow rates investigated may affect the multi-potency of hMSCs, and therefore influence the therapeutic efficiency of the injected cells. The capacity to differentiate into the three lineages was subsequently investigated.

Targeted cell lineage differentiation is sometimes important for the regenerative outcome of MSCs. The capacity for multi-lineage differentiation of the ejected hMSCs was also investigated in this study. All samples completed multi-lineage differentiation, which was induced using the manufacturer's recommended protocols. The progression of differentiation, indicated via qualitative markers of adipogenesis, osteogenesis and chondrogenesis, was consistent with previous studies in terms of retention of differentiation capacity [42, 213]. However, differentiation was visibly lower at the slower ejection rates, which was confirmed by standard staining methods. This may be due to lower cell numbers being ejected at these rates, impairing the capacity for differentiation. Elucidation of the extent of impact of ejection rate on differentiation capacity could not be concluded using qualitative staining methods alone. Therefore, a more detailed investigation into this effect on differentiation capacity was carried out. This work is described in Chapter 5.

Needle gauge also had a substantial impact on viability post-ejection. A smaller percentage of cell dose delivered was observed with the smaller needle diameter (51 µm). This can be explained by the magnitudes of the forces to which cells are exposed: smaller needles will result in higher forces being exerted on the cells. In addition, higher flow rates also caused significantly higher apoptotic cell proportions, which may be due to the higher, supra-physiological shear force levels exerted at this flow rate. In the case of 34G needles, both the prolonged ejection period at 10 µL/min and higher shear force value exerted at 300 µL/min adversely impacted cells post-ejection, causing significantly higher apoptotic cell proportions than control samples. Flow rates in between these lower and upper limits seemed to maintain a more favourable balance for the ejected cells.

Since cytotoxicity and apoptosis results did not fully account for the substantial differences in percentages of cell doses delivered, the likelihood of cells adhering to the inner walls of the delivery device was investigated, as hMSCs are highly adherent anchorage-dependent cells [216]. Results revealed that cells were mainly being retained in the syringe, and a smaller proportion was retained on the inner walls of the needle. These were only dislodged by PBS washes at 300 µL/min. Cell loss occurring at the slower ejection rates may be due to the longer period that the cells are in contact with the syringe's glass surface, which may allow the formation of transient adhesions to the injector as well as other cells, forming aggregates. The present results demonstrate that such adhesive interactions with the delivery device can be significant and could substantially affect the delivery of cells to the target site. This highlights the importance of developing materials that do not promote the attachment of cells for the manufacture of cell delivery devices. In addition, the optimisation of injection rates used in pre-clinical and clinical trials is critical to reduce mechanical stress and improve delivery success rates.

It was also important to investigate whether the characteristic morphological changes associated with apoptosis, such as cellular shrinkage and membrane blebbing [217], led to the increase in apoptotic cell proportions recovered at slower ejection rates, or whether it was due to the increased time exposed to mechanical forces within the delivery device. Percentage of cell dose delivery between apoptotic cells (induced using 10µM staurosporine) and viable cells ejected at 10 µL/min was compared. Despite the lower cell adhesion capability exhibited by apoptotic cells, shown by the statistically significant increase in cell dose delivered ($p<0.05$, Mann-Whitney Test), the increase in percentage delivered was not substantial. This suggests that the increase in apoptosis levels at slower flow rate is a combination of both factors: the prolonged

exposure to shear forces as well as the lower capacity of apoptotic cells to form transient adhesions to the syringe.

4.5 Conclusions

Reviewing current literature, there is a lack of comprehensive testing of the effects of injection-based cell delivery on the various parameters of cellular function. This study assesses an extensive range of viability and other cell health indicators in ejected hMSCs, a clinically relevant cell type, to comprehensively elucidate cellular responses to the ejection procedure.

In summary;

- Ejections at slower flow rates resulted in a lower percentage of the cell dose being delivered as viable cells.
- Apoptosis levels of samples ejected at 10 µL/min were statistically significantly higher than control.
- Immunophenotyping revealed a statistically significant down-regulation of CD105 expression in samples ejected at 10 µL/min.
- hMSCs ejected through 34G needles showed lower percentages of cell dose delivered relative to those ejected via 30G needles at the various flow rates investigated. Moreover, a different trend of apoptotic responses to varying ejection rate was displayed with the two needle sizes tested.
- Qualitative markers of adipogenesis, osteogenesis and chondrogenesis revealed that slower ejection rates exerted an effect on the differentiation capacity of ejected cells, thereby possibly influencing the success of cell-based therapies.

- Cells were being mostly retained in the syringe component of the delivery device. The time spent in the delivery device at the lowest ejection rate was shown to be sufficient to allow for the formation of transient adhesions between the cells and the glass surface.

Although great progress has been achieved, future research should focus on elucidating optimal strategies for injectable cell delivery, in order to revolutionise regenerative cellular therapies. Results of this study reveal that passing hMSCs through a needle at the slower injection rates previously utilised in clinical trials [111] is likely to induce apoptosis, which can bring about delayed death of the injected hMSCs, and phenotypic expression changes, which may affect their physiological functioning. Initial loss of injected cells may be due to a combination of cell disruption by mechanical forces and cell retention in the delivery device. Therefore, this study emphasises the importance of thorough consideration of administration protocols required for efficacious cell delivery.

Chapter 5| Effects of ejection rate on trilineage differentiation potential of ejected hMSCs

5.1 Introduction

A major defining characteristic of MSCs is their ability to differentiate into the three major mesenchymal lineages (bone, cartilage, and adipose) upon culture under specific *in vitro* conditions [218]. Results of flow cytometric immunophenotyping and qualitative assessment of differentiation of ejected cells (Chapter 4) raised questions about how varying the rate at which hMSCs are ejected may affect their trilineage differentiation potential, thus compromising their regenerative capacity. Elucidation of the extent of influence of ejection rate on differentiation capacity could not be concluded using qualitative staining methods alone. Therefore, a more detailed investigation into this effect on trilineage differentiation potential was carried out.

The field of mechanobiology, which comprises understanding how MSCs sense and respond to applied forces, has gained momentum in the past few years. This includes characterising the response of stem cells to controlled mechanical and physical loading, and in determining the biophysical mechanisms and biochemical pathways that regulate lineage commitment [219, 220]. Numerous dynamic mechanical forces, which biological tissues are exposed to, regulate various functions of MSCs [221, 222]. Differentiation of MSCs can be induced by various cocktails of biochemical agents and growth factors, including dexamethasone, β-glycerophosphate and ascorbic acid for osteogenesis [223], or serum-free medium and TGF-β for chondrogenesis

[179]. Recently, mechanical stimulation has been reported to play a critical role in proliferation and driving differentiation of MSCs [224].

Several studies have explored the effects of shear stress on osteoblastic differentiation of MSCs [225-232]. Flow perfusion inadvertently results in cells exposure to shear stress [233-235]. Perfusion culture of osteoprogenitor cells seeded within porous scaffolds enhanced deposition of a bone-like extracellular matrix, which was thought to be a result of flow-induced activation of mechanotransductive signalling pathways [226]. Increasing the viscosity of the perfused medium, which resulted in higher shear stress values at the same flow rates, enhanced calcium deposition by rat MSCs [235]. Exposure of MSCs to shear stress, whether controlled (fluid flow) or uncontrolled (flow perfusion), resulted in the increased expression of early markers [226, 230, 232] and enhanced osteogenic matrix production and maturation [225, 228, 229, 231, 233].

As discussed in Chapter 1, cells experience various types of mechanical forces, including shear forces, as it flows through a needle [74]. Therefore, the impact of shear stress on differentiation potential of hMSCs needs to be investigated. However, since it has been previously established that different percentages of the cell dose are delivered at different ejection rates (Chapters 3 and 4), it was deemed critical to assess the effect of cell numbers seeded on differentiation capacity first. Bipotential adipogenic/osteogenic inductive media were used in these investigations to remove any interfering effects of bioactive chemical components of the media, thereby exploring how mechanical forces exerted on the cells primes them in this setting.

The first part of this chapter focuses on the effects of initial cell seeding density on differentiation potential. After determining whether varying seeding cell density has

an effect on differentiation potential, the second part of this chapter focuses on the assessment of the impact of varying ejection rate on trilineage differentiation capacity of ejected cells. To explore whether varying ejection rate exerts a considerable effect on differentiation capacity, investigations were carried out using quantitative indicators of adipogenesis, osteogenesis, and chondrogenesis.

5.2 Experimental design

For more detailed methods describing hMSCs culture, trilineage differentiation protocols, cell ejection protocols and assay procedures, see Chapter 2: Materials and Methods.

For hMSC differentiation studies, differentiation to the osteoblastic and adipogenic lineages was examined in either monopotential osteogenic or adipogenic culture media, or in a bipotential 'mixed' medium. Bipotential 'mixed' media were formulated by combining adipogenic (#PT-3004; Lonza, Germany) and osteogenic media (#PT-3002; Lonza, Germany) in a 1:1 ratio. Differentiation medium was added to the cells 24 hours post-seeding, and cells were alternated between adipogenic induction/osteogenic induction media (1:1) and adipogenic maintenance/osteogenic induction media (1:1) every 3-4 days for 21 days. Uninduced controls were maintained in basal medium MSCGM (#PT-3001; Lonza, Germany).

For chondrogenic differentiation studies, pellet cultures were used as described by Penick *et al*. [178]. Ejected cell suspensions were seeded in U-type 96-well plates (Costar, Corning Life Sciences, UK). Chondrogenesis was induced for 28 days in culture volumes of 200 µL of chondrogenic induction medium (#PT-3003; Lonza, Germany). Media was changed three times a week.

5.2.1 **Effects of cell seeding density on differentiation potential of hMSCs**

Cell seeding densities tested range from 1000-70,000 cells per well in 12-well plates (Nunc, Thermo Fisher Scientific, UK), equivalent to 0.3-18.4 x 10^3 cells/cm^2. Twenty-four hours after seeding, the medium was replaced with differentiation medium (monopotential or bipotential), and cultures was incubated for 21 days. The differentiation medium was changed every 3-4 days for the duration of the differentiation period. The impact of initial seeding number on differentiation was quantified using either OsteoImage (Lonza, Germany) for osteogenesis or AdipoRed (Lonza, Germany) for adipogenesis.

5.2.2 **Effects of varying ejection rate on trilineage differentiation potential of hMSCs**

100 µL Hamilton GASTIGHT® syringes (model 1710RN), attached to 30G 20mm removable (RN) stainless steel needles were employed (Hamilton Bonaduz, Switzerland), as previously described in Chapter 2. Cell suspensions were drawn up using a Harvard® Infuse/Withdraw syringe pump (PHD 2000, Harvard Apparatus, USA) at 300 µL/min before being ejected at various rates (10-300 µL/min). The ejected samples were then transferred into 12-well plates. Differentiation media was added 24 hours post-ejection, and cultures were incubated for 21 days for adipogenic and osteogenic assays, and 28 days for chondrogenic assays.

5.2.3 **Multiplexing quantitative differentiation assays with nuclear staining**

Multiplexing of cell-specific differentiation assays and nuclear staining allowed for normalisation of differentiation to cell number. Differentiated cells were stained with

OsteoImage™ Staining Reagent (Lonza, Germany) for osteogenesis quantification, according to the manufacturer's instructions (Section 2.6.2). Afterwards, 100 µg/mL RNase A solution (AppliChem, Darmstadt, Germany) in Tris-EDTA buffer solution (Sigma-Aldrich, UK) was added to the fixed cells for ten minutes at room temperature. Finally, nuclear staining was carried out using 2 µg/mL PI (diluted in H_2O from 1 mg/mL; ThermoFisher Scientific, UK) for 5 minutes.

The fluorescence-based OsteoImage™ dye specifically binds to hydroxyapatite, and is therefore more specific than Alizarin red, which binds to calcium [236]. For the quantitation of differentiation, the mean fluorescence intensity of each well was determined using multiple readings of each well (>64 readings/well). The mean fluorescence intensity of each well was measured at $\lambda_{exc}/\lambda_{em}$: 492/520 nm.

The fluorescent AdipoRed™ assay was used to quantify adipogenic differentiation of hMSCs based on intracellular lipid content. Differentiated cells were stained with AdipoRed™ Assay Reagent (Lonza, Germany), according to the manufacturer's instructions (Chapter 2). Nuclear staining in adipogenic analysis was carried out using 2 µg/mL Hoechst 33258 (diluted in H_2O from 1 mg/mL; Sigma-Aldrich, UK) for 15 minutes. The mean fluorescence intensity of each well was determined on a Tecan Infinite M200 microplate reader (Tecan, Reading, UK) using 100 readings per well (Appendix 2).

5.2.4 **Biochemical characterisation of chondrogenic differentiation**

Triplicate cultures were removed from the culture medium after 28 days of *in vitro* culture and digested in 200 µL of a papain solution (125 µg/mL papain in 10 mM EDTA and 2 mM L-cysteine (Sigma)) for 18 hours at 65°C.

DNA content of the aggregates was quantified spectrofluorimetrically using the Quant-iT PicoGreen dsDNA Assay Kit (#P11496; Invitrogen), following the manufacturer's protocol. Quantification of sulphated GAGs in the digested aggregates was carried out spectrophotometrically using the dimethylmethylene blue dye (DMMB) assay. Absorbance at 525 nm was measured using a plate reader, and proteoglycan content was estimated using bovine chondroitin-4-sulphate as standard (# C6737, Sigma-Aldrich, UK). Collagen content was quantified by a colorimetric analysis using the hydroxyproline assay kit (#MAK008, Sigma), according to the manufacturer's instructions. Hydroxyproline, a major component of collagen [180, 181], was used as a measure of total collagen content. Hydroxyproline content was determined in duplicates by the oxidation of hydroxyproline residues in collagen with chloramine T, developed with p-dimethylaminobenzaldehyde (DMAB), resulting in a product that can be measured at 560 nm.

5.3 Results

5.3.1 Impact of initial cell seeding density on the osteogenic differentiation potential of hMSCs

Mineralisation is considered to mark the end of the osteoblast differentiation [237]. Hydroxyapatite (HA; $Ca_5((PO_4)(OH))$ is a mineral naturally found in bone tissue and can be used as a late marker for osteogenesis, since MSCs produce HA nodules as they form new bone tissue [238]. The fluorescent OsteoImage™ assay was used to quantify the osteogenic differentiation of hMSCs. The extent of differentiation was normalised to cell number.

- *Monopotential media formulation*

The effect of initial cell seeding number on hMSCs osteogenic differentiation capacity was evaluated. Figure 5.1 shows the results of OsteoImage staining of hMSCs, seeded at various densities. All samples underwent osteogenic differentiation, as determined by OsteoImage mineralisation assay at day 21. As shown in Figure 5.1A, the amount of hydroxyapatite deposition at day 21 is approximately the same with all initial seeding densities ≥5000 cells/well, with no statistically significant differences in amounts of hydroxyapatite deposited between the different cell numbers initially seeded ($p<0.05$ – Kruskal-Wallis test with Dunn's *post-hoc* test). Cells seeded at 1000 cells/well (263 cells/cm^2) deposited markedly less hydroxyapatite compared to the other seeding densities under investigation, both in terms of absolute (Figure 5.1A) and normalised values (Figure 5.1B).

Proliferation was investigated by quantification of the PI staining of the fixed cells, by means of multiple readings per well using a plate-reader, on day 21 of culture. Nuclear-based cell counts are shown in Figure 5.2. Cells seeded at 1000 cells/well exhibited significantly lower cell numbers at day 21 relative to a seeding cell density of 70,000 cells/well ($p<0.001$). However, when this data is expressed as fold change in cell number relative to the number of cells initially seeded, cells seeded at 1000 cells/well exhibited a significantly higher fold change in cell number relative to day 0 ($p<0.05$).

A

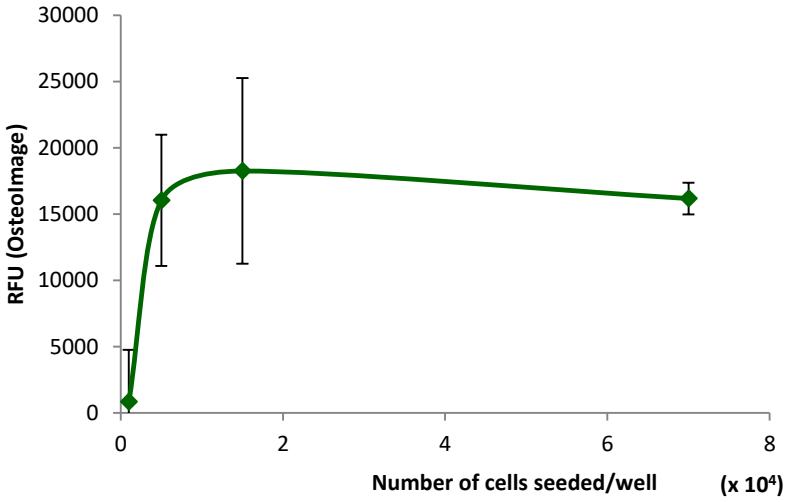

B

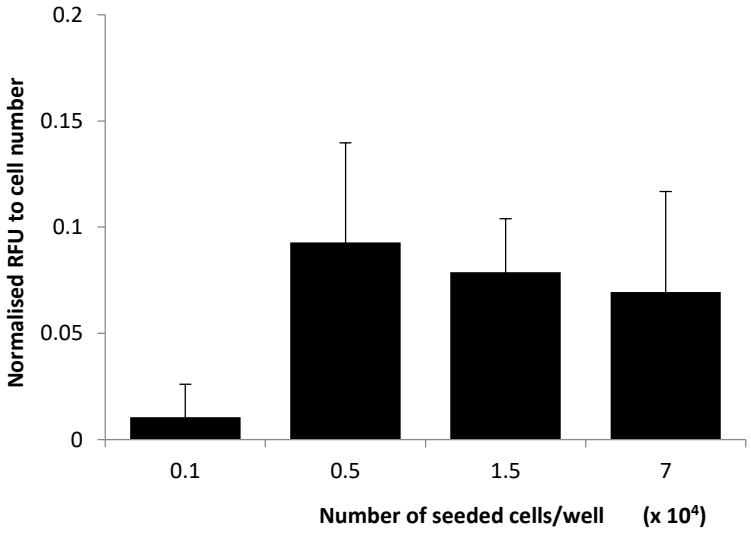

Figure 5.1: **Effect of initial cell seeding density of hMSCs on their osteogenic potential when cultured in monopotential osteogenic medium, quantified based on mineral deposition.** (A) OsteoImage fluorescent staining for hydroxyapatite in hMSCs from two donors seeded at different initial seeding densities in a 12-well plate, cultured in monopotential osteogenic media for 21 days. (B) OsteoImage fluorescence readings were normalised to cell counts based on nuclear staining using PI (mean ± SD, *n*=3 in triplicate). Statistical analysis was performed using Kruskal-Wallis test, with Dunn's *post-hoc* test.

A

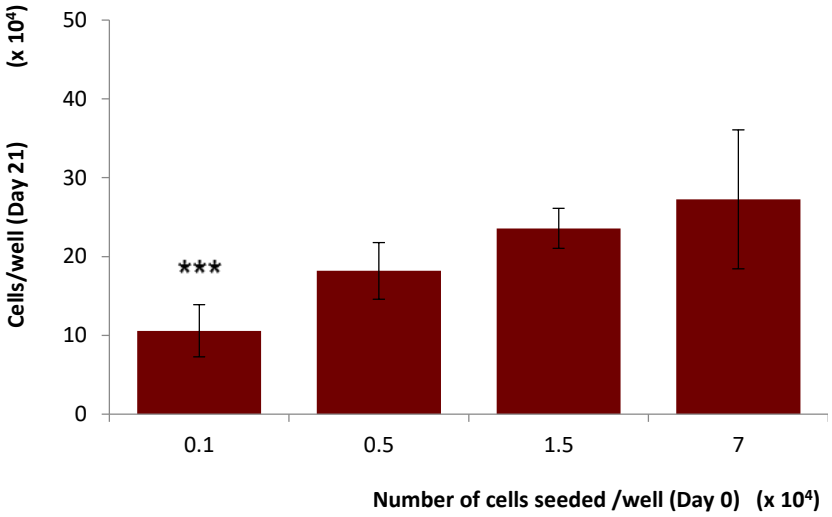

B

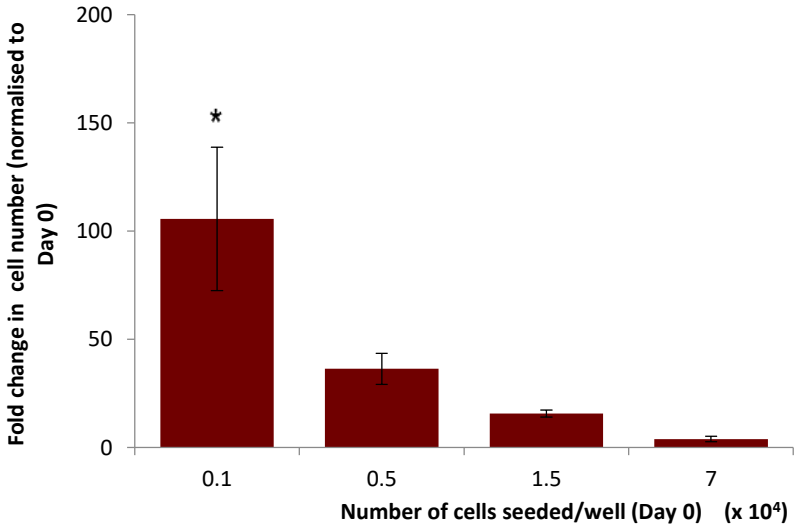

Figure 5.2: **Cell proliferation of hMSCs seeded at different initial seeding densities, based on PI staining of fixed cells, cultured in monopotential osteogenic media for 21 days**. (A) Number of cells at day 21, based on nuclear-based PI staining of hMSCs from two donors seeded at different initial seeding densities in a 12-well plate. (B) Each bar represents PI cell counts normalised to the respective initial cell numbers seeded, expressed as the fold change relative to initial cell seeding density (mean ± SD, *n*=3); Data represents averages from two donors (*n*=3; mean ± SD). Asterisks indicate statistically significant difference from the full seeding density of 70,000 cells/well (*p<0.05, ***p<0.001 - Kruskal-Wallis test, with Dunn's *post-hoc* test).

- *Bipotential media formulation*

Figure 5.3 presents the results for OsteoImage staining of hMSCs seeded at various cell seeding densities, after culturing in bipotential adipogenic/osteogenic media for 21 days. There was no significant difference in osteogenic differentiation between the different cell numbers initially seeded, as shown by the amounts of hydroxyapatite deposited ($p<0.05$ – Kruskal-Wallis test with Dunn's *post-hoc* test). Figure 5.3B shows no statistical difference in normalised mineral deposition values per cell for the various initial seeding densities under investigation.

Nuclear-based cell counts, quantified using PI staining of the fixed cells, are shown in Figure 5.4. All cell densities exhibited similar final cell numbers at day 21. When this data is expressed as fold change in cell number relative to the number of cells initially seeded (Figure 5.4B), lower initial cell seeding densities exhibited a significantly higher fold change in cell number relative to day 0 ($p<0.05$ – Kruskal-Wallis test with Dunn's *post-hoc* test).

Figure 5.4C shows representative fluorescence microscopy images of OsteoImage-stained hydroxyapatite bone nodules in hMSC cultures after 21 days of culture in bipotential media. There were no visible differences in hydroxyapatite deposition across the range of initial seeding densities investigated, which supports the quantitative results.

A

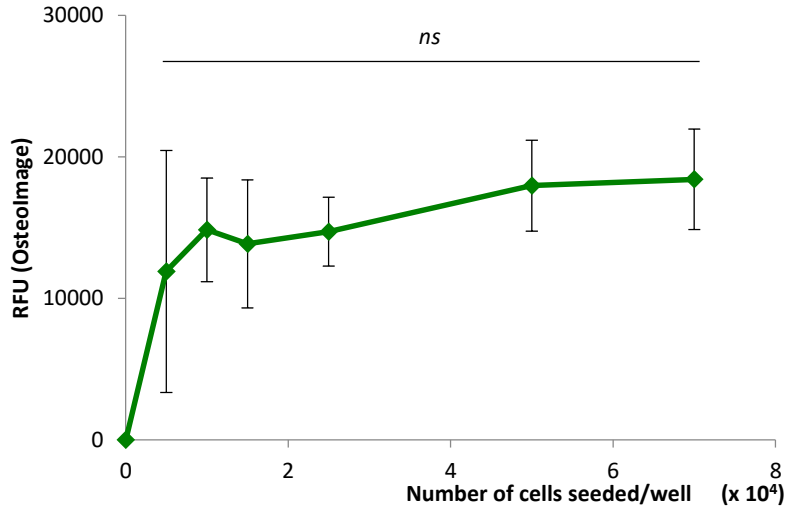

B

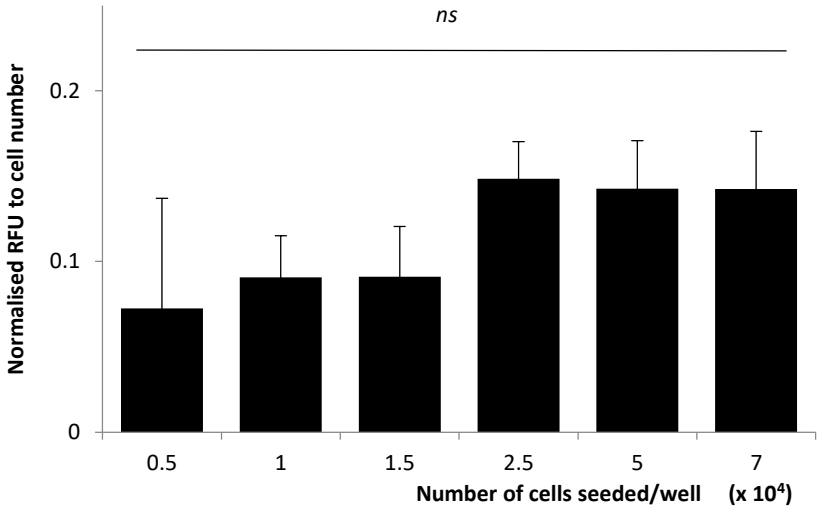

Figure 5.3: **Effect of initial cell seeding density of hMSCs on their osteogenic potential when cultured in bipotential adipogenic/osteogenic media, quantified based on mineral deposition.** (A) OsteoImage staining for hydroxyapatite in hMSCs from two donors seeded at different initial seeding densities in a 12-well plate, cultured in bipotential media for 21 days (mean ± SD, *n*=6). No significant difference was revealed between the various initial cell seeding densities, analysed using one-way ANOVA and Tukey's *post-hoc* test (B) OsteoImage fluorescence readings were normalised to cell count, based on nuclear staining using PI (mean ± SD, *n*=4). Statistical analysis was performed using Kruskal-Wallis test, with Dunn's *post-hoc* test; *ns*: no significant difference.

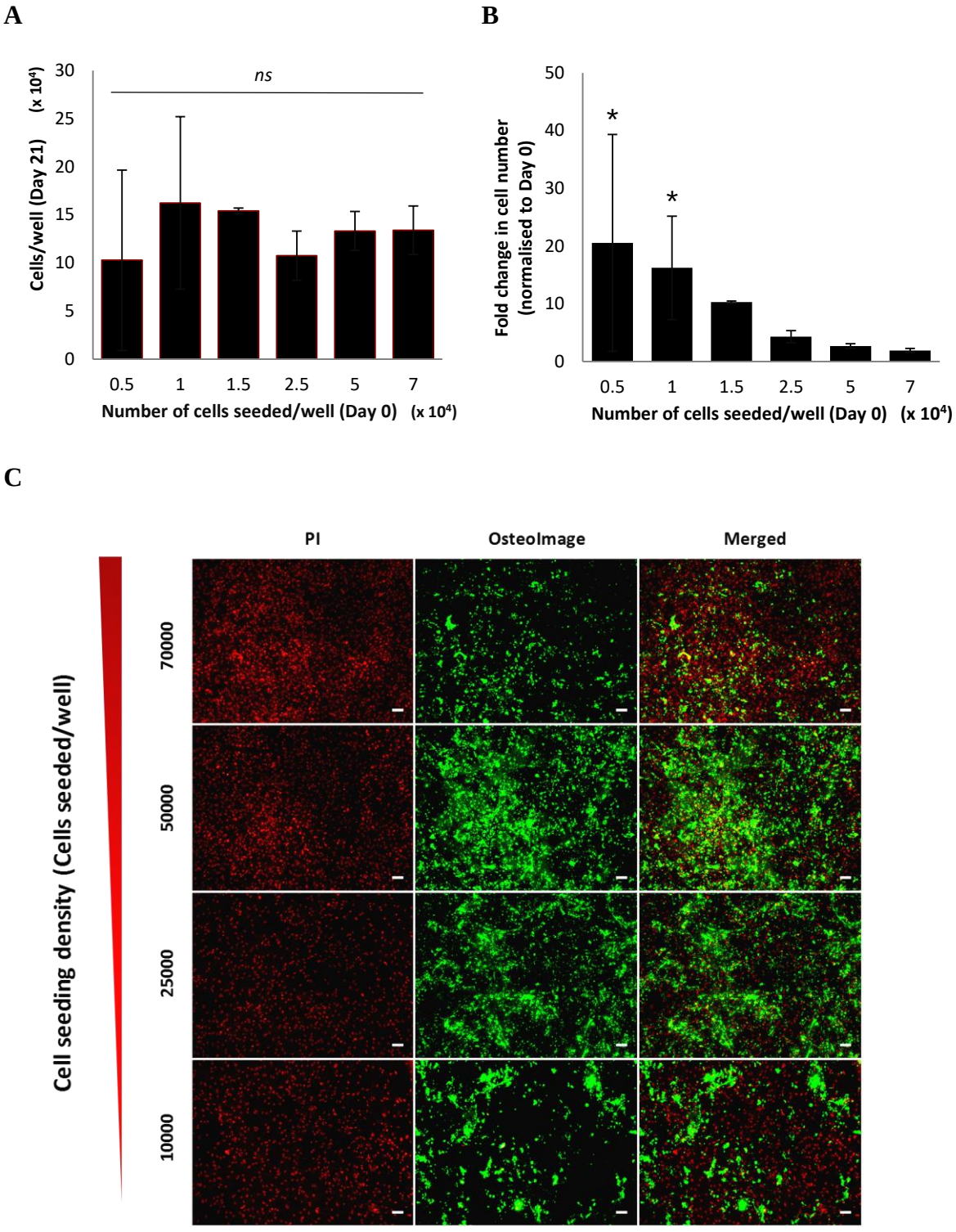

Figure 5.4: **Cell proliferation and differentiation of hMSCs seeded at different initial seeding densities, cultured in bipotential differentiation media**. (A) Number of cells at day 21, quantitated using nuclear-based PI staining of hMSCs from two donors seeded at different initial seeding densities in a 12-well plate, cultured in bipotential adipogenic/osteogenic media for 21 days (*ns*: no significant difference). (B) PI cell counts normalised to the respective initial cell numbers seeded, expressed as the fold change relative to initial cell seeding density (mean±SD, *n*=4). Data represents averages from two donors; Asterisks indicate statistically significant difference from full seeding density of 70,000 cells/well (*p<0.05 - Kruskal-Wallis test, with Dunn's *post-hoc* test). (C) Representative fluorescence microscopy images of hMSCs at day 21. Nuclei were stained with PI, and hydroxyapatite was fluorescently stained using OsteoImage (Scale bar=100 µm).

5.3.2 Impact of initial cell seeding density on the adipogenic differentiation potential of hMSCs

- *Monopotential media formulation*

In contrast with the OsteoImage results, a more obvious linear trend of increasing adipogenic differentiation with increasing seeding density was observed after culturing in monopotential adipogenic media for 21 days (Figure 5.5A). Intracellular lipid content at day 21 in samples initially seeded at 5000 cells/well was significantly lower than the maximum initial seeding density of 70,000 cells/well ($p<0.05$ – Kruskal-Wallis test with Dunn's *post-hoc* test). Normalisation of AdipoRed fluorescence to cell numbers (based on Hoechst staining) showed the same trend of increased differentiation efficiency with increasing initial cell seeding density (Figure 5.5B).

Nuclear-based cell counts, quantified using Hoechst staining of the fixed cells, are shown in Figure 5.6. There was a linear trend between number of cells initially seeded and the final cell number at day 21, whereby the higher the initial cell seeding density the higher the resultant cell numbers at day 21. However, when this data is expressed as fold change in cell number relative to the number of cells initially seeded (Figure 5.6B), cell proliferation appeared to be stimulated by lower cell seeding density. Cells seeded at 5000 cells/well exhibited a significantly higher fold change in cell number relative to day 0.

- *Bipotential media formulation*

Figure 5.7 presents the results for AdipoRed staining of hMSCs, seeded at the various cell seeding densities, after culturing in bipotential adipogenic/osteogenic media for 21 days. There was a clear linear correlation between initial seeding density and

adipogenesis, as shown by AdipoRed staining of intracellular lipid content. The lowest cell seeding densities under investigation exhibited significantly lower extent of adipogenesis relative to the full seeding density of 70,000 cells/well ($p<0.05$ – Kruskal-Wallis test with Dunn's *post-hoc* test). When AdipoRed fluorescence data is expressed as values normalised to the final cell counts at day 21 (Figure 5.7B), this linear correlation was still observed. The dependence of adipogenesis, as shown by accumulation of intracellular triglycerides, on initial cell seeding density is also shown in Figure 5.7C, where fluorescence microscopy images demonstrate an increasing intensity of fluorescent staining of intracellular lipids with increasing initial cell seeding numbers.

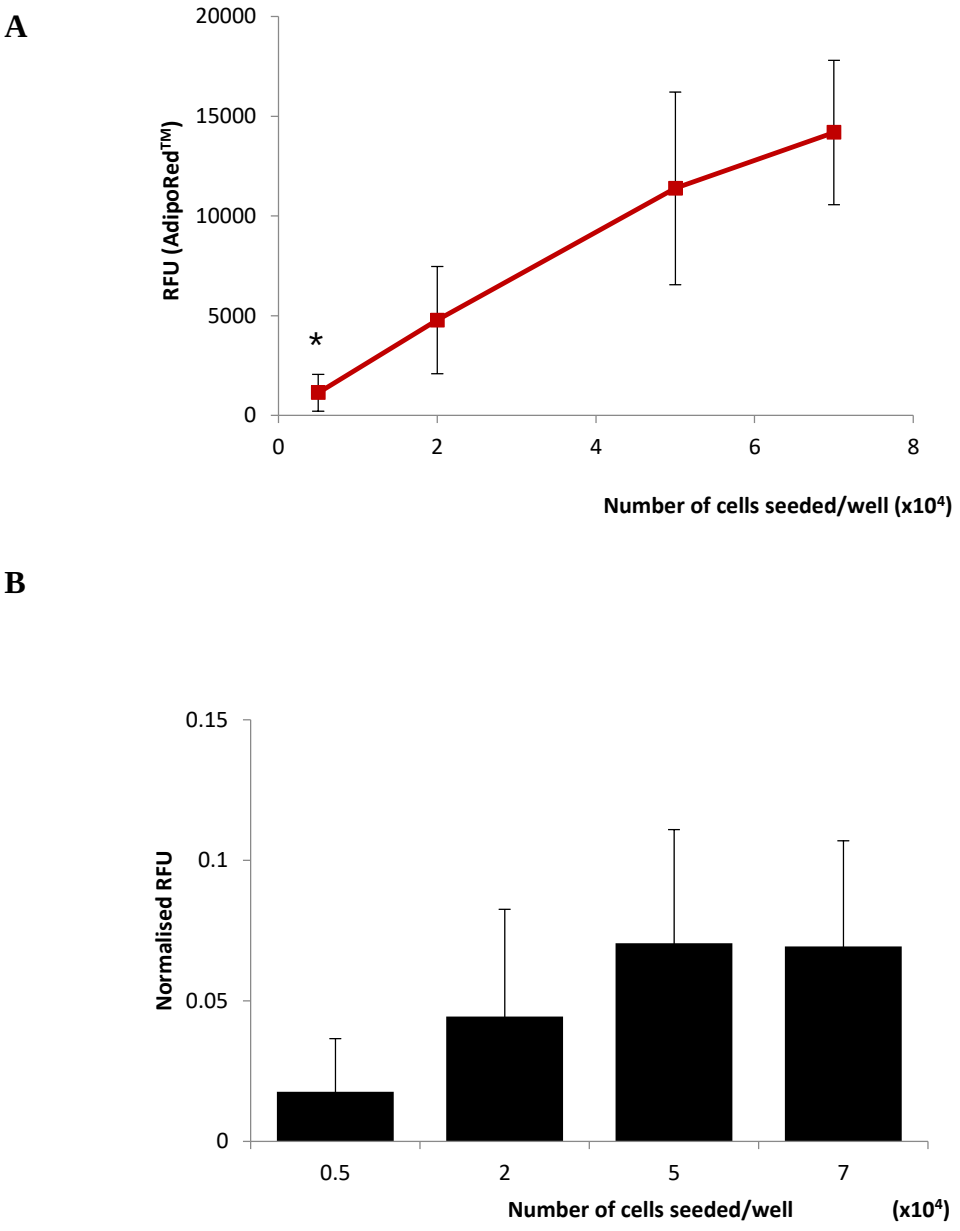

Figure 5.5: **Effect of initial cell seeding density of hMSCs on their adipogenic potential when cultured in monopotential differentiation medium, quantified based on intracellular lipid accumulation.** (A) AdipoRed staining for lipid content in hMSCs from two donors seeded at different initial seeding densities in a 12-well plate, cultured in monopotential adipogenic media for 21 days. Asterisks indicate statistically significant difference from the full seeding density of 70,000 cells/well (*p<0.05 - Kruskal-Wallis test, with Dunn's *post-hoc* test). (B) AdipoRed fluorescence readings, adjusted for cellular count based on nuclear staining using Hoechst 33258 (mean ± SD, n=3 in triplicates). Statistical analysis was performed using Kruskal-Wallis test, with Dunn's *post-hoc* test.

A

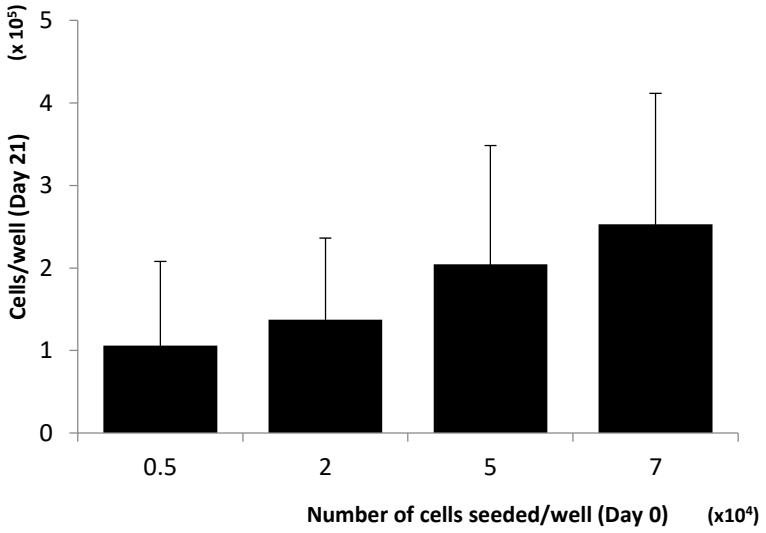

B

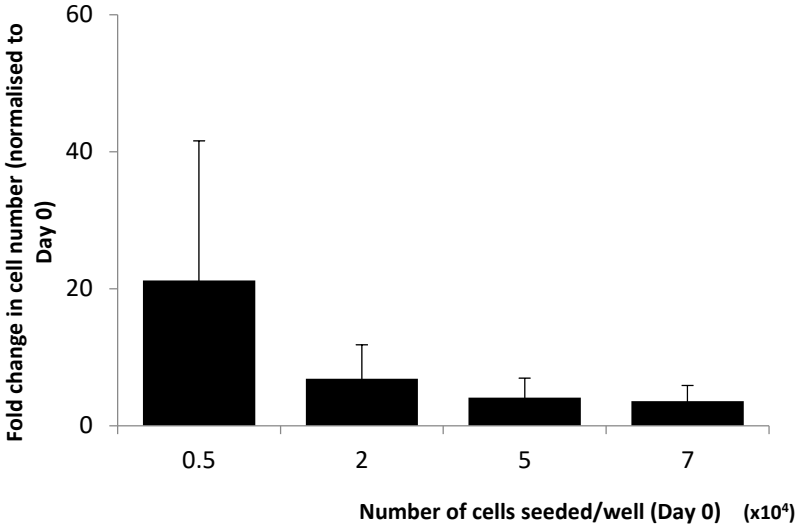

Figure 5.6: **Cell proliferation of hMSCs seeded at different initial seeding densities, based on Hoechst staining of fixed cells**. (A) Number of cells at day 21, based on nuclear staining using Hoechst 33258 of hMSCs (from two donors) seeded at different initial seeding densities in a 12-well plate, cultured in monopotential adipogenic media for 21 days. (B) Nuclear-based cell counts normalised to the respective initial cell numbers seeded, expressed as the fold change relative to initial cell seeding density (*n*=3 in triplicates); Data represents averages from two donors (mean ± SD).

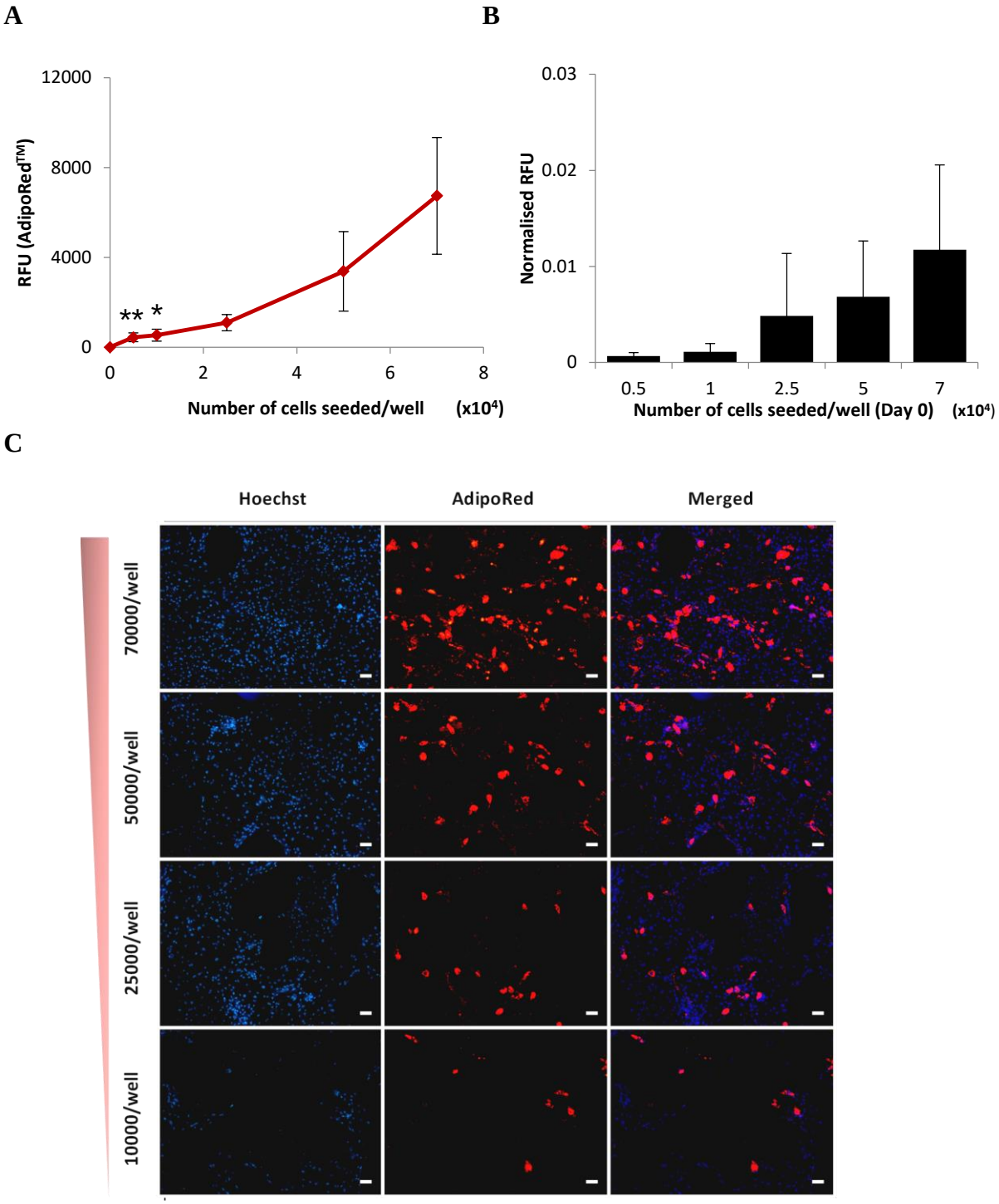

Figure 5.7: **Adipogenic differentiation of hMSCs seeded at different initial seeding densities, cultured in bipotential differentiation media.** (A) AdipoRed staining of hMSCs seeded at different initial seeding densities in a 12-well plate, cultured in bipotential adipogenic/osteogenic media for 21 days. (B) AdipoRed fluorescence readings were normalised to Hoechst-based cell counts (mean ± SD, n=4); Asterisks indicate statistically significant difference from the full seeding density of 70,000 cells/well (**p<0.01; *p<0.05 - Kruskal-Wallis test, with Dunn's *post-hoc* test). (C) Fluorescence microscopy images of hMSCs cultured in bipotential differentiation media at day 21. Lipid droplets were fluorescently stained using AdipoRed Adipogenesis Reagent, after which nuclei were counter-stained with Hoechst. (Scale bar=100 µm).

5.3.3 **Effects of varying ejection rate on the osteogenic differentiation capacity of ejected hMSCs**

Based on the results reported here regarding the influence of initial cell seeding density on osteogenic and adipogenic differentiation potentials, it was concluded that osteogenic differentiation is the most suitable differentiation model to be used for this study. It was therefore decided to focus on osteogenesis, where mineralisation at day 21 was shown to be independent of initial cell seeding density, as a model for investigating the potential impact of ejection rate on differentiation fate choice and capacity of ejected hMSCs. The effects of varying ejection rate on osteogenic differentiation potential was investigated next.

- *Monopotential media formulation*

Suspensions of hMSCs were ejected at rates ranging from 10 to 300 µL/minute. All ejected samples and the directly plated control deposited hydroxyapatite, as determined by the OsteoImage mineralisation assays at 21 days (Figure 5.8A). Samples ejected at the lowest flow rates under investigation (10 and 20 µL/min) deposited significantly less HA relative to the control (Figure 5.8B) in a monopotential setting.

- *Bipotential media formulation*

Directly plated control and ejected samples showed mixed populations of both adipocytes and osteoblasts. Samples ejected at 10 µL/min exhibited visibly less cells exhibiting the adipocyte morphology compared to the other samples. In addition, noticeably brighter OsteoImage staining of HA was evident in the samples ejected at 10 µL/min relative to directly plated controls and other ejected samples (Figure 5.9A).

All ejected samples gave similar absolute fluorescence values when stained with OsteoImage (Figure 5.9B), and samples ejected at 10 µL/min exhibited lower cell numbers at day 21 relative to the control (Figure 5.9C). However, samples ejected at 10 µL/min exhibited significantly higher normalised OsteoImage values (Figure 5.9D), being statistically significant over the directly plated control at 3 weeks ($p<0.05$ - one-way ANOVA and Dunnet's *post-hoc* test).

5.3.4 Effects of varying ejection rate on the adipogenic differentiation capacity of ejected hMSCs in monopotential media

There was significantly lower AdipoRed fluorescence values ($p<0.001$) in samples ejected at the lowest flow rates (10 and 20 µL/min) relative to the directly-plated control, indicating the lower extent of adipogenesis in those ejected samples (Figure 5.10). In addition, there was a clear trend of increasing adipogenesis with increasing flow rates.

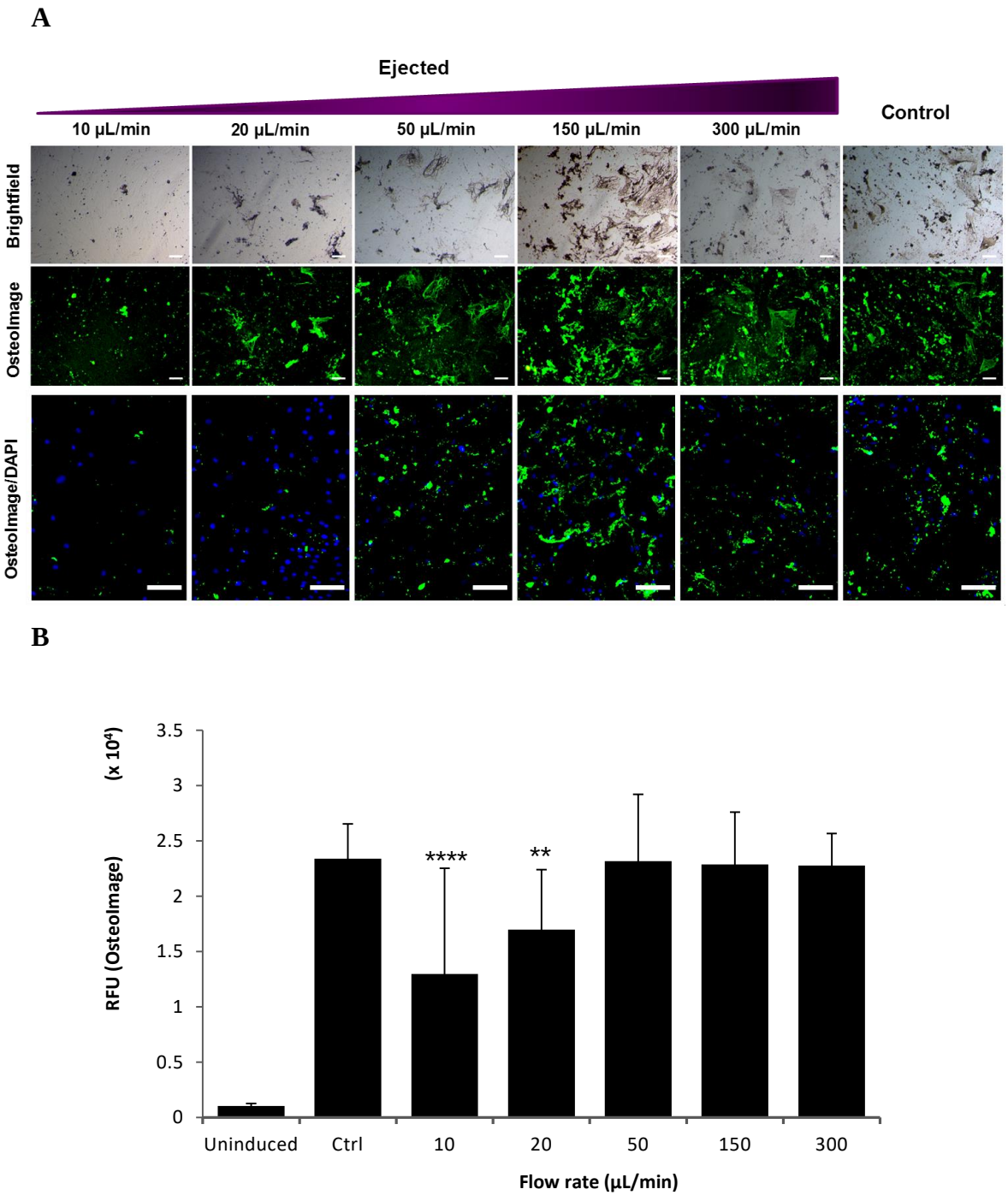

Figure 5.8: **Effect of ejection rate on differentiation potential of hMSCs ejected via 30G needles, cultured in monopotential osteogenic media**. (A) Representative bright field and fluorescence microscopic images showing ejected hMSCs after culturing for 21 days in osteogenic media. Cell nuclei appear blue (DAPI-stained), while mineralised areas are stained green with OsteoImage, which is HA-specific; Scale bar = 50 µm. (B) Quantitation of OsteoImage staining for hydroxyapatite in hMSCs cultured with osteogenic media for 21 days. Each bar represents mean fluorescence values ± SD, n=19 in four independent experiments and two donors (Repeated measures ANOVA, ****$p \leq 0.0001$, **$p \leq 0.01$)

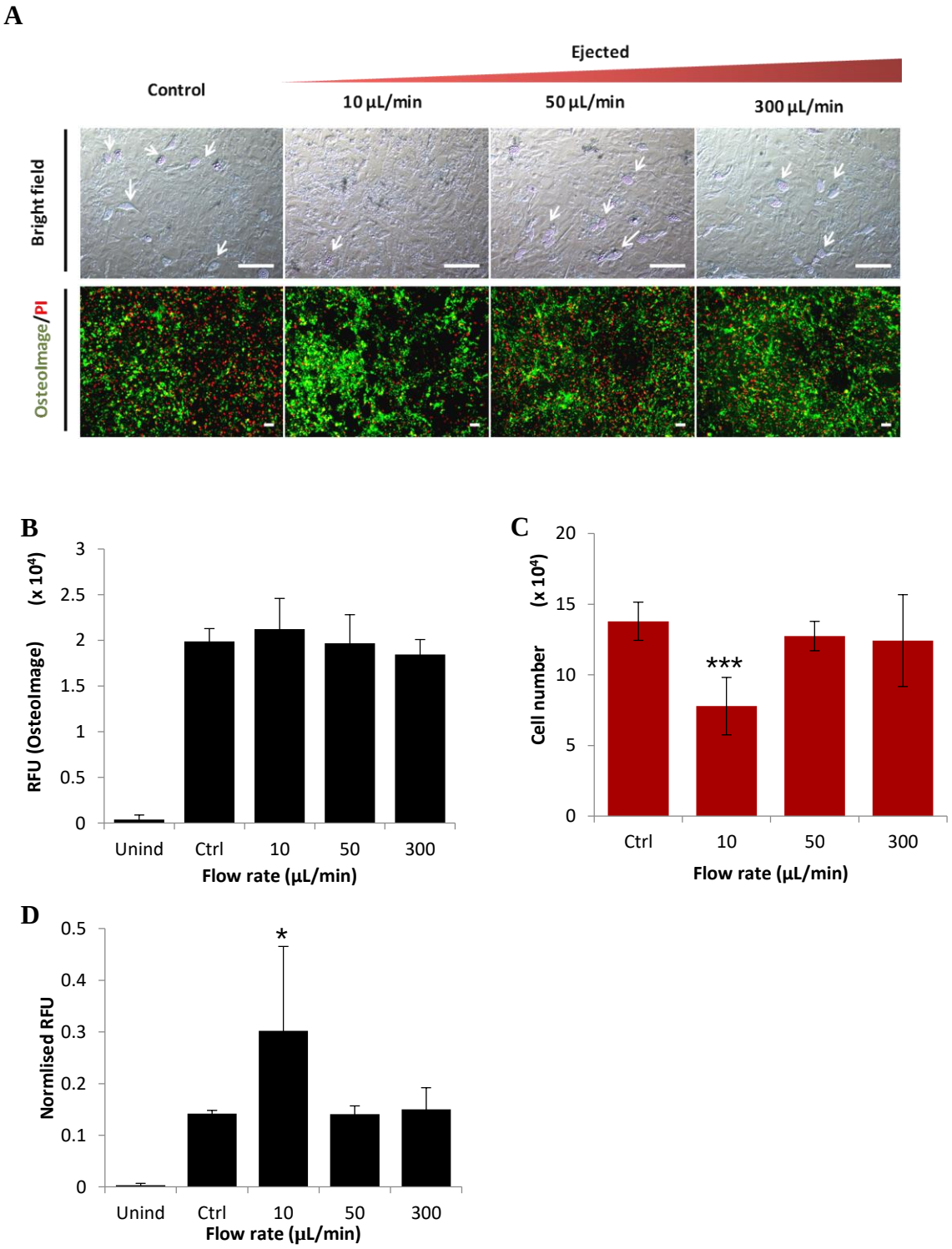

Figure 5.9: **Effect of ejection rate on osteogenic differentiation capacity of hMSCs ejected via 30G needles, cultured in bipotential osteogenic/adipogenic media for 21 days**. (A) Representative bright field and fluorescence microscopic images showing ejected hMSCs after culturing in bipotential media. Cell nuclei are stained red (PI), while mineralised areas are stained green (OsteoImage). Intracellular lipid accumulation is indicated by arrows (Scale bar = 100µm). (B) OsteoImage fluorescence values for ejected hMSCs. Each bar represents mean fluorescence values ± SD, n=9 in three independent experiments and two donors. (C) Number of cells at day 21 quantitated using PI staining of hMSCs from two donors. (mean ± SD, n=6). Asterisks represent statistically significant difference from directly plated control using ANOVA and Dunnet's *post-hoc* test; *$p \leq 0.05$, ***$p \leq 0.001$; Unind=Uninduced. (D) OsteoImage fluorescence readings were normalised to cell count, based on PI staining (mean ± SD, n=6).

A

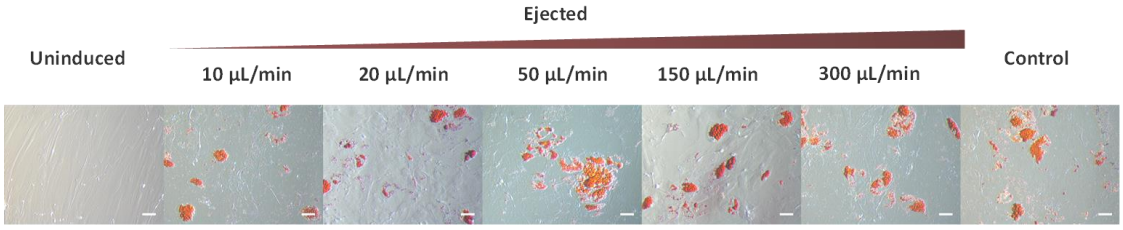

B

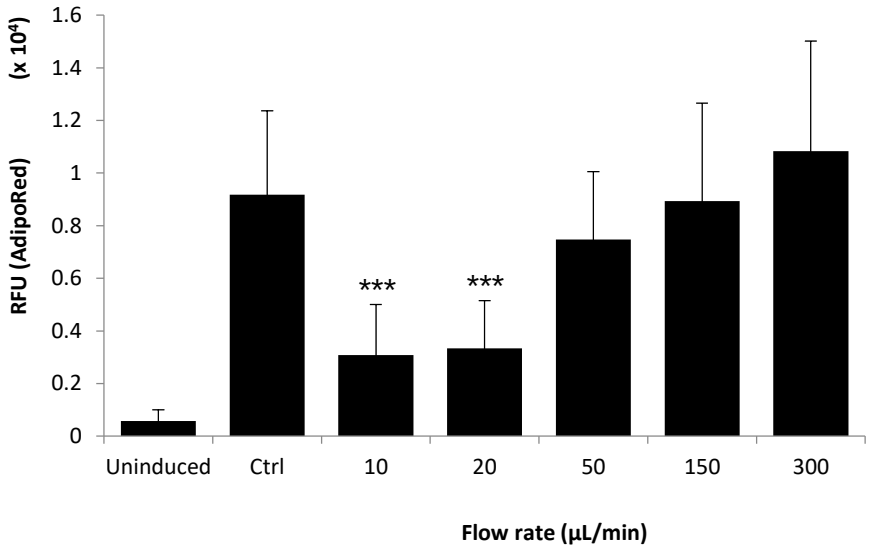

Figure 5.10: **Effect of ejection rate on differentiation potential of hMSCs ejected via 30G needles, cultured in monopotential adipogenic media.** (A) Representative bright field microscopic images showing ejected hMSCs after culturing in adipogenic media for 21 days. Adipogenic differentiation was assessed by Oil Red O staining (Scale bar=50µm). (B) Quantification of AdipoRed staining for intracellular lipid content in hMSCs cultured with adipogenic media for 21 days. Each bar represents mean fluorescence values ± SD, n=9 in three independent experiments using two donors. Asterisks represent statistically significant difference from directly plated control using ANOVA and Dunnet's *post-hoc* test (***$p \leq 0.001$).

5.3.5 Effects of varying ejection rate on the chondrogenic differentiation capacity of ejected hMSCs

To examine the possible effect of initial seeding density on chondrogenic differentiation capacity, an additional control was included, whereby 30% of the original seeding density was used (21,000 cells/aggregate) instead of the full seeding density of 70,000 cells/aggregate culture. This is roughly equivalent to the percentage of cell dose delivered as viable cells at the lowest flow rate under investigation (10 µL/min), as previously discussed in Chapter 4. This control is referred to as the low-density aggregate culture.

There was no significant difference between the amount of DNA content in the ejected hMSCs samples and the control samples (Figure 5.11A). However, there was a significantly lower amount of DNA in the lower cell density control relative to the full seeding density one.

Glycosaminoglycan (GAG) production results were similar to DNA content results, whereby the lower density control and samples ejected at 10 µL/min exhibited significantly lower total GAG content ($p<0.01$) relative to the full-density control (Figure 5.11B). However, there was no significant difference when GAG content was normalised to DNA content (Figure 5.11C), suggesting that, there were similar amounts of GAG deposition in hMSCs ejected at the various flow rates on a per cell basis, as well as at the two different seeding densities employed for the control samples.

Samples were assessed for total collagen content using a chloramine T hydroxyproline assay. There was no significant difference in total hydroxyproline content between the

two control cultures and the various ejected hMSC samples (Figure 5.11D). However, normalisation to DNA at day 28 showed significantly increased production of hydroxyproline in the low-density aggregate control sample ($p<0.0001$) and the one ejected at 10 µL/min ($p<0.05$) relative to the full-density control culture (Figure 5.11E). In addition, there was a significantly lower hydroxyproline content in the ejected sample (10 µL/min) relative to the low-density control culture ($p<0.05$).

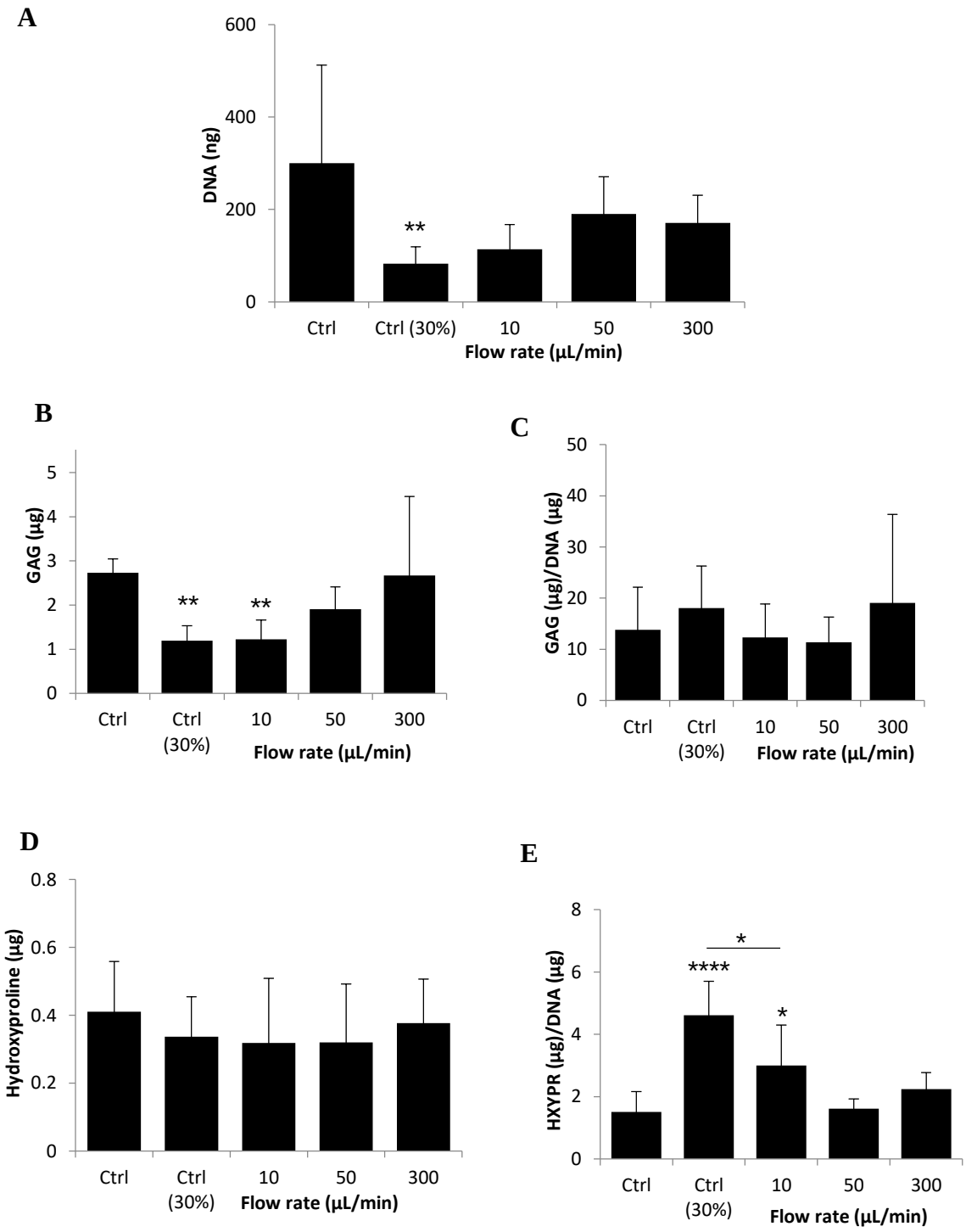

Figure 5.11: **Effect of ejection rate on chondrogenic differentiation capacity of hMSCs ejected via 30G needles, cultured in chondrogenic media for 28 days.** (A) Total cellular DNA content, quantified using PicoGreen, in hMSCs ejected at various flow rates. Bars represent mean ± SD ($n \geq 6$; two donors in three independent experiments); Asterisks represent statistically significant difference from control using Kruskal-Wallis test and Dunn's *post-hoc* test (**$p \leq 0.01$) (B) GAG production by hMSCs as a function of ejection rate. Values are mean ± SD ($n \geq 6$); Asterisks represent statistically significant difference from control using Kruskal-Wallis test and Dunn's *post-hoc* test (**$p \leq 0.01$). (C) GAG content was normalised to DNA content, revealing no significant difference between ejected MSCs and control at 28 days. (D) Hydroxyproline (HXYPR) production by hMSCs ($n \geq 6$). (E) HXYPR content was normalised against DNA ($n \geq 6$); Asterisks indicate statistically significant difference to control, using one-way ANOVA and Tukey's *post-hoc* test (*$p \leq 0.05$; ****$p \leq 0.0001$).

5.4 Discussion

The efficiency of differentiation of hMSCs is a critical factor for the clinical use of hMSCs in cellular therapy applications. Mechanical stimulation, such as shear stress, can directly influence the fate of undifferentiated stem cells [224, 239]. In this chapter, the trilineage differentiation capacity in ejected hMSCs was explored in more detail. Since one of the main consequences of varying ejection rate is achieving different percentages of the original cell dose being delivered, a separate set of experiments were carried out first to investigate the dependence of the differentiation capacity on initial cell number.

Deducing the impact of physical cues on cell differentiation fate is difficult to explore within the chemically defined environments of monopotential induction media. By using 'mixed' media, a bipotential setting is provided whereby the appropriate chemical differentiation cues required for both osteogenesis and adipogenesis are available in the media. This allows us to study the impact of physical cues, such as mechanical forces, on cell lineage fate.

5.4.1 Effect of initial cell seeding number on trilineage differentiation capacity of hMSCs

Osteogenic differentiation capacity of hMSCs when cultured at different initial seeding densities was first investigated by analysing the extent of mineralisation at day 21 using the OsteoImage^{TM} assay. The deposition of hydroxyapatite by hMSCs was analysed after culturing in either monopotential osteogenic or bipotential osteogenic/adipogenic media. No statistically significant differences were observed in both types of media, with a small decrease only at initial seeding of <5000 cells/well.

This corresponds to ~20% of the original cell dose used for these experiments. This data allowed us to postulate that the different initial cell seeding numbers from the various ejection rates tested will have negligible effects on mineralisation, even at the lowest flow rate under investigation (~35% of cell dose delivered at 10 µL/min). These results are consistent with findings from previous studies carried out on various scaffolds, which demonstrated that higher seeding densities do not necessarily produce enhanced results concerning proliferation and differentiation [240, 241]. Holy *et al.* investigated the effect of initial seeding density on rat bone marrow-derived cell differentiation on PLGA scaffolds, revealing that final mineralised tissue formation was independent of initial seeding density [242]. Another *in vivo* study also revealed a similar relationship between MSC density per cm^3 scaffold and bone yield, whereby doubling initial seeding density did not result in a significant increase in bone yield [243].

One uncontrolled aspect of these experiments was cell proliferation. Since cells continued to divide over the course of the 21-day experiment, cell density increased over time. A trend could be clearly observed, whereby the low initial seeding numbers corresponded to low final cell numbers at day 21. However, when expressed as fold change in cell number to day 0 (Figure 5.2 and Figure 5.4B), it was found that lower seeding densities corresponded to the highest proliferation rate. Thereby, proliferation rates were enhanced at lower seeding densities (Figure 5.2B and Figure 5.4B). This agrees with a previous study, which stated that proliferation rate of hMSCs increased at low plating densities [244].

In contrast to the effect of initial cell number on the osteogenesis marker quantified, adipogenic differentiation capacity was influenced by cell seeding number (Figure 5.5

and Figure 5.7). This result is in line with findings from studies by other groups [245-247].

For chondrogenesis studies, hMSC aggregate cultures made up of two different seeding densities were studied for their biochemical properties, in terms of absolute values per construct and values normalised to DNA content. In comparison with the full-density control, the low-seeding density control had significantly lower DNA content and total GAG content. This data agrees with a number of other studies using MSCs, which show an increase in GAG synthesis with increased seeding density up to a certain limit [248, 249] and where higher initial seeding density produced more proteoglycans when cultured in a gelatin matrix [250]. However, data normalised to DNA content showed that GAG synthetic capacity was similar for both seeding densities investigated. Total collagen content did not vary between both seeding densities, as shown by the hydroxyproline assay, but normalised HXYPR/DNA data showed a significant increase in hydroxyproline production per cell with the lower density culture relative to the higher seeding density one. This agrees with a previous study carried out by Revell *et al*., where increasing seeding density was shown to have an inverse relationship with total collagen content per wet weight [249], and the same was observed in MSCs cultured in hyaluronic acid hydrogels [251].

It was therefore decided to focus on osteogenesis, where mineralisation was shown to be independent of initial cell seeding density, as a model for studying the potential impact of ejection rate on differentiation fate choice and capacity of ejected hMSCs. A bipotential differentiation setting was used to allow the investigation of whether varying ejection rate would cause hMSCs to preferentially differentiate into certain lineages, independent of chemical dosing variables.

5.4.2 Effect of varying ejection rate on trilineage differentiation capacity of ejected hMSCs

To assess the influence of varying ejection rate on ejected hMSCs differentiation fate (cultured in bipotential adipogenic/osteogenic media formulation), the experiments performed to evaluate the impact of initial seeding density were replicated using hMSCs ejected at various flow rates.

In monopotential osteogenic media, two variables are in action to direct undifferentiated hMSCs down a certain differentiation pathway. The first is biochemical induction by the specialised media, and the second is the effect of exposure to mechanical forces of ejection. Staining of hydroxyapatite, a late osteogenic marker, revealed that the ejected hMSCs had passed all the differentiation stages when cultured in osteogenic media. In this case, the lowest flow rates exhibited the lowest levels of mineralisation and the lowest final cell numbers at day 21 (Figure 5.8B). This suggests that prolonged exposure to mechanical forces of ejection on hMSCs (at 10 µL/min) influenced the ability of the ejected cells to differentiate along the osteogenic lineage in a monopotential setting.

Bipotential media is permissive for both adipogenic and osteogenic differentiation, thereby allowing the investigation of the impact of ejection forces on differentiation independent of chemical induction. In this case, there was no significant difference in the degree of mineralisation between all samples. Normalised values showed a significantly higher level of mineralisation per cell at the lowest flow rate relative to control. This means that samples ejected at 10 µL/min yielded the same total mineral deposition as other samples but had more mineral deposition per cell. This suggests

that hMSCs ejected at this rate either preferentially underwent osteogenic differentiation relative to the control and other flow rates under investigation, started differentiating earlier, or had enhanced osteogenic efficiency per cell. Alternatively, this may be due to a selection of a sub-population of hMSCs ejected. These differentiation trends confirmed that prolonged exposure to the mechanical forces generated at 10 µL/min, rather than cell density and associated cell-cell interactions, contributed to cell differentiation fate.

It has been established (Section 5.3.2) that a lower cell number will adversely affect adipogenic differentiation capacity. This affected the adipogenic differentiation capacity of ejected hMSCs at the various flow rates under investigation. The lowest flow rates exhibited significantly lower levels of adipogenesis in monopotential adipogenic media, and there was a clear trend of increasing adipogenesis with increasing flow rates. This corresponded to a proportional relation between the extent of adipogenesis and cell recovery at the various flow rates under investigation.

The biochemical composition of pellet constructs, made up from hMSCs ejected at various rates, were analysed to determine the effects of ejection rate on chondrogenic differentiation capacity. It can be inferred from Figure 5.11A that the various ejection rates used in this study did not affect cell proliferation over the 28-day culture period. There were no significant differences in both absolute and normalised amounts of GAG and hydroxyproline between the full-seeding density control sample and samples ejected at 50 and 300 µL/min. This is probably due to the low duration of exposure to mechanical forces at these rates.

The lower-seeding density aggregate culture was used as an additional control to compare with samples ejected at 10 µL/min, in order to exclude the possible effects of the lower cell numbers ejected at this flow rate. Interestingly, results demonstrated that ejection of hMSCs at 10 µL/min contributed to a significant decrease in collagen deposition at day 28 relative to the comparable lower-seeding density control culture. It should be noted that the hydroxyproline assay does not distinguish types of collagen and thus, this difference is associated with a decreased production of total collagen and not necessarily of a specific type. Although previous studies have demonstrated an enhanced collagen synthesis in response to shear stress [252], a more detailed study has specified that there is a decrease in collagen type I expression in hMSCs cultured in a bioreactor (exposed to shear stress) relative to static cultures. There was also an increase in collagen type II production [253]. In addition, MSCs with hypertrophic phenotype produce collagen type I preferentially over collagen type II [254]. Promoting differentiation while preventing hypertrophy of chondrogenic MSCs is vital, and therefore a more detailed investigation of this observed effect on collagen content is required.

5.5 Conclusions

In summary,

- The amount of hydroxyapatite deposition at day 21 is approximately the same in all samples with initial seeding densities ≥5000 cells/well, with no statistically significant differences in amounts deposited between different initial cell numbers seeded. The cell numbers delivered at all flow rates are within the linear range. Therefore, it was postulated that differences in cell numbers would not influence final mineralisation results.

- In monopotential osteogenic and adipogenic media, the lowest flow rates exhibited the lowest levels of differentiation at day 21.
- In bipotential media, there was no significant difference in the degree of mineralisation between ejected samples at day 21. Normalised values showed a significantly higher level of mineralisation per cell at 10 µL/min. This suggests either preferential osteogenic differentiation or more efficient osteogenesis per cell upon prolonged exposure to mechanical forces of ejection, or alternatively due to a selection of a sub-population of hMSCs ejected from the delivery device.
- Biochemical composition of chondrogenic aggregate constructs showed that the ejection rates employed did not affect cell proliferation or absolute and normalised amounts of GAG over the 28-day culture period. Ejection of hMSCs at 10 µL/min contributed to a significant decrease in collagen deposition relative to the comparable lower-seeding density control culture.

MSC lineage commitment and differentiation are intricate processes, and can be sensitive to physical cues resulting from the injection process. Ejection rate should be carefully considered as a variable when injecting cells for regenerative medicine applications. The results from this study prove the potential of ejection rate to affect differentiation capacity of ejected hMSCs, whether as a result of the cell numbers delivered or through influencing fate choice of ejected hMSCs.

Chapter 6| Biomaterial-assisted delivery for improving delivery efficiency of hMSCs

6.1 Introduction

Cell suspensions can be easily administered via small diameter needles or cannulas to the target site with minimal invasiveness. However, cell loss has been reported to be observed within the first minutes of implantation [24], with typically only <10% of injected cells surviving and engrafting at the site of interest [22, 189, 255]. Consequently, increasing the percentage of viable cells delivered and retained post-injection is critical to the success of cell transplantation procedures [256].

Developing effective delivery systems poses major challenges to the clinical implementation of cell-based therapeutics [189]. Biomaterials have the potential to be used as cell delivery vehicles, where they can provide physical support and protection for cells to ensure retention at the target site, and as carriers to stimulate host cell recruitment and differentiation [257]. Therefore, one of the main translational challenges to the implementation of cell therapy for high accuracy applications is the need to develop injectable biomaterials that can be easily delivered, and fit both the mechanical and biological requirements of the proposed application. This will ensure sufficient cell survival and reproducibility of administration for maximal therapeutic efficacy [20].

An ideal cell carrier for injectable cell therapy applications should ensure maximal cell recovery and preservation of cell viability and functionality post-transplantation. It should encourage functional tissue growth *in situ*, possess appropriate biodegradation properties, maintain its mechanical integrity during injection, and have the capacity to control the spatial and temporal release of any incorporated biomolecules.

The success of hMSC-based therapies is also largely dependent on the ability to maintain multipotency and regulate differentiation. An important component of the cell microenvironment is the surrounding matrix, which includes numerous biophysical and chemical signals. Interactions of MSCs with their microenvironment play an important role in their morphogenesis and differentiation. Stem cell fate is known to be regulated by biochemical and biophysical cues from the microenvironment, including the ECM [258]. Numerous studies have highlighted that the material surrounding a stem cell is vital in determining its fate [259-264]. An intricate range of environmental effectors, experienced during the delivery procedure and post-transplantation, can have an impact on cell function (Figure 6.1) [265]. Biomaterials can mimic the physical, chemical, and mechanical properties of the ECM to promote cell retention, proliferation, and differentiation [266]. Biomaterial-assisted cell therapy can be utilised to provide appropriate environmental cues to support cell function, acting as an instructive and efficient cell delivery platform.

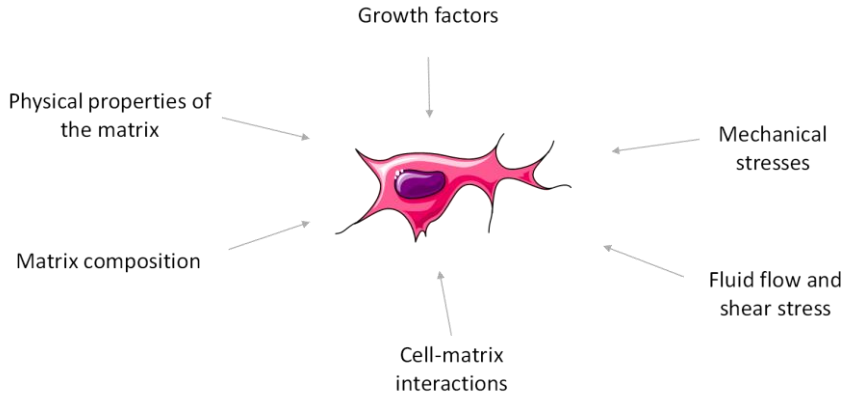

Figure 6.1: **A wide range of environmental factors can influence cell functionality during delivery and post-transplantation**. Figure produced using Servier Medical Art.

Naturally derived biomaterials, such as polysaccharides and glycosaminoglycans, have been used extensively in tissue engineering applications. This class of biomaterials possesses good biocompatibility and may exhibit inherent bioactivity and cellular interaction that can facilitate tissue integration. Artificial materials are usually easier to control [267], but the required conditions for the gelling of many synthetic hydrogels are not compatible with mammalian cells [268]. The biological characteristics of polymers of natural origin makes them one of the most appealing choices for cell delivery applications. Therefore, various natural biomaterials were selected to determine the impact of the addition of these carriers on cell recovery and differentiation capacity post-ejection via narrow-bore syringe needles.

Collagen has been widely investigated for tissue engineering applications due to its biocompatibility, ease of modification, biodegradability, and minimal immunogenicity [269-271]. It is also inherently cell-adhesive, being a major component of the ECM and providing support to connective tissues such as bones, cartilage, skin and blood vessels [272]. Collagen has been shown to support cell growth in 3D cell culture

studies and *in vivo* [269-271, 273-275]. Consequently, collagen matrices, preferably accompanied with added ECM components and/or growth factors, should provide a favourable environment for transplanted cells. Twenty-seven types of collagen have been identified, but collagen type I is the most investigated for biomedical applications [276]. Although the ECM of CNS tissue contains relatively little fibrous collagen and the brain normally expresses type IV collagen only, collagen type I is a better scaffold candidate than type IV for brain applications. Collagen type IV is the main ECM secreted by fibroblasts following trauma and has shown to induce scar formation and inhibit axonal regeneration [277]. In contrast, collagen type I has been widely applied as scaffolds for cell delivery in animal models of traumatic brain injury with good biocompatibility [278, 279]. Most reports of scaffolds for brain injury applications have employed type I collagen [280].

Gelatin is a denatured derivative of collagen that possesses biocompatible, biodegradable, and non-antigenic properties. It contains the Arg–Gly–Asp (RGD)-like sequence that promotes cell adhesion [281-283]. Gelatin is amphoteric, and the pH at which the net charge is zero is known as the isoelectric point [284]. Gelatin is obtained by acid or alkaline processing of collagen, resulting in two possible types of gelatin with different isoelectric points, depending on the collagen pre-treatment method prior to the extraction process [285]. Type A (acid) gelatin has a broad isoelectric range between pH 7-9. Type B (limed/alkaline) gelatin has a narrower isoelectric range between pH 4.7 and 5.4 [286]. Alkaline pre-treatment hydrolyses the amide groups of asparagine and glutamine into carboxyl groups. The higher density of carboxyl groups results in a negative charge and lowers the isoelectric point of gelatin to 5.0 [287]. On the other hand, the electrostatic nature of collagen is barely modified through the acidic treatment process, resulting in an isoelectric point similar to that of collagen [288].

ECM is a complex cellular environment largely made up of glycosaminoglycans and fibrous proteins (e.g., collagen, elastin, fibronectin and laminin) [289]. Tissue homeostasis necessitates dynamic reciprocity between cells and their microenvironment, in which cells maintain the ECM which, in turn, provides cues to regulate cell behaviour [290]. The ECM of mammalian tissues can be isolated, decellularised and used as biological scaffolds [291]. Scaffolds which have been obtained from tissues such as the small intestine have been reported to facilitate restoration of different tissues, such as musculoskeletal tissues [292, 293]. ECM plays a key role in modulating cell signalling and influences the functionality of cells with which it interacts [291].

Carboxymethyl cellulose (CMC) is a biodegradable anionic cellulose derivative with excellent film-forming properties [294]. It has gained interest due to its high viscosity, hydrophilicity, and biocompatibility [295], and has been used in various drug delivery applications [296-298]. Its carboxylic or hydroxyl groups serve as active sites for preparing CMC gels [299]. Despite these successful applications and their low cost, cellulose derivatives have not been widely used in the bioengineering field [300, 301].

The cellular models employed in the studies herein have provided valuable information into the impact of the ejection process on cell viability, functionality and differentiation. It has been demonstrated in previous chapters that delivery of cell suspensions at a low flow rate will negatively impact cell recovery. In this chapter, biomaterial-based formulations were selected as candidate biomimetic carriers to maximise hMSC recovery at low ejection rates. In addition, this study explored whether the use of naturally derived biomaterials, in an attempt to recreate ECM cues, will influence cellular differentiation and potentially stimulate endogenous

regeneration. Despite the availability of a wide variety of biomaterials for clinicians to use, there still remains a preference for simple biomaterials that have tuneable mechanical and biological properties, are easy to prepare, and can be used for a range of applications. The use of simple biomaterials as injectable cell carriers is explored to shed some light on the potential for future development of tailored biomaterials for efficient cell therapies.

Protein-based polymers have the advantage of mimicking the characteristics of the natural ECM, and thereby have the potential to influence the growth and organisation of transplanted cells in addition to protecting them [301]. Moreover, the supplementation of algal cultures with CMC, as a modifier of interfacial properties, has been reported to protect algal cells against hydrodynamic stress [302]. The impact of biomaterial-assisted delivery on cell viability, proliferation capacity and differentiation behaviour was investigated. A secondary aim was to evaluate whether there was a synergistic effect of cell carrier and mechanical forces on the differentiation of hMSCs when ejected.

6.2 Experimental Design

For a comprehensive description of materials and methods employed for culture of hMSCs, preparation of cell carriers, cell ejection and differentiation protocols, and assay procedures, see Chapter 2: Materials and Methods. The use of multipotent hMSCs for investigating biomaterial-assisted delivery allows us to examine the effects of biomaterial-assisted ejection on cell commitment and differentiation capacity in detail.

Herein, a simple biomaterial-based strategy is demonstrated to overcome the problem of low cell recovery at slow ejection rates. Several protein-based polymers (namely 1.75 mg/mL collagen, 1.75 mg/mL bone decellularised ECM [182], and 20 mg/mL (2%) gelatin type B), and one carbohydrate-derived biomaterial (5 mg/mL (0.5%) CMC) were selected to investigate injectable biomaterial-based delivery of hMSCs. The choice of biomaterials reflects the overarching aim of this work, which is to achieve convenient, reproducible and clinically relevant delivery of hMSCs to facilitate low-dosage cell therapies.

Osteogenic differentiation potential was selected as a model for the investigation of potential impact of biomaterial-assisted delivery on cell commitment. Osteogenesis is a robust, well-established *in vitro* cellular model of differentiation in hMSCs with well-defined assays and measurable outputs [303]. In addition, Chapter 5 shows that mineralisation at day 21 was not significantly affected by varying initial cell seeding numbers. Therefore, osteogenesis of hMSCs was used as a model to study potential impact of various cell carriers on differentiation capacity in bipotential 'mixed' media. The use of this bipotential setting permitted the examination of the impact of cell carriers on osteogenesis without the intrusive effects of chemical induction, thereby assessing how choice of cell carrier affects the osteogenic differentiation potential of ejected cells. Osteogenesis was assessed by measuring various markers of osteogenesis, including ALP activity, hydroxyapatite deposition, and osteocalcin (OCN) (Figure 6.2).

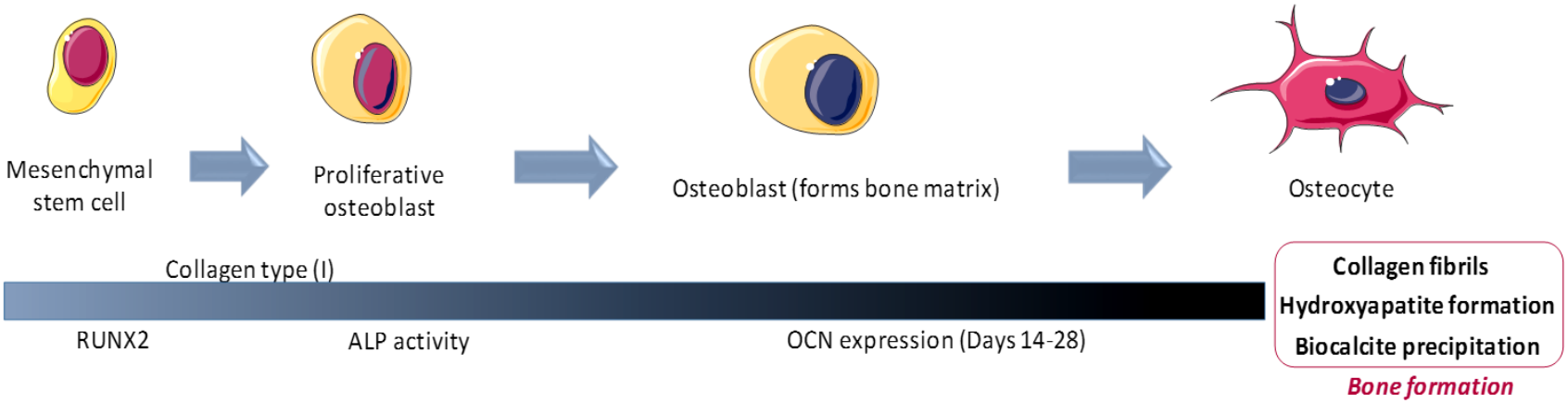

Figure 6.2: **Osteogenic differentiation pathway of MSCs**. Osteogenesis is characterised by the involvement of runt-related transcription factor 2 (Runx2), increased alkaline phosphatase (ALP) activity, collagen type I (COL1), osteopontin, osteocalcin (OCN), and calcification of the ECM [224]. Figure produced using Servier Medical Art.

hMSCs were suspended in PBS and incorporated into the carriers indirectly via gentle mixing to give a final cell density of $7x10^5$ cells/mL. Cell/carrier mixtures were set aside for 20 minutes, to represent delay time between loading and injection in cell transplantation procedures [101], before ejection through 30G needles at 10 µL/min using the syringe pump. The ejected samples were then transferred into the appropriate well plates. For differentiation studies, bipotential differentiation media was added 24 hours post-ejection. After culture in bipotential 'mixed' media for 21 days, osteogenesis was assessed by measuring various markers of osteogenesis, including ALP activity, hydroxyapatite deposition, and staining for osteocalcin (OCN). This experimental design is depicted schematically in Figure 6.3.

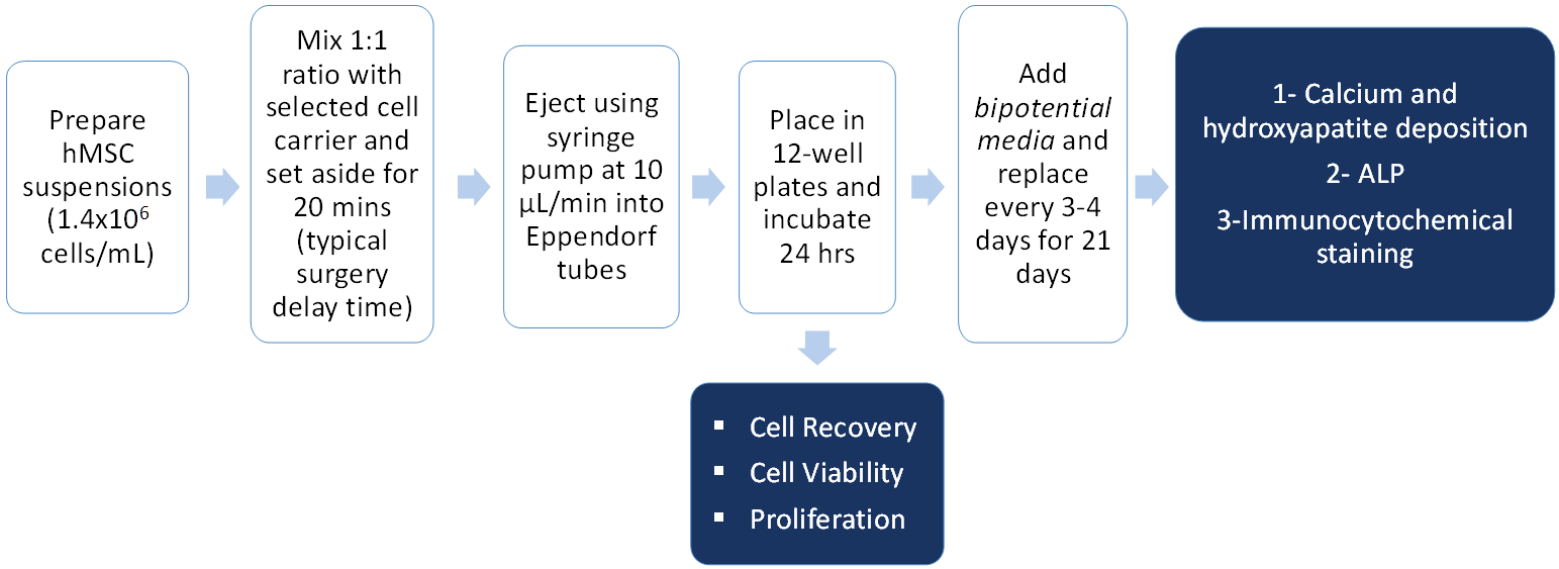

Figure 6.3: **Schematic presentation of the methodology used to explore the effects of various cell carriers on hMSC delivery.** Efficacy of delivery, in terms of cell recovery, viability and proliferation capacity, was assessed. In addition, various parameters of osteogenic differentiation were measured to determine the potential impact of various cell carriers on osteogenic differentiation capacity.

6.3 Results

6.3.1 Effects of biomaterial-assisted cell delivery on cell dose recovery and viability

As retention in the delivery device and shear stress experienced during the ejection process may result in a decrease in the number of viable cells delivered, it was hypothesised that co-injecting the cells with viscous carriers may improve recovery and viability. After screening various potential protein- and polysaccharide-based biomaterials for injectability, collagen, gelatin, bone decellularised ECM, and high viscosity CMC solutions were selected to test this hypothesis. The percentage of cell dose delivered as viable cells was assessed using the PrestoBlue assay. By incorporating the cells in a protective viscous medium, improved cell delivery was demonstrated (Figure 6.4A). Suspending cells within 2% gelatin type B exhibited the best cell recovery; with a significantly improved percentage of cell dose delivered as viable cells of 87.5 ± 14.1% compared to 32.1 ± 19.1% of the cell dose delivered when ejected in PBS. In contrast, collagen and ECM provided significantly lower percentages of viable cells delivered at 53.4 ± 24.4% and 60.7 ± 10.1% respectively relative to gelatin and CMC.

When comparing two different concentrations of CMC, it was noted that the lower concentration (0.25%) resulted in a markedly lower percentage of the dose being delivered as viable cells (Figure 6.4B). This difference in proportion of cell dose delivered was statistically significant (p=0.05).

A

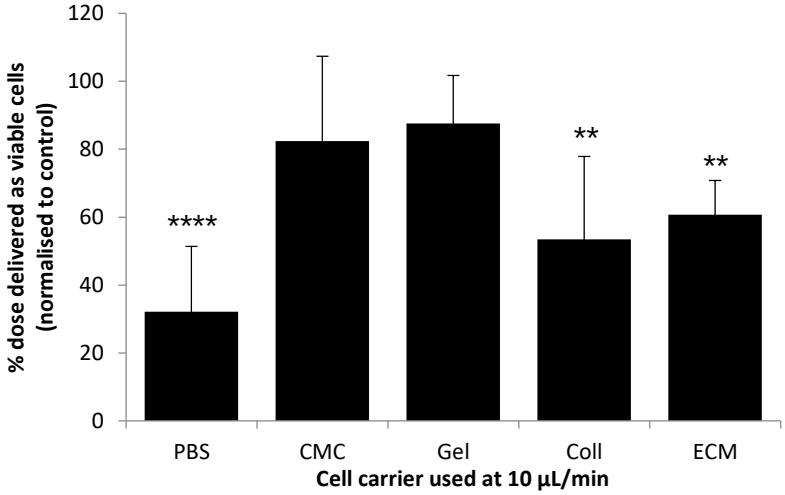

B

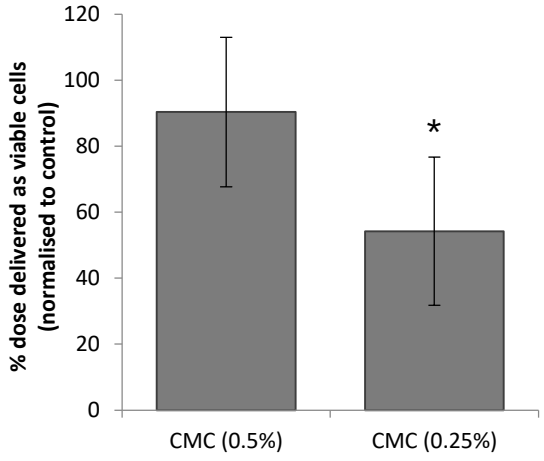

Figure 6.4: **Cell recovery, expressed as percentage of the cell dose delivered as viable cells, after ejecting hMSCs, suspended in various carriers, via 30G needles at 10 µL/min.** (A) Proportion of hMSCs delivered, measured using PrestoBlue, within phosphate buffered saline (PBS), carboxymethyl cellulose (CMC), gelatin (Gel), type I collagen (Coll) and bone extracellular matrix (ECM). Data represents averages from three donors in five independent experiments (n=5; mean ± SD). Data were normalised against control value of directly plated cells. (**$p \leq 0.01$, ****$p \leq 0.0001$ - one-way ANOVA with Dunnett's *post-hoc* test). (B) Percentage of cell dose delivered as viable cells when ejected at 10 µL/min via 30G needles when suspended within two concentrations of CMC (0.5% and 0.25%). Data represents averages from two donors (n=3; mean ± SD). Data were normalised against control value of directly plated cells. Asterisks indicate statistically significant differences between numbers of ejected cells compared with control ($^{*}p$=0.05- One-way ANOVA with Kruskal-Wallis analysis).

Live/Dead staining kit was used to assess viability within cells ejected, revealing a high proportion of viable cells among the various cell carriers investigated (Figure 6.5A). However, a visibly lower number of cells appeared in ejected samples suspended in PBS compared with other biomaterial-based carriers, endorsing results obtained using the PrestoBlue assay (Figure 6.4A).

All ejected cells attached to culture surfaces and displayed normal morphology. Brightfield images of the ejected samples 24 hours post-ejection (Figure 6.5B) displayed obvious presence of fibril-like structures along with the ejected hMSCs in samples ejected within collagen and bone ECM. The other investigated carriers showed no fibrillogenesis. All samples exhibited similar morphology to the directly plated control.

A

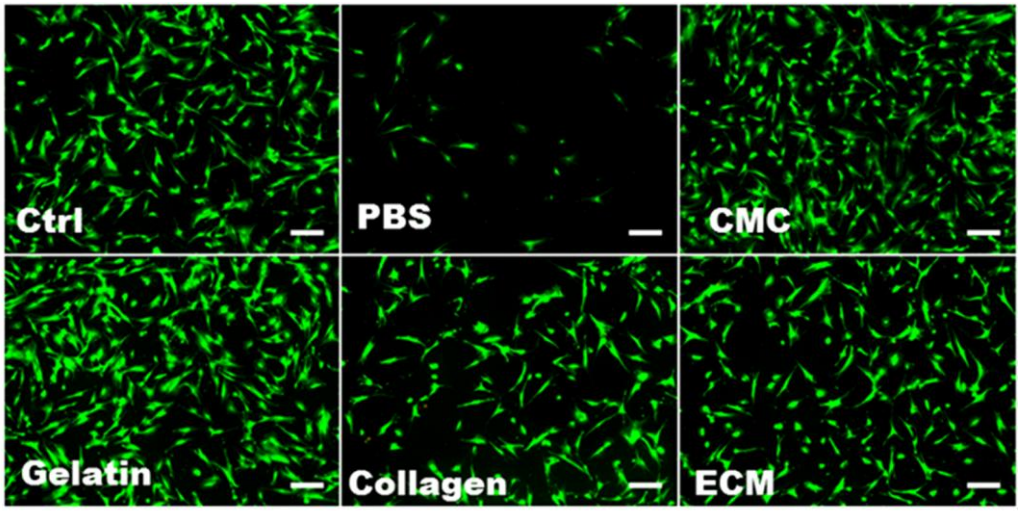

B

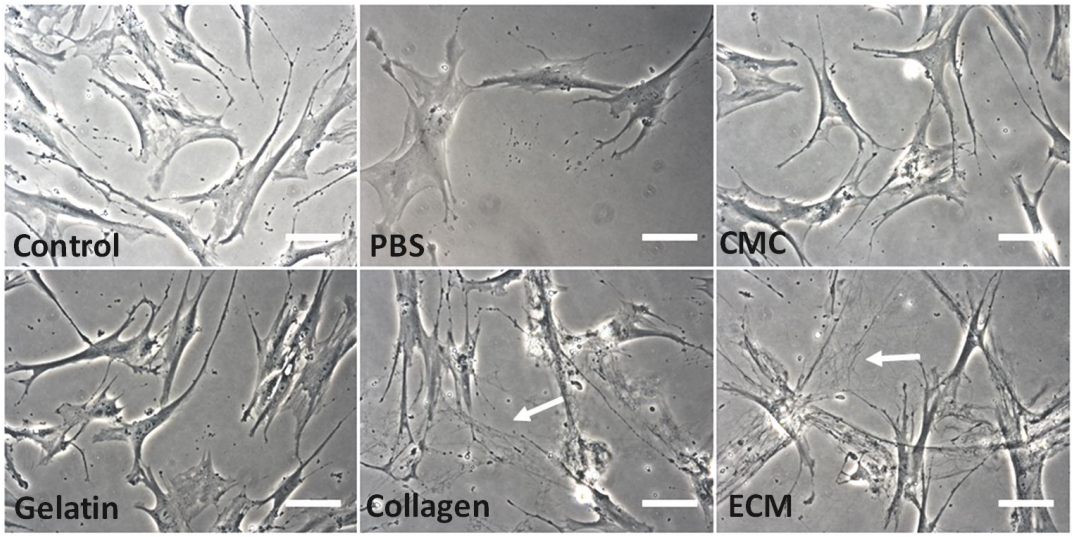

Figure 6.5: **Viability and morphology of hMSCs, suspended in various carriers, delivered via 30G needles at 10 µL/min**. (A) Representative Live/Dead-stained fluorescence images of hMSCs 24 hours following ejection at 10 µL/min, using various biomaterials as cell carriers (Scale bar=100 µm). (B) Representative brightfield images showing morphology of ejected hMSCs cultured for 24 hrs post-ejection. Bundles of fibrils surrounding the ejected cells are depicted by arrows (Scale bar=50 µm).

6.3.2 **Effect of biomaterial-assisted delivery on proliferation of ejected hMSCs**

Cells ejected within PBS and ECM showed significantly lower cell numbers relative to the directly-plated control cells at day 10 (Figure 6.6A). However, the proliferative ability of the ejected hMSCs was not significantly affected following ejection, with most cell carriers employed showing similar fold change in cell number at day 10 relative to the directly plated control (Figure 6.6B).

A

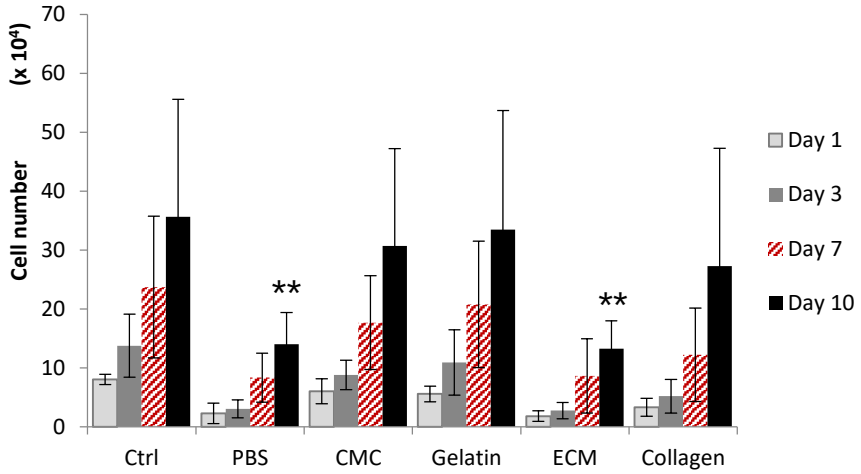

B

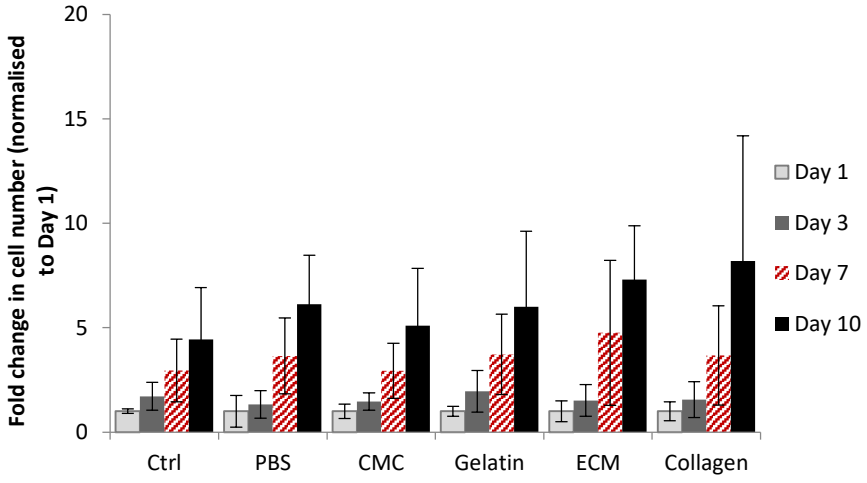

Figure 6.6: **Proliferation of hMSCs following ejection via 30G needles, suspended within PBS and in various biomaterial-based carriers, at 10 µL/min.** (A) Proliferation of hMSCs, measured using PrestoBlue, following ejection at 10 µL/min through a 30G needle. Results shown are mean values ± SD (*n*=4; two donors). Asterisks represent statistically significant difference to control at the corresponding day (**$p \leq 0.01$ - ANOVA and Dunnett's *post-hoc* test). (B) Proliferation of hMSCs given as fold change in number from day 1 of each sample, measured using PrestoBlue (mean ± SD; *n*=4, measured in two donors).

6.3.3 **Rheological studies of cell carriers employed**

The mechanical properties of the biomaterials used as cell carriers in this investigation were studied using rheology. Viscosity was determined at a constant shear rate of 1 s^{-1} using an Anton Paar cone plate (CP50-1) with a 50-mm diameter at 25°C. As shown in Figure 6.7A and Figure 6.7B, gelatin showed the lowest viscosity (0.010 ± 0.0007 Pa.s), while the viscosity of collagen employed was the highest at 0.655 ± 0.11 Pa.s.

The steady shear rheological properties of the biomaterial-based carriers used in this investigation are presented in Figure 6.7C. ECM, gelatin and collagen showed more significant shear-thinning profiles ($\Delta\eta \sim 10^4$ Pa.s) than both concentrations of CMC investigated ($\Delta\eta \sim 10^2$ Pa.s). Collagen had a viscosity of around 150 Pa.s at a shear rate of 0.01 s^{-1}, shearing down to 0.001 Pa.s at 1000 s^{-1}. It crossed over the 0.5% CMC profile at a shear rate of 2.6 s^{-1}. Gelatin exhibited a viscosity of around 1 Pa.s at a shear rate of 0.01 s^{-1}, shearing down to 0.002 Pa.s at a shear rate of 1000 s^{-1}, and not crossing over the profiles of both CMC concentrations under investigation.

A viscometric 3-step thixotropy test was also carried out using a PP25 plate to investigate recovery of material properties of the carriers following disruption by a high-magnitude shear-rate (Figure 6.7D). A high magnitude strain (10000 s^{-1}) was applied to break the biomaterial's structure, followed by a low level strain (1 s^{-1}) to observe the rate and extent of recovery of their bulk properties. This is considered a critical parameter for injectability [304]. CMC and collagen showed exceptionally fast and complete recovery of properties within seconds following stress-induced flow. ECM showed a more gradual recovery to almost 65% of its original properties at 180

seconds following strain removal. Gelatin recovered its viscosity within only a few seconds to almost 90% of its initial value, but started breaking down 70 seconds following strain removal. Due to their shear-thinning and self-healing properties, all carriers investigated were shown to be easily injectable through a narrow 30G needle (Figure 6.7E).

In addition, oscillatory rheological measurements were performed. Strain-amplitude sweeps were used to measure the storage (G′) and loss moduli (G'') of the employed biomaterials at varying shear strain (0.1% - 1000%). All cell carriers employed in this study, except CMC, showed higher storage moduli than loss moduli, with curves being parallel and almost linear, which confirmed their hydrogel nature. However, CMC, displayed a higher G'' than G', and should therefore be classified as a viscous carrier or a viscosity modifying excipient, and not a gel. As expected, the higher the viscosity of the material, the higher the values of the storage and loss moduli. The linear viscoelastic region (LVER), in which the sample can elastically strain and return to its original state once strain is removed, was also investigated using strain-dependent oscillatory rheology. All carriers displayed a broad linear viscoelastic region (Figure 6.8). Collagen and ECM also exhibited failure of the gel structure at high strains of around 65%.

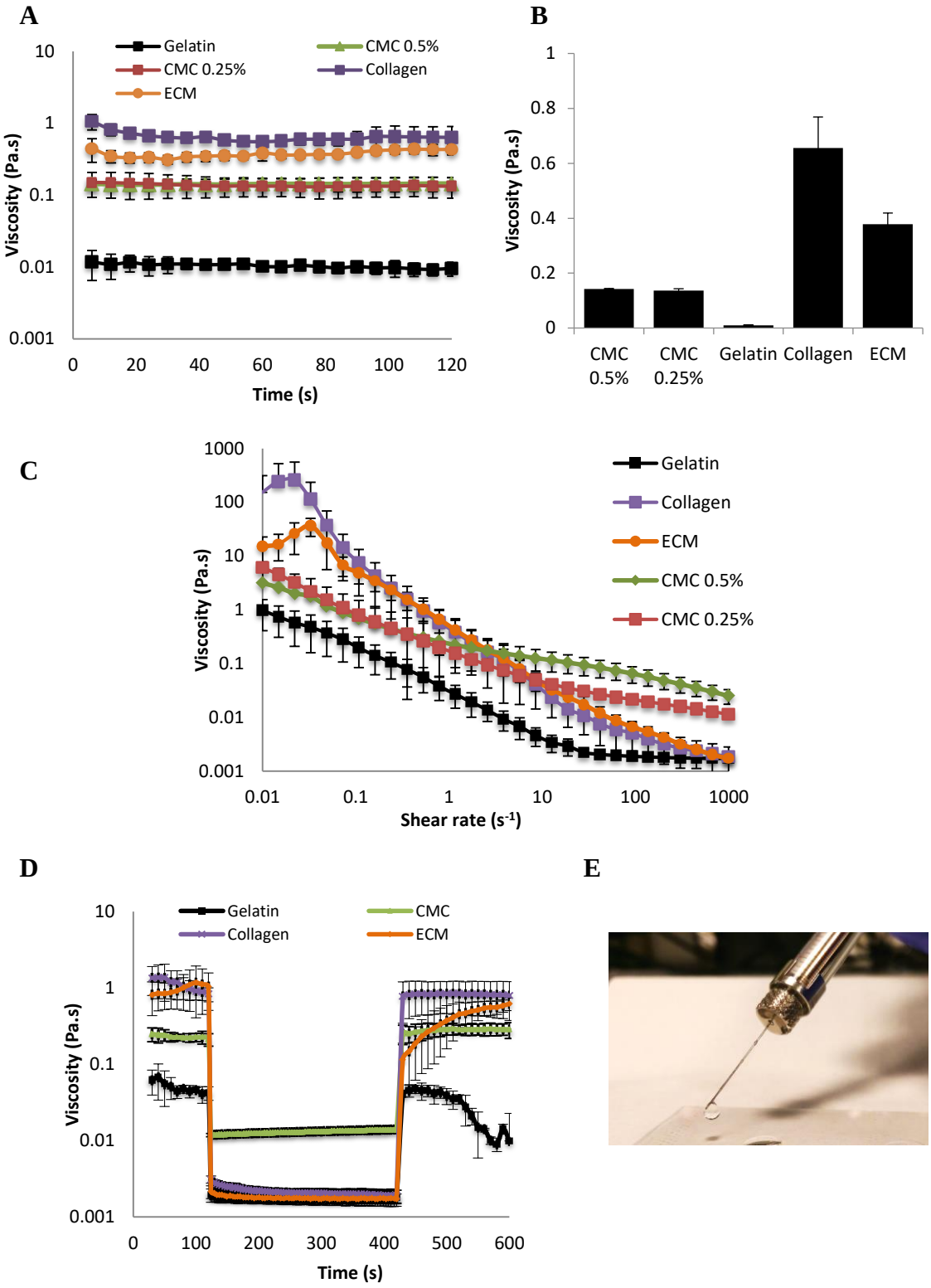

Figure 6.7: **Rheological characterisation of biomaterial-based cell carriers employed in this study (*n*≥3).** (A) Viscosities of the carriers were determined at 25°C with a constant shear rate of 1 s^{-1} (mean ± SD; *n*=3). (B) Viscosity of the carriers under investigation displayed on a linear scale, to clarify differences in viscosities. (C) Shear thinning properties of different carriers employed shown by steady shear rheological measurements. (D) Viscometric 3-step thixotropy test to display structure recovery of the hydrogel immediately after disruption due to a high-magnitude shear-rate strain (10000 s^{-1}), followed by a low magnitude strain (1 s^{-1}) to monitor recovery of bulk properties. (E) Figure shows 0.5% CMC ejected through a 30G needle, as a representative of injectability of biomaterials investigated.

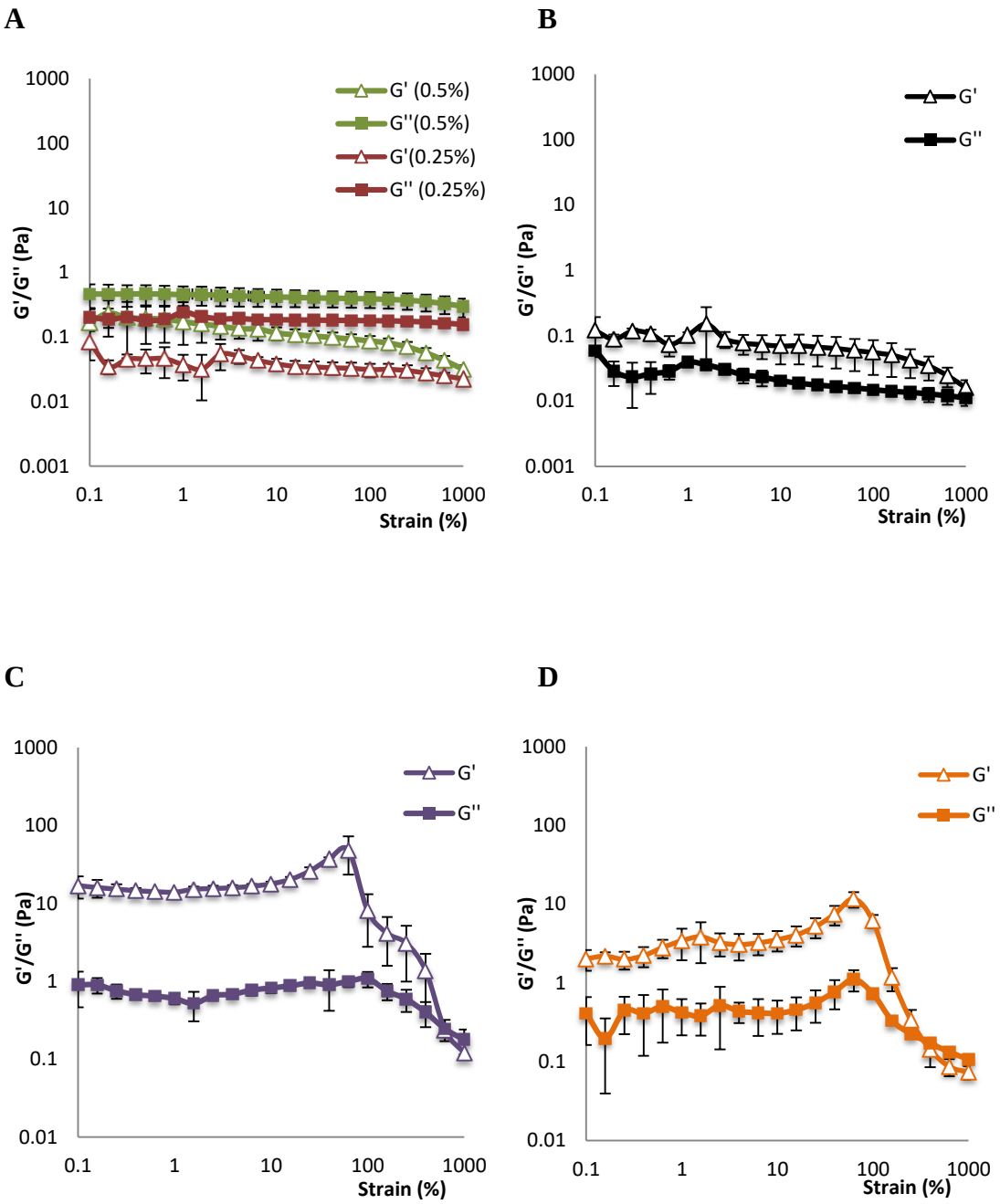

Figure 6.8: **Oscillatory rheological measurements of the biomaterial-based carriers to obtain storage (G') and loss (G'') moduli obtained from a strain-amplitude sweep (0.1–1000%) performed at 6 rad/s (*n*≥3).** (A) 5 (0.5%) and 2.5 (0.25%) mg/mL CMC (B) 20 mg/mL (2%) gelatin (C) 1.75 mg/mL collagen (D) 1.75 mg/mL bone ECM.

6.3.4 **Surface wettability of cell carriers employed**

A characteristic that may significantly influence cell adhesion is surface wettability, which is often determined by measuring the contact angle of the material. Contact angles of the various carriers under investigation were measured in order to examine the wettability of a glass surface. Soda-lime glass slides were used for measuring contact angles, which have similar wettability and surface tension in air to the borosilicate glass surfaces of the syringes [305]. A contact angle of 0° indicates total wetting and 180° indicates non-wetting.

All the biomaterials employed exhibited water contact angles ranging from 18° to 35° (Figure 6.9). PBS, collagen and ECM were the most hydrophilic, which was indicated by their lower contact angles. PBS displayed an angle of 18.6 ± 3.0°, while collagen was slightly less hydrophilic, displaying an angle of 24.0 ± 2.7°. Gelatin was the least hydrophilic among the biomaterials under investigation; displaying a contact angle of 34.3 ± 5.0° (Figure 6.9B). When comparing the two concentrations of CMC under investigation, it was found that the more dilute concentration exhibited a lower contact angle of 29.0 ± 5.8°, compared to 33.4 ± 4.1° for the higher concentration (Figure 6.9C).

A

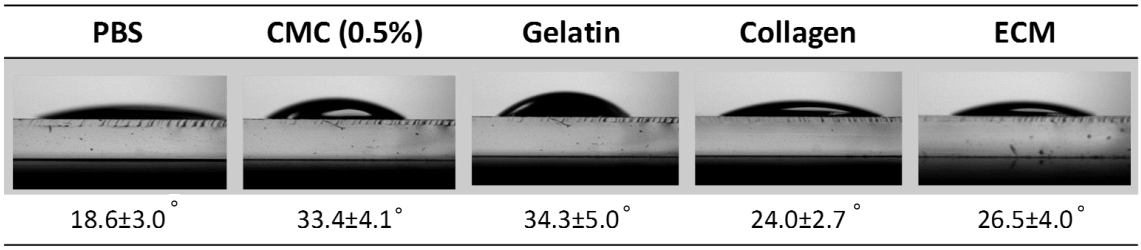

B

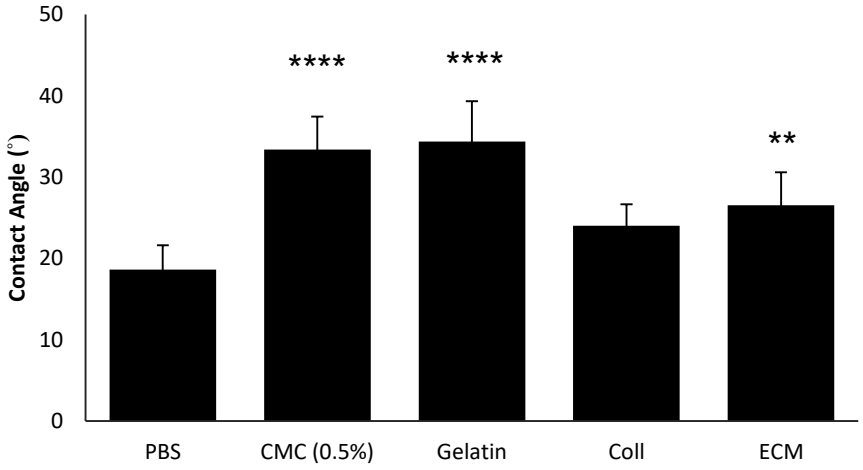

C

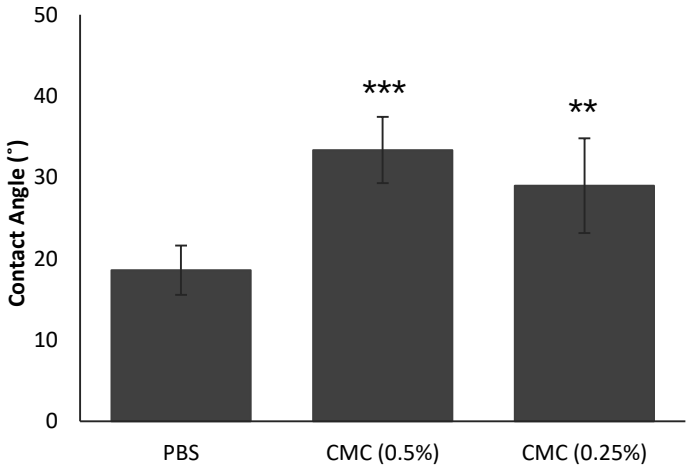

Figure 6.9: **Measurement of contact angles of biomaterial-based cell carriers on a glass surface.** (A) Contact angle images of various biomaterials employed on soda-lime glass slides measured at room temperature. (B, C) Measurement of contact angles of various carriers on a soda-lime glass surface. Each bar represents the mean ± SD (n = 5; **p<0.01; ***p<0.001; ****p<0.0001, relative to PBS).

6.3.5 Qualitative assessment of impact of using biomaterials as cell carriers on osteogenic differentiation capacity of ejected hMSCs

The ability of hMSCs to differentiate into multiple lineages is a functional criterion defining them [212]. Figure 6.10 represents the results obtained with cells from at least two separate donors, and shows that all directly plated control and ejected hMSCs completed osteogenic differentiation after 21 days of culture in bipotential conditions. Calcium mineralisation was first qualitatively measured by Alizarin Red S staining. Alizarin Red S stains calcium deposition orange-red, indicating mineralisation. Cells were also stained for hydroxyapatite deposition using the fluorescent OsteoImage™. All samples exhibited a mixture of cells displaying typical adipocyte morphology as well as mineralised bone nodules. PBS samples consistently displayed visibly lower numbers of cells exhibiting the adipocyte morphology, in addition to some cells displaying fibroblast-like morphology, typical of undifferentiated MSCs, at day 21 (Figure 6.10).

Production of mineral deposits is an important indicator of osteogenic differentiation [306]. At day 21, a higher extent of calcium and hydroxyapatite deposition in samples ejected within collagen and ECM was visible, compared to the directly plated control and other cell carriers (Figure 6.10). These findings suggested that osteogenic differentiation might be affected by the use of certain biomaterial-based carriers. This required further investigation to confirm these findings.

6.3.6 **Quantitative assessment of impact of using biomaterials as cell carriers on osteogenic differentiation capacity of ejected hMSCs**

A quantitative assessment of hydroxyapatite deposition and cell proliferation in ejected hMSCs was carried out. Fluorescence data from staining of hydroxyapatite deposition indicated that all control and ejected samples cultured in bipotential media showed mineralisation. Quantitative data in Figure 6.11A confirmed the qualitative assessment of images represented in Figure 6.10, by showing that cells co-injected with collagen, ECM and gelatin had significantly enhanced overall mineralisation relative to samples ejected within PBS (Figure 6.11A). PI-based cell counts of samples ejected within the various carriers under investigation are shown in Figure 6.11B. No significant difference in cell numbers was observed among all samples at day 21, despite differences in the number of cells initially ejected (Figure 6.4).

To determine whether ejection forces and biomaterial-based delivery have a synergistic effect on mineralisation in a bipotential differentiation setting, hydroxyapatite deposition in directly plated samples was compared with ejected cells, both suspended within the biomaterials under investigation (collagen and ECM). "Ejected" cells were ejected at 10 µL/min via 30G needles, and 60% of the initially ejected cell number was directly plated in 12-well plates as the "plated" control. The use of a lower cell number for directly plated sample was intended to account for the loss of cells during ejection (Figure 6.4). As shown in Figure 6.11C and D, there was no significant difference in hydroxyapatite deposition between the directly plated and ejected cells in collagen and ECM at day 21, both in terms of absolute and normalised values. This suggests that the more extensive mineralisation observed with these

carriers relative to PBS is due to interaction of hMSCs with the biomaterials, and is not augmented by the mechanical forces encountered by the cells during ejection.

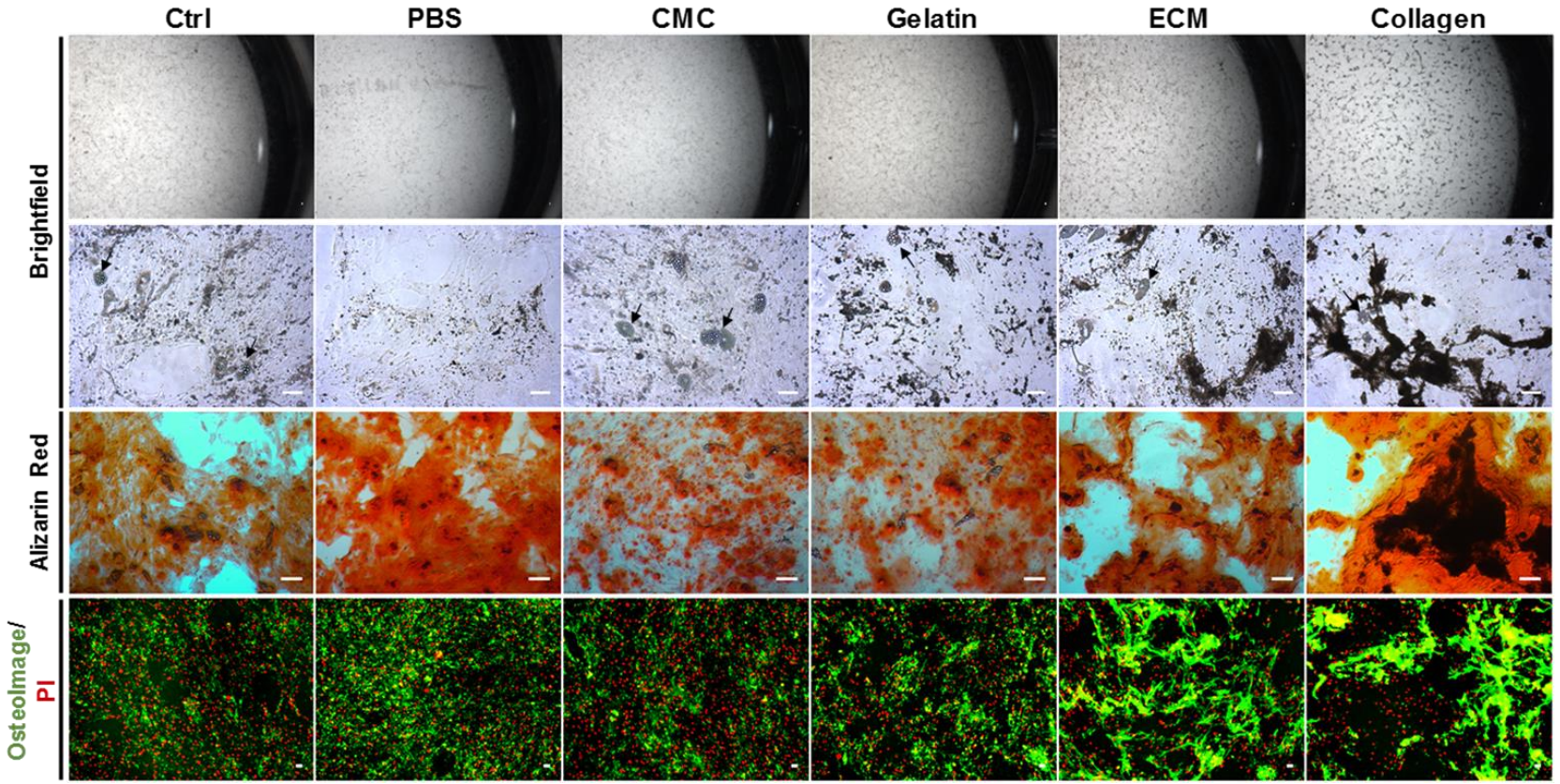

Figure 6.10: **Representative brightfield and fluorescence microscopy images displaying the qualitative assessment of osteogenic differentiation capacity of hMSCs post-ejection, after culturing in bipotential 'mixed' media for 21 days**. To assess the degree and distribution of mineralisation of the extracellular matrix, the last stage of osteogenesis, samples were observed using dissection microscopy, brightfield microscopy (10x), in addition to staining with Alizarin Red S (10x) and OsteoImage/PI (5x). Cells exhibiting typical adipocyte morphology are depicted in brightfield microscopy images using arrows (Scale=50 µm). Red represents calcium deposition, stained using Alizarin Red, and green depicts hydroxyapatite nodules stained using OsteoImage.

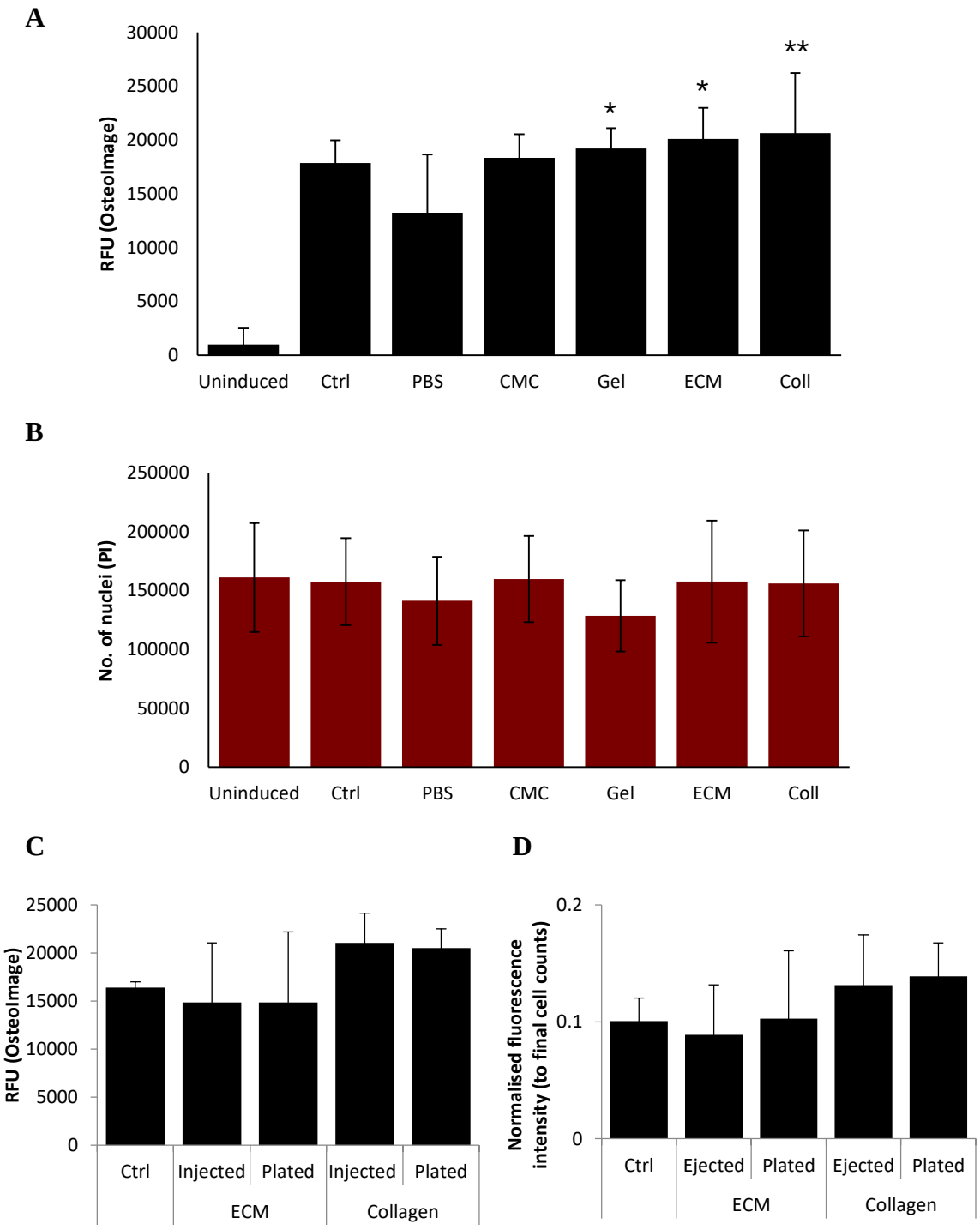

Figure 6.11: **Impact of biomaterial-based carriers on osteogenic differentiation capacity of hMSCs ejected via 30G needles, cultured in bipotential media for 21 days**. (A) OsteoImage fluorescence values, showing hydroxyapatite formation. Each bar represents mean fluorescence value ± SD, n=6 in 3 donors. Asterisks represent statistically significant difference relative to PBS using ANOVA and Dunnet's *post-hoc* test; *$p \leq 0.05$; **$p \leq 0.01$. (B) Number of cells at day 21, quantitated using PI staining of hMSCs from 3 donors (mean ± SD, n=5). (C) Ejected *vs* directly plated hMSCs, suspended within collagen and ECM, assessed for osteogenic differentiation capacity. "Ejected" cells were ejected at 10 µL/min, and "plated" cells were 60% of ejected cell number directly plated in 12-well plates. Results are mean fluorescence values ± SD, n=4 in 2 donors (D) OsteoImage fluorescence intensity readings were normalised to PI-based cell counts (mean ± SD, n=4; 2 donors).

6.3.7 **Effect of co-injection with biomaterials on ALP levels**

- *Media ALP activity*

To determine if ALP was released into the media during shear stress exposure, media were assayed for ALP activity 2 days following the addition of bipotential differentiation media, which was added 24 hours post-ejection. At day 2, media ALP activity was generally higher in ejected hMSC samples than in directly plated ones (Figure 6.12A). Ejection within PBS and ECM significantly increased released ALP activity compared with directly plated hMSCs ($p<0.05$).

To determine whether ejection forces and biomaterial-based delivery have a synergistic effect on released ALP, media ALP levels in directly plated versus ejected cells, both suspended within either collagen or ECM, were compared. "Ejected" cells were ejected at 10 µL/min via 30G needles, and 60% of the initially ejected cell number (to account for cell loss during ejection within those two carriers) was directly plated in 12-well plates. Figure 6.12B shows no significant difference in media ALP levels in ejected samples relative to directly plated ones within the same bECM carrier.

A

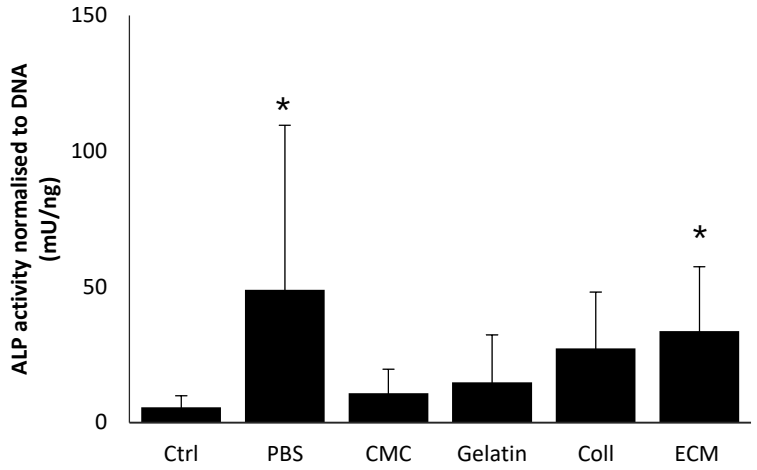

B

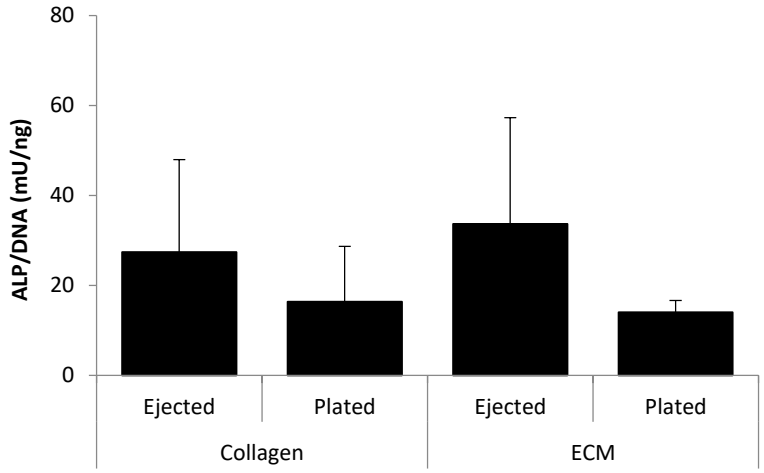

Figure 6.12: **Media alkaline phosphatase activity levels of hMSCs ejected at 10 µL/min, via 30G needles, and cultured in bipotential osteogenic/adipogenic media for 2 days.** (A) Media ALP was analysed 2 days after adding differentiation media 24 hrs post-ejection. Values shown are mean ± SD (n=3; 2 donors). Asterisks indicate statistically significant differences in ALP levels relative to control (Friedman test with Dunn's *post-hoc*; *p<0.05). (B) Released ALP levels in ejected versus directly plated hMSCs suspended within collagen and ECM. "Ejected" cells were ejected at 10 µL/min, and "plated" cells were 60% of the initially ejected cell number directly plated in 12-well plates. Results are mean fluorescence values ± SD (n=4 in 2 donors; Mann-Whitney test).

- *Cellular ALP activity*

Since release of ALP into the media during shear stress exposure significantly increased when ejected in PBS or co-injected with certain carriers, it was necessary to determine if cellular ALP levels were also affected.

On day 2, total cellular ALP activity was significantly lower for hMSCs ejected within PBS than for control samples (Figure 6.13A). However, when DNA content is factored in (as an indicator of cell number), it is found that levels of ALP production per cell is similar for all samples tested at this time point (Figure 6.13B).

Expression of normalised cellular ALP was found to peak earlier (day 4) for directly plated samples than ejected ones (day 7), which may indicate that these samples were undergoing differentiation more rapidly than ejected samples.

To explore whether shear forces contribute to this ALP expression pattern, directly plated and ejected hMSCs within ECM and collagen carriers were compared. Sixty percent of the initial ejected cell number was used for directly plated samples to account for cell loss during ejection and preclude any potential influence of initial seeding density on ALP production. The same pattern of normalised ALP levels peaking earlier (at day 4) in directly plated samples relative to ejected samples was observed again (Figure 6.13C). There was no significant difference in DNA content of plated hMSCs relative to ejected ones (Figure 6.13D).

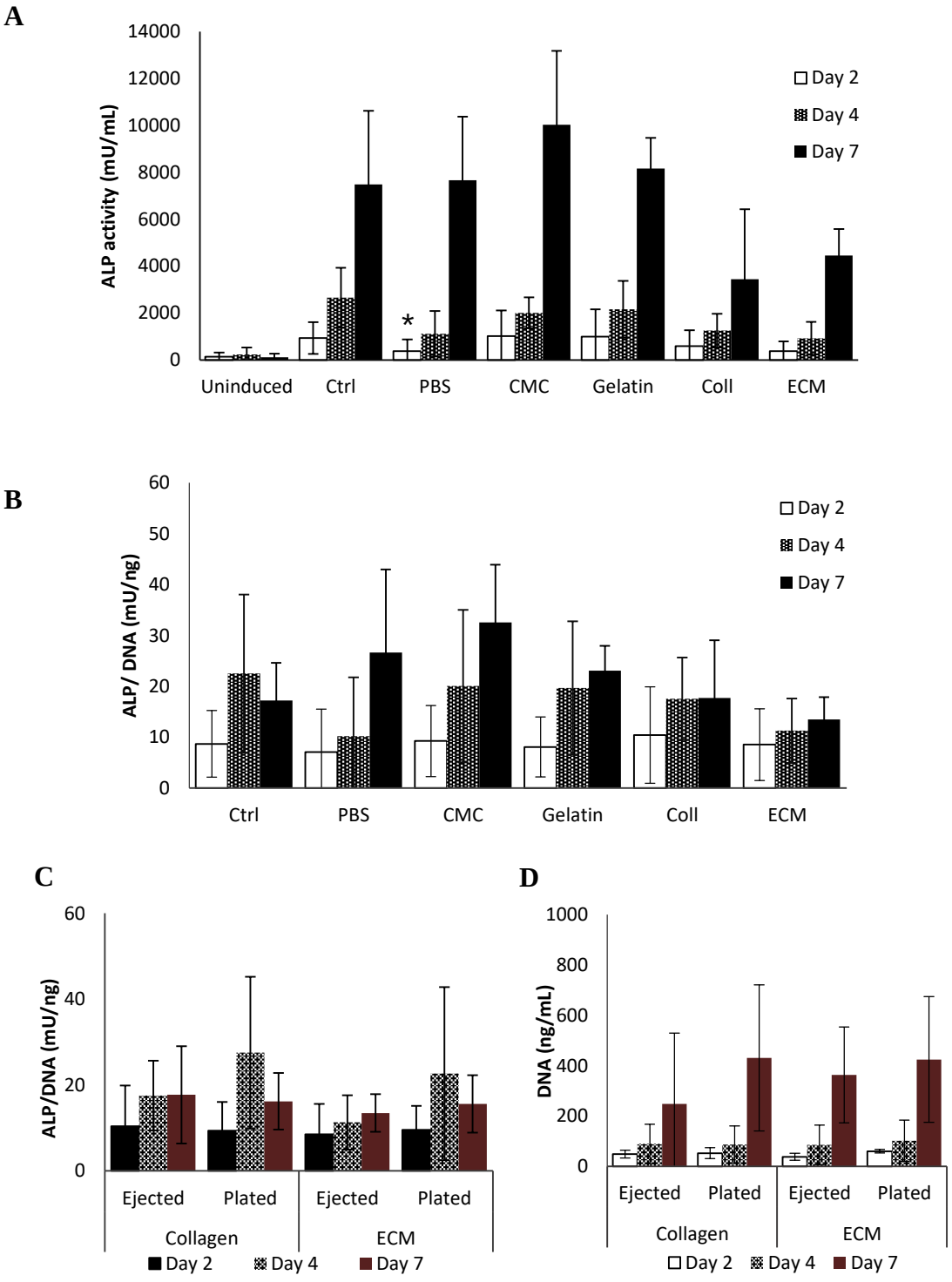

Figure 6.13: **Cellular alkaline phosphatase activity levels of hMSCs at different time points following ejection at 10 µL/min via 30G needles, and cultured in bipotential media**. (A) Cellular ALP was analysed 2, 4 and 7 days post-induction. Values shown are mean ± SD (n=3; 2 donors). Asterisks indicate statistically significant differences in ALP levels relative to control (Friedman test with Dunn's *post-hoc*; *p<0.05) (B) Cellular ALP values normalised to DNA content (mean ± SD; n=3; 2 donors) (C) Normalised cellular ALP levels in ejected versus directly-plated hMSCs suspended within collagen and ECM. "Ejected" cells were ejected at 10 µL/min, and "plated" cells were 60% of the initial cell number directly plated (mean ± SD; n=3 in 2 donors). (C) DNA content of hMSCs in ejected versus directly plated samples suspended within collagen and ECM (mean ± SD).

6.3.8 **Osteocalcin immunofluorescence staining**

The osteogenic differentiation of hMSCs was confirmed using immunofluorescence staining of osteocalcin (OCN), a bone specific ECM protein. After 21 days, immunostaining for osteocalcin showed a robust expression of this late osteogenic marker across all samples, with cell nuclei counter-stained with DAPI (blue), after 21 days of culture (Figure 6.14).

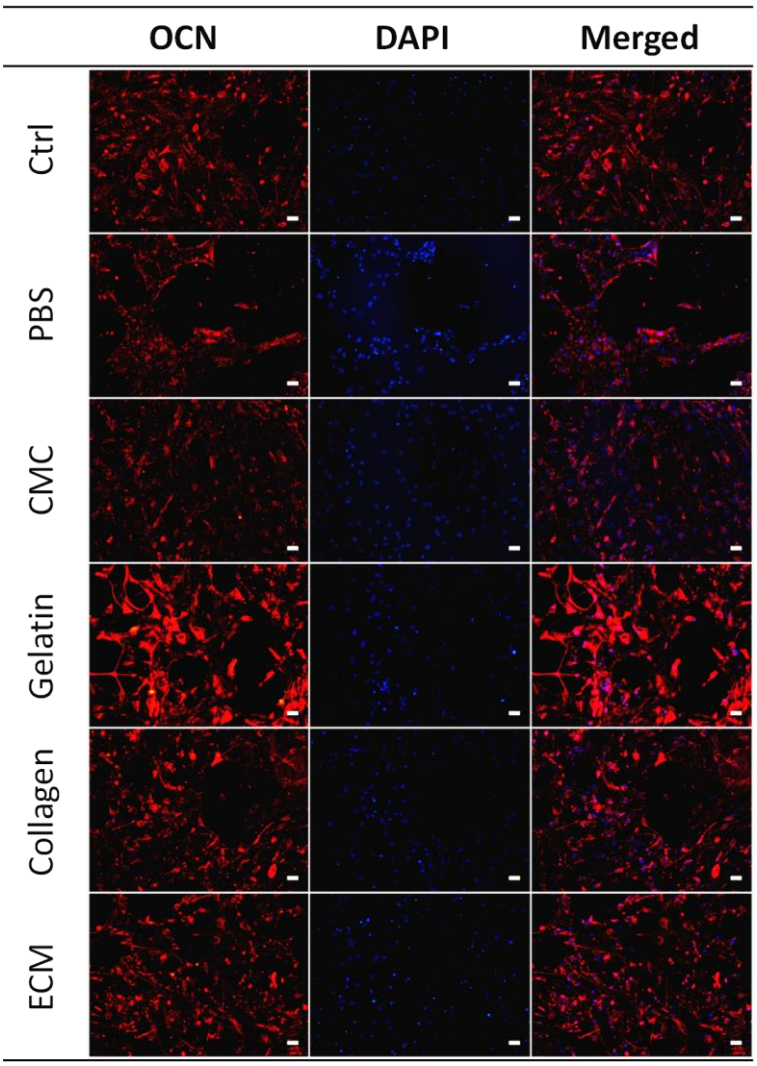

Figure 6.14: **Representative immunofluorescent staining of human osteocalcin (OCN) and nuclei counterstained with DAPI (blue) to confirm osteogenic differentiation of hMSCs**. Directly plated and ejected hMSCs (via 30G needles at 10 μL/min), were cultured in bipotential media at 21 days post-induction (Scale bar = 50 μm).

6.4 Discussion

The use of injectable biomaterials for cell delivery is a rapidly expanding discipline in the field of regenerative medicine. Biomaterials represent potentially adaptable cell delivery vehicles due to cytocompatibility, tuneability, and the possibility of use as injectable carriers. This study aimed to investigate the effects of using biomaterial-based cell carriers for ejection of hMSCs on cell recovery, commitment and differentiation capacity in a clinically relevant syringe/needle ejection scenario. MSCs are multipotent cells that can differentiate into osteoblasts, chondrocytes and adipocytes [212]. Although they do not readily differentiate into neural cells, they have been reported to promote recovery in CNS injury [111, 307].

It was hypothesised that cell ejection within biomaterial-based cell carriers may provide the protection required to prevent cells from adhering to the delivery device. To test this hypothesis, a range of biomaterial-based carriers was produced with varying viscoelastic properties and assessed their cell delivery capabilities. Results showed that utilising hydrogels and viscosity modifying excipients for cellular delivery demonstrated positive effects on cell recovery (Figure 6.4). A significant loss of cells at 10 µL/min was observed in unprotected (PBS) samples at 24 hours post-ejection. Gelatin (protein-based) and CMC (polysaccharide-based) cell carriers displayed the highest percentage of viable cells delivered, with no significant difference to directly plated control samples. In comparison, collagen and ECM carriers (both protein-based) resulted in lower cell recovery, yet significantly better than ejecting within PBS. An improvement in cell viability post-ejection was also previously obtained by Aguado *et al.* using alginate gels via a 28G needle and 1mL syringe [74]. This has been suggested to be due to hydrogels undergoing plug flow,

whereby the hydrogel adjacent to the walls undergoes shear thinning and forms a fluid layer that acts as a lubricant [87, 308]. Moreover, gel material and encapsulated cells within the plug flow region experienced low shear rate [308]. This lubricating fluid layer may be one explanation for the higher percentages of the cell doses delivered in this study, through keeping the cells in the central plug zone away from the walls. This protective mechanism and significant improvement in cell dose recovery through clinically relevant narrow-bore needles at low ejection rates [107, 309] may be vital to cells that display biological changes after exposure to mechanical forces and in high accuracy applications.

Live/Dead staining confirmed that all carriers under investigation conserved a high degree of viability of ejected cells (Figure 6.5A). Low cell recovery in samples ejected within PBS was also confirmed microscopically, where ejection at 10 µL/min resulted in a visibly lower number of cells relative to other cell carriers under investigation. In addition, brightfield microscopy revealed a dilute meshwork of what appears to be collagen fibrils dispersed between the cells, as they were not stained by calcein (Figure 6.5). Solubilised collagen I can be mixed with living cells during gelation to implant cells in a fibrillar collagen matrix [310]. Fibrils mingle laterally, resulting in a highly interconnected network of collagen gel [311]. Previous studies have also reported that when contractile cells are included in the mixture, they get entangled within the network of collagen fibrils during gelation [312]. The force generation and properties of collagen fibrils are comparable to biological filaments, such as actin or microtubules [313]. Non-covalent inter-fibril network interconnections have been reported to transmit cellular traction forces [314] and to result in the development of an integrin-independent component of adhesion for cell anchorage [312]. This may have given rise to extracellular cues that affected cell fate in samples ejected within collagen and

ECM relative to hMSCs ejected within PBS. Constant shear rate has been reported to influence collagen fibrillar alignment, with the best alignment of fibrils observed at the intermediate shear rates investigated [315]. Further investigations into harnessing shear forces generated within injectable systems is of interest in nervous system regeneration, where anisotropy is fundamental and tracts of aligned neurons and glia are required [316, 317].

Cell recovery did not correlate with the biochemical nature of the polymer (protein-*versus* polysaccharide-based), so rheological studies were carried out to investigate possible correlation of cell recovery with the mechanical properties of the biomaterials. Rheology was utilised to determine shear-thinning behaviour, thixotropic recovery and viscosity of the biomaterials under investigation. Shear-thinning behaviour of these biomaterials, which showed a relatively large change in the viscosity ($\Delta\eta \sim 10^2$ - 10^4 Pa.s) from low (0.01 s^{-1}) to high (1000 s^{-1}) shear rates, is a beneficial property for injection-based delivery through narrow-bore needles (Figure 6.7). Viscometric thixotropy testing revealed that biomaterials were able to recover after shearing, with some biomaterials (collagen and CMC) exhibiting more complete recovery than others. Oscillatory shear rheology of the biomaterials (Figure 6.8) also showed that the softer materials with lower storage moduli (G') resulted in the best cell recovery (0.1-1 Pa). However, rheological data was not sufficient to explain the significant improvement of cell recovery with gelatin and CMC carriers relative to collagen and ECM. In addition, viscosities and shear-thinning profiles of the two concentrations of CMC under investigation (0.5 and 0.25%) were not significantly different, thereby not explaining the significant difference in cell recovery between them. Moreover, gelatin and 0.25% displayed similar storage moduli, yet significantly different cell dose recovery rates.

Wetting is "the ability of a liquid to maintain contact with a solid surface, resulting from intermolecular interactions when the two are brought together" [318]. Surface wettability is an important physicochemical property of biomaterials that could control protein adsorption and, in turn, initial cell attachment. The process of physical adhesion is a function of wetting between surfaces [319]. Cell adhesion is similar to physical adhesion in that the cell membrane must make close molecular contact with the surface [320], and therefore it was hypothesised that better cell attachment occurs with surfaces of high wettability since cells can make better contact with these surfaces. However, it is difficult to obtain consistent correlation between surface wettability, protein adsorption and the subsequent initial cell attachment. Previously, studies have shown that hydrophilic surfaces produced a significant increase in the amount of protein adsorption and a high initial rate of cell attachment [321-324]. Cell adhesion has also been reported to be better on hydrophilic surfaces [325]. Additionally, cells adhered and proliferated more on surfaces with moderate hydrophilicity than on the more hydrophobic or hydrophilic spots [326]. Improvement of cell attachment with decreasing contact angles has been stated to be clearly observable at incubation times of up to 60 minutes [324].

The results detailed herein show that cell carriers with the lowest glass surface wettability showed the best cell dose recovery, which may correlate to lowest cell retention in the delivery device. This may be due to the lower contact that these carriers provide with the glass surface of the syringe, discouraging adhesion during time spent in the delivery device. It has been previously revealed in this work (Chapters 3 and 4) that the prevention of cell adhesion on the inner surfaces of the delivery device is critical to ensure successful injectable cell delivery [82, 100]. Contact angles displayed by the various carriers correlated well with cell recovery trends demonstrated (Figures

6.4 & 6.9). Gelatin resulted in high contact angles on glass despite being structurally similar to collagen. This has been suggested to be due to a preferred orientation of hydrophobic moieties at the air-gel interface, causing a specific arrangement of water molecules [327]. Such a noteworthy difference between contact angles (both made up of highly hydrophilic polymers) was explained by the difference in their molecular configuration. Gelatin molecules are randomly coiled polypeptides (denatured collagen), having a high degree of freedom to rearrange the distribution of hydrophilic moieties at the surface, whereas collagen's triple helices have less freedom to rearrange [328]. The ability of cells to attach to a surface will depend on the cell type and surface used. Therefore, experiments comparing the attachment of various cell types on different syringe material surfaces using various carriers is needed to confirm the influence of carrier wettability on cell retention in the delivery device. It should also be more helpful for understanding this property if a wider range of surface wettability were employed using various carriers, without a change in surface topography, as surface roughness also has an influence on the density and spreading of adhered cells [329].

Recently, the use of biomaterials that can interact with transplanted cells has been of significant interest [266]. A cell's fate is tightly regulated by its microenvironment, since cells commit to their fate by deriving information from its surroundings [330]. ECM proteins represent key components in the cell niche that dictates cell fate. These proteins are recognised by cell surface receptors and are involved in cell processes such as proliferation and differentiation. For example, fibronectin is a major component of the ECM that binds with integrins to promote cell adhesion and viability [331]. Hyaluronan, a naturally occurring polysaccharide found in the ECM of the CNS, can interact with various HA-receptors (e.g. CD44) present on diverse cell types to

promote cell adhesion and survival [332]. Therefore, it was hypothesised that biomimetic protein-based cell carriers will have a discernible impact on cell commitment and differentiation capacity. Alizarin Red S and OsteoImage staining were performed to qualitatively assess calcium and hydroxyapatite deposition respectively, which are parameters denoting late-stage osteogenic differentiation [303]. Quantification of alkaline phosphatase activity and staining for osteocalcin was also carried out in order to evaluate osteoblastic phenotype expression.

Late stage osteogenic differentiation was enhanced by the protein-based cell carriers, namely collagen, bone ECM, and gelatin, as demonstrated by mineralisation results (Figures 6.10 & 6.11). Final cell numbers at day 21 were all similar despite different initial cell numbers ejected using the various carriers, implying that cell proliferation was stimulated by the lower initial cell seeding density. The higher mineralisation levels in samples ejected within collagen ($p<0.01$) *versus* control at day 21 suggested that the use of a biomimetic cell carrier for the desired cell type can enhance the differentiation response. Results of this study show that the use of collagen as a cell carrier, in its pure form or as a component of bone ECM, resulted in the highest mineralisation results at day 21. The fibril-forming collagen type I (Col I) is the most investigated for biomedical applications, forming more than 90% of the organic mass of bone [276]. Bone ECM has been reported to contain 84.28 ± 10.20% of collagen, primarily type I [333]. In addition, bECM contains collagen III and V, adhesion proteins such as fibronectin, proteoglycans such as hyaluronan and decorin [334], angiogenic growth factors, such as VEGF, and growth factors of the TFG-β family [335]. Previous studies have demonstrated that contact with Col I alone may be sufficient to induce osteogenic differentiation of hMSCs, even in the absence of exogenous soluble stimuli in two-dimensional (2D) culture [336, 337]. Bone marrow

MSCs has also been reported to undergo osteogenesis when cultured on collagen I matrices *in vitro* by interaction with the Col-I-binding integrin α2β1 [337, 338]. ECM proteins typically influence cell behaviour by binding to specific integrin cell surface receptors [336]. One study concluded that adhesion to ECM proteins, in the absence of soluble osteogenic stimulants, can act as insoluble cues of osteogenesis [336]. ECM has been used to induce osteogenic differentiation of MSCs on scaffolds composed of titanium fibres [339].

ALP is used as an indicator of osteogenic commitment, and commonly precedes bone matrix mineralisation [227, 340-343]. A general trend of higher levels of media ALP was observed in ejected samples relative to directly plated ones, with a significantly higher release of ALP into the media especially notable in the unprotected PBS samples. A similar result was previously obtained by Yourek *et al*., whereby 24 hr exposure to shear stress resulted in higher ALP activity in the media than control cells [344]. Results of cellular ALP analysis may be due to mechanical forces caused by the ejection process, resulting in the promotion of slower commitment of ejected cells towards the osteogenic lineage *in vitro* (in comparison to direct plating), but stronger osteogenic expression. This is implied by the later peaking of normalised ALP expression in ejected samples at day 7, compared to directly plated samples at day 4, and enhanced mineralisation results with cells ejected within protein-based carriers at day 21. Results suggest that even though shear stress in combination with collagen-based carriers supported osteogenic differentiation more effectively relative to the directly plated control, the commitment process took longer. Correspondingly, Grellier *et al.* exposed hMSCs to short periods of fluid shear stress and showed that a 30-minute exposure upregulated ALP mRNA but 90 min decreased it to almost basal levels [75]. Additionally, MSCs exposed to oscillatory fluid flow displayed reduced ALP activity

despite upregulating OCN mRNA under the same conditions [227]. Evidently, the downstream effects of ALP are complex and the detailed mechanism of how ALP acts is unclear [345].

Future research into biomimetic tailoring of biomaterial-based injectable cell carriers, directly encapsulating cells within a 3D microenvironment that is rich in informational cues, will allow improved cell recovery and promotion of specific cellular responses for effective *in vivo* transplantation.

6.5 Conclusions

This study examines the effective use of various biomaterials for significant improvement of cell recovery, which was not associated with rheological properties as suggested by earlier studies [74]. In addition, results presented herein highlight the impact of cell carrier choice on cell fate, despite the limited contact time with the ejected cells pre-delivery and during the ejection procedure.

In summary,

- Biomaterial-assisted delivery significantly improved the percentage of cell dose delivered as viable cells. Certain carriers, e.g.: collagen, also improved the proliferative capacity of the delivered cells.
- Some of the cell carriers employed improved cell recovery more significantly than others. The trend of improvement in cell recovery correlated with the surface wettability of the various carriers with glass surfaces.
- Samples ejected using collagen and ECM as carriers showed significantly more extensive mineralisation at day 21 post-induction.
- Ejected samples displayed delayed peaking of normalised ALP expression

relative to directly plated ones. This suggests that ejection forces may cause the osteogenic commitment process to take longer.

Herein, it has been demonstrated that the use of natural biomaterials as cell carriers significantly influenced the percentage of the cell dose delivered as viable cells, as well as having an impact on the extent of differentiation of ejected hMSCs. Development of reproducible and well-defined biomaterial-assisted cell delivery systems will accelerate clinical translation of cell-based therapeutics and allow the utilisation of the synergistic effects of biomaterials for cell delivery, protection, and induction.

This study demonstrates an efficient approach to protect ejected cells from mechanical forces experienced during syringe/needle flow, as well as preventing retention in the delivery device. Using fewer cells to achieve a similar number of transplanted viable cells would greatly reduce the cost of cell transplantation protocols. Since the degree of commitment and extent of terminal differentiation was substantially altered by the selection of biomaterial carrier, it is recommended to identify optimal conditions, both biochemical and mechanophysical, to control MSC lineage commitment. Future investigations can investigate the possibility of using cell carriers to provide cues to direct differentiation without the need for biochemical factors. This approach is anticipated to provide a new paradigm in which regenerative medicine therapeutics use tailored cell carriers for the intended application.

Chapter 7| General discussion, conclusions and future perspectives

A crucial obstacle to the translation of promising cell-based therapeutics to the clinic is the ability to deliver adequate numbers of viable cells efficiently to the target site for functional regeneration. The current approach of administering large numbers of cells to overcome cell loss encountered post-injection is time- and cost-intensive, does not necessarily result in improved retention or better functionality, and can pose safety risks. Controversial results regarding the efficacy of injectable cell-based therapies and the effects of the injection process on transplanted cell viability (Chapter 1) have prompted us to step back and comprehensively explore injectable cell therapy protocols *in vitro*. A thorough understanding of the parameters affecting cell recovery and functionality post-ejection will assist researchers and clinicians in the field to provide clearer conclusions regarding cell therapy efficacy in patients.

This thesis aimed to address two fundamental issues concerning the translation of cell-based therapies to the clinic. The first central issue was to determine whether optimisation of certain delivery parameters through various narrow-bore needles, typically used for high accuracy cellular therapy applications, might improve delivered cell viability and functionality (Chapters 3-5). The second key issue was to explore improving injectable cell delivery using biomaterial-based delivery, and determine whether this could potentially influence cell fate post-injection (Chapter 6).

The novelty of this work lies in the comprehensive investigation of the responses of mammalian NIH 3T3 cells and the clinically relevant primary hMSCs to the ejection

process. In contrast to previous investigations, which have focused on viability as the chief indicator of cellular response to ejection through needle-based devices (Chapter 1), this work evaluates a wide range of viability and cellular health indicators, as well as impact on trilineage differentiation capacity. Furthermore, this study examines the successful use of various biomaterials for significant improvement of cell recovery, which was not associated with rheological properties as suggested by earlier studies [74]. In addition, the results presented herein highlight the notable impact of cell carrier choice on cell fate, despite limited contact time with the ejected cells during the delivery procedure.

7.1. The effect of cell delivery via narrow-bore needles on various aspects of cellular health

Numerous cell therapy procedures have used injection-based administration to deliver high-density cell preparations to the target site, either systemically or directly. The studies described in Chapters 3-5 assessed whether cell delivery through injection-based devices affected viability and a range of other characteristics of mammalian cells (NIH 3T3s and hMSCs). These studies determined whether cell viability, potency and fate could be improved and/or controlled by optimising the protocols employed for injectable cell delivery. An extensive toolset has been used, incorporating multiplex assays, for the assessment of cell delivery post-ejection. The effects of various ejection rates, needle sizes and cell suspension densities were assessed in terms of changes in viability, membrane integrity, apoptosis, senescence, and other key parameters of cellular health.

Guidance issued by the regulatory body CBER (Centre for Biologics Evaluation & Research) states that cell therapy products should have a viability of ≥70% and

demonstrate a repeatedly high level of potency [126]. Microscopical and flow cytometric Live/Dead analyses confirmed that cells ejected through 30 and 34G needles displayed ≥97% viability at all ejection rates under investigation. However, the percentage of cell dose being delivered as viable cells was lower at the lower ejection rates. The work described herein attributed this to cell retention in the delivery device (Chapters 3 and 4). The percentage of viable hMSCs delivered increased with increasing ejection rate, while the smaller NIH 3T3 cells had an optimum ejection rate of 150 µL/min, after which delivery efficiency dropped. This emphasises the importance of adapting cell administration protocols to the nature of the transplanted cells, as it can be assumed that the environment into which the cells would be injected would have further adverse effects on them.

Results of this study revealed that ejecting cells through a narrow-bore needle at the slower flow rates (e.g.: 10 µL/min), utilised in various clinical trials [111, 346], might induce apoptosis. This became apparent 24-48 hours after ejection, causing delayed death of the injected cells. It also resulted in phenotypic expression changes, with immunophenotyping revealing significant downregulation of CD105 expression in samples ejected at 10 µL/min ($p<0.05$), which may affect their physiological functionality. An impact on differentiation capacity was also observed, which could be attributed to both the different proportions of the cell dose delivered at the various ejection rates as well as being due to exposure to mechanical forces during the ejection process.

The range of shear stress values generated in this investigation is presented in Table A1.2. Calculated shear stress values for 10 and 20 µL/min in 30G needles are in the range expected physiologically: average wall shear stress is 1-6 dyn/cm^2 for venous

circulation, and 15 dyn/cm^2 for arterial circulation [78, 79]. All other flow rates have shear stress values outside of the ranges for venous and arterial circulations [78, 79]. The values calculated suggested that cells are being exposed to supra-physiological mechanical stresses during the injection process at most of the flow rates under investigation, and therefore it was deemed critical to assess the effects of such stresses on cellular health.

From the data obtained in this study, it can be concluded that passing hMSCs through narrow lumen needles at the flow rates under investigation is not likely to lead to clinically substantial changes in the viability of transplanted cells (viability ≥90%). This, in turn, validates the general safety of catheter-based delivery in cell-based therapeutics. However, various noteworthy biological and physiological functioning consequences of the ejection process have been observed in this work. These conclusions are based on a relatively small range of ejection rates, since clinical trials have employed flow rates of up to 6 mL/min [109, 110]. Therefore, the possibility that significant biological alterations (positive or negative) may be caused by injectable delivery of hMSCs, outside the scope of conditions examined in this study, cannot be excluded. There is a wealth of knowledge that could be gained by further investigating the effects of varying multiple parameters of the injection process to determine optimal protocols for utilisation in *in vivo* investigations.

7.2. The impact of biomaterials-based delivery on the injected cells

In most clinical trials, cells are directly injected via a syringe or catheter in saline, and often fewer than 5% of injected cells persist at the site of injection within days of transplantation. This makes improving viable cell recovery post-injection of the utmost importance. The use of biomaterials as cell delivery vehicles in this study aimed to

protect the cell payload and minimise cell retention in the delivery device. This would lead to an improvement of cell dose recovery, resulting in optimal cell delivery and thereby the continuous production of paracrine signalling at the target site [347]. In addition, the regenerative capability of naturally derived biomaterials may be enhanced by utilising components of the desired native ECM, or their derivatives, to act as cell instructive delivery systems.

For the commercial success of cell-based therapeutics, cell delivery systems must be efficient, simple to use and cost-effective. This introduces a potential contradiction between the current trend towards sophistication to enable accurate biomimicking of native cellular microenvironments, and the ease of production and clinical use. There is a growing interest in recreating extracellular cues in simplified systems, such as the use of basic chemistries to manipulate cell fate [348]. To enable the successful development and commercialisation of instructive materials for regenerative medicine, they need to display good clinical performance and cost-effectiveness. Focusing on the development and evaluation of convenient, manageable and efficient systems is likely to aid the reconciliation of clinical and commercial aspects of translating cell-based therapies to the clinic.

To facilitate the clinical translation of the results, identification of the gains needed in functional behaviour to improve injectable cell delivery and minimise cell retention in the delivery device was required. The aim of this work was to develop clinically translatable biomaterials that could be used to improve the efficiency of stem cell delivery. In this study, several injectable delivery systems were evaluated, that:

- Can serve as efficient cell delivery carriers;

- Possess shear-thinning properties that would allow injectability through narrow-bore needles and display plug flow behaviour to protect the cell payload.
- Have potentially tuneable mechanical characteristics to enable utilisation in numerous cell therapy applications.

Stem cells receive cues from numerous physical and chemical characteristics of their surrounding environment. Since there are unavoidable delays in any cell delivery procedure, cell carriers may provide cues within this time that would inevitably direct cell functionality outcomes, such as proliferation and differentiation. Within biomaterials, these cues may include material composition, degradation, adhesion and mechanics, as well as the external mechanical cues resulting from the exposure of cells to mechanical forces associated with injection procedures. Several protein-based biomaterials that are components of native ECM were investigated, to explore whether they would demonstrate bioactive properties and improve cell functionality.

This study demonstrated a significant improvement of *in vitro* cell recovery in cells co-ejected with naturally derived biomaterials relative to PBS, with gelatin and CMC solutions performing better than collagen and ECM hydrogels. All the biomaterials under investigation were shown to undergo shear thinning followed by self-healing, therefore indicating that the candidate biomaterials could recover their original form following the exposure to shear stress during injection, a necessary requirement for injection-based cell delivery applications. However, cell recovery trends appeared to be proportional to the surface wettability properties exhibited by the employed biomaterials and not their shear-thinning properties as had been suggested by previous studies [74, 155]. Further investigations are needed to confirm this conclusion and

make use of it to design more efficient cell delivery systems. Co-delivery of the cells within the biomaterials studied showed that cells were protected and remained viable *in vitro* up to ten days post-ejection.

Despite the relatively lower efficiency of collagen and bECM in improving cell recovery, they were investigated for potential impact on cell fate. Given the tissue specificity of ECM and the abundant presence of collagen in bone-derived ECM [333], these protein-based biomaterials have the potential of mimicking the native microenvironment pre-injection and closely mirror the target site once injected [349]. Collagen type I and bECM yielded significant increases in the amount of mineralised matrix deposited relative to cells delivered in PBS, demonstrating the potential capability of using biomaterial-based delivery to enhance the differentiation capacity of hMSCs and influence cell fate. These results highlight the potential of using tailored cell carriers for regenerative medicine applications.

7.3. Significance and future clinical perspectives

There is a growing number of clinical trials using MSCs for cellular therapy in a multitude of clinical targets. However, there is growing evidence in the literature of a problem with cell injection methods in various cellular therapy applications (Chapter 1). Delivery of cells in a minimally invasive manner, while ensuring maximum cell survival and retention, poses considerable challenges. Because of the large number of variables involved, studies that have been carried out have still not been able to evaluate all combinations of parameters for potential interactions. The specific combinations of cell preparation procedure, cell dose, density, interval between filling of the cannula/needle and fixing to the stereotaxic frame prior to injection, instruments, and angles of delivery will not be consistent for all clinical trials. These factors must

be considered and empirically validated prior to use in clinical practice. However, the available results demonstrate that such interactions can be significant and could substantially alter cell delivery.

The potential implications of this study on regenerative medicine applications are notable. This study has established that standardisation of injection parameters is a critical aspect of designing and comparing clinical studies. Pre-clinical planning and testing of the planned administration protocol with the specific cell type to be used must be a key component of clinical trial design. This study demonstrated that lower ejection rates had substantial impact on the percentage of cell dose delivered and cellular health post-ejection. The novel findings presented herein, concerning the impact of ejection rate on cell recovery and the comprehensive assessment of various parameters of cellular health and function, can be used to improve delivery using fine needles. Although some *in vitro* and *in vivo* studies have investigated optimal cell dosage (Chapter 1), limited work has been carried out to assess the effects of injectable cell delivery on the various cell health parameters.

This study has opened up numerous future opportunities for research. Although this study has investigated the effects of varying ejection rate and needle size on hMSC viability and cell function in depth, one potential area of research is the evaluation of varying stem cell concentrations. Increasing cell concentrations being ejected may increase shearing forces leading to increased cell death. However, it has been found, during the course of this study, that increasing NIH 3T3 concentration causes cell clumping and increases the number of viable cells delivered. Investigations into other cell types such as hMSCs and neural stem cells are essential to elucidate the effects of cell concentration.

In order to maximise cell delivery success, researchers need to optimise ejection rate using the target cells before embarking on clinical trials, and preferably use the widest and shortest possible needles to minimise undesirable impact on cellular health parameters. Further studies will enable us to optimise protocols utilising finer needles to minimise the physical damage of cell implantation, particularly for degenerative diseases accompanying neuronal damage.

Results presented in this thesis have suggested that the ejected cells were viable after the delivery process, and capable of attaching to cell culture surfaces and undergoing proliferation. However, other vital cellular functions, key in a clinical setting, were affected by the ejection process. This included increases in apoptosis levels and an impact on phenotype and differentiation capacity at slower flow rates (Section 4.3). Further studies are needed to explore the impact on differentiation in more detail, since it is reasonable to believe that injectable delivery may impair the cells ability to differentiate into the required cell type, or even cause differentiation into other undesirable cell types.

The main focus of the present study has been to thoroughly examine the impact of injectable delivery on primary human mesenchymal stem cells (hMSCs), mainly because of the great amount of interest in MSCs as a potential cell-based therapy for various conditions (as discussed in Chapters 1 and 4). However, MSCs may not be representative of the wide range of other cell types currently investigated for cell therapy. Therefore, studies using various clinically relevant cell types are required to determine the effects of different injection scenarios. Since one of the main factors affecting cell health is the mechanical stresses that the cells are exposed to as they are pass through the syringe-based delivery device, the physical parameters of cell size

and morphology will influence how they react to such stresses. These physical parameters may be one of the main reasons behind the difference in cell recovery trends observed in this study with NIH 3T3 cells and hMSCs (Sections 3.3.1 and 4.3.2). The most obvious step would be to move on to carrying out this study on neuronal or retinal cell models, which would be more applicable to various high accuracy applications.

In addition, further studies are required to investigate whether, in the absence of chemical differentiation factors, certain biomaterials will induce differentiation. More detailed studies into the impact of shear forces and cell delivery vehicles on different differentiation pathways are also necessary.

To improve the success of clinical translation, several issues must be addressed. An integrated approach to the evaluation of cell delivery success is needed to improve the assessment of delivery efficacy and to allow for sound interpretations of clinical results. Improved cell delivery tools are also required to streamline the delivery of cell-based therapeutics from the donor to the patient without compromising quality. The findings reported herein, regarding the retention of cells on the glass surfaces of the syringe (Section 4.3.7), highlights the importance of developing materials which do not promote cell attachment for the manufacture of cell delivery devices. In terms of design of clinical trial protocols, it is vital that the cell dose, needle size and rate of injection are carefully evaluated. At this stage, it is no longer feasible to simply inject cells in a saline carrier. Moreover, cell doses that are too high are costly, hinder clinical translation due to practicability issues, and may cause unwanted side effects post-injection. The effects of injection rate must be carefully characterised and optimised, using both *in vitro* and *in vivo* models, prior to embarking on clinical trials. Coupling

in vitro studies using target cell types with mathematical modelling may improve our understanding of the effects of the injection procedure on transplanted cells.

Generating optimal efficacy using convenient biomaterial-based approaches will positively influence patient outcomes in the future. This study highlights that the use of injectable biomaterials is effective at significantly improving cell recovery, as well as having the potential to direct cell fate. The complexity of physiological development suggests the need for more sophisticated delivery systems that can regulate cell fate. At the translation stage, it is important to seek advice from clinicians, industry, and regulatory officials, to make sure that delivery systems and clinical studies are carefully designed to make regulatory approval as efficient as possible.

References

1. Mason, C. and P. Dunnill, *A brief definition of regenerative medicine.* Regen Med, 2008. **3**(1): p. 1-5.

2. Yang, J., et al., *Cell delivery in regenerative medicine: the cell sheet engineering approach.* J Control Release, 2006. **116**(2): p. 193-203.

3. Slaughter, B.V., S.S. Khurshid, O.Z. Fisher, A. Khademhosseini, and N.A. Peppas, *Hydrogels in regenerative medicine.* Adv Mater, 2009. **21**(32-33): p. 3307-29.

4. Tan, H.P. and K.G. Marra, *Injectable, Biodegradable Hydrogels for Tissue Engineering Applications.* Materials, 2010. **3**(3): p. 1746-1767.

5. Bidarra, S.J., C.C. Barrias, and P.L. Granja, *Injectable alginate hydrogels for cell delivery in tissue engineering.* Acta Biomater, 2014. **10**(4): p. 1646-62.

6. Chen, F.M., L.A. Wu, M. Zhang, R. Zhang, and H.H. Sun, *Homing of endogenous stem/progenitor cells for in situ tissue regeneration: Promises, strategies, and translational perspectives.* Biomaterials, 2011. **32**(12): p. 3189-3209.

7. Fichera, G., *Impianti omoplastici feto-umani nel cancro e nel diabete,* Tumoi, 1928. **14**, 434.

8. Ishii, T. and K. Eto, *Fetal stem cell transplantation: Past, present, and future.* World J Stem Cells, 2014. **6**(4): p. 404-20.

9. Freed, C.R., et al., *Transplantation of embryonic dopamine neurons for severe Parkinson's disease.* N Engl J Med, 2001. **344**(10): p. 710-9.

10. Olanow, C.W., et al., *A double-blind controlled trial of bilateral fetal nigral transplantation in Parkinson's disease.* Ann Neurol, 2003. **54**(3): p. 403-14.

11. Bachoud-Levi, A.C., et al., *Effect of fetal neural transplants in patients with Huntington's disease 6 years after surgery: a long-term follow-up study.* Lancet Neurol, 2006. **5**(4): p. 303-9.

12. Hauser, R.A., P.R. Sandberg, T.B. Freeman, and A.J. Stoessl, *Bilateral human fetal striatal transplantation in Huntington's disease.* Neurology, 2002. **58**(11): p. 1704; author reply 1704.

13. Lunn, J.S., S.A. Sakowski, J. Hur, and E.L. Feldman, *Stem cell technology for neurodegenerative diseases.* Ann Neurol, 2011. **70**(3): p. 353-61.

14. Savitz, S.I. and K. Parsha, *60 - Enhancing Stroke Recovery with Cellular Therapies*, in *Stroke (Sixth Edition)*. Wong, Editor. 2016, Elsevier: London. p. 981-991.

15. Kondziolka, D., et al., *Neurotransplantation for patients with subcortical motor stroke: a phase 2 randomized trial.* J Neurosurg, 2005. **103**(1): p. 38-45.

16. Bliss, T.M., R.H. Andres, and G.K. Steinberg, *Optimizing the success of cell transplantation therapy for stroke.* Neurobiol Dis, 2010. **37**(2): p. 275-83.

17. Mackay-Sim, A., et al., *Autologous olfactory ensheathing cell transplantation in human paraplegia: a 3-year clinical trial.* Brain, 2008. **131**(Pt 9): p. 2376-86.

18. Jones, L.A., et al., *A phase 2 autologous cellular therapy trial in patients with acute, complete spinal cord injury: pragmatics, recruitment, and demographics.* Spinal Cord, 2010. **48**(11): p. 798-807.

19. Kalladka, D., Sinden, J., et al., *Human neural stem cells in patients with chronic ischaemic stroke (PISCES): a phase 1, first-in-man study.* Lancet, 2016. **388**(10046): p. 787-96.

20. Srijaya, T.C., T.S. Ramasamy, and N.H. Kasim, *Advancing stem cell therapy from bench to bedside: lessons from drug therapies.* Journal of Translational Medicine, 2014. **12**: p. 243.

21. Stover, N.P., et al., *Intrastriatal implantation of human retinal pigment epithelial cells attached to microcarriers in advanced Parkinson disease.* Arch Neurol, 2005. **62**(12): p. 1833-7.

22. Rossetti, T., F. Nicholls, and M. Modo, *Intracerebral Cell Implantation: Preparation and Characterization of Cell Suspensions.* Cell Transplant, 2016. **25**(4): p. 645-64.

23. Templin, C., T.F. Luscher, and U. Landmesser, *Cell-based cardiovascular repair and regeneration in acute myocardial infarction and chronic ischemic cardiomyopathy-current status and future developments.* Int J Dev Biol, 2011. **55**(4-5): p. 407-17.

24. Teng, C.J., J. Luo, R.C. Chiu, and D. Shum-Tim, *Massive mechanical loss of microspheres with direct intramyocardial injection in the beating heart: implications for cellular cardiomyoplasty.* J Thorac Cardiovasc Surg, 2006. **132**(3): p. 628-32.

25. Hicks, A.U., et al., *Transplantation of human embryonic stem cell-derived neural precursor cells and enriched environment after cortical stroke in rats: cell survival and functional recovery.* European Journal of Neuroscience, 2009. **29**(3): p. 562-74.

26. Muller-Ehmsen, J., et al., *Survival and development of neonatal rat cardiomyocytes transplanted into adult myocardium.* J Mol Cell Cardiol, 2002. **34**(2): p. 107-16.

27. Hubschman, J.P., S. Reddy, and S.D. Schwartz, *Age-related macular degeneration: current treatments.* Clin Ophthalmol, 2009. **3**: p. 155-66.

28. Wang, G., et al., *Analysis of the indel at the ARMS2 3'UTR in age-related macular degeneration.* Hum Genet, 2010. **127**(5): p. 595-602.

29. Laflamme, M.A. and C.E. Murry, *Heart regeneration.* Nature, 2011. **473**(7347): p. 326-35.

30. Wang, H., et al., *Injectable biodegradable hydrogels for embryonic stem cell transplantation: improved cardiac remodelling and function of myocardial infarction.* J Cell Mol Med, 2012. **16**(6): p. 1310-20.

31. Dunnett, S.B., A. Bjorklund, and O. Lindvall, *Cell therapy in Parkinson's disease - stop or go?* Nat Rev Neurosci, 2001. **2**(5): p. 365-9.

32. Lindvall, O. and A. Bjorklund, *Cell therapy in Parkinson's disease.* NeuroRx, 2004. **1**(4): p. 382-93.

33. Selden NR, G.D., Huhn SL, Koch TK, Al-Uzri A, Steiner RD, *CNS transplantation of purified neural stem cells in neuronal ceroid lipofuscinoses: Phase I trial.*, in *American Association of Neurological Surgeons Annual Meeting.* 2010: Philadelphia, PA.

34. Laflamme, M.A., et al., *Cardiomyocytes derived from human embryonic stem cells in pro-survival factors enhance function of infarcted rat hearts.* Nat Biotechnol, 2007. **25**(9): p. 1015-24.

35. Silva, E.A., E.S. Kim, H.J. Kong, and D.J. Mooney, *Material-based deployment enhances efficacy of endothelial progenitor cells.* Proc Natl Acad Sci U S A, 2008. **105**(38): p. 14347-52.

36. Wang, L., J. Shansky, C. Borselli, D. Mooney, and H. Vandenburgh, *Design and fabrication of a biodegradable, covalently crosslinked shape-memory alginate scaffold for cell and growth factor delivery.* Tissue Eng Part A, 2012. **18**(19-20): p. 2000-7.

37. Guest, J., F. Benavides, K. Padgett, E. Mendez, and D. Tovar, *Technical aspects of spinal cord injections for cell transplantation. Clinical and translational considerations.* Brain Res Bull, 2011. **84**(4-5): p. 267-79.

38. Skuk, D., M. Paradis, M. Goulet, and J.P. Tremblay, *Ischemic central necrosis in pockets of transplanted myoblasts in nonhuman primates: implications for cell-transplantation strategies.* Transplantation, 2007. **84**(10): p. 1307-15.

39. Schwartz, S.D., E. Anglade, R. Lanza, and G. Ocata Macular Disease Investigator, *Stem cells in age-related macular degeneration and Stargardt's macular dystrophy - Authors' reply.* Lancet, 2015. **386**(9988): p. 30.

40. Borlongan, C.V. and M.D. Weiss, *Baby STEPS: a giant leap for cell therapy in neonatal brain injury.* Pediatr Res, 2011. **70**(1): p. 3-9.

41. Vadala, G., et al., *Mesenchymal stem cells injection in degenerated intervertebral disc: cell leakage may induce osteophyte formation.* J Tissue Eng Regen Med, 2012. **6**(5): p. 348-55.

42. Walker, P.A., et al., *Effect of needle diameter and flow rate on rat and human mesenchymal stromal cell characterization and viability.* Tissue Eng Part C Methods, 2010. **16**(5): p. 989-97.

43. Potts, M.B., M.T. Silvestrini, and D.A. Lim, *Devices for cell transplantation into the central nervous system: Design considerations and emerging technologies.* Surg Neurol Int, 2013. **4**(Suppl 1): p. S22-30.

44. Chen, Y., et al., *Effects of storage solutions on the viability of human umbilical cord mesenchymal stem cells for transplantation.* Cell Transplant, 2013. **22**(6): p. 1075-86.

45. Watts, C., M.A. Caldwell, and S.B. Dunnett, *The development of intracerebral cell-suspension implants is influenced by the grafting medium.* Cell Transplant, 1998. **7**(6): p. 573-83.

46. Mathew, A.J., J.M. Baust, R.G. Van Buskirk, and J.G. Baust, *Cell preservation in reparative and regenerative medicine: evolution of individualized solution composition.* Tissue Eng, 2004. **10**(11-12): p. 1662-71.

47. Silvestrini, M.T., et al., *Radially Branched Deployment for More Efficient Cell Transplantation at the Scale of the Human Brain.* Stereotact Funct Neurosurg, 2013. **91**(2): p. 92-103.

48. Kopyov, O.V., D. Jacques, A. Lieberman, C.M. Duma, and R.L. Rogers, *Outcome following intrastriatal fetal mesencephalic grafts for Parkinson's patients is directly related to the volume of grafted tissue.* Exp Neurol, 1997. **146**(2): p. 536-545.

49. Breeze, R.E., T.H. Wells, Jr., and C.R. Freed, *Implantation of fetal tissue for the management of Parkinson's disease: a technical note.* Neurosurgery, 1995. **36**(5): p. 1044-7; discussion 1047-8.

50. Gutierrez, J., et al., *Preclinical Validation of Multilevel Intraparenchymal Stem Cell Therapy in the Porcine Spinal Cord.* Neurosurgery, 2015. **77**(4): p. 604-12; discussion 612.

51. Usvald, D., et al., *Analysis of dosing regimen and reproducibility of intraspinal grafting of human spinal stem cells in immunosuppressed minipigs.* Cell Transplant, 2010. **19**(9): p. 1103-22.

52. Yamout, B., et al., *Bone marrow mesenchymal stem cell transplantation in patients with multiple sclerosis: a pilot study.* J Neuroimmunol, 2010. **227**(1-2): p. 185-9.

53. Kishk, N.A., et al., *Case control series of intrathecal autologous bone marrow mesenchymal stem cell therapy for chronic spinal cord injury.* Neurorehabil Neural Repair, 2010. **24**(8): p. 702-8.

54. Eckert, M.A., et al., *Evidence for high translational potential of mesenchymal stromal cell therapy to improve recovery from ischemic stroke.* J Cereb Blood Flow Metab, 2013. **33**(9): p. 1322-34.

55. Taguchi, A., et al., *Intravenous Autologous Bone Marrow Mononuclear Cell Transplantation for Stroke: Phase1/2a Clinical Trial in a Homogeneous Group of Stroke Patients.* Stem Cells Dev, 2015. **24**(19): p. 2207-18.

56. Heng, B.C., et al., *Transcatheter injection-induced changes in human bone marrow-derived mesenchymal stem cells.* Cell Transplant, 2009. **18**(10): p. 1111-21.

57. Kebriaei, P., et al., *Adult human mesenchymal stem cells added to corticosteroid therapy for the treatment of acute graft-versus-host disease.* Biol Blood Marrow Transplant, 2009. **15**(7): p. 804-11.

58. Shehadah, A., et al., *Human placenta-derived adherent cell treatment of experimental stroke promotes functional recovery after stroke in young adult and older rats.* PLoS One, 2014. **9**(1): p. e86621.

59. Qiao, L.Y., et al., *A two-year follow-up study of cotransplantation with neural stem/progenitor cells and mesenchymal stromal cells in ischemic stroke patients.* Cell Transplant, 2014. **23 Suppl 1**: p. S65-72.

60. Miljan, E.A. and J.D. Sinden, *Stem cell treatment of ischemic brain injury.* Curr Opin Mol Ther, 2009. **11**(4): p. 394-403.

61. Bjarkam, C.R., et al., *Safety and function of a new clinical intracerebral microinjection instrument for stem cells and therapeutics examined in the Gottingen minipig.* Stereotact Funct Neurosurg, 2010. **88**(1): p. 56-63.

62. Brecknell, J.E. and J.W. Fawcett, *A device for the implantation of multiple cellular deposits into a large volume of brain from a single cannula site.* Exp Neurol, 1996. **138**(2): p. 338-44.

63. Mendez, I., M. Hong, S. Smith, A. Dagher, and J. Desrosiers, *Neural transplantation cannula and microinjector system: experimental and clinical experience. Technical note.* J Neurosurg, 2000. **92**(3): p. 493-9.

64. Lammertse, D.P., et al., *Autologous incubated macrophage therapy in acute, complete spinal cord injury: results of the phase 2 randomized controlled multicenter trial.* Spinal Cord, 2012. **50**(9): p. 661-671.

65. Tabakow, P., et al., *Transplantation of Autologous Olfactory Ensheathing Cells in Complete Human Spinal Cord Injury.* Cell Transplant, 2013. **22**(9): p. 1591-1612.

66. Feron, F., et al., *Autologous olfactory ensheathing cell transplantation in human spinal cord injury.* Brain, 2005. **128**(Pt 12): p. 2951-60.

67. Knoller, N., et al., *Clinical experience using incubated autologous macrophages as a treatment for complete spinal cord injury: Phase I study results.* Journal of Neurosurgery-Spine, 2005. **3**(3): p. 173-181.

68. Deda, H., et al., *Treatment of chronic spinal cord injured patients with autologous bone marrow-derived hematopoietic stem cell transplantation: 1-year follow-up.* Cytotherapy, 2008. **10**(6): p. 565-74.

69. Savitz, S.I., et al., *Neurotransplantation of fetal porcine cells in patients with basal ganglia infarcts: A preliminary safety and feasibility study.* Cerebrovascular Diseases, 2005. **20**(2): p. 101-107.

70. Kondziolka, D., G.K. Steinberg, S.B. Cullen, and M. McGrogan, *Evaluation of surgical techniques for neuronal cell transplantation used in patients with stroke.* Cell Transplant, 2004. **13**(7-8): p. 749-754.

71. Mendez, I., et al., *Cell type analysis of functional fetal dopamine cell suspension transplants in the striatum and substantia nigra of patients with Parkinson's disease.* Brain, 2005. **128**(Pt 7): p. 1498-510.

72. Burguera, E.F., H.H. Xu, and L. Sun, *Injectable calcium phosphate cement: effects of powder-to-liquid ratio and needle size.* J Biomed Mater Res B Appl Biomater, 2008. **84**(2): p. 493-502.

73. Tol, M., A.R. Akar, S. Durdu, E. Ayyildiz, and O. Ilhan, *Comparison of different needle diameters and flow rates on bone marrow mononuclear stem cell viability: an ex vivo experimental study.* Cytotherapy, 2008. **10**(1): p. 98-99.

74. Aguado, B.A., W. Mulyasasmita, J. Su, K.J. Lampe, and S.C. Heilshorn, *Improving viability of stem cells during syringe needle flow through the design of hydrogel cell carriers.* Tissue Eng Part A, 2012. **18**(7-8): p. 806-15.

75. Grellier, M., R. Bareille, C. Bourget, and J. Amedee, *Responsiveness of human bone marrow stromal cells to shear stress.* J Tissue Eng Regen Med, 2009. **3**(4): p. 302-9.

76. Stolberg, S. and K.E. McCloskey, *Can shear stress direct stem cell fate?* Biotechnol Prog, 2009. **25**(1): p. 10-9.

77. Bird, R.B., W.E. Stewart, and E.N. Lightfoot, *Transport Phenomena*. 2007: Wiley.

78. Reneman, R.S. and A.P. Hoeks, *Wall shear stress as measured in vivo: consequences for the design of the arterial system.* Med Biol Eng Comput, 2008. **46**(5): p. 499-507.

79. Malek, A.M., S.L. Alper, and S. Izumo, *Hemodynamic shear stress and its role in atherosclerosis.* JAMA, 1999. **282**(21): p. 2035-42.

80. Korenaga, R., et al., *Negative transcriptional regulation of the VCAM-1 gene by fluid shear stress in murine endothelial cells.* American Journal of Physiology-Cell Physiology, 1997. **273**(5): p. C1506-C1515.

81. Wang, H., et al., *Shear stress induces endothelial differentiation from a murine embryonic mesenchymal progenitor cell line.* Arterioscler Thromb Vasc Biol, 2005. **25**(9): p. 1817-23.

82. Amer, M.H., L.J. White, and K.M. Shakesheff, *The effect of injection using narrow-bore needles on mammalian cells: administration and formulation considerations for cell therapies.* J Pharm Pharmacol, 2015. **67**(5): p. 640-50.

83. Doran, P.M., *Bioprocess Engineering Principles, 2nd Edition.* Bioprocess Engineering Principles, 2nd Edition, 2013: p. 1-919.

84. Sutera, S.P., *Flow-induced trauma to blood cells.* Circ Res, 1977. **41**(1): p. 2-8.

85. Lee, S.S., Y. Yim, K.H. Ahn, and S.J. Lee, *Extensional flow-based assessment of red blood cell deformability using hyperbolic converging microchannel.* Biomed Microdevices, 2009. **11**(5): p. 1021-7.

86. Tanzeglock, T., M. Soos, G. Stephanopoulos, and M. Morbidelli, *Induction of mammalian cell death by simple shear and extensional flows.* Biotechnol Bioeng, 2009. **104**(2): p. 360-70.

87. Olsen, B.D., J.A. Kornfield, and D.A. Tirrell, *Yielding Behavior in Injectable Hydrogels from Telechelic Proteins.* Macromolecules, 2010. **43**(21): p. 9094-9099.

88. Dong, J., et al., *A novel and precise method for simultaneous measurement of serum HDL and LDL subfractions and lipoprotein (a) cholesterol by ultracentrifugation and high-performance liquid chromatography.* Clin Chim Acta, 2012. **413**(13-14): p. 1071-6.

89. Kondziolka, D., G.T. Gobbel, W. Fellows-Mayle, Y.F. Chang, and M. Uram, *Injection parameters affect cell viability and implant volumes in automated cell delivery for the brain.* Cell Transplant, 2011. **20**(11-12): p. 1901-6.

90. Mazzini, L., et al., *Human neural stem cell transplantation in ALS: initial results from a phase I trial.* J Transl Med, 2015. **13**: p. 17.

91. Riley, J.P., B. Raore, J.S. Taub, T. Federici, and N.M. Boulis, *Platform and cannula design improvements for spinal cord therapeutics delivery.* Neurosurgery, 2011. **69**(2 Suppl Operative): p. ons147-54; discussion ons155.

92. Riley, J., et al., *Intraspinal stem cell transplantation in amyotrophic lateral sclerosis: a phase I safety trial, technical note, and lumbar safety outcomes.* Neurosurgery, 2012. **71**(2): p. 405-16; discussion 416.

93. Zarembinski, T.I., et al., *Thiolated hyaluronan-based hydrogels crosslinked using oxidized glutathione: an injectable matrix designed for ophthalmic applications.* Acta Biomater, 2014. **10**(1): p. 94-103.

94. Ballios, B.G., M.J. Cooke, D. van der Kooy, and M.S. Shoichet, *A hydrogel-based stem cell delivery system to treat retinal degenerative diseases.* Biomaterials, 2010. **31**(9): p. 2555-64.

95. van Asten, F., et al., *Are Intravitreal Injections with Ultrathin 33-G Needles Less Painful Than the Commonly Used 30-G Needles?* Retina, 2015. **35**(9): p. 1778-85.

96. Nikkhah, G., et al., *A microtransplantation approach for cell suspension grafting in the rat Parkinson model: a detailed account of the methodology.* Neuroscience, 1994. **63**(1): p. 57-72.

97. Mehta, T., et al., *Subarachnoid placement of stem cells in neurological disorders.* Transplant Proc, 2008. **40**(4): p. 1145-7.

98. Karussis, D., et al., *Safety and immunological effects of mesenchymal stem cell transplantation in patients with multiple sclerosis and amyotrophic lateral sclerosis.* Arch Neurol, 2010. **67**(10): p. 1187-94.

99. Veraitch, F.S., R. Scott, J.W. Wong, G.J. Lye, and C. Mason, *The impact of manual processing on the expansion and directed differentiation of embryonic stem cells.* Biotechnol Bioeng, 2008. **99**(5): p. 1216-29.

100. Amer, M.H., F.R.A.J. Rose, L.J. White, and K.M. Shakesheff, *A Detailed Assessment of Varying Ejection Rate on Delivery Efficiency of Mesenchymal Stem Cells Using Narrow-Bore Needles.* Stem Cells Translational Medicine, 2016. **5**(3): p. 366-378.

101. Torres, E.M., M. Trigano, and S.B. Dunnett, *Translation of cell therapies to the clinic: characteristics of cell suspensions in large-diameter injection cannulae.* Cell Transplant, 2015. **24**(4): p. 737-49.

102. Heaton, J.T., et al., *Modification and testing of a pneumatic dispensing device for controlled delivery of injectable materials.* Laryngoscope, 2012. **122**(9): p. 2023-2028.

103. Guo, B.L., A. Finne-Wistrand, and A.C. Albertsson, *Molecular Architecture of Electroactive and Biodegradable Copolymers Composed of Polylactide and Carboxyl-Capped Aniline Trimer.* Biomacromolecules, 2010. **11**(4): p. 855-863.

104. Bayoussef, Z., J.E. Dixon, S. Stolnik, and K.M. Shakesheff, *Aggregation promotes cell viability, proliferation, and differentiation in an in vitro model of injection cell therapy.* J Tissue Eng Regen Med, 2012. **6**(10): p. e61-73.

105. Ma, Y., et al., *Dyskinesia after fetal cell transplantation for parkinsonism: a PET study.* Ann Neurol, 2002. **52**(5): p. 628-34.

106. Borlongan, C.V., et al., *Potential of stem/progenitor cells in treating stroke: the missing steps in translating cell therapy from laboratory to clinic.* Regen Med, 2008. **3**(3): p. 249-50.

107. Glass, J.D., et al., *Lumbar intraspinal injection of neural stem cells in patients with amyotrophic lateral sclerosis: results of a phase I trial in 12 patients.* Stem Cells, 2012. **30**(6): p. 1144-51.

108. Yoon, S.H., et al., *Complete spinal cord injury treatment using autologous bone marrow cell transplantation and bone marrow stimulation with granulocyte macrophage-colony stimulating factor: Phase I/II clinical trial.* Stem Cells, 2007. **25**(8): p. 2066-73.

109. Misra, V., A. Lal, R. El Khoury, P.R. Chen, and S.I. Savitz, *Intra-arterial delivery of cell therapies for stroke.* Stem Cells Dev, 2012. **21**(7): p. 1007-15.

110. Rosado-de-Castro, P.H., P.M. Pimentel-Coelho, L.M. da Fonseca, G.R. de Freitas, and R. Mendez-Otero, *The rise of cell therapy trials for stroke: review of published and registered studies.* Stem Cells Dev, 2013. **22**(15): p. 2095-111.

111. Steinberg, G.K., D. Kondziolka, et al., *Clinical Outcomes of Transplanted Modified Bone Marrow-Derived Mesenchymal Stem Cells in Stroke: A Phase 1/2a Study.* Stroke, 2016. **47**(7): p. 1817-24.

112. Myers, R.D., *Injection of Solutions into Cerebral Tissue - Relation between Volume and Diffusion.* Physiology & Behavior, 1966. **1**(2): p. 171-&.

113. Peterson, S.L., *Drug microinjection in discrete brain regions.* Kopf Carrier, 1998. **50**: p. 1-6.

114. Janowski, M., et al., *Cell size and velocity of injection are major determinants of the safety of intracarotid stem cell transplantation.* Journal of Cerebral Blood Flow and Metabolism, 2013. **33**(6): p. 921-927.

115. Morrison, P.F., M.Y. Chen, R.S. Chadwick, R.R. Lonser, and E.H. Oldfield, *Focal delivery during direct infusion to brain: role of flow rate, catheter diameter, and tissue mechanics.* Am J Physiol, 1999. **277**(4 Pt 2): p. R1218-29.

116. Gobbel, G.T., D. Kondziolka, W. Fellows-Mayle, and M. Uram, *Manual vs automated delivery of cells for transplantation: accuracy, reproducibility, and impact on viability.* Neurosurgery, 2010. **67**(6): p. 1662-8; discussion 1668.

117. Massensini, A.R., et al., *Concentration-dependent rheological properties of ECM hydrogel for intracerebral delivery to a stroke cavity.* Acta Biomater, 2015. **27**: p. 116-30.

118. Miyanji, F., J.C. Furlan, B. Aarabi, P.M. Arnold, and M.G. Fehlings, *Acute cervical traumatic spinal cord injury: MR imaging findings correlated with neurologic outcome--prospective study with 100 consecutive patients.* Radiology, 2007. **243**(3): p. 820-7.

119. Valles, F., et al., *Anatomic compression caused by high-volume convection-enhanced delivery to the brain.* Neurosurgery, 2009. **65**(3): p. 579-85; discussion 585-6.

120. Yin, D., et al., *Optimal region of the putamen for image-guided convection-enhanced delivery of therapeutics in human and non-human primates.* Neuroimage, 2011. **54 Suppl 1**: p. S196-203.

121. Mamidi, M.K., et al., *Impact of passing mesenchymal stem cells through smaller bore size needles for subsequent use in patients for clinical or cosmetic indications.* Journal of Translational Medicine, 2012. **10**.

122. Agashi, K., D.Y.S. Chau, and K.M. Shakesheff, *The effect of delivery via narrow-bore needles on mesenchymal cells.* Regen Med, 2009. **4**(1): p. 49-64.

123. Chen, X. and S. Thibeault, *Effect of DMSO concentration, cell density and needle gauge on the viability of cryopreserved cells in three dimensional hyaluronan hydrogel.* Conf Proc IEEE Eng Med Biol Soc, 2013. **2013**: p. 6228-31.

124. Gobbel, G.T., D. Kondziolka, W. Fellows-Mayle, and M. Uram, *Cellular transplantation for the nervous system: impact of time after preparation on cell viability and survival.* J Neurosurg, 2010. **113**(3): p. 666-72.

125. Nikkhah, G., et al., *Microtransplantation of dopaminergic cell suspensions: further characterization and optimization of grafting parameters.* Cell Transplant, 2009. **18**(2): p. 119-33.

126. Center for Biologics Evaluation and Research, C., *Guidance for FDA Reviewers and Sponsors: Content and Review of Chemistry, Manufacturing, and Control (CMC) Information for Human Somatic Cell Therapy Investigational New Drug Applications (INDs)*. 2008.

127. Mamidi, M.K., et al., *Comparative cellular and molecular analyses of pooled bone marrow multipotent mesenchymal stromal cells during continuous passaging and after successive cryopreservation.* J Cell Biochem, 2012. **113**(10): p. 3153-64.

128. El Khoury, R., et al., *The effect of transcatheter injections on cell viability and cytokine release of mononuclear cells.* AJNR Am J Neuroradiol, 2010. **31**(8): p. 1488-92.

129. Bankiewicz, K.S., et al., *Technique for bilateral intracranial implantation of cells in monkeys using an automated delivery system.* Cell Transplant, 2000. **9**(5): p. 595-607.

130. Ott, H.C., et al., *Intramyocardial microdepot injection increases the efficacy of skeletal myoblast transplantation.* Eur J Cardiothorac Surg, 2005. **27**(6): p. 1017-21.

131. Richard, P.L., et al., *A first semimanual device for clinical intramuscular repetitive cell injections.* Cell Transplant, 2010. **19**(1): p. 67-78.

132. Brundin, P., et al., *Bilateral caudate and putamen grafts of embryonic mesencephalic tissue treated with lazaroids in Parkinson's disease.* Brain, 2000. **123 (Pt 7)**: p. 1380-90.

133. Schwartz, S.G., *Re: Awh et al.: CFH and ARMS2 Genetic polymorphisms predict response to antioxidants and zinc in patients with age-related macular degeneration (Ophthalmology 2013;120:2317-23).* Ophthalmology, 2014. **121**(8): p. e38.

134. Rajan, A., et al., *Optimized cell survival and seeding efficiency for craniofacial tissue engineering using clinical stem cell therapy.* Stem Cells Transl Med, 2014. **3**(12): p. 1495-503.

135. Zakaria, N., et al., *Results of a phase I/II clinical trial: standardized, non-xenogenic, cultivated limbal stem cell transplantation.* J Transl Med, 2014. **12**: p. 58.

136. Reyes, S., N. Tajiri, and C.V. Borlongan, *Developments in intracerebral stem cell grafts.* Expert Rev Neurother, 2015. **15**(4): p. 381-93.

137. Harting, M.T., L.E. Sloan, F. Jimenez, J. Baumgartner, and C.S. Cox, Jr., *Subacute neural stem cell therapy for traumatic brain injury.* J Surg Res, 2009. **153**(2): p. 188-94.

138. Pearson, R.A., et al., *Restoration of vision after transplantation of photoreceptors.* Nature, 2012. **485**(7396): p. 99-103.

139. Mazzini, L., et al., *Mesenchymal stem cell transplantation in amyotrophic lateral sclerosis: A Phase I clinical trial.* Exp Neurol, 2010. **223**(1): p. 229-37.

140. Cristante, A.F., et al., *Stem cells in the treatment of chronic spinal cord injury: evaluation of somatosensitive evoked potentials in 39 patients.* Spinal Cord, 2009. **47**(10): p. 733-8.

141. Riley, J., et al., *Intraspinal stem cell transplantation in amyotrophic lateral sclerosis: a phase I trial, cervical microinjection, and final surgical safety outcomes.* Neurosurgery, 2014. **74**(1): p. 77-87.

142. Hare, J.M., et al., *A Randomized, Double-Blind, Placebo-Controlled, Dose-Escalation Study of Intravenous Adult Human Mesenchymal Stem Cells (Prochymal) After Acute Myocardial Infarction.* Journal of the American College of Cardiology, 2009. **54**(24): p. 2277-2286.

143. Bidarra, S.J., C.C. Barrias, and P.L. Granja, *Injectable alginate hydrogels for cell delivery in tissue engineering.* Acta Biomaterialia, 2014. **10**(4): p. 1646-62.

144. Slaughter, B.V., S.S. Khurshid, O.Z. Fisher, A. Khademhosseini, and N.A. Peppas, *Hydrogels in regenerative medicine.* Advanced Materials, 2009. **21**(32-33): p. 3307-29.

145. Hamdi, H., et al., *Cell delivery: intramyocardial injections or epicardial deposition? A head-to-head comparison.* Ann Thorac Surg, 2009. **87**(4): p. 1196-203.

146. Smith, R.R., E. Marban, and L. Marban, *Enhancing retention and efficacy of cardiosphere-derived cells administered after myocardial infarction using a hyaluronan-gelatin hydrogel.* Biomatter, 2013. **3**(1).

147. Qian, L., et al., *Hemodynamic contribution of stem cell scaffolding in acute injured myocardium.* Tissue Eng Part A, 2012. **18**(15-16): p. 1652-63.

148. Sortwell, C.E., *Strategies for the augmentation of grafted dopamine neuron survival.* Frontiers in Bioscience, 2003. **8**: p. S522-S532.

149. Guarino, V., A. Gloria, M.G. Raucci, and L. Ambrosio, *Hydrogel-Based Platforms for the Regeneration of Osteochondral Tissue and Intervertebral Disc.* Polymers, 2012. **4**(3): p. 1590-1612.

150. Seif-Naraghi, S.B., M.A. Salvatore, P.J. Schup-Magoffin, D.P. Hu, and K.L. Christman, *Design and characterization of an injectable pericardial matrix gel: a potentially autologous scaffold for cardiac tissue engineering.* Tissue Eng Part A, 2010. **16**(6): p. 2017-27.

151. Uemura, M., et al., *Matrigel supports survival and neuronal differentiation of grafted embryonic stem cell-derived neural precursor cells.* J Neurosci Res, 2010. **88**(3): p. 542-51.

152. Sortwell, C.E., *Strategies for the augmentation of grafted dopamine neuron survival.* Frontiers in Bioscience, 2003. **8**: p. s522-32.

153. Hunt, J.A., R. Chen, T. van Veen, and N. Bryan, *Hydrogels for tissue engineering and regenerative medicine.* Journal of Materials Chemistry B, 2014. **2**(33): p. 5319-5338.

154. Sivashanmugam, A., R. Arunkumar, M.V. Priya, S.V. Nair, and R. Jayakumar, *An overview of injectable polymeric hydrogels for tissue engineering.* European Polymer Journal, 2015.

155. Yan, C., et al., *Injectable solid peptide hydrogel as a cell carrier: effects of shear flow on hydrogels and cell payload.* Langmuir, 2012. **28**(14): p. 6076-87.

156. Guvendiren, M., H.D. Lu, and J.A. Burdick, *Shear-thinning hydrogels for biomedical applications.* Soft Matter, 2012. **8**(2): p. 260-272.

157. Bartlett, R.D., D. Choi, and J.B. Phillips, *Biomechanical properties of the spinal cord: implications for tissue engineering and clinical translation.* Regen Med, 2016. **11**(7): p. 659-73.

158. Kong, H.J., M.K. Smith, and D.J. Mooney, *Designing alginate hydrogels to maintain viability of immobilized cells.* Biomaterials, 2003. **24**(22): p. 4023-9.

159. Bible, E., et al., *Non-invasive imaging of transplanted human neural stem cells and ECM scaffold remodeling in the stroke-damaged rat brain by (19)F- and diffusion-MRI.* Biomaterials, 2012. **33**(10): p. 2858-71.

160. Zeng, Q. and W. Chen, *The functional behavior of a macrophage/fibroblast co-culture model derived from normal and diabetic mice with a marine gelatin-oxidized alginate hydrogel.* Biomaterials, 2010. **31**(22): p. 5772-81.

161. Ryu, J.H., et al., *Implantation of bone marrow mononuclear cells using injectable fibrin matrix enhances neovascularization in infarcted myocardium.* Biomaterials, 2005. **26**(3): p. 319-26.

162. Barbero, A., et al., *Growth factor supplemented matrigel improves ectopic skeletal muscle formation--a cell therapy approach.* J Cell Physiol, 2001. **186**(2): p. 183-92.

163. Bible, E., et al., *Attachment of stem cells to scaffold particles for intra-cerebral transplantation.* Nat Protoc, 2009. **4**(10): p. 1440-53.

164. Bible, E., et al., *The support of neural stem cells transplanted into stroke-induced brain cavities by PLGA particles.* Biomaterials, 2009. **30**(16): p. 2985-94.

165. Mahoney, M.J. and W.M. Saltzman, *Transplantation of brain cells assembled around a programmable synthetic microenvironment.* Nat Biotechnol, 2001. **19**(10): p. 934-9.

166. Salama, H., et al., *Peripheral vein infusion of autologous mesenchymal stem cells in Egyptian HCV-positive patients with end-stage liver disease.* Stem Cell Res Ther, 2014. **5**(3): p. 70.

167. Moriya, K., et al., *Embryonic stem cells reduce liver fibrosis in CCl4-treated mice.* Int J Exp Pathol, 2008. **89**(6): p. 401-9.

168. Casanova, F., P.R. Carney, and M. Sarntinoranont, *Effect of needle insertion speed on tissue injury, stress, and backflow distribution for convection-enhanced delivery in the rat brain.* PLoS One, 2014. **9**(4): p. e94919.

169. Guo, L., et al., *A novel method for efficient delivery of stem cells to the ischemic brain.* Stem Cell Res Ther, 2013. **4**(5): p. 116.

170. Kim, H.J., et al., *Stereotactic brain injection of human umbilical cord blood mesenchymal stem cells in patients with Alzheimer's disease dementia: A phase 1*

clinical trial. Alzheimer's & Dementia: Translational Research & Clinical Interventions, 2015. **1**(2): p. 95-102.

171. Park SS, Bauer G, et al. *Intravitreal Autologous Bone Marrow CD34+ Cell Therapy for Ischemic and Degenerative Retinal Disorders: Preliminary Phase 1 Clinical Trial Findings*. Investigative Ophthalmology & Visual Science. 2015. **56**(1): p. 81-89.

172. Boncler, M., M. Rozalski, U. Krajewska, A. Podsedek, and C. Watala, *Comparison of PrestoBlue and MTT assays of cellular viability in the assessment of anti-proliferative effects of plant extracts on human endothelial cells.* J Pharmacol Toxicol Methods, 2014. **69**(1): p. 9-16.

173. Quent, V.M.C., D. Loessner, T. Friis, J.C. Reichert, and D.W. Hutmacher, *Discrepancies between metabolic activity and DNA content as tool to assess cell proliferation in cancer research.* Journal of Cellular and Molecular Medicine, 2010. **14**(4): p. 1003-1013.

174. Debacq-Chainiaux, F., J.D. Erusalimsky, J. Campisi, and O. Toussaint, *Protocols to detect senescence-associated beta-galactosidase (SA-betagal) activity, a biomarker of senescent cells in culture and in vivo.* Nat Protoc, 2009. **4**(12): p. 1798-806.

175. Campisi, J. and F. d'Adda di Fagagna, *Cellular senescence: when bad things happen to good cells.* Nat Rev Mol Cell Biol, 2007. **8**(9): p. 729-40.

176. Rieger, A.M., K.L. Nelson, J.D. Konowalchuk, and D.R. Barreda, *Modified annexin V/propidium iodide apoptosis assay for accurate assessment of cell death.* J Vis Exp, 2011(50).

177. Greenberger, J.S., *Corticosteroid-dependent differentiation of human marrow preadipocytes in vitro.* In Vitro, 1979. **15**(10): p. 823-8.

178. Penick, K.J., L.A. Solchaga, and J.F. Welter, *High-throughput aggregate culture system to assess the chondrogenic potential of mesenchymal stem cells.* Biotechniques, 2005. **39**(5): p. 687-91.

179. Johnstone, B., T.M. Hering, A.I. Caplan, V.M. Goldberg, and J.U. Yoo, *In vitro chondrogenesis of bone marrow-derived mesenchymal progenitor cells.* Exp Cell Res, 1998. **238**(1): p. 265-72.

180. Bean, A.C. and R.S. Tuan, *Fiber diameter and seeding density influence chondrogenic differentiation of mesenchymal stem cells seeded on electrospun poly(epsilon-caprolactone) scaffolds.* Biomed Mater, 2015. **10**(1): p. 015018.

181. Wang, L., K. Seshareddy, M.L. Weiss, and M.S. Detamore, *Effect of initial seeding density on human umbilical cord mesenchymal stromal cells for fibrocartilage tissue engineering.* Tissue Eng Part A, 2009. **15**(5): p. 1009-17.

182. Sawkins, M.J., et al., *Hydrogels derived from demineralized and decellularized bone extracellular matrix.* Acta Biomater, 2013. **9**(8): p. 7865-73.

183. Macosko, C.W., *Rheology Principles, Measurements, and Applications*. Advances in interfacial engineering series. 1994, VCH, New York: Wiley.

184. Goodwin, J.W. and R.W. Hughes, *Rheology for Chemists: An Introduction.* Rheology for Chemists: An Introduction, 2008: p. 1-264.

185. Larson, R.G., *The Structure and Rheology of Complex Fluids*. 1999: Oxford University Press.

186. Mezger, T.G., *The Rheology Handbook*. 2006., Hannover, Germany: Vincentz Network GmbH and Co.

187. Pethrick, R.A., *Polymer surface modification and characterization, edited by Chi-Ming Chan. Carl Hanser Verlag, Munich, Vienna, New York, 1993.* Polymer International, 1995. **37**(1).

188. Bang, O.Y., J.S. Lee, P.H. Lee, and G. Lee, *Autologous mesenchymal stem cell transplantation in stroke patients.* Ann Neurol, 2005. **57**(6): p. 874-82.

189. Mooney, D.J. and H. Vandenburgh, *Cell delivery mechanisms for tissue repair.* Cell Stem Cell, 2008. **2**(3): p. 205-13.

190. Karp, J.M. and G.S. Leng Teo, *Mesenchymal stem cell homing: the devil is in the details.* Cell Stem Cell, 2009. **4**(3): p. 206-16.

191. Bliss, T.M., et al., *Transplantation of hNT neurons into the ischemic cortex: Cell survival and effect on sensorimotor behavior.* Journal of Neuroscience Research, 2006. **83**(6): p. 1004-1014.

192. Spielmann, H., et al., *The International EU/COLIPA In Vitro Phototoxicity Validation Study: Results of Phase II (Blind Trial). Part 1: The 3T3 NRU Phototoxicity Test.* Toxicol In Vitro, 1998. **12**(3): p. 305-27.

193. Ranzato, E., M. Patrone, M. Pedrazzi, and B. Burlando, *Hmgb1 promotes wound healing of 3T3 mouse fibroblasts via RAGE-dependent ERK1/2 activation.* Cell Biochem Biophys, 2010. **57**(1): p. 9-17.

194. Kuonen, R., et al., *Effects of Lipophilic Extract of Viscum album L. and Oleanolic Acid on Migratory Activity of NIH/3T3 Fibroblasts and on HaCat Keratinocytes.* Evid Based Complement Alternat Med, 2013. **2013**: p. 718105.

195. Khalili, A.A. and M.R. Ahmad, *A Review of Cell Adhesion Studies for Biomedical and Biological Applications.* Int J Mol Sci, 2015. **16**(8): p. 18149-84.

196. Fletcher, D.A. and R.D. Mullins, *Cell mechanics and the cytoskeleton.* Nature, 2010. **463**(7280): p. 485-92.

197. Lowe, N.J., P.L. Lowe, and J. St Clair Roberts, *A phase IIa open-label dose-escalation pilot study using allogeneic human dermal fibroblasts for nasolabial folds.* Dermatol Surg, 2010. **36**(10): p. 1578-85.

198. Chugh, A.R., et al., *Administration of cardiac stem cells in patients with ischemic cardiomyopathy: the SCIPIO trial: surgical aspects and interim analysis of myocardial function and viability by magnetic resonance.* Circulation, 2012. **126**(11 Suppl 1): p. S54-64.

199. Schwartz, S.D., et al., *Embryonic stem cell trials for macular degeneration: a preliminary report.* Lancet, 2012. **379**(9817): p. 713-20.

200. Orozco, L., et al., *Treatment of knee osteoarthritis with autologous mesenchymal stem cells: a pilot study.* Transplantation, 2013. **95**(12): p. 1535-41.

201. Takashina, T. and M. Nakayama, *Modifications enhance the apoptosis-inducing activity of FADD.* Mol Cancer Ther, 2007. **6**(6): p. 1793-803.

202. Gallant, N.D., J.R. Capadona, A.B. Frazier, D.M. Collard, and A.J. Garcia, *Micropatterned surfaces to engineer focal adhesions for analysis of cell adhesion strengthening.* Langmuir, 2002. **18**(14): p. 5579-5584.

203. Khalili, A., and Ahmad, M.R., *A review of cell adhesion studies for biomedical and biological applications.* International journal of molecular sciences, 2015. **16**(8): p. 18149-18184.

204. Bayoussef, Z., J.E. Dixon, S. Stolnik, and K.M. Shakesheff, *Aggregation promotes cell viability, proliferation, and differentiation in an in vitro model of injection cell therapy.* Journal of Tissue Engineering and Regenerative Medicine, 2012. **6**(10): p. e61-e73.

205. Lin, S.Z., *Translational Cell Therapies in Regenerative Medicine and Cancers.* Cell Transplantation, 2016. **25**(5): p. 781-782.

206. Mendez, I., et al., *Cell type analysis of functional fetal dopamine cell suspension transplants in the striatum and substantia nigra of patients with Parkinson's disease.* Brain, 2005. **128**: p. 1498-1510.

207. Phinney, D.G. and D.J. Prockop, *Concise review: Mesenchymal stem/multipotent stromal cells: The state of transdifferentiation and modes of tissue repair - Current views.* Stem Cells, 2007. **25**(11): p. 2896-2902.

208. Caplan, A., *Why are MSCs therapeutic? New data: new insight.* Journal of Pathology, 2009. **217**(2): p. 318-324.

209. Martens, T.P., et al., *Mesenchymal lineage precursor cells induce vascular network formation in ischemic myocardium.* Nat Clin Pract Cardiovasc Med, 2006. **3 Suppl 1**: p. S18-22.

210. Suzuki, K., et al., *Role of interleukin-1beta in acute inflammation and graft death after cell transplantation to the heart.* Circulation, 2004. **110**(11 Suppl 1): p. II219-24.

211. Srijaya, T.C., T.S. Ramasamy, and N.H. Abu Kasim, *Advancing stem cell therapy from bench to bedside: lessons from drug therapies.* Journal of Translational Medicine, 2014. **12**.

212. Dominici, M., et al., *Minimal criteria for defining multipotent mesenchymal stromal cells. The International Society for Cellular Therapy position statement.* Cytotherapy, 2006. **8**(4): p. 315-7.

213. Mamidi, M.K., et al., *Impact of passing mesenchymal stem cells through smaller bore size needles for subsequent use in patients for clinical or cosmetic indications.* J Transl Med, 2012. **10**: p. 229.

214. Baer, P. C., Griesche, N., et al. *Human adipose-derived mesenchymal stem cells in vitro: evaluation of an optimal expansion medium preserving stemness*. Cytotherapy, 2010. **12**(1): p. 96-106.

215. Jin, H.J., et al., *Down-regulation of CD105 is associated with multi-lineage differentiation in human umbilical cord blood-derived mesenchymal stem cells.* Biochem Biophys Res Commun, 2009. **381**(4): p. 676-81.

216. Jung, S., K.M. Panchalingam, L. Rosenberg, and L.A. Behie, *Ex vivo expansion of human mesenchymal stem cells in defined serum-free media.* Stem Cells Int, 2012. **2012**: p. 123030.

217. Mills, J.C., N.L. Stone, and R.N. Pittman, *Extranuclear apoptosis. The role of the cytoplasm in the execution phase.* J Cell Biol, 1999. **146**(4): p. 703-8.

218. Pittenger, M.F., et al., *Multilineage potential of adult human mesenchymal stem cells.* Science, 1999. **284**(5411): p. 143-7.

219. Hao, J., et al., *Mechanobiology of mesenchymal stem cells: Perspective into mechanical induction of MSC fate.* Acta Biomater, 2015. **20**: p. 1-9.

220. Wang, J.H. and B.P. Thampatty, *Mechanobiology of adult and stem cells.* Int Rev Cell Mol Biol, 2008. **271**: p. 301-46.

221. Ku, C.H., et al., *Collagen synthesis by mesenchymal stem cells and aortic valve interstitial cells in response to mechanical stretch.* Cardiovasc Res, 2006. **71**(3): p. 548-56.

222. MacQueen, L., Y. Sun, and C.A. Simmons, *Mesenchymal stem cell mechanobiology and emerging experimental platforms.* Journal of the Royal Society Interface, 2013. **10**(84).

223. Jaiswal, N., S.E. Haynesworth, A.I. Caplan, and S.P. Bruder, *Osteogenic differentiation of purified, culture-expanded human mesenchymal stem cells in vitro.* J Cell Biochem, 1997. **64**(2): p. 295-312.

224. Potier, E., J. Noailly, and K. Ito, *Directing bone marrow-derived stromal cell function with mechanics.* J Biomech, 2010. **43**(5): p. 807-17.

225. Kreke, M.R. and A.S. Goldstein, *Hydrodynamic shear stimulates osteocalcin expression but not proliferation of bone marrow stromal cells.* Tissue Eng, 2004. **10**(5-6): p. 780-8.

226. Kreke, M.R., L.A. Sharp, Y.W. Lee, and A.S. Goldstein, *Effect of intermittent shear stress on mechanotransductive signaling and osteoblastic differentiation of bone marrow stromal cells.* Tissue Eng Part A, 2008. **14**(4): p. 529-37.

227. Li, Y.J., et al., *Oscillatory fluid flow affects human marrow stromal cell proliferation and differentiation.* J Orthop Res, 2004. **22**(6): p. 1283-9.

228. Holtorf, H.L., J.A. Jansen, and A.G. Mikos, *Flow perfusion culture induces the osteoblastic differentiation of marrow stroma cell-scaffold constructs in the absence of dexamethasone.* J Biomed Mater Res A, 2005. **72**(3): p. 326-34.

229. Meinel, L., et al., *Bone tissue engineering using human mesenchymal stem cells: effects of scaffold material and medium flow.* Ann Biomed Eng, 2004. **32**(1): p. 112-22.

230. Stiehler, M., et al., *Effect of dynamic 3-D culture on proliferation, distribution, and osteogenic differentiation of human mesenchymal stem cells.* J Biomed Mater Res A, 2009. **89**(1): p. 96-107.

231. Zhao, F., R. Chella, and T. Ma, *Effects of shear stress on 3-D human mesenchymal stem cell construct development in a perfusion bioreactor system: Experiments and hydrodynamic modeling.* Biotechnol Bioeng, 2007. **96**(3): p. 584-95.

232. Scaglione, S., et al., *Effects of fluid flow and calcium phosphate coating on human bone marrow stromal cells cultured in a defined 2D model system.* J Biomed Mater Res A, 2008. **86**(2): p. 411-9.

233. Bancroft, G.N., et al., *Fluid flow increases mineralized matrix deposition in 3D perfusion culture of marrow stromal osteoblasts in a dose-dependent manner.* Proc Natl Acad Sci U S A, 2002. **99**(20): p. 12600-5.

234. Sikavitsas, V.I., G.N. Bancroft, and A.G. Mikos, *Formation of three-dimensional cell/polymer constructs for bone tissue engineering in a spinner flask and a rotating wall vessel bioreactor.* J Biomed Mater Res, 2002. **62**(1): p. 136-48.

235. Sikavitsas, V.I., G.N. Bancroft, H.L. Holtorf, J.A. Jansen, and A.G. Mikos, *Mineralized matrix deposition by marrow stromal osteoblasts in 3D perfusion culture increases with increasing fluid shear forces.* Proc Natl Acad Sci U S A, 2003. **100**(25): p. 14683-8.

236. Wang, Y.H., Y. Liu, P. Maye, and D.W. Rowe, *Examination of mineralized nodule formation in living osteoblastic cultures using fluorescent dyes.* Biotechnol Prog, 2006. **22**(6): p. 1697-701.

237. Stein, G.S. and J.B. Lian, *Molecular Mechanisms Mediating Proliferation Differentiation Interrelationships during Progressive Development of the Osteoblast Phenotype.* Endocrine Reviews, 1993. **14**(4): p. 424-442.

238. Logan, N., et al., *TiO2-coated CoCrMo: improving the osteogenic differentiation and adhesion of mesenchymal stem cells in vitro.* J Biomed Mater Res A, 2015. **103**(3): p. 1208-17.

239. Estes, B.T., J.M. Gimble, and F. Guilak, *Mechanical signals as regulators of stem cell fate.* Curr Top Dev Biol, 2004. **60**: p. 91-126.

240. Shearn, J., L. Hellmann, and G. Boivin, *Effect of initial cell-seeding density on postoperative cell number and dispersion.* Tissue Eng, 2005. **11**(11-12): p. 1898-904.

241. Grayson, W.L., et al., *Effects of initial seeding density and fluid perfusion rate on formation of tissue-engineered bone.* Tissue Eng Part A, 2008. **14**(11): p. 1809-20.

242. Holy, C.E., M.S. Shoichet, and J.E. Davies, *Engineering three-dimensional bone tissue in vitro using biodegradable scaffolds: investigating initial cell-seeding density and culture period.* J Biomed Mater Res, 2000. **51**(3): p. 376-82.

243. Kruyt, M., et al., *Analysis of the dynamics of bone formation, effect of cell seeding density, and potential of allogeneic cells in cell-based bone tissue engineering in goats.* Tissue Eng Part A, 2008. **14**(6): p. 1081-8.

244. McBeath, R., D.M. Pirone, C.M. Nelson, K. Bhadriraju, and C.S. Chen, *Cell shape, cytoskeletal tension, and RhoA regulate stem cell lineage commitment.* Dev Cell, 2004. **6**(4): p. 483-95.

245. Ni, X.F., et al., *On-chip differentiation of human mesenchymal stem cells into adipocytes.* Microelectronic Engineering, 2008. **85**(5-6): p. 1330-1333.

246. Gobaa, S., et al., *Artificial niche microarrays for probing single stem cell fate in high throughput.* Nature Methods, 2011. **8**(11): p. 949-955.

247. McBeath, R., D.M. Pirone, C.M. Nelson, K. Bhadriraju, and C.S. Chen, *Cell shape, cytoskeletal tension, and RhoA regulate stem cell lineage commitment.* Developmental Cell, 2004. **6**(4): p. 483-495.

248. Kavalkovich, K.W., R.E. Boynton, J.M. Murphy, and F. Barry, *Chondrogenic differentiation of human mesenchymal stem cells within an alginate layer culture system.* In Vitro Cell Dev Biol Anim, 2002. **38**(8): p. 457-66.

249. Revell, C.M., C.E. Reynolds, and K.A. Athanasiou, *Effects of initial cell seeding in self assembly of articular cartilage.* Ann Biomed Eng, 2008. **36**(9): p. 1441-8.

250. Ponticiello, M.S., R.M. Schinagl, S. Kadiyala, and F.P. Barry, *Gelatin-based resorbable sponge as a carrier matrix for human mesenchymal stem cells in cartilage regeneration therapy.* J Biomed Mater Res, 2000. **52**(2): p. 246-55.

251. Erickson, I.E., et al., *High mesenchymal stem cell seeding densities in hyaluronic acid hydrogels produce engineered cartilage with native tissue properties.* Acta Biomater, 2012. **8**(8): p. 3027-34.

252. Jin, M., E.H. Frank, T.M. Quinn, E.B. Hunziker, and A.J. Grodzinsky, *Tissue shear deformation stimulates proteoglycan and protein biosynthesis in bovine cartilage explants.* Arch Biochem Biophys, 2001. **395**(1): p. 41-8.

253. Alves da Silva, M.L., et al., *Chondrogenic differentiation of human bone marrow mesenchymal stem cells in chitosan-based scaffolds using a flow-perfusion bioreactor.* J Tissue Eng Regen Med, 2011. **5**(9): p. 722-32.

254. Scotti, C., et al., *Recapitulation of endochondral bone formation using human adult mesenchymal stem cells as a paradigm for developmental engineering.* Proc Natl Acad Sci U S A, 2010. **107**(16): p. 7251-6.

255. Hofmann, M., et al., *Monitoring of bone marrow cell homing into the infarcted human myocardium.* Circulation, 2005. **111**(17): p. 2198-2202.

256. Zhang, G., Q. Hu, E.A. Braunlin, L.J. Suggs, and J. Zhang, *Enhancing efficacy of stem cell transplantation to the heart with a PEGylated fibrin biomatrix.* Tissue Eng Part A, 2008. **14**(6): p. 1025-36.

257. Kearney, C.J. and D.J. Mooney, *Macroscale delivery systems for molecular and cellular payloads.* Nat Mater, 2013. **12**(11): p. 1004-17.

258. Watt, F.M. and B.L.M. Hogan, *Out of Eden: Stem cells and their niches.* Science, 2000. **287**(5457): p. 1427-1430.

259. Sun, Y., C.S. Chen, and J. Fu, *Forcing stem cells to behave: a biophysical perspective of the cellular microenvironment.* Annu Rev Biophys, 2012. **41**: p. 519-42.

260. Discher, D.E., D.J. Mooney, and P.W. Zandstra, *Growth factors, matrices, and forces combine and control stem cells.* Science, 2009. **324**(5935): p. 1673-7.

261. Huebsch, N., et al., *Harnessing traction-mediated manipulation of the cell/matrix interface to control stem-cell fate.* Nat Mater, 2010. **9**(6): p. 518-26.

262. Trappmann, B., et al., *Extracellular-matrix tethering regulates stem-cell fate.* Nat Mater, 2012. **11**(7): p. 642-649.

263. Engler, A.J., S. Sen, H.L. Sweeney, and D.E. Discher, *Matrix elasticity directs stem cell lineage specification.* Cell, 2006. **126**(4): p. 677-689.

264. Higuchi, A., Q.D. Ling, Y. Chang, S.T. Hsu, and A. Umezawa, *Physical Cues of Biomaterials Guide Stem Cell Differentiation Fate.* Chemical Reviews, 2013. **113**(5): p. 3297-3328.

265. Lutolf, M.P., *Integration column: artificial ECM: expanding the cell biology toolbox in 3D.* Integr Biol (Camb), 2009. **1**(3): p. 235-41.

266. Tam, R.Y., T. Fuehrmann, N. Mitrousis, and M.S. Shoichet, *Regenerative therapies for central nervous system diseases: a biomaterials approach.* Neuropsychopharmacology, 2014. **39**(1): p. 169-88.

267. Mei, Y., et al., *Combinatorial development of biomaterials for clonal growth of human pluripotent stem cells.* Nat Mater, 2010. **9**(9): p. 768-778.

268. Olabisi, R.M., *Cell microencapsulation with synthetic polymers.* J Biomed Mater Res A, 2015. **103**(2): p. 846-59.

269. Gonen-Wadmany, M., L. Gepstein, and D. Seliktar, *Controlling the cellular organization of tissue-engineered cardiac constructs.* Ann N Y Acad Sci, 2004. **1015**: p. 299-311.

270. Boccafoschi, F., J. Habermehl, S. Vesentini, and D. Mantovani, *Biological performances of collagen-based scaffolds for vascular tissue engineering.* Biomaterials, 2005. **26**(35): p. 7410-7.

271. Kofidis, T., et al., *Clinically established hemostatic scaffold (tissue fleece) as biomatrix in tissue- and organ-engineering research.* Tissue Eng, 2003. **9**(3): p. 517-23.

272. Chevallay, B. and D. Herbage, *Collagen-based biomaterials as 3D scaffold for cell cultures: applications for tissue engineering and gene therapy.* Med Biol Eng Comput, 2000. **38**(2): p. 211-8.

273. Gingras, M., M.M. Beaulieu, V. Gagnon, H.D. Durham, and F. Berthod, *In vitro study of axonal migration and myelination of motor neurons in a three-dimensional tissue-engineered model.* Glia, 2008. **56**(3): p. 354-64.

274. Dewitt, D.D., S.N. Kaszuba, D.M. Thompson, and J.P. Stegemann, *Collagen I-matrigel scaffolds for enhanced Schwann cell survival and control of three-dimensional cell morphology.* Tissue Eng Part A, 2009. **15**(10): p. 2785-93.

275. Phillips, J.B. and R. Brown, *Micro-structured materials and mechanical cues in 3D collagen gels.* Methods Mol Biol, 2011. **695**: p. 183-96.

276. Gelse, K., E. Poschl, and T. Aigner, *Collagens--structure, function, and biosynthesis.* Adv Drug Deliv Rev, 2003. **55**(12): p. 1531-46.

277. Hermanns, S., N. Klapka, and H.W. Muller, *The collagenous lesion scar - an obstacle for axonal regeneration in brain and spinal cord injury.* Restorative Neurology and Neuroscience, 2001. **19**(1-2): p. 139-148.

278. Lu, D., et al., *Collagen scaffolds populated with human marrow stromal cells reduce lesion volume and improve functional outcome after traumatic brain injury.* Neurosurgery, 2007. **61**(3): p. 596-602; discussion 602-3.

279. Xiong, Y., et al., *Delayed transplantation of human marrow stromal cell-seeded scaffolds increases transcallosal neural fiber length, angiogenesis, and hippocampal neuronal survival and improves functional outcome after traumatic brain injury in rats.* Brain Res, 2009. **1263**: p. 183-91.

280. Wong, F.S. and A.C. Lo, *Collagen-Based Scaffolds for Cell Therapies in the Injured Brain.* Journal of Stem Cell Research & Therapy, 2015. **2015**.

281. Zhao, F., W.L. Grayson, T. Ma, B. Bunnell, and W.W. Lu, *Effects of hydroxyapatite in 3-D chitosan-gelatin polymer network on human mesenchymal stem cell construct development.* Biomaterials, 2006. **27**(9): p. 1859-1867.

282. Takahashi, Y., M. Yamamoto, and Y. Tabata, *Osteogenic differentiation of mesenchymal stem cells in biodegradable sponges composed of gelatin and beta-tricalcium phosphate.* Biomaterials, 2005. **26**(17): p. 3587-3596.

283. Huang, Y., S. Onyeri, M. Siewe, A. Moshfeghian, and S.V. Madihally, *In vitro characterization of chitosan-gelatin scaffolds for tissue engineering.* Biomaterials, 2005. **26**(36): p. 7616-7627.

284. Janus, J.W., A.W. Kenchington, and A.G. Ward, *A rapid method for the determination of the isoelectric point of gelatin using mixed bed deionization.* Research, 1951. **4**(5): p. 247-8.

285. Djagny, V.B., Z. Wang, and S. Xu, *Gelatin: a valuable protein for food and pharmaceutical industries: review.* Crit Rev Food Sci Nutr, 2001. **41**(6): p. 481-92.

286. Puoci, F., *Advanced Polymers in Medicine*. 2014: Springer International Publishing.

287. Ikada, Y. and Y. Tabata, *Protein release from gelatin matrices.* Adv Drug Deliv Rev, 1998. **31**(3): p. 287-301.

288. Young, S., M. Wong, Y. Tabata, and A.G. Mikos, *Gelatin as a delivery vehicle for the controlled release of bioactive molecules.* Journal of Controlled Release, 2005. **109**(1-3): p. 256-74.

289. Baker, E.L., R.T. Bonnecaze, and M.H. Zaman, *Extracellular matrix stiffness and architecture govern intracellular rheology in cancer.* Biophys J, 2009. **97**(4): p. 1013-21.

290. Santin, M., *Strategies in Regenerative Medicine: Integrating Biology with Materials Design*. 2009: Springer New York.

291. Badylak, S.F., D.O. Freytes, and T.W. Gilbert, *Extracellular matrix as a biological scaffold material: Structure and function.* Acta Biomater, 2009. **5**(1): p. 1-13.

292. Turner, N.J., et al., *Xenogeneic extracellular matrix as an inductive scaffold for regeneration of a functioning musculotendinous junction.* Tissue Eng Part A, 2010. **16**(11): p. 3309-17.

293. Valentin, J.E., N.J. Turner, T.W. Gilbert, and S.F. Badylak, *Functional skeletal muscle formation with a biologic scaffold.* Biomaterials, 2010. **31**(29): p. 7475-84.

294. Tharanathan, R.N., *Biodegradable films and composite coatings: past, present and future.* Trends in Food Science & Technology, 2003. **14**(3): p. 71-78.

295. Barkhordari, S., M. Yadollahi, and H. Namazi, *pH sensitive nanocomposite hydrogel beads based on carboxymethyl cellulose/layered double hydroxide as drug delivery systems.* Journal of Polymer Research, 2014. **21**(6).

296. Barbucci, R., G. Leone, and A. Vecchiullo, *Novel carboxymethylcellulose-based microporous hydrogels suitable for drug delivery.* Journal of Biomaterials Science-Polymer Edition, 2004. **15**(5): p. 607-619.

297. Rodriguez, R., C. Alvarez-Lorenzo, and A. Concheiro, *Cationic cellulose hydrogels: kinetics of the cross-linking process and characterization as pH-/ion-sensitive drug delivery systems.* Journal of Controlled Release, 2003. **86**(2-3): p. 253-265.

298. Alvarez-Lorenzo, C., B. Blanco-Fernandez, A.M. Puga, and A. Concheiro, *Crosslinked ionic polysaccharides for stimuli-sensitive drug delivery.* Advanced Drug Delivery Reviews, 2013. **65**(9): p. 1148-1171.

299. Feng, X.B., H.B. Hu, and M. Pritsker, *Network effects, cascades and CCP interoperability.* International Journal of Modern Physics C, 2014. **25**(9).

300. Lee, K.Y. and D.J. Mooney, *Hydrogels for tissue engineering.* Chemical Reviews, 2001. **101**(7): p. 1869-79.

301. Malafaya, P.B., G.A. Silva, and R.L. Reis, *Natural-origin polymers as carriers and scaffolds for biomolecules and cell delivery in tissue engineering applications.* Adv Drug Deliv Rev, 2007. **59**(4-5): p. 207-33.

302. Camacho, F.G., E.M. Grima, A.S. Miron, V.G. Pascual, and Y. Chisti, *Carboxymethyl cellulose protects algal cells against hydrodynamic stress.* Enzyme and Microbial Technology, 2001. **29**(10): p. 602-610.

303. Hoemann, C.D., H. El-Gabalawy, and M.D. Mckee, *In vitro osteogenesis assays: Influence of the primary cell source on alkaline phosphatase activity and mineralization.* Pathologie Biologie, 2009. **57**(4): p. 318-323.

304. Appel, E.A., et al., *Self-assembled hydrogels utilizing polymer-nanoparticle interactions.* Nat Commun, 2015. **6**: p. 6295.

305. *Polymer Interface and Adhesion - Wu,Sh.* Textile Research Journal, 1983. **53**(7): p. 452-452.

306. Kotobuki, N., et al., *Observation of osteogenic differentiation cascade of living mesenchymal stem cells on transparent hydroxyapatite ceramics.* Biomaterials, 2005. **26**(7): p. 779-85.

307. Hofstetter, C.P., et al., *Marrow stromal cells form guiding strands in the injured spinal cord and promote recovery.* Proc Natl Acad Sci U S A, 2002. **99**(4): p. 2199-204.

308. Yan, C., et al., *Injectable solid hydrogel: mechanism of shear-thinning and immediate recovery of injectable beta-hairpin peptide hydrogels.* Soft Matter, 2010. **6**(20): p. 5143-5156.

309. Jolkkonen, J. and P. Walczak, *Clinical Trials: Intracerebral cell therapy in stroke patients*, in *Cell-based therapies in stroke*. 2013, Springer Science & Business Media.

310. Lund, A.W., J.A. Bush, G.E. Plopper, and J.P. Stegemann, *Osteogenic differentiation of mesenchymal stem cells in defined protein beads.* J Biomed Mater Res B Appl Biomater, 2008. **87**(1): p. 213-21.

311. Zhu, W., J.C. Iatridis, V. Hlibczuk, A. Ratcliffe, and V.C. Mow, *Determination of collagen-proteoglycan interactions in vitro.* J Biomech, 1996. **29**(6): p. 773-83.

312. Jiang, H. and F. Grinnell, *Cell-matrix entanglement and mechanical anchorage of fibroblasts in three-dimensional collagen matrices.* Mol Biol Cell, 2005. **16**(11): p. 5070-6.

313. Shayegan, M. and N.R. Forde, *Microrheological characterization of collagen systems: from molecular solutions to fibrillar gels.* PLoS One, 2013. **8**(8): p. e70590.

314. Grinnell, F. and C.R. Lamke, *Reorganization of hydrated collagen lattices by human skin fibroblasts.* J Cell Sci, 1984. **66**: p. 51-63.

315. Saeidi, N., E.A. Sander, and J.W. Ruberti, *Dynamic shear-influenced collagen self-assembly.* Biomaterials, 2009. **30**(34): p. 6581-92.

316. O'Rourke, C., R.A. Drake, G.W. Cameron, A.J. Loughlin, and J.B. Phillips, *Optimising contraction and alignment of cellular collagen hydrogels to achieve reliable and consistent engineered anisotropic tissue.* J Biomater Appl, 2015. **30**(5): p. 599-607.

317. Phillips, J.B., S.C. Bunting, S.M. Hall, and R.A. Brown, *Neural tissue engineering: a self-organizing collagen guidance conduit.* Tissue Eng, 2005. **11**(9-10): p. 1611-7.

318. Bormashenko, E., *Wetting of real solid surfaces: new glance on well-known problems.* Colloid and Polymer Science, 2013. **291**(2): p. 339-342.

319. Garrett, H.E., *Aspects of Adhesion*, in *Chemistry & Industry*. 1966. p. 355-357.

320. Grinnell, F., M. Milam, and P.A. Srere, *Atachment of normal and transformed hamster kidney cells to substrata varying in chemical composition.* Biochem Med, 1973. **7**(1): p. 87-90.

321. Grinnell, F. and M.K. Feld, *Fibronectin adsorption on hydrophilic and hydrophobic surfaces detected by antibody binding and analyzed during cell adhesion in serum-containing medium.* J Biol Chem, 1982. **257**(9): p. 4888-93.

322. Hao, L. and J. Lawrence, *Albumin and fibronectin protein adsorption on CO2-laser-modified biograde stainless steel.* Proc Inst Mech Eng H, 2006. **220**(1): p. 47-55.

323. Anselme, K., *Osteoblast adhesion on biomaterials.* Biomaterials, 2000. **21**(7): p. 667-81.

324. Wei, J., et al., *Influence of surface wettability on competitive protein adsorption and initial attachment of osteoblasts.* Biomed Mater, 2009. **4**(4): p. 045002.

325. Altankov, G. and T. Groth, *Reorganization of Substratum-Bound Fibronectin on Hydrophilic and Hydrophobic Materials Is Related to Biocompatibility.* Journal of Materials Science-Materials in Medicine, 1994. **5**(9-10): p. 732-737.

326. Lee, J.H., G. Khang, J.W. Lee, and H.B. Lee, *Interaction of Different Types of Cells on Polymer Surfaces with Wettability Gradient.* J Colloid Interface Sci, 1998. **205**(2): p. 323-330.

327. Bialopiotrowicz, T. and B. Janczuk, *Surface properties of gelatin films.* Langmuir, 2002. **18**(24): p. 9462-9468.

328. Yasuda, T., T. Okuno, and H. Yasuda, *Contact-Angle of Water on Polymer Surfaces.* Langmuir, 1994. **10**(7): p. 2435-2439.

329. Gristina, R., et al., *Increasing cell adhesion on plasma deposited fluorocarbon coatings by changing the surface topography.* J Biomed Mater Res B Appl Biomater, 2009. **88**(1): p. 139-49.

330. Murry, C.E. and G. Keller, *Differentiation of embryonic stem cells to clinically relevant populations: lessons from embryonic development.* Cell, 2008. **132**(4): p. 661-80.

331. Prowse, A.B., F. Chong, P.P. Gray, and T.P. Munro, *Stem cell integrins: implications for ex-vivo culture and cellular therapies.* Stem Cell Res, 2011. **6**(1): p. 1-12.

332. Jiang, D., J. Liang, and P.W. Noble, *Hyaluronan in tissue injury and repair.* Annu Rev Cell Dev Biol, 2007. **23**: p. 435-61.

333. Viswanath, A., et al., *Extracellular Matrix-Derived Hydrogels for Dental Stem Cell Delivery.* J Biomed Mater Res A, 2016.

334. Shekaran, A. and A.J. Garcia, *Extracellular matrix-mimetic adhesive biomaterials for bone repair.* J Biomed Mater Res A, 2011. **96**(1): p. 261-72.

335. Papadimitropoulos, A., C. Scotti, P. Bourgine, A. Scherberich, and I. Martin, *Engineered decellularized matrices to instruct bone regeneration processes.* Bone, 2015. **70**: p. 66-72.

336. Salasznyk, R.M., W.A. Williams, A. Boskey, A. Batorsky, and G.E. Plopper, *Adhesion to Vitronectin and Collagen I Promotes Osteogenic Differentiation of Human Mesenchymal Stem Cells.* J Biomed Biotechnol, 2004. **2004**(1): p. 24-34.

337. Mizuno, M. and Y. Kuboki, *Osteoblast-related gene expression of bone marrow cells during the osteoblastic differentiation induced by type I collagen.* J Biochem, 2001. **129**(1): p. 133-8.

338. Xiao, G., D. Wang, M.D. Benson, G. Karsenty, and R.T. Franceschi, *Role of the alpha2-integrin in osteoblast-specific gene expression and activation of the Osf2 transcription factor.* J Biol Chem, 1998. **273**(49): p. 32988-94.

339. Datta, N., H.L. Holtorf, V.I. Sikavitsas, J.A. Jansen, and A.G. Mikos, *Effect of bone extracellular matrix synthesized in vitro on the osteoblastic differentiation of marrow stromal cells.* Biomaterials, 2005. **26**(9): p. 971-7.

340. Faia-Torres, A.B., et al., *Differential regulation of osteogenic differentiation of stem cells on surface roughness gradients.* Biomaterials, 2014. **35**(33): p. 9023-32.

341. Stenderup, K., J. Justesen, E.F. Eriksen, S.I. Rattan, and M. Kassem, *Number and proliferative capacity of osteogenic stem cells are maintained during aging and in patients with osteoporosis.* J Bone Miner Res, 2001. **16**(6): p. 1120-9.

342. Prins, H.J., et al., *In vitro induction of alkaline phosphatase levels predicts in vivo bone forming capacity of human bone marrow stromal cells.* Stem Cell Res, 2014. **12**(2): p. 428-40.

343. Koide, H., et al., *Mice Deficient in AKAP13 (BRX) Are Osteoporotic and Have Impaired Osteogenesis.* J Bone Miner Res, 2015. **30**(10): p. 1887-95.

344. Yourek, G., S.M. McCormick, J.J. Mao, and G.C. Reilly, *Shear stress induces osteogenic differentiation of human mesenchymal stem cells.* Regen Med, 2010. **5**(5): p. 713-24.

345. Golub, E.E., G. Harrison, A.G. Taylor, S. Camper, and I.M. Shapiro, *The role of alkaline phosphatase in cartilage mineralization.* Bone Miner, 1992. **17**(2): p. 273-8.

346. Savitz, S.I., et al., *Neurotransplantation of fetal porcine cells in patients with basal ganglia infarcts: a preliminary safety and feasibility study.* Cerebrovasc Dis, 2005. **20**(2): p. 101-7.

347. Hastings, C.L., et al., *Drug and cell delivery for cardiac regeneration.* Adv Drug Deliv Rev, 2015. **84**: p. 85-106.

348. Place, E.S., N.D. Evans, and M.M. Stevens, *Complexity in biomaterials for tissue engineering.* Nat Mater, 2009. **8**(6): p. 457-70.

349. Seif-Naraghi, S.B., et al., *Safety and efficacy of an injectable extracellular matrix hydrogel for treating myocardial infarction.* Sci Transl Med, 2013. **5**(173): p. 173ra25.

350. Barnes, J.M., J.T. Nauseef, and M.D. Henry, *Resistance to fluid shear stress is a conserved biophysical property of malignant cells.* PLoS One, 2012. **7**(12): p. e50973.

351. Munson, B.R., D.F. Young, and T.T.H. Okiishi, *Fundamentals of fluid mechanics*. 2002: John Wiley & Sons Australia, Limited.

Appendix 1| Flow parameters and shear stress calculations

A1.1 Needle diameters for needle gauges employed

Table A1.1: **Needle gauges employed in this study, and their corresponding internal needle diameters (µm).**

Needle Gauge	Internal Needle Diameter (µm)
30	159
32	108
34	51

A1.2 Shear stress calculations

The use of a syringe pump for this work allowed accurate control over flow rates, which are determined based on the pusher block travel rate (rate at which the syringe pump moves the syringe plunger) and syringe characteristics programmed into the pump's software. Substituting the rate of µL/min (which is equivalent to mm^3/min) for the volume and the length for the rate in mm/s gives this equation,

$$\text{Flow rate } (cm^3/s) = \text{rate } (\mu L/min) / (60 \times 1000);$$

where we divided by 60 to convert mins to secs and by 1000 to convert µL to cm^3. The equation $\pi R^2 l$ was used to determine the volume of the needle studied (where R is the needle radius and l is the length of needle used). Transit time was calculated by dividing volume by flow rate.

Since fluid shear stress varies with distance from the wall of the syringe/needle (parabolic velocity profile explained in Chapter 1), wall shear stress is specified. The

wall shear stress can be stated as a function of volume flow using Poiseuille's law. Volume fraction of the cell suspensions was calculated to be <0.3%, thereby is dilute enough to conform to Poiseuille flow relationships [350]. Poiseuille's equation was used to calculate shear stress,

$$\tau = \frac{4Q\eta}{\pi R^3} \quad (1)$$

where τ_{max} is shear stress (dyn/cm^2); Q is flow rate (cm^3/s); η is dynamic viscosity of the medium (PBS treated as water at room temperature; 0.01 dyn*s/cm^2); and R is needle radius (30G internal radius = 7.9X10^{-3} cm; 34G internal radius = 2.55X10^{-3} cm).

Reynolds number is a dimensionless parameter used in fluid mechanics to distinguish between laminar (smooth) and turbulent (irregular) flow [351]. Reynolds number was calculated to determine flow conditions:

$$\mathrm{Re} = \frac{\rho Q}{15\pi D\eta} \quad (2)$$

where ρ is density of PBS (treated as water at room temperature at 0.999 g/cm^3), Q is volumetric flow rate (mL/min), D is the needle diameter (cm), and η is the dynamic viscosity of the medium (0.01 g/cms^{-1}). For the lowest flow rate (10 µL/min), Re is 1.33; for the highest flow rate (300 µL/min), *Re* is 39.98 for 30G needles and 124.6 for 34G ones. These values are well below the critical value of 2100 [351], and therefore it can be safely assumed that flow in the employed needles is laminar.

The range of shear stress values and Reynold's numbers encountered in this investigation is presented in Table A1.2. It illustrates that shear forces exerted on the

cells ejected through 34G needles at the lowest flow rate under investigation are higher than those calculated for all flow rates with a 30G needle.

Table A1.2: **Shear stress values, transit times and Reynolds numbers for cell suspensions ejected through a 100 µL Hamilton syringe attached to 30- and 34G 20mm needles at the investigated flow rates, calculated using equations 1 and 2**

Flow rate (µL/min)	Shear stress τ_{max} in 100 µL syringe (dyn/cm^2)	Shear stress τ_{max} in 30G needle (dyn/cm^2)	Shear stress τ_{max} in 34G needle (dyn/cm^2)	Transit time through syringe (s)	Transit time through needle lumen (s)	Re (in a 30G needle)	Re (in a 34G needle)
10	0.006	4.25	128.2	600	2.38	1.3	4.2
20	0.011	8.48	253.4	300	1.19	2.7	8.3
50	0.027	21.20	637.3	120	0.48	6.6	20.8
150	0.082	63.59	2037.2	40	0.158	20.0	62.3
300	0.16	127.18	3839.4	20	0.079	40.0	124.6

Appendix 2| Confirming linearity of chosen cell quantitation methods

One required element of this work was the ability to quantitate cell numbers in various hMSC samples. Here the linearity of the chosen methods employed to quantify cell numbers is confirmed, using either PI (as a counter-stain for OsteoImage^{TM} staining) or Hoechst 33258 dye (as a counter-stain for AdipoRed^{TM} staining) and the Tecan Infinite M200 microplate reader. These assays provided linear results over the range of cell numbers under investigation.

Table A2.1: **Values for excitation (λ_{exc}) and emission (λ_{em}) wavelengths for individual fluorochromes used in this study**

	λ_{exc}	λ_{em}
PI	535	617
OsteoImage	492	520
Hoechst 33258	355	465
AdipoRed	485	535
PrestoBlue	560	590

A2.1 Quantitation of cell number using propidium iodide

Nuclear staining was carried out using 2 µg/mL PI (diluted in H_2O from 1 mg/mL; ThermoFisher Scientific, UK) for 5 minutes.

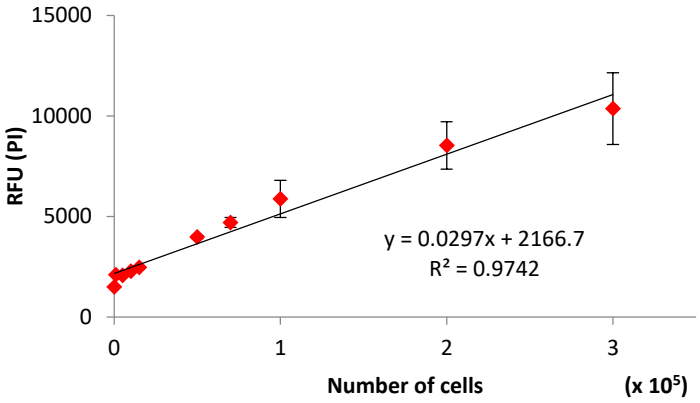

Figure A2.1: **Linearity of PI assay for quantification of cell number.** A calibration curve of cell numbers from 0 to 300,000 cells per well were stained using 2 µg/mL PI solution with linear regression analysis. Fluorescence was determined using a on a Tecan Infinite M200 microplate reader using 100 reads per well in five independent experiments using *h*MSCs from three different donors (mean values ± SD).

A2.2 Quantitation of cell number using Hoechst 33258

Nuclear staining in adipogenic analysis was carried out using 2 µg/mL Hoechst 33258 (diluted in H_2O from 1 mg/mL; Sigma-Aldrich, UK) for 15 minutes.

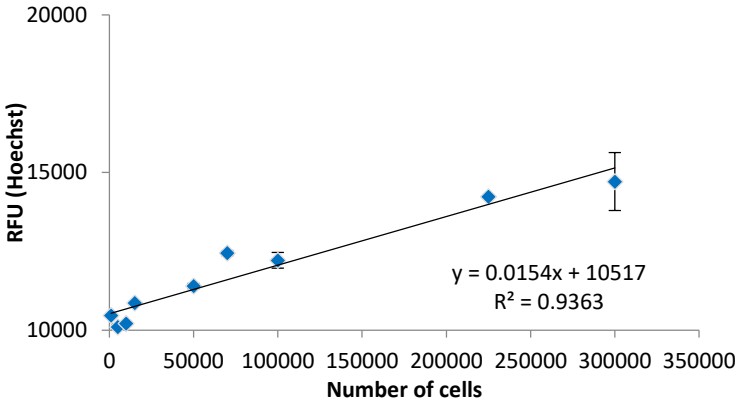

Figure A2.2: **Linearity of Hoechst assay for quantification of cell number**. A calibration curve of cell numbers from 0 to 300,000 cells per well were stained using 2 µg/mL Hoechst 33258 solution with linear regression analysis. Fluorescence was determined using a on a Tecan Infinite M200 microplate reader using 100 reads per well in five independent experiments using *h*MSCs from three different donors (mean values ± SD).

A2.3 Quantitation of cell numbers using PrestoBlue

The Presto Blue assay was used to assess the metabolic activity of cells over time (described in Chapters 3-6). Standard calibration curves were generated to enable the extrapolation of the number of metabolically active cells present from the fluorescence measurements obtained. To confirm linearity over a large range of cell numbers for cell proliferation investigations, cell suspensions were made up containing cellular concentrations ranging from $8x10^4$-$1x10^6$ NIH 3T3s/well and $7x10^3$ - $4.5x10^5$ hMSCs/well using the PrestoBlue assay reagent. These solutions were incubated in a tissue culture incubator for the appropriate time (see Chapter 2), and analysed fluorometrically using a Tecan Infinite M200 microplate reader ($\lambda_{exc}/\lambda_{em:}$ 560/590 nm). Once linearity was established, standard curves were generated with every experiment to enable the extrapolation of cell numbers.

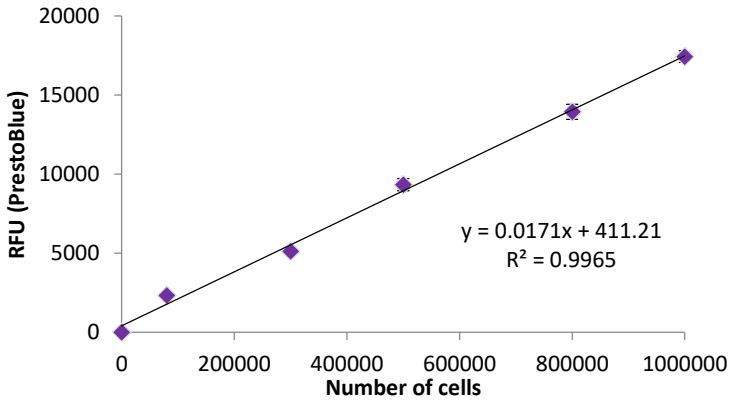

Figure A2.3: **Linearity of Presto blue for quantification of NIH 3T3 cell numbers**. A standard calibration curve of cell numbers from 0 to 1,000,000 cells per well were stained using PrestoBlue reagent at a 1:10 dilution in culture media. Fluorescence was determined using a on a Tecan Infinite M200 microplate reader (*n*=5; mean values ± SD).

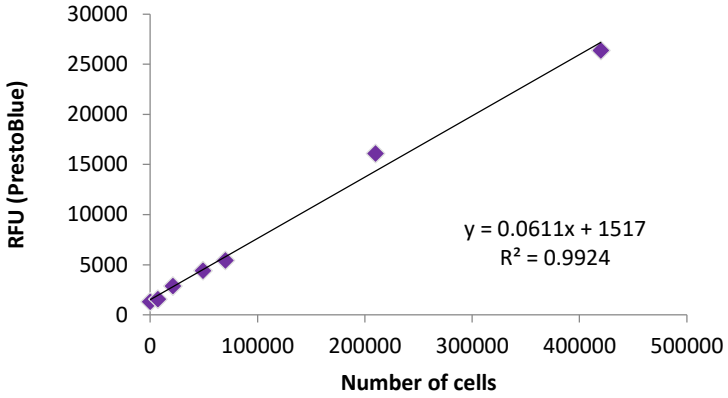

Figure A2.4: **Linearity of PrestoBlue for quantification of hMSC cell numbers**. A representative standard calibration curve of cell numbers from 0 to 450,000 cells per well were stained using PrestoBlue reagent at a 1:10 dilution in culture media. Fluorescence was determined using a on a Tecan Infinite M200 microplate reader (mean values ± SD).